Nuclear spin and isospin excitations

Franz Osterfeld

Institut für Kernphysik, Forschungszentrum Jülich GmbH, Postfach 1913, 5170 Jülich, Germany

A review is given of our present knowledge of collective spin-isospin excitations in nuclei. Most of this knowledge comes from intermediate-energy charge-exchange reactions and from inelastic electron- and proton-scattering experiments. The nuclear-spin dynamics is governed by the spin-isospin-dependent two-nucleon interaction in the medium. This interaction gives rise to collective spin modes such as the giant Gamow-Teller resonances. An interesting phenomenon is that the measured total Gamow-Teller transition strength in the resonance region is much less than a model-independent sum rule predicts. Two physically different mechanisms have been discussed to explain this so-called quenching of the total Gamow-Teller strength: coupling to subnuclear degrees of freedom in the form of Δ-isobar excitation and ordinary nuclear configuration mixing. Both detailed nuclear structure calculations and extensive analyses of the scattering data suggest that the nuclear configuration mixing effect is the more important quenching mechanism, although subnuclear degrees of freedom cannot be ruled out. The quenching phenomenon occurs for nuclear-spin excitations at low excitation energies ($\omega \sim 10$–20 MeV) and small-momentum transfers ($q \leq 0.5$ fm^{-1}). A completely opposite effect is anticipated in the high (ω, q)-transfer region ($0 \leq \omega \leq 500$ MeV, $0.5 \leq q \leq 3$ fm^{-1}). The nuclear spin-isospin response might be enhanced due to the attractive pion field inside the nucleus. Charge-exchange reactions at GeV incident energies have been used to study the quasifree peak region and the Δ-resonance region. An interesting result of these experiments is that the Δ excitation in the nucleus is shifted downwards in energy relative to the Δ excitation of the free proton. The physical origin of this shift is discussed, and it is shown that it may be related to the energy-dependent, attractive one-pion exchange interaction in the medium.

CONTENTS

I. INTRODUCTION

In this article we review the present status of collective spin and isospin excitations in nuclei. Over the last decade impressive development has taken place in this field of nuclear physics. The progress has been made through both outstanding experimental work at the intermediate-energy hadron and electron facilities and intriguing theoretical ideas. The hadron facilities contributing to this field of physics are IUCF in Bloomington, IPN in

Orsay, LAMPF in Los Alamos, SATURNE in Saclay, TRIUMF in Vancouver, and SIN in Villigen. The electron facilities in question are DALINAC in Darmstadt, MAMI in Mainz, MIT Bates Laboratories in Boston, NIKHEF in Amsterdam, and the (γ,γ') facilities at Giessen and Urbana.

Traditionally a considerable amount of the experimental work at nuclear physics accelerators is devoted to the study of giant multipole resonances. These are elementary modes of nuclear excitation which involve the coherent motion of many nucleons in the nucleus. Typical examples are the shape and density oscillations of the nucleus around its equilibrium configuration. The appropriate nuclear reactions to excite these modes are the inelastic scattering of electrons or hadrons from nuclei. Inelastic scattering processes are particularly sensitive to any coherent aspects of the nucleonic motion, since they lead to enhanced or diminished inelastic-scattering cross sections as compared to, say, a single-particle transition between shell-model orbitals. Furthermore, in the inelastic-scattering event, energy and momentum can be transferred independently to the target. This makes it possible to measure both excitation functions and angular distributions, the latter of which are needed to determine the multipolarity of the given state under investigation.

By 1980 various electric collective modes like the isoscalar giant quadrupole resonance with spin-parity $J^\pi=2^+$ (Pitthan and Walcher, 1971; Lewis and Bertrand, 1972) and the isoscalar giant monopole resonance with spin-parity $J^\pi=0^+$ (Marty *et al.*, 1975; Harakeh *et al.*, 1977; Youngblood *et al.*, 1977; Buenerd *et al.*, 1979; Lebrun *et al.*, 1980; Rosza *et al.*, 1980; Youngblood *et al.*, 1981) were well established. The isoscalar ($T=0$) modes are vibrations in which the neutrons and protons move in phase. Modes in which protons and neutrons move in opposite phase are called isovector ($T=1$). The giant electric dipole resonance ($J^\pi=1^-$, $T=1$) is the classical example for the latter class of states. This resonance is very strongly and selectively excited by photon absorption (Baldwin and Klaiber, 1947, 1948; Berman and Fultz, 1975). The electric dipole radiation induces a polarization oscillation of the protons against the neutrons, leaving the center of mass of the nucleus at rest (Goldhaber and Teller, 1948; Steinwedel and Jensen, 1950).

Similar oscillations to those in isospin space are also possible in spin space. Nucleons with spin up and spin down may move either in phase (spin-scalar $S=0$ modes) or out of phase (spin-vector $S=1$ modes). The latter class of states is also referred to as spin excitations or spin-flip transitions. The spin excitations are again subdivided into isoscalar spin-flip ($S=1$, $T=0$) and isovector spin-flip ($S=1$, $T=1$) states. The interesting aspect of the collective spin modes is that they provide direct information on the spin- and spin-isospin-dependent effective interactions in the nuclear medium. These forces are represented on the microscopic level by the residual particle-hole (p-h) interaction, which correlates the individual p-h transitions forming collective states.

The fields that can be used as a probe of spin excitations are the weak, the electromagnetic, and the strong interactions. In the weak interaction it is the axial-vector current which couples to the spin of the nucleon and which induces the Gamow-Teller (GT) transitions of nuclear $\beta_\pm$ decay. In the nonrelativistic form of the β current, these transitions are mediated by the spin-isospin operator $g_A\boldsymbol{\sigma}\tau_\pm$, where g_A is the axial-vector coupling constant. Hence, by studying these transitions, one obtains valuable information on the spin-isospin properties of nuclei. Unfortunately, β decay has access to nuclear states only in a very limited energy window and misses the strongest states in the spectrum. Therefore, to map out the complete response function in the $\boldsymbol{\sigma}\tau_\pm$ channels, one needs probes that allow the independent variation of both energy transfer and momentum transfer to the target. This is possible with hadronic probes such as the (p,n) and (n,p) charge-exchange reactions, the properties of which we shall describe in this article.

The electromagnetic field couples to the spin of the nucleon through the nuclear magnetization current, which consists of an isoscalar part proportional to $(\mu_p+\mu_n)\boldsymbol{\sigma}\times\mathbf{q}$ and an isovector part proportional to $(\mu_p-\mu_n)\boldsymbol{\sigma}\times\mathbf{q}\tau_3$. Here, the nonrelativistic limit of the current is assumed, and $\mu_p=2.79$ and $\mu_n=-1.91$ are the intrinsic magnetic moments of the proton and neutron, respectively; $\mathbf{q}$ is the momentum transfer. Since the difference of the magnetic moments, $(\mu_p-\mu_n)=4.71$, is much larger than the sum, $(\mu_p+\mu_n)=0.88$, it is apparent that the electromagnetic interaction preferentially probes spin transitions in the inelastic isovector $(\boldsymbol{\sigma}\tau_3)$ channel (Morpurgo, 1958, 1959). Note that the spin operator $\boldsymbol{\sigma}$ and the momentum transfer $\mathbf{q}$ couple transversely, i.e., like $\boldsymbol{\sigma}\times\mathbf{q}$. Therefore the electromagnetic interaction measures the transverse spin response of nuclei. The appropriate spectroscopic tool to study this response is backward-angle inelastic electron scattering.

Because of the nucleon's spin and isospin structure, the strong interaction has several couplings that allow many different types of nuclear excitations to be investigated. In a meson-exchange picture of nuclear forces it is the π- and ρ-meson exchange which generates the spin-isospin-dependent interaction terms. Here the pion plays a special role for the following reasons: (i) Since the pion has a small mass it can be exchanged over large distances. This feature is especially important for the inelastic scattering of nucleons from nuclei and for charge-exchange reactions, where the exchange of neutral or charged pions between the projectile and the target excites the nuclear spin-isospin degrees of freedom at small-momentum transfers. (ii) Because of its pseudoscalar nature the pion couples longitudinally, i.e., by $\boldsymbol{\sigma}\cdot\mathbf{q}$, to the spin of the nucleon, and thus can give complementary information about nuclear-spin properties to that from the electromagnetic interaction. In particular, the pionic coupling can be used to study the virtual-pion field inside the nucleus. (iii) The pion field itself strongly couples to

the $\Delta(1232, s=\frac{3}{2}, t=\frac{3}{2})$ isobar, which in the quark picture of baryons can be viewed as the internal spin-isospin-flip excitation of the nucleon. A central issue in the study of nuclear spin-isospin modes is therefore whether these Δ degrees of freedom of the nucleon can also influence the properties of normal GT nuclear β decay.

This question was first discussed in 1973 by Ericson *et al.* (1973) and Wilkinson (1973a, 1973b), who suggested a renormalization of the axial-vector coupling constant g_A for nucleons embedded in a nucleus. Their arguments were based on the partially conserved axial-vector current (PCAC) hypothesis, which states that the divergence of the axial-vector current is proportional to the pion field (Gell-Mann and Levy, 1960). Ericson *et al.* (1973) pointed out that the pion field within the nucleus might be suppressed at small momenta ($|\mathbf{q}| \sim 0$) because of the strong, short-range repulsion between nucleons in the medium. Then, via PCAC, the Gamow-Teller β decay would also be suppressed. This argument was worked out in more detail by Rho (1974), and Ohta and Wakamatsu (1974), who showed that the Δ isobar would be the main mediator of the subnucleonic influences on the GT strength function. A quenching of GT strength was indeed observed in all (p,n) charge-exchange experiments (Gaarde *et al.*, 1981), as we shall discuss later. Whether or not this quenching is due to a Δ-isobar effect is, however, not so clear. There are other many-body corrections arising from short-range central and tensor correlations between nucleons which also reduce the observable strength (Shimizu *et al.*, 1974; Bertsch and Hamamoto, 1982).

The GT states test the spin-isospin correlations in nuclei at small-momentum transfers. Another interesting problem is the nature and magnitude of these correlations at higher-momentum transfers of $q \sim (1-2)$ fm^{-1}. This is particularly interesting in view of the possible existence of an enhanced pion field in nuclei in this momentum-transfer region, as was first discussed by Migdal (1972, 1978, 1979), Sawyer (1972), and Scalapino (1972) (see also Sawyer, 1979). These authors pointed out that the correlations could possibly be very attractive at $q \sim (1-2)$ fm^{-1} because of the strong attraction of the one-pion-exchange interaction, and that this attraction might even lead to a phase transition into a pion condensate at sufficiently high nuclear densities. From the study of the GT states over the last decade we know that the short-range correlations in the spin-isospin channel are sufficiently repulsive to screen the attraction of the one-pion exchange and hinder pion condensates as well as their precursors. In addition, the strong attractive tensor force of the π-exchange interaction, which would be the driving interaction for formation of a pion condensate, is reduced by the repulsive tensor component of the ρ-exchange potential because of their mutual cancellation at larger-momentum transfers.

In spite of the absence of collectivity, it is of great interest to study the spin-isospin-dependent effective interaction in the high-momentum-transfer region. In particular, one expects that the interaction in the spin-longitudinal and spin-transverse channels might show a quite different q dependence. The former involves the pion, while the latter is governed by the ρ meson. Now the ρ meson couples to the spin of the nucleon transversely ($\boldsymbol{\sigma} \times \mathbf{q}$), while the pion couples to it longitudinally ($\boldsymbol{\sigma} \cdot \mathbf{q}$). Therefore their relative contribution to the residual p-h interaction can, in principle, be separated by measuring the longitudinal and transverse spin responses of nuclei, respectively. The relevant region in which to look for such effects in the nuclear excitation spectrum is the quasielastic peak region. The longitudinal isovector spin response function should be enhanced and shifted downwards in energy relative to the free-Fermi-gas response due to the attraction of the π exchange (Alberico *et al.*, 1982), while the transverse isovector spin response should be quenched and shifted upwards in energy due to the repulsive transverse p-h interaction. The transverse spin response can be studied by means of inelastic magnetic electron scattering, while the measurement of the longitudinal spin response requires complete spin-flip transfer measurements with hadronic probes.

Another very interesting problem is the spin response of nuclei in the $\Delta(1232)$ resonance region. Again the longitudinal and transverse spin responses are expected to behave differently. The longitudinal response gives information about pion propagation in the nucleus and, closely connected to this, about the Δ dynamics in the medium. A great deal of information on the Δ resonance in nuclei has been obtained from pion-nucleus scattering and γ absorption (see, for example, Eisenberg and Koltun, 1980; Oset *et al.*, 1982; Ericson and Weise, 1988). New and complementary information comes from the high-energy (p,n), $(^3\mathrm{He},t)$, and $(d,2p)$ charge-exchange reactions as well as from high-energy (e,e') experiments. These reactions have a different selectivity and explore a different kinematic region of the spin-isospin response function than pion-nucleus scattering and γ absorption.

This article is organized as follows: In Sec. II we derive some very general, model-independent sum rules for Fermi and Gamow-Teller transitions starting from the fundamental current algebra of weak interactions. These sum rules have to be respected by all nuclear structure models used for the description of Fermi and Gamow-Teller transitions. In Sec. III we give an overview of the experimental development in inelastic scattering and charge-exchange reactions, with emphasis on collective spin excitations in nuclei. We discuss only selected experiments, by means of which we try to explain the physics of spin excitations in a broad way. In Sec. IV we present the direct nuclear reaction theory needed for the interpretation of the scattering data. We shall find that at intermediate projectile energies ($E_p \geq 100$ MeV) inelastic nucleon-nucleus scattering and charge-exchange reactions mainly proceed via a direct, single-step reaction mechanism. Therefore the measured cross section can be rather reliably calculated within the distorted-wave im-

pulse approximation (DWIA). This allows for a separation of the scattering problem into a nuclear reaction part and a nuclear structure part. It turns out that the probe-target nucleon interaction can be well described by the free nucleon-nucleon t-matrix interaction, particularly in the $\sigma\tau$ channel. Thus one may regard the probe-target coupling to be known and one can focus attention on the nuclear structure aspect of the problem. In Sec. V we review the nuclear structure aspects of the spin and isospin excitations. The nuclear-spin response is calculated either within the various versions of the random-phase approximation (RPA) or by complete diagonalization of a shell-model Hamiltonian. The observed properties of the spin and isospin modes are related to the residual p-h interaction. The couplings responsible for the damping width of the spin modes are discussed. In Sec. VI we review various microscopic analyses of complete forward-angle $(p,n),(p,p')$, and (n,p) spectra as well as spectra obtained with other probes. These analyses are intended to decompose the spectra into the various multipoles in order to determine the strength distribution functions of states with different spin-parity J^π. Of special interest is the strength function of the GT states because of the possible quenching of GT strength due to subnuclear degrees of freedom. Section VII will deal with the spin-isospin response function in the quasifree peak region ($E_x \sim 100$ MeV) and in the Δ-resonance ($E_x \sim 300$ MeV) region. Research in this area is still in progress, and we shall therefore only review the experimental facts and give some tentative explanations of the data. Section VIII contains a short summary and conclusions.

II. SUM RULES

The charge-changing reactions that we study in this article involve matrix elements between nuclear states very similar to the matrix elements required for weak-interaction processes. This gives rise to parallels between the treatment of nuclear matrix elements, which is usually made with a nonrelativistic reduction of the operators, and matrix elements in hadron physics, which are always written in covariant form. An important guidepost in both areas is the existence of sum rules for operators of interest. In this section we shall briefly review the relevant strong-interaction theory and derive the sum rules needed for nuclear physics.

At the most fundamental level, which is the Standard Model, the weak and electromagnetic interactions are coupled to hadrons by matrix elements in the quark fields. There are two types of matrix elements, connected either with the vector (V) or the axial-vector (A) current. The currents themselves are matrices in flavor SU(3) space. In the following we shall be concerned only with ordinary (nonstrange) hadrons, in which case the matrix structure is just that of SU(2) or isospin. In terms of the quark fields the vector and axial-vector currents are defined by

$$V_\lambda^j(\mathbf{x},t)=\hat{\bar{q}}(\mathbf{x},t)\gamma_\lambda\left[\frac{\tau_j}{2}\right]\hat{q}(\mathbf{x},t)\ ,\quad j=1,2,3\ , \tag{2.1}$$

$$A_\lambda^j(\mathbf{x},t)=\hat{\bar{q}}(\mathbf{x},t)\gamma_\lambda\gamma_5\left[\frac{\tau_j}{2}\right]\hat{q}(\mathbf{x},t)\ ,\quad j=1,2,3\ , \tag{2.2}$$

where the γ_λ ($\lambda=0,1,2,3$) denote the usual Dirac matrices with $\gamma_5\equiv i\gamma_0\gamma_1\gamma_2\gamma_3$ and $\hat{\bar{q}}(\mathbf{x},t)\equiv\hat{q}^\dagger(\mathbf{x},t)\gamma_0$. The τ_j are the Pauli isospin operators acting on the quark isospin doublet consisting of a d and u quark. The weak-interaction Hamiltonian describing low-energy β-decay processes is then given by the effective coupling (Fermi, 1934a, 1934b)

$$H_{\text{weak}}(x)=-\frac{G}{\sqrt{2}}[l^\lambda(x)]^\dagger[V_\lambda^+(x)-A_\lambda^+(x)]+\text{H.c.} \tag{2.3}$$

Here $l_\lambda(x)$ is the leptonic four-vector current and $V_\lambda^\pm=V_\lambda^1\pm iV_\lambda^2$ and $A_\lambda^\pm=A_\lambda^1\pm iA_\lambda^2$ are the charge-changing vector and axial-vector currents, respectively. The weak Fermi coupling constant G is given by

$$G=1.15\times10^{-5}\ \text{GeV}^{-2} \tag{2.4}$$

in natural units ($\hbar=c=1$).

Although the currents of Eqs. (2.1) and (2.2) are defined in terms of the fundamental quark fields, they are not easy to use directly because the wave functions of hadrons in terms of quark fields are not known. Nevertheless general statements, derivable from the symmetry properties of the Lagrangian in the Standard Model, can be made. This is the current algebra, which we now briefly review.

A. Current algebra

Current algebra is based on equal-time commutation relations among the various components of the currents (Gell-Mann, 1962, 1964). Naively taking the commutators of the operators of Eqs. (2.1) and (2.2) one obtains

$$[V_\lambda^j(\mathbf{x},t),V_\lambda^k(\mathbf{y},t)]=i\epsilon_{jkl}V_0^l(\mathbf{x},t)\delta^3(\mathbf{x}-\mathbf{y})\ ,\quad \lambda=0,1,2,3\ , \tag{2.5}$$

$$[V_\lambda^j(\mathbf{x},t),A_\lambda^k(\mathbf{y},t)]=i\epsilon_{jkl}A_0^l(\mathbf{x},t)\delta^3(\mathbf{x}-\mathbf{y})\ ,\quad \lambda=0,1,2,3\ , \tag{2.6}$$

$$[A_\lambda^j(\mathbf{x},t),A_\lambda^k(\mathbf{y},t)]=i\epsilon_{jkl}V_0^l(\mathbf{x},t)\delta^3(\mathbf{x}-\mathbf{y})\ ,\quad \lambda=0,1,2,3\ , \tag{2.7}$$

where ϵ_{jkl} is the Levi-Civita antisymmetric tensor defining the structure constants of the SU(2) group. However, contradictions arise in field theory for all these relations except those involving only the timelike components of the fields. One may integrate the currents over space to get the vector and axial-vector charges

$$Q_V^j(t)=\int V_0^j(\mathbf{x},t)\,d^3\mathbf{x}\ ,\quad j=1,2,3\ , \tag{2.8}$$

$$Q_A^j(t)=\int A_0^j(\mathbf{x},t)\,d^3\mathbf{x}\ ,\quad j=1,2,3\ , \tag{2.9}$$

which, in general, are time dependent. If one of the currents is conserved, that is,

$$\partial^\lambda V_\lambda^i(x)=0 , \tag{2.10}$$

then the corresponding charge Q_V^i is a constant of the motion,

$$\frac{dQ_V^i}{dt}=0 . \tag{2.11}$$

For example, the vector current $V_\lambda^+=V_\lambda^1+iV_\lambda^2$ and its conjugate, $V_\lambda^-=V_\lambda^1-iV_\lambda^2$, are partners of the isovector electromagnetic current V_λ^3 in an isospin triplet. The corresponding charges are the isospin operators $T_\pm\equiv Q_V^\pm$ and $T_3\equiv Q_V^3$, which, in the absence of the electromagnetic effects, are conserved. This is the *conserved vector current* (CVC) hypothesis of Feynman and Gell-Mann (1958) and Gershtein and Zeldovich (1956). The isospin charges generate the isospin SU(2) group and satisfy the familiar commutation relations

$$[T_+,T_-]=2T_3 , \tag{2.12}$$

$$[T_3,T_\pm]=\pm T_\pm . \tag{2.13}$$

In the presence of symmetry-breaking effects in the Lagrangian, the charges are no longer constants of the motion. As Gell-Mann (1962, 1964) pointed out, however, even in this case the charges will satisfy the *equal-time* commutation relations

$$[Q_V^i(t),Q_V^k(t)]=i\epsilon_{jkl}Q_V^l(t) , \tag{2.14}$$

$$[Q_V^i(t),Q_A^k(t)]=i\epsilon_{jkl}Q_A^l(t) , \tag{2.15}$$

$$[Q_A^i(t),Q_A^k(t)]=i\epsilon_{jkl}Q_V^l(t) . \tag{2.16}$$

Equation (2.14) states that the SU(2) algebra generated by the vector charges $Q_V^i(t)$ holds independently of the conservation of the charges and of the validity of the continuity equation for the currents. These relations are usually referred to as *charge algebra* (Gell-Mann, 1962, 1964). Equation (2.15) sets a relative scale for the various vector and axial-vector charges. From Eq. (2.16) it is obvious that the axial charges alone do not form a closed algebra. This is due to their odd-parity character. Since Eq. (2.16) is bilinear in axial charges, and since the right-hand side contains vector charges, the relative scale between vector and axial-vector quantities is also fixed.

The vector and axial-vector charges together, connected by the commutation relations of Eqs. (2.14)–(2.16), define the so-called chiral $SU(2)_L\otimes SU(2)_R$ algebra. The current-algebra hypothesis of Gell-Mann states that these relations hold independently of any explicit form of the currents. (For a general discussion of current algebra, see, for example, Adler and Dashen 1968; de Alfaro *et al.*, 1973; Cheng and Li, 1984.)

B. Fermi sum rule

The discussion in Sec. II.A is directly applicable to the Fermi sum rule, which is obtained by sandwiching the commutator of Eq. (2.12) between nucleon states. For a neutron state, for example, we have

$$\langle n|[T_+,T_-]|n\rangle=\langle n|T_+T_--T_-T_+|n\rangle =2\langle n|T_3|n\rangle . \tag{2.17}$$

By inserting a complete set of physical intermediate states into the commutator we obtain

$$\sum_f\langle n|T_+|f\rangle\langle f|T_-|n\rangle-\sum_f\langle n|T_-|f\rangle\langle f|T_+|n\rangle=1 , \tag{2.18}$$

where we used the (nuclear physics) convention $T_3|n\rangle=\frac{1}{2}|n\rangle(T_3|p\rangle=-\frac{1}{2}|p\rangle)$. Since $V_\lambda^\pm$ is a conserved current, the operators T_+ and T_- allow transitions only between particles belonging to the same multiplet. Therefore in the first sum the only allowed intermediate state is the proton, whereas no allowed intermediate states appear in the second sum. We thus obtain the well known result

$$|\langle p|T_-|n\rangle|^2=1 . \tag{2.19}$$

Next we extend this sum rule to nuclei and assume that the initial state $|\Psi_i\rangle$ of the nucleus has good isospin $T_0=T_3=(N-Z)/2$. For a nucleus with neutron excess ($N\geq Z$) we have $T_+|\Psi_i\rangle\equiv T_+|T_0,T_0\rangle=0$. Therefore the Fermi sum rule reads

$$S_{\beta_-}(F)=\sum_f|\langle\Psi_f|T_-|\Psi_i\rangle|^2=2\langle\Psi_i|T_3|\Psi_i\rangle =(N-Z) . \tag{2.20}$$

Because isospin is conserved, all the Fermi strength $S_{\beta_-}(F)$ has to be concentrated in one single final state $|f\rangle$. This state is the so-called isobaric analog (IAS) of the target ground state. It is defined by

$$|\mathrm{IAS}\rangle=\frac{1}{\sqrt{(N-Z)}}T_-|\Psi_0\rangle =\frac{1}{2\sqrt{(N-Z)}}\sum_{j=1}^{A}\tau_-(j)|\Psi_0\rangle , \tag{2.21}$$

where $|\Psi_0\rangle$ denotes the target ground state and $\tau_-(j)\equiv\tau_1(j)-i\tau_2(j)$ denotes the isospin lowering operator that converts the neutron j into a proton without changing its spatial wave function.

C. Gamow-Teller sum rule

If we take the nonrelativistic reduction of two space-like axial currents, we obtain a second sum rule that is very useful for the analysis of nuclear charge-exchange reactions. But note that such a commutator is not one of the permissible ones in Sec. II.A. In low-energy nuclear physics the nucleons are usually treated as pointlike particles which interact via an effective two-nucleon interaction resulting from meson exchange. Explicit mesonic degrees of freedom are not considered. In this situation

we can construct the nucleonic weak currents as follows. We group neutron (n) and proton (p) into an isospin doublet $N=\binom{n}{p}$, and assume that the nucleon field can be described by the Dirac field operators $\hat{\Psi}_N(\mathbf{x},t)$ for pointlike particles. Then, in the impulse approximation, the vector and axial-vector currents associated with the SU(2) transformations are given by

$$V^j_\lambda(\mathbf{x},t)=\hat{\bar{\Psi}}_N(\mathbf{x},t)\gamma_\lambda\left[\frac{\tau_j}{2}\right]\hat{\Psi}_N(\mathbf{x},t)\ , \quad j=1,2,3\ , \tag{2.22}$$

$$A^j_\lambda(\mathbf{x},t)=\hat{\bar{\Psi}}_N(\mathbf{x},t)\gamma_\lambda\gamma_5\left[\frac{\tau_j}{2}\right]\hat{\Psi}_N(\mathbf{x},t)\ , \quad j=1,2,3\ , \tag{2.23}$$

where $\hat{\bar{\Psi}}_N(\mathbf{x},t)\equiv\hat{\Psi}^\dagger_N(\mathbf{x},t)\gamma_0$. The currents fulfill the commutation relations of Eqs. (2.5)–(2.7), as can be immediately verified by inserting them into these equations and by making use of the canonical anticommutation relations for the Dirac field operators, $\{\hat{\Psi}_i(\mathbf{x},t),\hat{\Psi}^\dagger_j(\mathbf{y},t)\}=\delta_{ij}\delta^3(\mathbf{x}-\mathbf{y})$. Note that in Eq. (2.23) we have put $g_A=1$ since we assume that there is no substructure of the nucleon in the present model. In Sec. II.D we shall discuss the mesonic effects on g_A.

In allowed β decay, and for the purposes of the present discussion, we are interested only in the nonrelativistic situation. Under these circumstances, the time and space components of the vector current reduce to

$$\begin{aligned}&\hat{\bar{\Psi}}_N(\mathbf{x},t)\gamma_0\left[\frac{\tau_j}{2}\right]\hat{\Psi}_N(\mathbf{x},t)\to\hat{\Psi}^\dagger_N(\mathbf{x},t)\left[\frac{\tau_j}{2}\right]\hat{\Psi}_N(\mathbf{x},t)\ ,\\ &\hat{\bar{\Psi}}_N(\mathbf{x},t)\gamma_k\left[\frac{\tau_j}{2}\right]\hat{\Psi}_N(\mathbf{x},t)\to 0\ , \quad k=1,2,3\ ,\end{aligned} \tag{2.24}$$

while those of the axial-vector current become

$$\begin{aligned}&\hat{\bar{\Psi}}_N(\mathbf{x},t)\gamma_0\gamma_5\left[\frac{\tau_j}{2}\right]\hat{\Psi}_N(\mathbf{x},t)\to 0\ ,\\ &\hat{\bar{\Psi}}_N(\mathbf{x},t)\gamma_k\gamma_5\left[\frac{\tau_j}{2}\right]\hat{\Psi}_N(\mathbf{x},t)\\ &\qquad\to\hat{\Psi}^\dagger_N(\mathbf{x},t)\sigma_k\left[\frac{\tau_j}{2}\right]\hat{\Psi}_N(\mathbf{x},t)\ , \quad k=1,2,3\ .\end{aligned} \tag{2.25}$$

Here the σ_k are the Pauli spin matrices, and the field operators on the right-hand side of Eqs. (2.24) and (2.25) are supposed to be nonrelativistic ones acting in the two-component Pauli spin space. The connection between the charge-changing vector and axial-vector currents and the corresponding configuration-space operators is established by the following relationship (see, for example, Fetter and Walecka, 1971):

$$\hat{\Psi}^\dagger_N(\mathbf{x},t)\left[\frac{\tau_\pm}{2}\right]\hat{\Psi}_N(\mathbf{x},t)\to\tfrac{1}{2}\sum_{i=1}^{A}\delta(\mathbf{x}-\mathbf{r}_i)\tau_\pm(i)\ , \tag{2.26}$$

$$\hat{\Psi}^\dagger_N(\mathbf{x},t)\sigma_k\left[\frac{\tau_\pm}{2}\right]\hat{\Psi}_N(\mathbf{x},t)\to\tfrac{1}{2}\sum_{i=1}^{A}\delta(\mathbf{x}-\mathbf{r}_i)\sigma_k(i)\tau_\pm(i)\ , \tag{2.27}$$

where the sum runs over all A nucleons in the nucleus. The operators on the right-hand side are charge-changing density operators, which describe the probability for finding nucleons at the space point $\mathbf{x}$ with the corresponding spin and isospin specifications. These operators belong to a larger set of 16 local one-particle density operators $\rho(\mathbf{x},\sigma,\tau)$, which form a 4×4 matrix in the spin-isospin variables.

Inserting the results of Eqs. (2.26) and (2.27) into Eq. (2.7), we obtain after integration over coordinates $\mathbf{x}$ and $\mathbf{y}$, the following commutation relation:

$$[\beta_+(\mu),\beta_-(\mu)]=2T_3\ , \quad \mu=-1,0,+1\ , \tag{2.28}$$

where

$$\beta_\pm(\mu)=\tfrac{1}{2}\sum_{i=1}^{A}\sigma_\mu(i)\tau_\pm(i) \tag{2.29}$$

and

$$T_3=\tfrac{1}{2}\sum_{i=1}^{A}\tau_3(i)\ . \tag{2.30}$$

Here, $\beta_\pm$ is the nonrelativistic Gamow-Teller (GT) operator, $\sigma_\mu(i)$ is the nucleon spin operator in spherical basis, and T_3 is the third component of the total isospin. By taking the expectation value of the commutator of Eq. (2.28) with respect to the initial state of the nucleus $|\Psi_i\rangle$ and by inserting a complete set of final states $|\Psi_f\rangle$ between the operators $\beta_+(\mu)$ and $\beta_-(\mu)$, we obtain the nonrelativistic GT sum rule

$$\begin{aligned}S_{\beta_-}(\mathrm{GT})-S_{\beta_+}(\mathrm{GT})&=\sum_{f,\mu}|\langle\Psi_f|\beta_-(\mu)|\Psi_i\rangle|^2\\ &\quad-\sum_{f,\mu}|\langle\Psi_f|\beta_+(\mu)|\Psi_i\rangle|^2\\ &=3(N-Z)\ .\end{aligned} \tag{2.31}$$

Note that the wave functions $|\Psi_f\rangle$ represent either the wave functions of the $(Z+1,N-1)$ or $(Z-1,N+1)$ daughter nuclei, respectively. The sum rule is expressed in terms of the difference between the total transition strengths $S_{\beta_-}(\mathrm{GT})$ and $S_{\beta_+}(\mathrm{GT})$ measured in β_- and β_+ decay, respectively. This difference depends only on the neutron excess $(N-Z)$ and is totally independent of the states $|\Psi_i\rangle$ and $|\Psi_f\rangle$. This reflects the model independence of the sum rule.

A Gamow-Teller sum rule can also be derived within the constituent quark model, which allows us to discuss possible effects of the internal nucleonic degrees of freedom on the GT sum rule. In the quark model (Gell-Mann, 1964; Zweig, 1964) the baryons are supposed to consist of three-quark (qqq) bound states. The baryons occur in SU(3) singlets (**1**), octets (**8**), and decuplets (**10**).

The neutron and proton belong to the octet of $J^\pi=\frac{1}{2}^+$ baryons, which are three-quark states with total orbital angular momentum $L=0$ and with total quark spin $J^\pi=\frac{1}{2}^+$. The states in which the quark spins add up to $J^\pi=\frac{3}{2}^+$ represent the SU(3) decuplet of baryon resonances. The $\Delta(1232)$ isobar belongs to this latter multiplet.

The derivation of the sum rule within the constituent quark model starts from the definition of the quark currents in Eqs. (2.5)–(2.7). Then the nonrelativistic limit of the quark currents is taken in analogy to Eqs. (2.24) and (2.25). Insertion of the currents into Eq. (2.7) and integration over coordinates **x** and **y** then gives us the commutation relation of Eq. (2.28) in terms of the quark spin-isospin operators

$$\beta^q_\pm(\mu)=\tfrac{1}{2}\sum_{i=1}^{3A}\sigma_\mu(i)\tau_\pm(i)\ , \tag{2.32}$$

where the sum now runs over all quarks in the nucleus. To explain the properties of the quark operators, let us consider the operator $\beta^q_-(\mu=-1)$ as an example. This operator transforms d quarks with spin $\uparrow$ into u quarks with spin $\downarrow$ while it gives zero for all other quark states. Therefore, if we apply this operator to a neutron wave function that contains the quark configuration $|u\uparrow d\uparrow d\downarrow\rangle$, this configuration is changed into $|u\uparrow u\downarrow d\downarrow\rangle$, which is a component of the proton as well as of the $\Delta^+(1232)$. Thus $\beta^q_-(\mu=-1)$ changes the neutron either into a proton or into a Δ^+. Similarly it transforms a proton into a Δ^{++}.

With the quark spin-isospin operators of Eq. (2.32) we obtain the following sum rule for the neutron:

$$\begin{aligned}\langle n|[\beta^q_+(0),\beta^q_-(0)]|n\rangle&=|\langle p|\beta^q_-(0)|n\rangle|^2\\&\quad+|\langle\Delta^+|\beta^0_-(0)|n\rangle|^2\\&\quad-|\langle\Delta^-|\beta^q_+(0)|n\rangle|^2\\&=\tfrac{25}{9}+\tfrac{8}{9}-\tfrac{8}{3}=1\ .\end{aligned}\tag{2.33}$$

Here, the matrix elements were calculated within the constituent quark model (see Kokkedee, 1969), and the nuclear physics convention for the isospin was used, that is, $T_3|d\rangle=\frac{1}{2}|d\rangle$ and $T_3|u\rangle=-\frac{1}{2}|u\rangle$. The sum-rule value for the proton turns out to be just the negative of that for the neutron, i.e., $\langle p|[\beta^q_+(0),\beta^q_-(0)]|p\rangle=-1$. From the value of $|\langle p|\beta^q_-(0)|n\rangle|=\frac{5}{3}$ we recognize that the axial-vector coupling constant in the constituent quark model is $\frac{5}{3}$. This deviation from the experimental value ($g_A=1.26$) is assumed to be due to strong-interaction effects not included in the constituent quark model.

To estimate the importance of Δ-h excitations for the Gamow-Teller sum rule we make a naive model of the nucleus assuming that it is composed of A nucleons, each of which is represented by a bag containing three confined quarks. The ground state of the nucleus is then described by a Slater determinant of A noninteracting bags with the energetically lowest single-particle orbitals being occupied. The action of the operator $\beta^q_-(\mu)$ on the ground-state wave function produces p-h as well as Δ-h excitations. The sum rule reads

$$\begin{aligned}S_{\beta^q_-}(\mathrm{GT})-S_{\beta^q_+}(\mathrm{GT})&=\sum_{\text{p-h},\mu}|\langle \mathrm{p}|\beta^q_-(\mu)|\mathrm{h}\rangle|^2-\sum_{\text{p-h},\mu}|\langle \mathrm{p}|\beta^q_+(\mu)|\mathrm{h}\rangle|^2+\sum_{\Delta\text{-h},\mu}|\langle\Delta|\beta^q_-(\mu)|\mathrm{h}\rangle|^2-\sum_{\Delta\text{-h},\mu}|\langle\Delta|\beta^q_+(\mu)|\mathrm{h}\rangle|^2\\&=\tfrac{75}{9}(N-Z)+\tfrac{24}{9}(N+3Z)-\tfrac{24}{9}(Z+3N)\\&=3(N-Z)\ ,\end{aligned}\tag{2.34}$$

where the sum over h is performed with respect to all occupied single-particle states. We notice that in individual $\beta_\pm$ directions the total transition strength to the Δ-h states is very large. This reflects the fact that there exists no Pauli blocking for Δ-h excitations, so that all nucleons in the nucleus can participate in Δ-h transitions. For the usual p-h excitations, however, the total transition strength remains proportional to the neutron excess $(N-Z)$. A comparison of Eqs. (2.31) and (2.34) reveals that in the quark model the dominant part of the GT strength is carried by the Δ-h excitations.

D. Adler-Weisberger sum rule

It is still possible to make a useful sum rule involving the axial current by introducing a new relation, the partially conserved axial coupling (PCAC), which relates the divergence of the axial current to the pion field. This sum rule is based on the commutator of Eq. (2.16) and is the so-called Adler-Weisberger sum rule (Adler, 1965; Weisberger, 1966). In the following we shall only describe the main ideas for its derivation and refer the reader to the original papers by Adler (1965), Weisberger (1966), and Fubini and Furlan (1965) for details (see also, Adler and Dashen, 1968). Unlike the vector current $V^\pm_\lambda(\mathbf{x},t)$, the axial-vector current $A^\pm_\lambda(\mathbf{x},t)$ is not an exactly conserved quantity. Therefore the intermediate states to be inserted into the commutator of Eq. (2.16) belong to a much wider class of states than just to a single multiplet. The coupling to states outside the multiplet is due to the nonconservation of the axial charges $Q_A(t)$.

In order to determine the possible intermediate states, we make use of the partially conserved axial current theory, due originally to Gell-Mann and Levy (1960). The PCAC theory states that the divergence of the axial current is proportional to the pion field

$$\partial^\lambda A_\lambda^\pm(\mathbf{x},t)=m_\pi^2 f_\pi \hat{\Phi}^\pm(\mathbf{x},t)\ , \tag{2.35}$$

where $\hat{\Phi}^\pm(\mathbf{x},t)$ is the pion field operator creating or annihilating a pion at point $(\mathbf{x},t)$, $m_\pi \simeq 140$ MeV is the pion mass, and $f_\pi \simeq 93$ MeV is the pion-decay constant.

Integrating Eq. (2.35) over $\mathbf{x}$ and using the fact that the spatial part $\mathbf{A}(\mathbf{x},t)$ of the axial current vanishes for large distances, we find that the time derivative of the axial charge operator is given by

$$\frac{dQ_A^\pm(t)}{dt}=\int d^3\mathbf{x}\frac{\partial A_0(\mathbf{x},t)}{\partial t}=\int d^3\mathbf{x}\,\partial^\lambda A_\lambda(\mathbf{x},t)$$
$$=m_\pi^2 f_\pi \int d^3\mathbf{x}\,\hat{\Phi}^\pm(\mathbf{x},t)\ . \tag{2.36}$$

Since $\hat{\Phi}^\pm(\mathbf{x},t)$ is a pion field operator, Eq. (2.36) shows that $Q_A^\pm(t)$ can connect states differing in pion occupation number by unity. This means that in the evaluation of the expectation value of the commutator (2.16) we have to consider, besides the one-nucleon states $|n\rangle$, also one-nucleon plus one-pion states $|k\rangle$ as intermediate states. Now we sandwich the commutator of Eq. (2.16) between proton states $|p\rangle$ and insert a complete set of intermediate states into the commutator. We obtain

$$-\sum_n \langle p|Q_A^-|n\rangle\langle n|Q_A^+|p\rangle$$
$$+\sum_k \langle p|Q_A^+|k\rangle\langle k|Q_A^-|p\rangle-(Q_A^+\leftrightarrow Q_A^-)$$
$$=2\langle p|Q_V^3|p\rangle=-1\ , \tag{2.37}$$

where we have separated out the one-nucleon (the neutron) term. In the last step, we made use of the fact that the vector charge Q_V^3 is conserved. The calculation of the various matrix elements in Eq. (2.37) can be found in the original papers by Adler (1965) and Weisberger (1966), and we state only the final result here. The first term is just the negative of the axial-vector coupling constant squared, $-g_A^2$, while the second term can be related to an energy integral over the total pion-nucleon cross section for zero-mass pion scattering ($m_\pi \to 0$). The result is the Adler-Weisberger relation,

$$1=g_A^2+\frac{2f_\pi^2}{\pi}\int_{m_\pi}^\infty dE_\pi \frac{E_\pi+m_N}{E_\pi(E_\pi+2m_N)}$$
$$\times[\sigma_{\rm tot}^{\pi^-p}(E_\pi)-\sigma_{\rm tot}^{\pi^+p}(E_\pi)]\ . \tag{2.38}$$

Here, $\sigma_{\rm tot}^{\pi^\pm p}(E_\pi)$ is the total cross section for scattering of a zero-mass $\pi^\pm$ on a proton at the pion center-of-mass energy E_π. This cross section can be estimated by extrapolation from the experimental cross section for finite-mass pions. Using the experimental values one obtains $g_A \simeq 1.24$, which agrees quite well with the most recent experimental value of $g_A=1.262\pm0.005$ (Klemt *et al.*, 1988).

The Adler-Weisberger relation was generalized to nuclei by Kim and Primakoff (1965) and Ericson (1971). In the nuclear case the commutator of Eq. (2.16) is sandwiched between nuclear states $|\Psi_i\rangle$. Following a similar procedure to that described before for the nucleon, one obtains

$$(N-Z)=(N-Z)(g_A)_{\rm eff}^2$$
$$+\frac{f_\pi^2}{\pi}\int_{m_\pi}^\infty \frac{dE_\pi}{E_\pi}[\sigma_{\rm tot}^{\pi^+A}(E_\pi)-\sigma_{\rm tot}^{\pi^-A}(E_\pi)]\ , \tag{2.39}$$

where $(g_A)_{\rm eff}$ is the effective axial-vector coupling constant of the nucleon in the medium, and $\sigma_{\rm tot}^{\pi^\pm A}(E_\pi)$ is the total pion-nucleus cross section for soft pions ($m_\pi \to 0$). Assuming a complete suppression of the dispersive integral on the right-hand side of Eq. (2.39) due to the strong shadowing effect in pion-nucleus scattering, one obtains $(g_A)_{\rm eff} \simeq 1$ (Delorme *et al.*, 1982).

The fact that $(g_A)_{\rm eff}$ might be different from g_A has been discussed for some time (Ericson, 1971; Wilkinson, 1973a, 1973b; Ohta and Wakamatsu, 1974; Rho, 1974). This conjecture is based on the PCAC relation of Eq. (2.35) and the possible modification of the pion field inside the nucleus. The nuclear medium has two major effects on the pion field. First, when a nucleon is surrounded by other nucleons a virtual pion emitted by it will be successively scattered by these nucleons as it propagates through the nucleus. In addition, of course, the other nucleons will also act as sources of pions and so contribute to the total pion field. Second, there is a renormalization of the strength of the pionic source due to correlations between nucleons. These correlations produce a "correlation" hole around the nucleon, similar to the hole around an electric dipole in a dielectric medium which leads to the famous Lorentz-Lorenz effect. In the case of the pion field, the axial dipole strength of the nucleon ($\sim g_A \sigma \tau_i$) is renormalizable in an analogous way, as was first pointed out by Ericson and Ericson (1966). Estimates of this effect in nuclear matter lead to a quenching of g_A, that is, to $(g_A)_{\rm eff} \simeq 1$ (Delorme *et al.*, 1976). To what extent g_A is quenched in finite nuclei is still an open problem. There are significant surface and other many-body effects that will modify this estimate. We shall come back to this point in Secs. V, VI, and VII.

III. EXPERIMENTAL OVERVIEW OF SPIN-ISOSPIN EXCITATIONS

In this section we try to give an overview of the experimental development in nuclear-spin physics over the past decade. In the presentation of the scattering data we shall sometimes make use of results from nuclear reaction and nuclear structure theory, which is described in more detail in Secs. IV and V. If necessary, the reader may go on to these sections to find the appropriate information and explanations.

A. The Gamow-Teller (GT) resonance

The experimental breakthrough in our understanding of spin-isospin correlations in nuclei came in 1980 with the beautiful (p,n) charge-exchange experiments at the Indiana University Cyclotron Facility (IUCF). These experiments demonstrated the existence of very collective spin-isospin modes in nuclei (Moake *et al.*, 1979; Anderson *et al.*, 1980; Bainum *et al.*, 1980; Goodman *et al.*, 1980; Horen *et al.*, 1980, 1981; Gaarde *et al.*, 1981). Figure 1 shows measured zero-degree (p,n) spectra of various targets at an incident energy of $E_p = 200$ MeV (from Gaarde *et al.*, 1981). The spectra of nuclei with neutron excess are seen to be dominated by one prominent peak, which is interpreted as the giant Gamow-Teller resonance. This collective mode was predicted by Ikeda, Fujii, and Fujita (1963) as early as 1963. These authors inferred the existence of the GT resonance from the absence of spin-isospin strength at low excitation energies. Assuming a collective GT state at high excitation energies, they could show that the empirically observed hindrance (quenching) of allowed GT β decays in medium and heavy-mass nuclei could be explained as a core-polarization effect. Core polarization means that the energetically high-lying GT state, which is inaccessible to β decay, couples destructively into the low-lying GT states and reduces their strength. Such an effect had been introduced earlier by Blin-Stoyle (1953) and Arima and Horie (1954a, 1954b) in order to explain the systematic deviation of nuclear magnetic moments in odd-A nuclei from the Schmidt values of the extreme single-particle picture. First experimental indications of the GT resonance were observed in 1975 in a 45-MeV ^{90}Zr(p,n) experiment by Doering *et al.* (1975), and thereafter in various low-energy ^{90}Zr(^{3}He,t) experiments (Galonsky *et al.*, 1978, Ovazza *et al.*, 1978).

The GT resonance is a collective spin-isospin oscillation in which the excess neutrons coherently change the direction of their spins and isospins without changing their orbital motion. In the (p,n) reaction this spin-isospin mode is excited by the $V_{\sigma\tau}\sigma_p\cdot\sigma_j\tau_p\cdot\tau_j$ component of the projectile-target nucleon interaction. The labels p and j refer to the projectile and the struck target nucleon, respectively. With respect to the target the (p,n) probe has a similar spin-isospin operator structure to the GT operator of β decay. However, the (p,n) reaction is connected with β decay only if the GT cross section is measured at very-small-momentum transfers q, since allowed β decay takes place at essentially $q=0$. In the (p,n) reaction this condition can be met only for zero degree scattering and at high bombarding energies ($E_p \rightarrow \infty$).

The fact that the orbital motion of the nucleons is unchanged in the GT excitation can be observed from the angular distribution of the GT resonance, which has a characteristic $L=0$ shape, with the maximum cross section at zero degrees. This means that no orbital angular momentum (L) is transferred in the reaction. In the left panel of Fig. 2 the angular distribution of two GT states in ^{90}Zr are shown. Both show the characteristic $L=0$ shape. A spin transfer of $S=1$ in the reaction can be derived only indirectly from the incident-energy dependence of the GT cross section, as we shall discuss shortly. For a target ground state with spin-parity $J^\pi = 0^+$, the spin transfer then makes the GT resonance a $J^\pi = 1^+$ state. The isospin transfer of $T_3 = -1$ is obvious because of the charge-exchange requirement. The single-particle

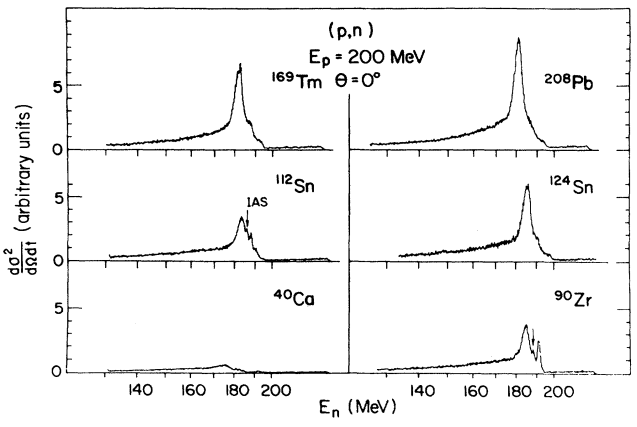

FIG. 1. Neutron time-of-flight spectra of various target nuclei at $E_p = 200$ MeV, measured at the Indiana University Cyclotron Facility (IUCF). The spectra are normalized to show relative cross sections. From Gaarde *et al.* (1981).

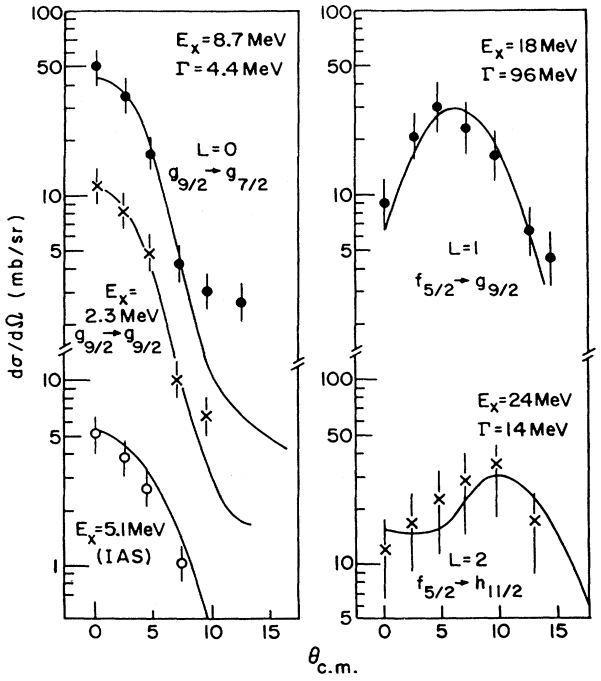

FIG. 2. Angular distributions from the ^{90}Zr$(p,n)^{90}$Nb reaction for different excitation energy regions. The curves (with arbitrary normalization) are angular distributions calculated in the DWIA for typical single-particle transitions. From Gaarde *et al.* (1981).

transitions contributing to the GT oscillation are shown schematically in Fig. 3(b) for the closed-shell nucleus ^{90}Zr.

The GT resonance appears energetically somewhat above the well known isobaric analog of the target ground state. The isobaric analog state was first discovered in 1961 by Anderson and Wong (1961) in a ^{51}V$(p,n)^{51}$Cr experiment at $E_p=14$ MeV. The single-particle transitions involved in case of the isobaric analog excitation are schematically shown for the nucleus ^{90}Zr in Fig. 3(a). The (p,n) reaction excites the isobaric analog through the force component $V_\tau \tau_p \cdot \tau_j$, which requires no spin flip ($S=0$). While the isobaric analog state is the dominant peak in the spectrum at low incident energies ($E_p \leq 100$ MeV), it is completely swamped by the large GT cross section at $E_p=200$ MeV. In Fig. 1 the isobaric analog state is hidden in the envelope of the GT resonance and its position is indicated by the arrow. This large difference in the excitation strengths of isobaric analog state and GT resonance as a function of the incident projectile energy is due to the strong energy dependence of the V_τ term in the projectile-target nucleon interaction. The force strength V_τ gets strongly reduced with increasing projectile energy, while the force strength $V_{\sigma\tau}$ is nearly independent of the incident energy (Goodman, 1980; Love, 1980; Petrovich, 1980). Empirically this can best be seen from the reaction ^{14}C$(p,n)^{14}$N, where the GT transition to the $J^\pi=1^+$, $E_x=3.95$ MeV state, and the isobaric analog transition to the $J^\pi=0^+$, $E_x=2.31$ MeV state are energetically well separated. The relative strength for these transitions in ^{14}C between 60 and 650 MeV is shown in Fig. 4 (Gaarde, 1985; Rapaport, 1988). Here the spectra have been arbitrarily normalized to give a constant peak height for the GT transition to the 3.95-MeV state in ^{14}N. The relative energy dependence of the $V_{\sigma\tau}$ and V_τ interactions causes the cross section to the 0^+ isobaric analog state to decrease between 60 and 200 MeV and then to increase slightly at 650 MeV relative to the GT transition. The physical origin of this different behavior of the two force components will be explained in more detail in Sec. IV.

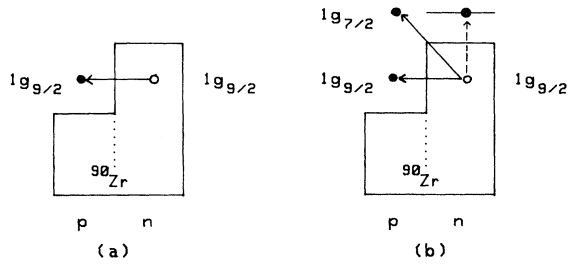

FIG. 3. Schematic picture of single-particle transitions involved in the (a) Fermi and (b) Gamow-Teller transitions. The transitions are excited by the operators T_- and $\beta_-(\mu)$, respectively. The dashed line indicates an $M1$ transition excited by (e,e') and (p,p') reactions.

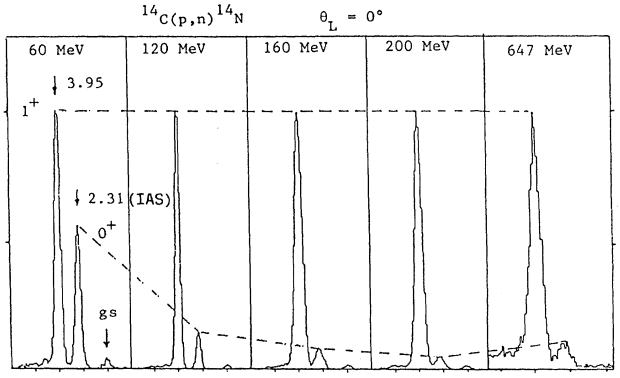

FIG. 4. Zero-degree cross-section spectra for the ^{14}C$(p,n)^{14}$N reactions at the indicated bombarding energies. The spectra have been arbitrarily normalized. From Gaarde (1985) and Rapaport (1989).

From Fig. 1 it is clear that the GT resonance is very selectively excited by the (p,n) reaction at $E_p=200$ MeV. Actually it provides us with one of the most beautiful examples of a giant resonance in nuclei [besides the giant electric dipole resonance, which is very selectively excited by photon absorption (Baldwin and Klaiber, 1947, 1948; Berman and Fultz, 1975)]. With increasing neutron excess the GT cross section increases, indicating that a large fraction of the excess neutrons is participating in the oscillation. In the doubly closed-shell nucleus ^{40}Ca, where all nucleonic spins are saturated, no strong GT state appears, as one expects from the shell model and the Pauli principle. In heavy nuclei, like ^{208}Pb, most of the GT transition strength is concentrated in one collective state at a high excitation energy. This concentration of strength in one collective state that is pushed up in excitation energy proves that there exist strong, repulsive spin-isospin correlations in the nucleus. These are generated on the microscopic level by the residual particle-hole (p-h) interaction in the $\sigma\tau$ channel. The p-h interaction can be simply related to π and ρ-meson exchange with important corrections coming from short-range correlations between the nucleons in the medium (Speth *et al.*, 1980). This will be discussed in more detail in Sec. V.

The GT resonance is characterized by a rather broad peak with a width of about 4 MeV in all heavy-mass nuclei, while the isobaric analog state is a rather sharp peak. This difference in width is due to the different isospin properties of the two states. To explain this let us consider the excitation of an isovector vibration in a nucleus with neutron excess and ground-state isospin $T_0=T_3=(N-Z)/2$. The isobaric analog state is obtained by applying the isospin lowering operator T_- to the ground state $|T_0\ T_0\rangle$ of the parent nucleus and thus has isospin quantum numbers $|T_0\ T_0-1\rangle$, as is schematically illustrated in Fig. 5 (from Satchler, 1983). Since Fermi transitions occur only between members of an isomultiplet, the whole Fermi strength is concentrated in

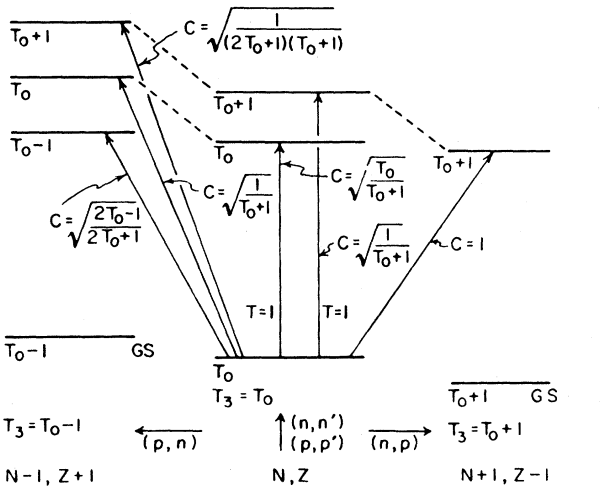

FIG. 5. Isospin transitions in a nucleus with ground-state isospin $T_0=T_3=(N-Z)/2$. The isospin Clebsch-Gordan coefficients are denoted by C. From Satchler (1983).

the isobaric analog state. In the neighborhood of the isobaric analog there are no other states with the same isospin T_0, since such states are much higher in excitation energy. Therefore the isobaric analog state has practically no states to mix with and the resulting width is small. The situation is different for the GT states. Here the GT strength is spread over a triplet of states with isospins $T_f=T_0-1$, T_0, T_0+1, as is shown in Fig. 5. Most of the strength goes to the states with $T_f=T_0-1$, as can be seen from a simple application of the Wigner-Eckart theorem to the isospin transition matrix element $\langle T_f\ T_0-1|\beta_-(\mu)|T_0T_0\rangle$. This matrix element is proportional to the usual Clebsch-Gordan coefficient $C=(T_0\ T_0\ 1\ -1|T_f\ T_0-1)$, which, for a nucleus with neutron excess ($T_0\gg0$), is largest for $T_f=T_0-1$. The corresponding values of C for different isospins T_f are given in Fig. 5. The GT state with isospin $T_f=T_0-1$ is now surrounded by a large number of 2p-2h states with the same isospin, which couple into the GT mode and lead to a fragmentation of the strength. This so-called nuclear configuration mixing effect will be addressed in Sec. V.

As was shown in Sec. II, there exist very general model-independent sum rules for both the Gamow-Teller and the Fermi operators. The Fermi sum rule states that if the initial state $|\Psi_i\rangle$ has good isospin $T_0=T_3=(N-Z)/2$, the Fermi strength $S_{\beta_-}(F)$ has to be concentrated in one state because of isospin conservation. Consequently the $S_{\beta_+}(F)$ has to vanish. Experimentally nearly all the $S_{\beta_-}(F)$ strength is found in the isobaric analog state, showing that isospin SU(2) is a good symmetry of nuclei. For GT transitions such a conservation law does not hold because SU(4) is not a good symmetry. Therefore the $S_{\beta_+}(\mathrm{GT})$ strength is generally nonvanishing. In spite of this fact one can use the sum rule of Eq. (2.31) to give a lower bound for the total amount of $S_{\beta_-}(\mathrm{GT})$ strength to be expected. This lower bound is obtained from the sum rule by putting $S_{\beta_+}(\mathrm{GT})=0$; that is, $S^{\min}_{\beta_-}(\mathrm{GT})=3(N-Z)$. The condition $S_{\beta_+}(\mathrm{GT})=0$ is approximately fulfilled for nuclei with a large neutron excess, since in this case all states for transferring a proton into a neutron within the same major shell are Pauli blocked. For example, if we assume an independent-particle shell-model ground state for ^{90}Zr, as is done in Fig. 3, we find that $S_{\beta_+}(\mathrm{GT})=0$ due to the Pauli blocking. In the independent-particle model the ground state is described by a single Slater determinant. On the other hand, every nucleus shows ground-state correlations, that is, the true ground state can only be represented by a sum of various Slater determinants instead of a single one. In the case of a correlated ground state the sum-rule result of the independent-particle model is changed, since the ground-state correlations always give rise to $S_{\beta_+}(\mathrm{GT})\neq0$ because the sharp proton and neutron Fermi surfaces are smeared out. Therefore the $S_{\beta_-}(\mathrm{GT})$ strength is also changed and now becomes larger than the $3(N-Z)$ sum-rule bound.

The GT cross section measured in the (p,n) experiments can be converted into GT sum-rule strength. The procedure for this conversion will be described in Sec. IV. The surprising result is that experimentally only 60% of the expected total GT strength of $S^{\min}_{\beta_-}(\mathrm{GT})=3(N-Z)$ can be located in the excitation energy region where the major GT peaks occur. This means that at least 40% of GT strength is missing from the spectrum. This feature is found for many nuclei all over the periodic table. A summary of the results obtained for the total GT strength as extracted from 160-MeV (p,n) data (Rapaport, 1983; Gaarde, 1985) is shown in Fig. 6. For the lighter nuclei the GT strength is often concentrated in a few individual peaks, as can be seen, for example, in Fig. 4. In heavy nuclei the GT resonance appears on top of a large continuum (background), the shape and magnitude of which is not known. A few examples of spectra are shown in Fig. 1. Although the

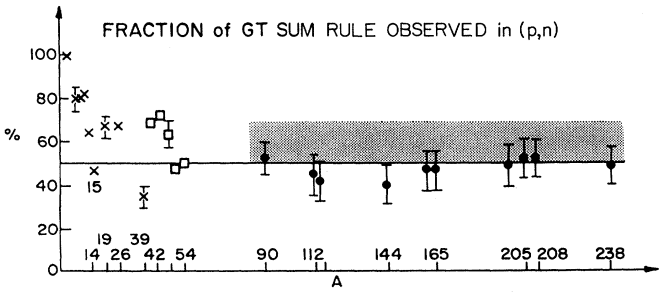

FIG. 6. Fraction of the Gamow-Teller sum-rule strength observed in the (p,n) reactions from different targets. For the heavier targets the full points represent the strength concentrated in the peaks, whereas the shaded area also includes the strength under the collective states. From Gaarde (1985).

peak-background ratio is very good for the GT states, the decomposition of the spectra into resonance and background seriously limits the accuracy with which the amount of sum-rule strength exhausted by the GT resonance can be determined (Osterfeld, 1982). This uncertainty is indicated by the error band in Fig. 6.

The question of the "missing" GT strength has stimulated much experimental and theoretical work in recent years. Two physically different mechanisms have been brought forward to explain this so-called quenching of the total GT strength. The first is that Δ(1232)-isobar–nucleon-hole (Δ-h) states couple into the proton-particle–neutron-hole (pn^{-1}) GT mode and remove part of the strength from the low-lying excitation spectrum (Ericson *et al.*, 1973; Wilkinson, 1973a, 1973b, 1974, 1977; Ohta and Wakamatsu, 1974; Rho, 1974; Delorme *et al.*, 1976; Oset and Rho, 1979; Knüpfer *et al.*, 1980; Toki and Weise, 1980; Bohr and Mottelson, 1981; Brown and Rho, 1981; Härting *et al.*, 1981; Krewald *et al.*, 1981; Suzuki *et al.*, 1981; Osterfeld *et al.*, 1982). This mechanism invalidates the sum rule of Eq. (2.31), which is based on the assumption that only structureless nucleons are the building blocks of the system. The consideration of the internal nucleonic degrees of freedom changes the sum rule, and we have to consider a sum rule like that of Eq. (2.34). The latter sum rule says that in the quark model the dominant part of the strength is carried by Δ-h excitations. A schematic picture of the strength function is shown in Fig. 7.

With no mixing between p-h and Δ-h states, the low-energy strength excited in (p,n) reactions would still be greater than or equal to $3(N-Z)$, since the rest of the sum-rule strength is located at 300 MeV excitation energy in the Δ-resonance region. However, if there is a strong coupling between the low-lying GT modes and the high-lying Δ-h states, then these states will influence each other. This will happen in spite of the fact that these states are 300 MeV apart in excitation energy. It is just the large number of Δ-h configurations which is able to bridge the energy gap of 300 MeV and bias the low-lying

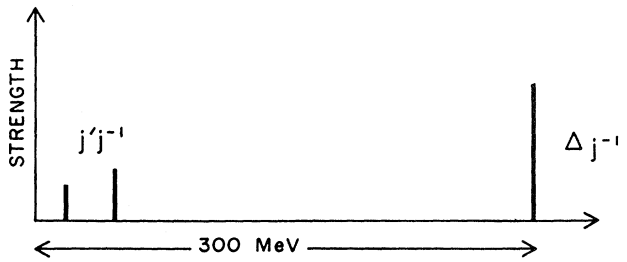

FIG. 7. A schematic picture of the Gamow-Teller strength function, including the Δ-h excitations in the spectrum. The overall strength in the delta region is higher because there are no Pauli restrictions on the excited nucleons. Depending on the coupling to the states in the low-energy region, the residual interaction may shift substantial strength out of the low states. From Bertsch and Esbensen (1987).

GT modes. If the coupling is repulsive the transition strength to the low-lying GT states will be reduced while that to the Δ-h states will be enhanced. Whether or not this mechanism plays a major role in the quenching of the total GT strength depends critically on the strength of the residual interaction which couples the p-h states with the Δ-h states. The properties of this interaction will be discussed in more detail in Sec. V.

The second mechanism for explaining the "missing" GT strength is ordinary nuclear configuration mixing (Shimizu *et al.*, 1974; Towner and Khanna, 1979, 1983; Bertsch and Hamamoto, 1982; Towner, 1984, 1987; Drożdż *et al.*, 1986a, 1986b; Drożdż *et al.* 1987; Nishizaki *et al.*, 1988). Here, energetically high-lying two-particle/two-hole (2p-2h) states mix with the 1p-1h GT states and shift GT strength into the energy region far beyond the GT resonance. Again the importance of this effect depends sensitively on the coupling strength between the 1p-1h and 2p-2h states. If this mechanism is the right one, then the so-called missing GT strength would actually be located in the physical background below and beyond the giant GT state. The detection of this strength would not be an easy task from an experimental point of view because the cross section on the high-energy side of the GT resonance in the 0° spectrum is continuous and structureless. This makes it difficult to extract information from it. Some estimates of the amount of GT strength in the continuum can be given by a careful analysis of the continuum spectra within microscopic nuclear structure and reaction models. We shall come back to this problem in Sec. VI.

B. The magnetic dipole (M1) resonance

The GT state with isospin $T_f=T_0$ is the analog of the magnetic dipole (M1) transition in the parent nucleus, as is indicated in Fig. 5. The M1 operator is a one-body operator

$$\begin{aligned}\boldsymbol{\mu}&=\mu_0\sum_{j=1}^{A}[g_l\boldsymbol{l}_j+g_s\mathbf{s}_j]\\&=\mu_0\sum_{j=1}^{A}\left[\frac{1}{2}\left[g_l\boldsymbol{l}_j+\frac{g_p+g_n}{2}\mathbf{s}_j\right]\right.\\&\qquad\left.-\frac{1}{2}\left[g_l\boldsymbol{l}_j+\frac{g_p-g_n}{2}\mathbf{s}_j\right]\tau_3(j)\right]\end{aligned}\tag{3.1}$$

consisting of an orbital part $\boldsymbol{l}$ ($g_l=1$ for protons and $g_l=0$ for neutrons) and a spin part $\mathbf{s}$ (the gyromagnetic factors are $g_p=5.58$ for protons and $g_n=-3.82$ for neutrons), where $\mu_0=e\hbar/2M_pc$ is the nuclear magneton (e is the proton charge and M_p is the proton mass). In Eq. (3.1) the M1 operator is written as a sum of an isoscalar and an isovector term, the spin parts of which measure the isoscalar (σ) and isovector ($\sigma\tau_3$) spin correlations in the nucleus, respectively. According to the shell model, for a closed-shell nucleus with spin unsaturated j-shell

closures, the M1 strength should be concentrated in a few p-h states. In ^{90}Zr, for example, there is only one p-h transition possible in the independent-particle model, namely, the neutron transition $[\nu g_{7/2}(\nu g_{9/2})^{-1}]_{1^+}$ [see Fig. 3(b)].

Before 1980, strong M1 transitions were known only in light nuclei (in *p*-shell and *sd*-shell nuclei; Fagg, 1975; Hanna, 1974, 1977, 1980). Searches for M1 strength in heavy-mass nuclei mostly failed because of the high-level density of states in the excitation energy region where the shell model would predict the M1 states to be, and because of the difficulties in making the right parity assignments to M1 candidates under consideration (Hanna, 1980; Raman, 1979; Brown and Raman, 1980). In 1980, however, a strong and isolated M1 transition was discovered in ^{48}Ca at $E_x=10.23$ MeV in a high-resolution inelastic electron-scattering experiment at the DALINAC in Darmstadt (Steffen *et al.*, 1980). The observed 1^+ state corresponds to a $[\nu f_{5/2}(\nu f_{7/2})^{-1}]_{1^+}$ neutron spin-flip transition. At the same time, the analog of this state was also discovered in the ^{48}Ca$(p,n)^{48}$Sc reaction at $E_p=160$ MeV (Anderson *et al.*, 1980). A zero-degree ^{48}Ca(p,n) spectrum measured in a later experiment at $E_p=135$ MeV (Anderson *et al.*, 1985a) is shown in Fig. 8 and the (e,e') spectrum of several Ca isotopes is shown in Fig. 9. In the zero-degree ^{48}Ca(p,n) spectrum, one can clearly identify the isobaric analog state at $E_x=6.67$ MeV and the three 1^+ states over which the GT strength is distributed in ^{48}Sc. The narrow 1^+, $T_f=4$ state at $E_x=16.8$ MeV is the isobaric analog of the $J^\pi=1^+$ state at $E_x=10.23$ MeV in ^{48}Ca shown in the upper part of the (e,e') spectrum of Fig. 9. The analog states have a narrow width, as expected from their isospin character ($T_f=4$), and stand out strongly from the underlying background.

The 1^+ state in ^{48}Ca carries a large transition strength of B(M1)$\uparrow=4.3\ \mu_0^2$, which is roughly $\frac{1}{3}$ of the value predicted in the independent-particle model ($12\ \mu_0^2$). In addition to this giant M1 resonance, further weakly excited 1^+ states are identified, which lead to a total observed strength of $5.3\pm0.6\mu_0^2$. This value is quenched compared to the independent-particle model value of $12\mu_0^2$. The amount of quenching is similar to that observed for GT states.

It is important to notice that there exists no model-independent sum rule for M1 transitions. The total M1 strength strongly depends on the properties of the nuclear ground-state wave function. If the ground-state wave function is strongly mixed among various Slater determinants, an elaborate microscopic nuclear structure calculation is needed to define a quenching factor. The shell-model calculations of McGrory and Wildenthal (1981) performed within the full *pf*-shell-model space give a total 1^+ strength of $7.3\mu_0^2$ in ^{48}Ca. Microscopic RPA calculations (Suzuki, Krewald, and Speth, 1981) give a similar value of $8.2\ \mu_0^2$. This shows that even in the doubly magic nucleus ^{48}Ca there exist strong ground-state correlations that produce a quenching of the total M1 strength by $\sim$25–30% relative to the independent-particle model estimate. A further quenching of $\sim$30% is needed to explain the experimental data. This additional quenching can be either due to the Δ-hole mechanism or due to the 2p-2h nuclear configuration mixing effect. We remark that the renormalization of the $\sigma\tau_3$ operator suggested by the excitation strength of these 1^+ states is essentially the same as that required for ground-state magnetic moments (see Arima *et al.*, 1987).

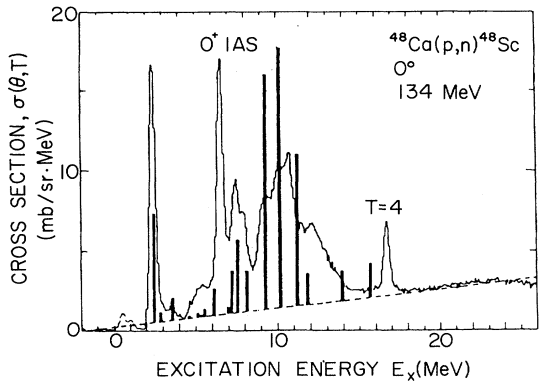

FIG. 8. Neutron energy spectrum for the ^{48}Ca$(p,n)^{48}$Sc reaction at $\theta=0°$ and $E_p=135$ MeV (from Anderson *et al.*, 1985a). The vertical bars indicate the location and relative strength of 1^+ states predicted by the shell-model calculations of Anderson *et al.* (1985b). Similar shell-model calculations were also performed by Gaarde *et al.* (1980).

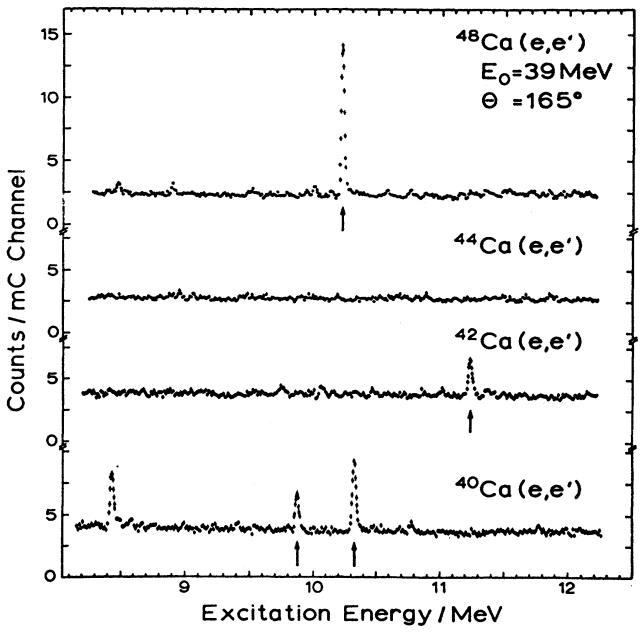

FIG. 9. Inelastic electron-scattering spectra from the even-even Ca isotopes. The arrows point to strong $J^\pi=1^+$ states. From Steffen *et al.* (1980).

From the lower part of Fig. 9, it can be seen that two relatively strong 1^+ states also appear in the "spin-saturated" nucleus ^{40}Ca where the independent-particle model would not predict any. These 1^+ states are the result of the ground-state correlations, which break the spin-saturated j-shell closure. Amazingly, in the nucleus ^{44}Ca, where one would expect several 1^+ states because of the partially filled $f_{\frac{7}{2}}$ neutron shell, no strong 1^+ state appears. A closer inspection of the spectrum shows, however, that the 1^+ strength is distributed over very many weak lines, indicating an extreme fragmentation of the strength due to the strong configuration mixing in ^{44}Ca.

The strong 1^+ state in ^{48}Ca was confirmed by various high-resolution (p,p') experiments (Berg *et al.*, 1982; Fujita *et al.*, 1982; Rehm *et al.*, 1982; Crawley *et al.*, 1983). In these experiments a similar amount of quenching is observed to that in (e,e'). In the other Ca isotopes, however, significant differences occur between the (p,p') and the (e,e') results. Sometimes more 1^+ states are seen in (p,p') than in (e,e') and vice versa. A possible explanation is that some of the 1^+ states correspond predominantly to the orbital (l) transitions, which are strongly excited by electrons but only weakly by protons (Bohle *et al.*, 1986; Hartmann *et al.*, 1987). In some cases a destructive interference between the orbital and spin parts of the M1 operator might occur in (e,e'). This could lead to a suppression of certain states in (e,e') but not in (p,p'). In the latter case only the spin excitation contributes to the cross section. Many similar observations (See Crawley *et al.*, 1983; Bohle *et al.*, 1986) have been made in other nuclei, and the origin of the difference between the (e,e') and (p,p') results is not always obvious. One trivial reason is that since the M1 states occur in a region of high-level density, and since they themselves are strongly fragmented, many of them might simply escape experimental detection.

For a long time neither backward-angle inelastic electron scattering (Richter, 1979; Meuer *et al.*, 1980) nor inelastic proton scattering (Cecil *et al.*, 1974) could clearly identify M1 strength in heavy-mass nuclei like ^{90}Zr or ^{208}Pb. However, the strong excitation of the $T_f = T_0$ component of the GT states in the ^{90}Zr(p,n) reaction (Horen *et al.*, 1980) suggested where to look for the M1 strength in the ^{90}Zr(p,p') experiments. Such experiments were carried out at the Synchrocyclotron in Orsay at $E_p = 201$ MeV. In the ^{90}Zr(p,p') reaction (Anantaraman *et al.*, 1981) a broad peak riding on a huge background was observed close to the expected excitation energy. The angular distribution of this peak was found to be of $L=0$ shape, as expected for 1^+ transition. Similar bumps were also detected in the other Zr isotopes. The corresponding spectra are shown in Fig. 10. These (p,p') experiments provided the first identification of the giant M1 resonance in heavy-mass nuclei. These measurements were confirmed by Bertrand *et al.* (1981) and extended by the Los Alamos group (Nanda *et al.*, 1983, 1984). The Los Alamos group used a high-energy polarized proton (p) beam to determine the inelastic spin-flip spectrum by measuring the polarization of the outgoing proton (p'). In this way they could separate the spin excitations from the otherwise complicated inelastic excitation spectrum, which is mainly governed by non-spin-flip transitions. In these experiments a fine structure of the M1 resonance in ^{90}Zr could be observed. In addition, much additional spin-flip strength at higher excitation energies was identified, but no spin assignment could be made.

Both the (e,e') and (p,p') experiments have difficulties in giving an accurate value for the total M1 strength in heavy-mass nuclei because of the large background, which is of both physical and experimental origin (Richter, 1979; Anantaraman *et al.*, 1981). In ^{208}Pb the

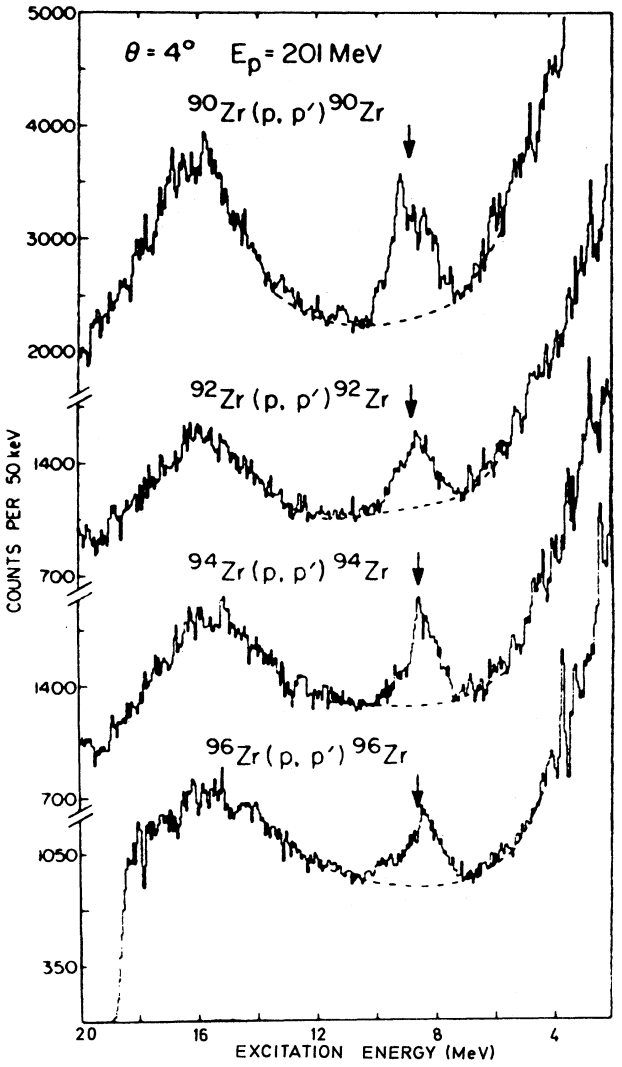

FIG. 10. Spectra of protons inelastically scattered from ^{90}Zr, ^{92}Zr, ^{94}Zr, and ^{96}Zr at $\theta = 4°$. The arrows indicate the centroids of the $M1$ resonance. From Crawley *et al.* (1983).

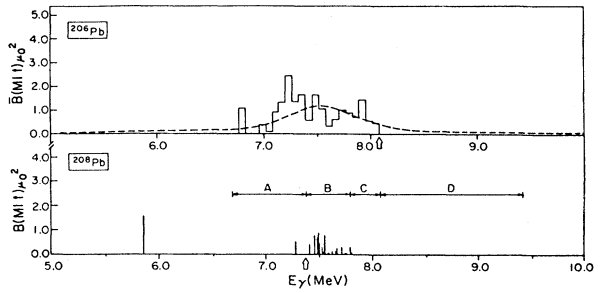

FIG. 11. The measured $M1$ transition strength in ^{206}Pb and ^{208}Pb (Laschewski *et al.*, 1986, 1987, 1988). The data are compared to calculations (dashed line) by Cha *et al.* (1984). The arrows indicate the neutron emission thresholds (From Laschewski and Wambach, 1985).

M1 strength could not be identified with these reactions just for this reason (Djalali, 1984).

The longstanding problem of the "missing" M1 strength in heavy-mass nuclei like ^{208}Pb was finally solved by the beautiful photon scattering experiments of Laszewski, Rullhusen, *et al.* (1985, 1986), and Laszewski, Alarcon, *et al.* (1987, 1988). These authors used highly polarized elastically scattered photons to measure the M1 strength in heavy-mass nuclei. In these (γ,γ') experiments essentially all of the isovector M1 strength below the neutron emission threshold could be detected. The amount of the observed strength is found to be comparable with microscopic RPA calculations, including 2p-2h spreading effects (Laszewski and Wambach, 1985). The experimental spectrum, together with a microscopic calculation (Cha *et al.*, 1984), is shown for the nucleus ^{206}Pb in Fig. 11.

C. The isoscalar M1 strength

The isoscalar M1 strength can be measured with electromagnetic probes like the (γ,γ') and the (e,e') reactions, as well as with inelastic hadron scattering, like (p,p'). The better probe is the (p,p') reaction, since isoscalar states are strongly suppressed in electromagnetic transitions, as can be immediately noticed from the isoscalar M1 transition operator of Eq. (3.1), which is proportional to $\mu_p+\mu_n=0.88$ and therefore small. An isoscalar 1^+ transition was observed in ^{208}Pb in photofluorescence (Wienhard *et al.*, 1982) and various (e,e') (Müller *et al.*, 1983) and (p,p') experiments (Hayakawa *et al.*, 1982). In *sd*-shell nuclei various new isoscalar 1^+ states were identified by means of the (p,p') reaction (Anantaraman *et al.*, 1984; Crawley *et al.*, 1989). Especially interesting are even-even, spin-unsaturated nuclei with a $T_0=0$ ground state, like ^{28}Si, since both $T_f=0$ and $T_f=1$, 1^+ states exist in these nuclei, and these states are excited by isoscalar and isovector transition operators, respectively. It is found that both isoscalar and isovector 1^+ transitions are quenched by a similar amount; that is, there is no tendency for $T_f=1$ states to be more quenched than $T_f=0$ states. This is interesting in connection with Δ-h quenching, since this mechanism can apply only to the $T_f=1$ states. Elaborate shell-model calculations show that both type of states suffer from a similar quenching due to nuclear configuration mixing (Brown and Wildenthal, 1983, 1987, 1988). It is concluded that the Δ-h explanation of the quenching is not the most important one.

D. The Gamow-Teller strength in the τ_+ channel

The (n,p) reaction is a unique tool for measuring the GT strength of nuclei in the τ_+ channel. In $N>Z$ nuclei this reaction exclusively excites states with isospin T_0+1 (see Fig. 5). Fermi transitions are not allowed in this case because of the isospin selection rules. Therefore intermediate-energy (n,p) reactions at forward angles provide an excellent filter of GT strength with

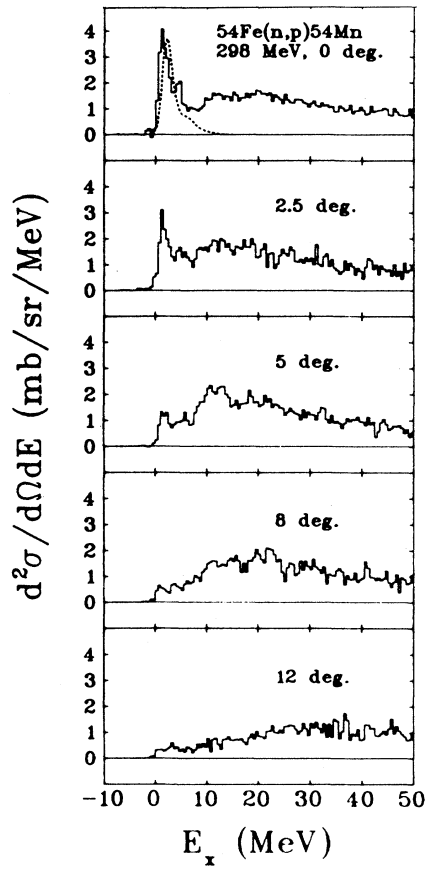

FIG. 12. Cross sections for the reaction ^{54}Fe$(n,p)^{54}$Mn at $E_n=298$ MeV for five angles between 0° and 12°. The strongly forward-peaked feature below 10 MeV excitation energy is the Gamow-Teller resonance. The dashed curve in the 0° spectrum represents a shell-model calculation of the GT strength by Bloom and Fuller (1985). The calculated curve was renormalized by a factor of about 0.45. From Vetterli *et al.* (1987).

$T_f = T_0 + 1$. One of the aims of the (n,p) experiments is to solve the problem of the missing GT strength observed in the (p,n) experiments. By measuring both the zero-degree (p,n) and (n,p) spectra at the same incident energy, i.e., with the same hadronic transition operator, one can subtract the (n,p) from the (p,n) data. The remaining cross section should then be proportional to $3(N-Z)$ if the sum rule of Eq. (2.31) is valid.

The (n,p) reaction is very difficult to measure, since it is not easy to produce a neutron beam with sharp energy. For a long time the only (n,p) studies were performed at the University of California at Davis at beam energies below 60 MeV (Brady, Castaneda *et al.*, 1982; Brady, Needman *et al.*, 1983). For a quantitative measurement of the β_+ strength function, however, one needs a neutron beam at higher energies. Such a new (n,p) facility was recently installed at TRIUMF in Vancouver (Helmer, 1987; Yen, 1987) and the first (n,p) measurements were carried out. For the majority of targets these experiments open up an uncharted spectroscopic territory. Here we discuss the reaction ^{54}Fe$(n,p)^{54}$Mn at $E_n = 298$ MeV, in which substantial S_{β_+}(GT) strength has been observed (Vetterli *et al.*, 1987). The measured spectra are shown in Fig. 12. The large peak below 10 MeV excitation energy in the 0° spectrum is the GT resonance. Its location and shape are reasonably well reproduced by the shell-model calculations of Bloom and Fuller (1985). The measured strength, however, is again overestimated by the theory. Experimentally only 3.8 ± 1.0 GT strength units are identified, while the shell-model calculations predict total sum-rule values in the range $5.1 \leq S_{\beta_+}(\mathrm{GT}) \leq 9.4$, depending on the choice of the model space (Bloom and Fuller, 1985; Muto, 1986). These values are appreciably larger than the experimental one. Of course, there is again the question of how much GT strength might reside in the high-energy tail of the spectrum.

The ^{54}Fe(n,p) measurements, when combined with the ^{54}Fe(p,n) data of Rapaport *et al.* (1983) and Vetterli *et al.* (1989), provide a full test of the GT sum rule. Rapaport *et al.* determined an S_{β_-}(GT) value of 7.8 ± 1.9. Together with the (n,p) result, this gives for the sum-rule estimate $S_{\beta_-}(\mathrm{GT}) - S_{\beta_+}(\mathrm{GT}) = 4.0 \pm 2.1$, which is 67% of the expected value of 6, or even agrees with the sum rule within errors. Note, however, that this result is questionable, since a sizable fraction of the GT strength is shifted out of the low-energy shell-model region in both the (p,n) and the (n,p) cases. A definitive test of the sum rule is made difficult by the need to determine the $L=0$ fraction of the cross section—notably at high excitation energy where other multipoles dominate.

Similar spectra to those of the (n,p) reaction are also obtained with the $(d,2p)$ reaction at $E_d = 650$ MeV at Saturne in Saclay (Ellegaard, 1987; Ellegaard *et al.*, 1987, 1989; Gaarde, 1988). Obviously, with the (n,p) and $(d,2p)$ reaction we now have excellent spectroscopic tools at hand to study the $\sigma\tau_+$ response function.

E. The giant spin-flip dipole and spin-flip quadrupole charge-exchange resonances

The GT and M1 states represent $0\hbar\omega$ excitations that are most strongly excited at very forward angles. The (p,n) spectra at higher scattering angles show clear evidence for the collective spin-flip dipole and spin-flip quadrupole charge-exchange modes characterized by angular momentum transfers of $L=1$ and $L=2$, respectively. These modes can be interpreted as a manifestation of strength corresponding to the multipole operators

$$\sum_{j=1}^{A} r_j^L [Y_L(\hat{r}_j) \otimes \sigma(j)]_{J^\pi} \tau_-(j) \ . \tag{3.2}$$

The spin-flip dipole ($L=1, S=1$) resonance is a $1\hbar\omega$ excitation and has been observed in many nuclei. In the 200-MeV ^{90}Zr(p,n) reaction it appears at an excitation energy of $E_x \sim 25$ MeV and has its peak cross section at the scattering angle of $\theta = 4.5°$ (see Fig. 13; Gaarde *et al.*, 1981). The angular distribution of the bump around $E_x \sim 25$ MeV has a characteristic $L=1$ shape, as can be

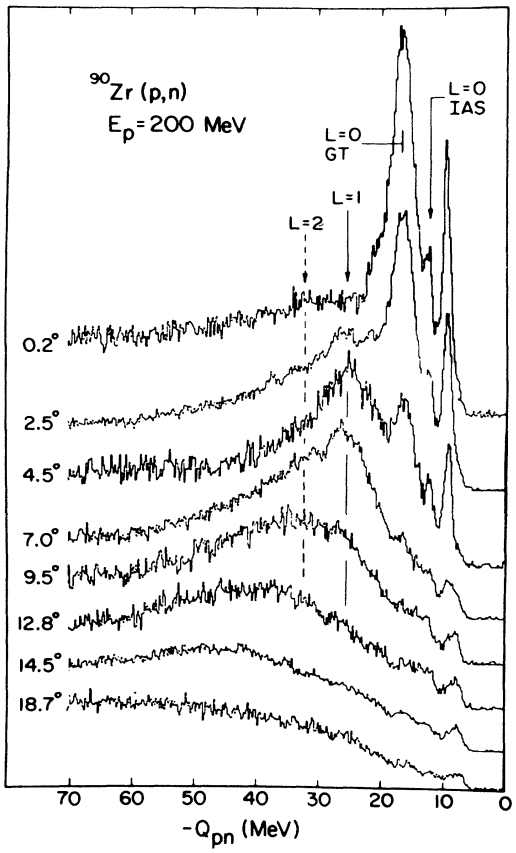

FIG. 13. Neutron spectra at $E_p = 200$ MeV for the ^{90}Zr$(p,n)^{90}$Nb reaction at different scattering angles. The positions of the various giant resonances are indicated by the arrows. The angular distributions of these giant resonances are shown in Fig. 3. From Gaarde *et al.* (1981).

seen from the right-hand panel of Fig. 2. The cross section varies with incident projectile energy like that of the GT resonance. This indicates that a spin transfer of $S=1$ is involved. The width of the resonance structure is about 10 MeV. The resonance can be interpreted as the superposition of three collective modes with spin-parity $J^\pi=0^-$, 1^-, and 2^-. This interpretation is supported by microscopic RPA calculations (Krmpotić *et al.*, 1980; Osterfeld *et al.*, 1981; Klein *et al.*, 1985; Osterfeld, Cha, and Speth, 1985). Experimentally, however, it has not yet been possible to resolve the broad resonance into the different spin components.

In the (^{3}He,t) reaction at $E=130$ MeV (Galonsky *et al.*, 1978) and in the (p,n) reaction at $E_p=45$ MeV (Sterrenburg *et al.*, 1980) one also finds an $L=1$ resonance structure in medium and heavy-mass nuclei, but this time at a slightly higher excitation energy than that of the spin-flip dipole resonance. This bump, observed with low-incident-energy beams ($E_p=45$ MeV), is interpreted as the (T_0-1) component of the giant isovector electric dipole resonance which carries quantum numbers $J^\pi=1^-$, $L=1$, $S=0, T=1$. This interpretation is based on the incident energy dependence of the cross section (energies around $E_p=45$ MeV favor non-spin-flip excitations) and on calculations (Krmpotić and Osterfeld, 1980; Osterfeld *et al.*, 1981; Krmpotić, 1981a, 1981b; Krmpotić *et al.*, 1983; Cha *et al.*, 1984). The corresponding multipole transition operator is obtained from Eq. (3.2) by replacing the spin operator σ by the identity operator.

In ^{208}Pb the excitation energy of the $J^\pi=1^-$, $S=0$ state is roughly 5 MeV higher than that of the spin-flip dipole resonance, although both modes represent $1\hbar\omega$ excitations. This difference in excitation energy is an effect of the residual p-h interaction, which turns out to be more repulsive in the τ channel than in the $\sigma\tau$ channel (Osterfeld, *et al.*, 1981).

The spin-flip quadrupole resonance ($L=2, S=1$) is a $2\hbar\omega$ excitation and is observed in many heavy-mass nuclei. In the 200-MeV ^{90}Zr(p,n) reaction it appears as a broad structure at $E_x\sim35$ MeV and obtains its peak cross section at a scattering angle of $\theta=9.5°$ (see Fig. 13). The angular distribution of this bump has an $L=2$ shape (see the right-hand panel of Fig. 2!), and the spin transfer of $S=1$ is again deduced from the incident energy dependence of the cross-section magnitude. The resonance is very broad and strongly overlapping with the $L=1$ resonance. Therefore one has to decompose the spectrum into the various multipoles in order to determine the strength distribution functions of states with different J^π. The resonance is interpreted as a superposition of three collective modes with spin-parity $J^\pi=1^+,2^+$, and 3^+ (Klein *et al.*, 1985; Osterfeld *et al.*, 1985).

A promising tool for resolving experimentally the different multipolarities is the $(\mathbf{p},\mathbf{n})$ spin-flip transfer reaction (Taddeucci *et al.*, 1984, 1986; Watson *et al.*, 1986, 1987; Taddeucci, 1987) which, in principle, is sensitive to different J^π values (Cornelius *et al.*, 1981; Seestrom-Morris *et al.*, 1982; McClelland *et al.*, 1984), as we shall discuss in Sec. VI.

Until recently there was no clear signature for the corresponding spin modes in the neutral (τ_3) channel. However, a large amount of M2 strength was identified in the (e,e') reaction (Knüpfer *et al.*, 1978; Richter, 1982). The M2 strength is found to suffer from a similar amount of quenching as the M1 and GT states (Richter, 1982). The $(\mathbf{p},\mathbf{p}')$ spin-flip transfer measurements at LAMPF (Nanda *et al.*, 1983, 1984) could identify a large amount of spin-flip cross section in the nucleus ^{90}Zr up to excitation energies of $E_x=40$ MeV, but the interpretation of this cross section relies heavily on microscopic nuclear structure calculations (Yabe *et al.*, 1986). More recent measurements of Glashausser *et al.* (1987) and Baker *et al.* (1988, 1989) give evidence for the spin-flip dipole and spin-flip quadrupole resonances in the ^{40}Ca$(\mathbf{p},\mathbf{p}')$ reaction. The ^{40}Ca target is particularly useful for the study of $L>0$ spin-flip resonances, since, owing to its being spin saturated, very little $L=0$, $S=1$ strength is expected [and has been observed in ^{40}Ca(e,e'); Richter, 1982]. The inelastic spin-flip dipole resonance is found to have its peak cross section at $E_x\sim15$–20 MeV, showing a broad asymmetric width. The $L=2$ spin-flip quadrupole strength is centered around $E_x=30$ MeV and has an even broader width. Both strength distributions were obtained by performing a multipole decomposition of the spin-flip cross section at various scattering angles. The multipole decomposition is based on the assumption that the measured spin-flip cross section is background free; that is, it is only the result of one-step processes. This assumption obtains strong support from microscopic cross-section calculations, as will be shown in Sec. VI.

F. The spin-flip isovector monopole resonance

The existence of an isoscalar giant monopole resonance ($J^\pi=0^+$, $T=0$) in medium and heavy-mass nuclei has been well established for many years (Marty *et al.*, 1975; Harakeh *et al.*, 1977, 1979; Youngblood *et al.*, 1977; Buenerd *et al.*, 1979; Lebrun *et al.*, 1980; Rosza *et al.*, 1980; Youngblood *et al.*, 1981). The monopole resonance is a volume mode that is connected with the compression and expansion of the nucleus as a whole. Neutrons and protons move in phase, and the spin degrees of freedom of the nucleons are untouched. Some years ago the pion charge-exchange experiments ($\pi^\pm,\pi^0$) (Bowman *et al.*, 1983; Erell *et al.*, 1986) were successful in observing the isovector monopole mode ($J^\pi=0^+$, $T=1$). In this case the nucleus performs a monopole oscillation in which neutrons and protons move in opposite phase. If, in addition, nucleons with spin $\uparrow$ and spin $\downarrow$ oscillate against each other, then one may have a spin-isovector monopole excitation with quantum numbers $J^\pi=1^+$, $L=0$, $S=1$, $T=1$. The relevant transition operator for the spin-isovector monopole is

$$\sum_{j=1}^{A} r_j^2 \sigma(j)\tau_\mu(j) \tag{3.3}$$

where $\mu=\pm 1$ or 0. Since the spin-isovector monopole has total spin $J^\pi=1^+$ it can, in principle, couple to other 1^+ states which involve $L=2$ and $S=1$. A realistic tensor force actually does mix the $L=0$, $J^\pi=1^+$ and $L=2$, $J^\pi=1^+$ modes.

The radial transition density of any monopole excitation has a characteristic shape (Auerbach, 1971, 1974; Bohr and Mottelson, 1975) with a node near the nuclear surface. This is a consequence of mass conservation and the spherical symmetry of the motion. The transition density has a positive peak outside the nuclear surface and a compensating negative peak in the nuclear interior, so that its volume integral is vanishing. In order to excite a monopole resonance one therefore needs a strongly absorbed projectile which only probes the nuclear surface part, but not the volume part, of the transition density. The cross section is then determined only from the surface, and hence may take a large value.

The (p,n) reaction at intermediate energies is not the best probe to excite the spin-isovector monopole because the nucleus is quite transparent to protons and neutrons at these incident energies. A better probe is the $(^3\mathrm{He},t)$ reaction. The ^{3}He projectile is strongly absorbed but still shows a strong selectivity for spin-isospin excitations at intermediate energies. This can be seen from Fig. 14, where 900-MeV ^{90}Zr$(^3\mathrm{He},t)$ spectra (Gaarde, 1985) are shown at three scattering angles and for a large excitation energy range. A dramatic change of the spectra as a function of scattering angle can be observed. The GT resonance in the 0° spectrum and the spin-flip dipole resonance in the 1.3° spectrum are excited with a similar selectivity to that in the (p,n) reaction. The main difference between the $(^3\mathrm{He},t)$ and the (p,n) spectra at a given incident energy per nucleon is the appearance of a larger 0° cross section at $E_x\sim 35$–40 MeV in $(^3\mathrm{He},t)$ than in (p,n) (Ellegaard *et al.*, 1983). This excitation energy region corresponds to that of the $2\hbar\omega$ collective states. Microscopic reaction calculations show (Schulte *et al.*, 1987; Udagawa *et al.*, 1987; Auerbach *et al.*, 1989) that the $2\hbar\omega$ collective states of spin-parity 1^+ and 2^+ give a significant contribution to the 0° $(^3\mathrm{He},t)$ cross section. The angular distribution of the strongest 1^+ state has a characteristic $L=0$ shape, as expected for a spin-isovector monopole state. We conclude that the $(^3\mathrm{He},t)$ reaction is very selective in exciting the spin-isovector monopole.

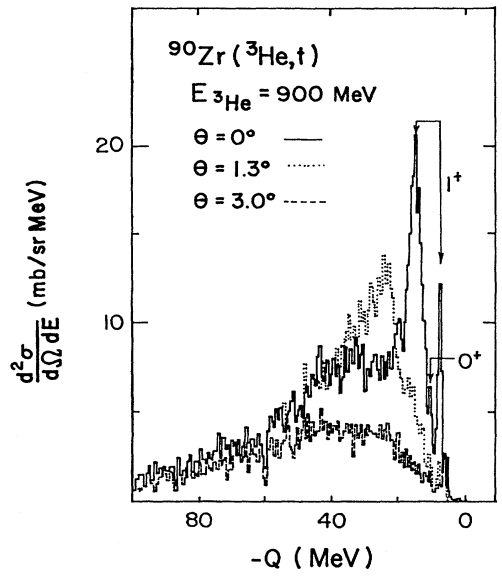

FIG. 14. Spectra for the ^{90}Zr$(^3\mathrm{He},t)^{90}$Nb reaction at three scattering angles. The positions of the isobaric analog state and of the GT states are marked by arrows. Note the enhanced $\theta=0°$ cross section around $Q\sim -40$ MeV, which gives evidence for the existence of the spin-isovector monopole resonance. From Gaarde (1985).

G. The magnetic high-spin states

So far we have discussed the spin-isospin modes of low multipolarity which are excited at small-momentum transfers ($q\leq 1$ fm^{-1}). Another interesting class of spin-flip transitions is provided by the magnetic high-spin states (M4 to M14 transitions). They dominate the inelastic excitation spectrum at excitation energies of $1\hbar\omega$ and large-momentum transfers ($q\sim 2$ fm^{-1}). Of special interest are the so-called "stretched" (s) states, which are characterized by having the total angular momentum $J_s=j_p+j_h$, where $j_p=l_p+\frac{1}{2}$ and $j_h=l_h+\frac{1}{2}$ are the highest single-particle angular momenta found in the first open shell and the last filled shell of the nucleus, respectively. Examples of stretched states are the 4^- states in $1p$-shell nuclei, involving the stretched configuration $[1d_{\frac{5}{2}}(1p_{\frac{3}{2}})^{-1}]_{4^-}$, or the 6^- states in $2s1d$-shell nuclei, involving $[1f_{\frac{7}{2}}(1d_{\frac{5}{2}})^{-1}]_{6^-}$. What makes the stretched states most interesting is that, although their wave functions will contain thousands of complex multiparticle-multihole components in a $1\hbar\omega$ shell-model space, only the stretched configuration can contribute to the inelastic excitation in a direct one-step reaction. As a result, inelastic scattering measures the distribution of this unique configuration among all the others.

In terms of the orbital and spin angular momentum quantum numbers, which are transferred to the target in the reaction, the "stretched" transitions require $J_s=L+S$, where $L=l_p+l_h$ and $S=1$. As a consequence of the spin-flip, the stretched states can only be excited by the single multipole operator

$$\sum_k j_L(qr_k)[i^L Y_L(\hat{r}_k)\otimes\sigma(k)]^{J_s}_M \tau_3^{(m)}(k) \tag{3.4}$$

where $j_L(qr_k)$ is the spherical Bessel function of order $L=(J_s-1)$ and $\tau_3^{(m)}=1$, τ_3 for $m=0,1$. This operator can involve only a single spin density, which provides a

common source for the cross section in electron, nucleon, and pion inelastic-scattering reactions. The isovector-spin transition density can be uniquely determined from the (e,e') reaction. By combining this result with the (p,p') or $(\pi^{\pm},\pi^{\pm\prime})$ measurements, one can gain useful new information on the hadronic reaction mechanism and the form of the effective projectile-target nucleon interaction (Moffa and Walker, 1974; Lindgren *et al.*, 1979; Petrovich *et al.*, 1980; Petrovich and Love, 1981). It turns out that the stretched transitions give definite information on the high-momentum components of the isovector tensor part of the nucleon-nucleon tensor force (Lindgren *et al.*, 1979). This will be described in more detail in Secs. IV.C.3 and IV.E.

Most of the available experimental and theoretical information on the electromagnetic and hadronic excitation of the high-spin stretched transitions relates to $1\hbar\omega$ negative-parity states between adjacent shells. A complete survey of this material is given in the recent review papers by Lindgren and Petrovich (1984). Petrovich, Carr, and McManus (1986), Lindgren *et al.* (1987), and Raman, Fagg, and Hicks (1991). Historically the first stretched states were detected in ^{12}C and ^{16}O (the 4^- states!) by means of the (e,e') reaction (Donnelly *et al.*, 1968; Sick *et al.*, 1969). The states with highest spin observed so far are the 12^- and 14^- states in ^{208}Pb with the stretched proton and neutron configurations $[1i_{13/2}(1h_{11/2})^{-1}]_{12^-}$ and $[1j_{15/2}(1i_{13/2})^{-1}]_{14^-}$, respectively (Lichtenstadt *et al.*, 1979; Bacher *et al.*, 1980). Of considerable interest also are the isoscalar and isovector 6^- states in the self-conjugate nucleus ^{28}Si which were measured in the (e,e') (Yen *et al.*, 1980), (p,p') (Adams *et al.*, 1977), and $(\pi^{\pm},\pi^{\pm\prime})$ (Olmer *et al.*, 1979) reactions. These states give important information on the nuclear structure aspects of the isoscalar and isovector stretched states. It turns out that the experimental cross sections for these states are less than 50% of the 1p-1h prediction. This quenching of the stretched strength can be explained by the nuclear configuration mixing effect, as will be discussed in Sec. V.J.

IV. REACTION THEORY OF INELASTIC NUCLEON-NUCLEUS SCATTERING AND CHARGE-EXCHANGE REACTIONS

In this section we describe the appropriate direct-reaction theory needed in the analysis of the experimental data. We limit the discussion to nucleon-induced reactions, since most of the recent progress in our understanding of spin excitations comes from these reactions. Particular emphasis is placed on the description of the effective projectile-target nucleon interaction, since a knowledge of the coupling between the probe and the nucleus is essential for the interpretation of the scattering data. The intrinsic relation between the measured zero-degree (p,n) cross section and the β-decay matrix elements is derived.

A. Scattering observables

The evaluation and interpretation of nucleon-nucleus inelastic scattering observables involves the construction of the transition amplitude $\mathcal{T}_{fi}$, which describes the transition of the scattering system from the initial (i) to the final (f) reaction channel. Denoting the spin quantum numbers of the projectile by $|\frac{1}{2}m\rangle$ and those of the target by $|IM\rangle$, we find that the transition matrix element of the transition operator $\mathcal{T}$ can be written as

$$\mathcal{T}_{fi}=\langle \mathbf{k}_f,I_fM_f,\tfrac{1}{2}m_f|\mathcal{T}|\mathbf{k}_i,I_iM_i,\tfrac{1}{2}m_i\rangle \ , \tag{4.1}$$

where $\mathbf{k}_i$ and $\mathbf{k}_f$ are the projectile momenta before and after the collision. A quantity related to the transition amplitude is the scattering amplitude $\mathcal{M}$, which is defined by

$$\mathcal{M}_{fi}=-\frac{\mu}{2\pi\hbar^2}\left[\frac{k_f}{k_i}\right]^{1/2}\mathcal{T}_{fi} \ , \tag{4.2}$$

where μ is the reduced mass (note that $\mu_i=\mu_f$ for inelastic scattering and charge-exchange reactions).

Once the scattering amplitude is known, the various scattering observables can be constructed. For example, the differential cross section for an unpolarized (u) beam is given by

$$\begin{aligned}\sigma_u(\theta)&=\frac{d\sigma}{d\Omega}\\ &=\frac{1}{2(2I_i+1)}\sum_{\substack{M_iM_f\\ m_im_f}}|\langle I_fM_f,\tfrac{1}{2}m_f|\mathcal{M}|I_iM_i,\tfrac{1}{2}m_i\rangle|^2\\ &\equiv\frac{1}{2(2I_i+1)}\mathrm{Tr}(\mathcal{M}\mathcal{M}^{\dagger})\equiv\sum_{m_im_f}\sigma_{m_im_f} \ .\end{aligned} \tag{4.3}$$

Here, an average over the initial spin orientations and a sum over the final spin orientations of both the projectile and the target spin states has been performed, since we assume that neither of them was observed. The meaning of the trace (Tr) is then obvious. The cross section σ_u is a function of the scattering angle θ between $\mathbf{k}_i$ and $\mathbf{k}_f$.

Next we assume that the incident beam is polarized. Then the state of polarization of the beam is completely described by a polarization vector $\mathbf{P}(i)=(P_x(i),P_y(i),P_z(i))$, whose components are the expectation values of the projectile spin operator σ_i $(i=x,y,z)$ along the three orthogonal directions of a Cartesian coordinate system. According to the Madison convention (Barschall and Haeberli, 1970), we choose the z axis (z' axis) along the beam direction $\mathbf{k}$ ($\mathbf{k}'$) and the y axis perpendicular to the scattering plane parallel to $\hat{\mathbf{n}}=(\mathbf{k}\times\mathbf{k}')/|\mathbf{k}\times\mathbf{k}'|$. The x axis is then chosen so as to obtain a right-handed coordinate frame, i.e., $\hat{\mathbf{x}}=\hat{\mathbf{y}}\times\hat{\mathbf{z}}$ ($\hat{\mathbf{x}}'=\hat{\mathbf{y}}\times\hat{\mathbf{z}}'$). Note that the coordinate frames in the incident and exit channels are related through a rotation around the y axis by the angle θ. The cross section for a polarization (p) beam is given by

$$\sigma_p = \sigma_u (1 + p_y A_y) , \tag{4.4}$$

where the analyzing power A_y is defined by

$$A_y = \frac{\mathrm{Tr}(\mathcal{M}\boldsymbol{\sigma}\cdot\hat{\mathbf{y}}\mathcal{M}^\dagger)}{\mathrm{Tr}(\mathcal{M}\mathcal{M}^\dagger)} . \tag{4.5}$$

The other components of the analyzing power A_x, A_z vanish identically because of parity conservation.

In the next step we consider polarization transfer experiments. In these experiments one uses a polarized beam of polarization $\mathbf{P}(i)$ and measures the polarization $\mathbf{P}(f)$ of the outgoing particle in a secondary scattering experiment. The components of the polarization vectors $\mathbf{P}(i)$ and $\mathbf{P}(f)$ are related through the equation (Ohlsen, 1972)

$$\sigma_p \begin{bmatrix} P_{x'}(f) \\ P_{y'}(f) \\ P_{z'}(f) \end{bmatrix} = \sigma_u \begin{bmatrix} 0 \\ D_{0y'} \\ 0 \end{bmatrix} + \sigma_u \begin{bmatrix} D_{xx'} & 0 & D_{zx'} \\ 0 & D_{yy'} & 0 \\ D_{xz'} & 0 & D_{zz'} \end{bmatrix} \begin{bmatrix} P_x(i) \\ P_y(i) \\ P_z(i) \end{bmatrix} \tag{4.6}$$

where

$$D_{mm'}(\mathbf{k}_i,\mathbf{k}_f) = \frac{\mathrm{Tr}(\mathcal{M}\sigma_m\mathcal{M}^\dagger\sigma_{m'})}{\mathrm{Tr}(\mathcal{M}\mathcal{M}^\dagger)} , \quad m,m' = 0,1,2,3 \tag{4.7}$$

are the Cartesian polarization transfer coefficients. The primed index on $D_{mm'}$ reminds us that the initial and final states of polarization do not need to be referred to the same coordinate frame. The Pauli spin operators are defined as $\sigma_0 = 1$, $\sigma_1 = \sigma_x$, $\sigma_2 = \sigma_y$, $\sigma_3 = \sigma_z$, and correspondingly for the outgoing channel. With our choice of axes ($\hat{\mathbf{y}}$ parallel to $\hat{\mathbf{y}}'$), the only nonvanishing functions $D_{mm'}$ are $D_{00} = 1$, $D_{y0} = A_y$ (analyzing power), $D_{0y'}$ (induced polarization), $D_{xx'}$, $D_{yy'}$, $D_{zz'}$, $D_{zx'}$, and $D_{xz'}$, which are altogether eight independent quantities. Note the absence of coefficients transferring an in-plane polarization (along the $\hat{\mathbf{x}}$ or $\hat{\mathbf{z}}$ axis) into the perpendicular direction (along the $\hat{\mathbf{y}}$ axis) or vice versa. These transfers are forbidden by parity conservation.

Recently complete polarization transfer experiments have become feasible for both inelastic $A(\mathbf{p},\mathbf{p}')B$ scattering (Moss, 1984) and $A(\mathbf{p},\mathbf{n})B$ charge-exchange reactions (Taddeucci *et al.*, 1984, 1986; Watson *et al.*, 1986; Taddeucci, 1987; Watson *et al.*, 1987). This is due to the great advances made in polarimeter techniques (Moss, 1984). In these experiments one can directly measure the spin transfer to the target and can thus separate the spin-flip from the non-spin-flip excitations. To demonstrate this, let us consider the polarization transfer coefficient D_{yy} as an example. This coefficient can be expressed in terms of the cross section $\sigma_{m_i m_f}$ as

$$D_{yy} = \frac{\sigma_{\uparrow\uparrow} - \sigma_{\uparrow\downarrow}}{\sigma_{\uparrow\uparrow} + \sigma_{\uparrow\downarrow}} , \tag{4.8}$$

where the incoming nucleon is polarized along the $\hat{\mathbf{y}} = \hat{\mathbf{y}}'$ axis (spin projection $\uparrow$) and the polarization of the outgoing particle is measured with respect to the same axis (spin projection $\uparrow$ or $\downarrow$). In case of a spin-independent reaction the spin-flip cross section $\sigma_{\uparrow\downarrow}$ is vanishing and $D_{yy} = 1$. On the other hand, if there is a spin dependence, then D_{yy} takes a value between -1 and $+1$. In Sec. VI we shall show that the $D_{mm'}$ functions can be used to separate the longitudinal from the transverse spin response of the nucleus for given momentum and energy transfer.

B. The distorted-wave approximation

In general, the transition operator $\mathcal{T}$ of Eq. (4.1) represents a complicated many-body operator which can only approximately be calculated. Fortunately, at incident energies above 100 MeV, the operator simplifies because the reaction mechanism operative at these energies is preferentially of a direct, one-step nature. This means that the inelastic transition between target states can be evaluated to first order in an effective interaction $V_{pt} = \sum_{j=1}^{A} V_{pj}$ between the projectile nucleon p and the nucleons j in the target. The interaction V_{pt} also has large diagonal matrix elements in the target states. These matrix elements represent average one-body potentials which govern the relative-motion wave function of projectile and target before and after the inelastic scattering event, making them distorted waves (Kerman *et al.*, 1959). This procedure leads to the distorted-wave approximation to the scattering amplitude

$$\mathcal{T}_{if}^{\mathrm{DW}} = \int d\mathbf{r}_p \chi_f^{(-)*}(\mathbf{k}_f,\mathbf{r}_p) \langle I_f M_f, \tfrac{1}{2} m_f | \sum_{j=1}^{A} V_{pj} | I_i M_i, \tfrac{1}{2} m_i \rangle \chi_i^{(+)}(\mathbf{k}_i,\mathbf{r}_p) . \tag{4.9}$$

Here $\chi_i^{(+)}$ and $\chi_f^{(-)*}$ are the distorted waves of the projectile in the initial and final states, respectively, and $|I_i M_i\rangle$ and $|I_f M_f\rangle$ are the associated many-particle wave functions of the target states. The expression for the distorted-wave amplitude in Eq. (4.9) is oversimplified in that it assumes distinguishability between the projectile nucleon p and the nucleons j in the target. In actual calculations one has to include the exchange effects by replacing V_{pj} through $\bar{V}_{pj} = V_{pj}(1 - \mathcal{P}_{pj})$, where $\mathcal{P}_{pj}$ is the exchange operator that exchanges the space, spin, and isospin coordinates of nucleons p and j. This leads to a nonlocal effective interaction. For high incident energies, however, the nonlocal operator can be well approximated by a local form (Petrovich *et al.*, 1969; Love, 1978), and we shall assume in the following that this is the case.

With these assumptions one can show that the transi-

tion amplitude in Eq. (4.9) is factorizable into a nuclear structure part and a nuclear reaction part (see, for instance, Satchler, 1983; Petrovich, Philpott, *et al.*, 1984; Petrovich, Carr, and McManus, 1986). This factorization is most easily seen for the special case of a central spin-independent interaction depending only on the relative distance $r_{pj}=|\mathbf{r}_p-\mathbf{r}_j|$ between the probe and the target nucleon j. To show this we first define a nuclear transition potential:

$$U_{fi}(\mathbf{r}_p)\equiv\langle I_fM_f|\int d\mathbf{r}\,V(\mathbf{r}-\mathbf{r}_p)\sum_{j=1}^{A}\delta(\mathbf{r}-\mathbf{r}_j)|I_iM_i\rangle$$
$$\equiv\int d\mathbf{r}\,V(\mathbf{r}-\mathbf{r}_p)\rho_{I_fI_i}(\mathbf{r})\ . \tag{4.10}$$

Here $\rho_{I_fI_i}(\mathbf{r})$ is the nuclear one-body transition density defined by

$$\rho_{I_fI_i}(\mathbf{r})=\langle I_fM_f|\sum_{j=1}^{A}\delta(\mathbf{r}-\mathbf{r}_j)|I_iM_i\rangle\ . \tag{4.11}$$

It contains all the nuclear structure information with respect to the transition $I_i\rightarrow I_f$ as long as the probe acts on the target system as a one-body operator. Expressing V_{pj} in terms of its Fourier components $V_{pj}(\mathbf{q})$,

$$V_{pj}(|\mathbf{r}_j-\mathbf{r}_p|)=\frac{1}{(2\pi)^3}\int d\mathbf{q}\exp[i\mathbf{q}\cdot(\mathbf{r}_j-\mathbf{r}_p)]V_{pj}(\mathbf{q})\ , \tag{4.12}$$

and inserting this expansion into Eq. (4.9), we obtain the distorted-wave transition amplitude in the form

$$\mathcal{T}_{fi}^{\mathrm{DW}}(\mathbf{k}_f,\mathbf{k}_i)=\int d\mathbf{q}\,D(\mathbf{k}_f,\mathbf{k}_i,\mathbf{q})V(\mathbf{q})\rho_{I_fI_i}(\mathbf{q})\ , \tag{4.13}$$

where

$$\rho_{I_fI_i}(\mathbf{q})\equiv\langle I_fM_f|\sum_{j=1}^{A}\exp[i\mathbf{q}\cdot\mathbf{r}_j]|I_iM_i\rangle \tag{4.14}$$

is the nuclear transition density in $\mathbf{q}$ space, and where $D(\mathbf{k}_f,\mathbf{k}_i,\mathbf{q})$ is the projectile distortion function defined by

$$D(\mathbf{k}_f,\mathbf{k}_i,\mathbf{q})=\frac{1}{(2\pi)^3}\int d\mathbf{r}_p\chi^{(-)*}_{\frac{1}{2}m_f}(\mathbf{k}_f,\mathbf{r}_p)\times\exp[-i\mathbf{q}\cdot\mathbf{r}_p]\chi^{(+)}_{\frac{1}{2}m_i}(\mathbf{k}_i,\mathbf{r}_p)\ . \tag{4.15}$$

From Eqs. (4.10) and (4.13) one can see that the nuclear transition potential U_{fi} is separable in $\mathbf{q}$ space:

$$U_{fi}(\mathbf{q})=V(\mathbf{q})\rho_{I_fI_i}(\mathbf{q})\ . \tag{4.16}$$

Clearly, $\mathcal{T}_{fi}$ of Eq. (4.13) is factorized into a nuclear structure part and a nuclear reaction part. In the plane-wave approximation the distorted waves $\chi_i^{(+)}$ and $\chi_f^{(-)*}$ of Eq. (4.15) are replaced by plane waves, and the distortion function $D(\mathbf{k}_f,\mathbf{k}_i,\mathbf{q})$ becomes $\delta(\mathbf{q}-\mathbf{k}_i+\mathbf{k}_f)$, leading to the simple result

$$\mathcal{T}_{fi}^{\mathrm{PW}}(\mathbf{q})=V(\mathbf{q})\rho_{I_fI_i}(\mathbf{q})\ . \tag{4.17}$$

Here $\mathbf{q}=\mathbf{k}_f-\mathbf{k}_i$ is the asymptotic momentum transfer between incoming projectile and outgoing ejectile. Although quantitatively unreliable, the plane-wave result of Eq. (4.17) is extremely useful for the interpretation of more accurate distorted-wave calculations. The inclusion of distortions introduces a distribution of momenta $\mathbf{q}$, but one expects them to be peaked near $(\mathbf{k}_f-\mathbf{k}_i)$ for sufficiently high energies and at scattering angles where the cross section is large. From Eq. (4.17) it is clear that one needs a strong force component $V(\mathbf{q})$ in order to explore the corresponding Fourier components of the nuclear transition density, $\rho_{I_fI_i}(\mathbf{q})$, and that both $V(\mathbf{q})$ and $\rho_{I_fI_i}(\mathbf{q})$ have to be large in order to obtain a large cross section.

By transforming Eq. (4.13) into $\mathbf{r}$ space we obtain

$$\mathcal{T}_{fi}^{\mathrm{DW}}(\mathbf{k}_f,\mathbf{k}_i)=\int d\mathbf{r}\,\rho_{I_fI_i}(\mathbf{r})P(\mathbf{k}_f,\mathbf{k}_i,\mathbf{r}) \tag{4.18}$$

where

$$P(\mathbf{k}_f,\mathbf{k}_i,\mathbf{r})=\int d\mathbf{q}\exp[i\mathbf{q}\cdot\mathbf{r}]D(\mathbf{k}_f,\mathbf{k}_i,\mathbf{q})V(\mathbf{q}) \tag{4.19}$$

is known as the hadronic transition operator (Bernstein, 1970; see also Satchler, 1983). This is the interaction operator or probe seen by the target during the collision. It is the extent to which this operator resembles the transition operators of other probes which determines whether or not their transition rates and sum-rule strengths can be compared. A few comparisons of the hadronic probe function $P(\mathbf{k}_f,\mathbf{k}_i,\mathbf{r})$ with the electric multipole operators r^LY_{LM} have been performed in the case of inelastic proton scattering (Osterfeld *et al.*, 1979) and in the case of inelastic α scattering (Bernstein, 1970). Bernstein finds that for inelastic α scattering the electromagnetic and hadronic transition operators are rather similar, since both operators favor the nuclear surface region: the multipole operator r^LY_{LM} because of its r^L dependence and the hadronic transition operator because of the strong absorption of the α particles. There can be, however, substantial differences between the radial dependence of the electromagnetic and hadronic transition operators in the case of high-energy proton scattering (Osterfeld *et al.*, 1979). Considering the charge-exchange reactions at intermediate energies we can argue that the (p,n) reaction is a weakly absorbed probe, while the $(^3\mathrm{He},t)$ reaction is a strongly absorbed probe. This different feature of both reactions is useful to identify volume oscillations such as the spin-isovector monopole state.

Another useful limit to the distorted-wave transition amplitude is the strong-absorption limit (Blair, 1959). Especially at high beam energies ($E_p\geq 500$ MeV), where the eikonal approximation applies and where the real part of the optical potential can be ignored, the product of the optical model wave functions in Eq. (4.9) can be estimated by

$$\chi_f^{(-)*}(\mathbf{k}_f,\mathbf{r}_p)\chi_i^{(+)}(\mathbf{k}_i,\mathbf{r}_p) \sim \exp[-i\mathbf{q}\cdot\mathbf{r}_p]\exp\left[-\frac{1}{\hbar v_0}\int_{-\infty}^{\infty} dz\, W(\mathbf{r}_p)\right] . \quad (4.20)$$

Here the second factor on the right-hand side of Eq. (4.20) is a so-called attenuation factor, which describes the damping of the distorted waves inside the nucleus. The attenuation factor is a function of the imaginary part of the optical potential $W(\mathbf{r}_p)$. The z integration is along an axis parallel to the beam direction, and v_0 is the beam velocity. Because of the strong absorption, the attenuation factor implies that the major contribution to the $\mathbf{r}_p$ integration in Eq. (4.9) is localized in a narrow ring around the target nucleus.

Bertsch and Esbensen (1987) have applied the strong-absorption limit to the evaluation of the charge-exchange cross sections. They assume the target transition density (4.11) to be of the form

$$\rho_{I_fI_i}(\mathbf{r})=\delta\rho_{fi,\lambda}(r)Y^*_{\lambda\mu}(\theta,\phi)/(2\lambda+1)^{1/2} \quad (4.21)$$

and assume a momentum-dependent contact interaction for the projectile-target nucleon interaction. The latter assumption reduces the six-dimensional integral of Eq. (4.9) to a three-dimensional one. In this case the transition amplitude can be expressed as

$$\mathcal{T}^{\mathrm{SA}}_{fi}(\mathbf{q})=\frac{V(q)}{\sqrt{(2\lambda+1)}}\int d\mathbf{r}_p\exp[-i\mathbf{q}\cdot\mathbf{r}_p] \times\exp\left[-\frac{1}{\hbar v_0}\int dz\, W(\mathbf{r}_p)\right] \times\delta\rho_{fi,\lambda\mu}(r_p)Y^*_{\lambda\mu}(\theta_p,\phi_p) . \quad (4.22)$$

Using the axial symmetry of the problem around the beam axis, one can perform the integration over the azimuthal angle ϕ_p analytically:

$$\int_0^{2\pi} d\phi_p\exp[-iqb\cos\phi_p]\exp[-i\mu\phi_p]=2\pi J_\mu(qb) . \quad (4.23)$$

Here $b\equiv r_p\sin\theta_p$ is the impact parameter of the reaction and $J_\mu(qb)$ is the spherical Bessel function of integer order. Since the main contribution to the integral in Eq. (4.22) comes from a narrow ring near $\theta_p\simeq\pi/2$ and $b\simeq R_0$, where R_0 is the strong-absorption radius, the integral can be approximately factorized according to

$$\mathcal{T}^{\mathrm{SA}}_{fi}(\mathbf{q})=N_D^{1/2}V(q)Y_{\lambda\mu}(\pi/2,0)J_\mu(qR_0)M_{fi,\lambda} \quad (4.24)$$

with the nuclear matrix element

$$M_{fi,\lambda}=\int d^3\mathbf{r}_p\delta\rho_{fi,\lambda}(r_p)/(2\lambda+1)^{1/2} \quad (4.25)$$

and the distortion factor

$$N_D=\left|\int d^3\mathbf{r}_p\delta\rho_{fi,\lambda}(r_p)\exp\left[-\frac{1}{\hbar v_0}\int dz\, W(\mathbf{r}_p)\right]M^{-1}_{fi\lambda}\right|^2 . \quad (4.26)$$

The latter factor describes the attentuation of the projectile wave function inside the target nucleus in an average way. From Eq. (4.24) we obtain the following simple expression for the double-differential cross section:

$$\frac{d^2\sigma}{d\Omega\,dE}=\left[\frac{\mu}{2\pi\hbar^2}\right]^2 N_D\sum_{f,\mu}\frac{k_f}{k_i}|V(q)Y_{\lambda\mu}(\pi/2,0)J_\mu(qR)|^2 \times|M_{fi\lambda}|^2\delta(E-\omega_{fi}) . \quad (4.27)$$

The angular dependence of the cross section is determined by the product of the interaction $V(q)$ and the Bessel function. Thus, for a given angular momentum transfer λ, the cross section has a maximum at an angle that is mainly determined by the position of the maximum of the Bessel function. The Blair approach to the transition amplitude is particularly suited for the description of heavy-ion charge-exchange reactions at incident energies $E\geq 100$ MeV/nucleon.

C. The effective projectile-target nucleon interaction

From Eqs. (4.13) and (4.16) it is clear that in order to extract the nuclear structure information from $\mathcal{T}_{fi}$ one needs to know the effective interaction V_{pj}. This effective interaction is, in general, very complicated. It depends on the incident projectile energy E_p and on the specific properties of the target, such as its ground-state density distribution and inelastic excitation spectrum. In principle it should be calculated for each scattering situation anew, starting from a bare nucleon-nucleon (NN) potential V_{NN} which, when used in a two-body Schrödinger equation, describes the free NN scattering data.

Modern NN potentials are the Bonn potential (Holinde *et al.*, 1972; Erkelenz, 1974; Holinde and Machleidt, 1977; Holinde; 1981; Machleidt, Holinde, and Elster, 1987), the Paris potential (Lacombe *et al.*, 1980), and the Nijmegen potential (Nagels *et al.*, 1979a, 1979b), all of which are based on meson-exchange models. The long-range part in these potentials is provided by the one-pion exchange, since the pion is the lightest meson. The medium-range attraction is produced by correlated two-pion exchange, which is simulated by an effective, low-mass scalar meson ("σ" meson). The short-range repulsion is due to the exchange of heavy vector (ω) mesons. In the Paris potential, instead of the ω exchange, a purely phenomenological short-range part is added to the meson exchange potential in order to reproduce the NN phase shifts in the partial-wave expansion of the NN scattering amplitude. Because of the strong repulsion in the NN potentials at short distances, they cannot be used directly in a perturbative calculation. First the repulsive core has to be properly regularized by converting the bare potentials

V_{NN} into weak *effective* interactions. In the free NN scattering problem this is done by solving the two-body Schrödinger equation or, equivalently, the Lippmann-Schwinger equation with V_{NN}. The Lippmann-Schwinger equation is an integral equation that allows the two nucleons to interact any number of times via the strong interaction V_{NN}, but the final sum of all these interactions is a weak *effective* interaction *represented* by the free NN scattering matrix t_F.

In the case of the scattering of a projectile nucleon p from a nucleon j in the nucleus, one has to incorporate the nuclear medium effects into the two-nucleon scattering amplitude. The effective interaction so constructed is known as Brueckner's scattering matrix G (Brueckner, 1954; Brueckner and Levinson, 1955; Day, 1967, 1981; Bethe, 1971), which is the solution of the Bethe-Goldstone equation (Bethe and Goldstone, 1957) defined by

$$G(\omega)=V_{NN}+V_{NN}\frac{Q}{\omega-H_0+i\epsilon}G(\omega)\ . \tag{4.28}$$

Here Q is the Pauli projection operator, which restricts the two-nucleon intermediate states to those unoccupied by the nuclear medium, H_0 is a single-particle Hamiltonian composed of the kinetic-energy operator and the single-particle potential, and ω represents the starting energy of the two interacting nucleons. The nuclear medium effects enter in two ways, namely, by the Pauli operator Q, which hinders the interacting nucleons p and j from scattering into already occupied states, and by the single-particle Hamiltonian H_0, which modifies the single-particle energies and single-particle wave functions as compared to those in free space.

For finite nuclei it is very difficult to solve Eq. (4.28) because of the complicated Pauli operator, which involves a double integration over intermediate states. Therefore one first calculates the G matrix in symmetric nuclear matter at several densities and applies $G(\omega)$ to finite nuclei by using the local-density approximation (Negele, 1970; Siemens, 1970). The medium corrections to the effective interaction are found to be very large at lower energies, $E_p \ll 100$ MeV (Jeukenne *et al.*, 1976; Brieva and Rook, 1977a, 1977b, 1978; Brieva *et al.*, 1978; Mahaux, 1983; Yamaguchi *et al.*, 1983; Nakayama *et al.*, 1984, 1986; Rikus *et al.*, 1984; Rikus and von Geramb, 1984; Nakayama and Love, 1988). For high incident-projectile energies, however, i.e., for energies large compared to the Fermi energy ($\epsilon_F \sim 37$ MeV) of the nucleons in the target, the G matrix approaches the free t_F matrix. The replacement of G by t_F is the impulse approximation (Kerman *et al.*, 1959), which becomes a good approximation for incident energies, say, greater than 400 MeV. The appeal of the impulse approximation is obvious: the effective interaction can be constructed directly from the phase-shift analysis of NN scattering data without the intervention of a potential.

1. The free nucleon-nucleon t_F-matrix interaction

Nowadays the NN scattering data are rather complete up to energies of 1 GeV (Arndt *et al.*, 1983), so that the interesting properties of the free NN transition matrix t_F can be derived. In analogy to Eq. (4.2), the t_F matrix is related to the NN scattering amplitude M by

$$\begin{aligned} t_F &= -\frac{4\pi(\hbar c)^2}{E_{\rm CM}}M(E_{\rm CM},\theta)\ , \\ E_{\rm CM}^2 &= m^2c^4+(\hbar ck)^2\ , \end{aligned} \tag{4.29}$$

where $E_{\rm CM}$ and $\hbar k$ are the energy and momentum in the two-nucleon center-of-mass frame, respectively, m is the nucleon rest mass, and θ is the scattering angle between the initial and final momenta $\mathbf{k}$ and $\mathbf{k}'$ of either particle. The scattering amplitude $M(E_{\rm CM},\theta)$ is represented by a 4×4 matrix in the spin space of the two nucleons. It can be written as a sum of five linearly independent scalar, time-reversible, parity-conserving and charge-independent operators (Wolfenstein and Ashkin, 1952; Kerman *et al.*, 1959; MacGregor *et al.*, 1960),

$$\begin{aligned} M(E_{\rm CM},\theta) = {} & A+B\boldsymbol{\sigma}_1\cdot\hat{\mathbf{n}}\boldsymbol{\sigma}_2\cdot\hat{\mathbf{n}}+C(\boldsymbol{\sigma}_1+\boldsymbol{\sigma}_2)\cdot\hat{\mathbf{n}} \\ & +E\boldsymbol{\sigma}_1\cdot\hat{\mathbf{q}}\boldsymbol{\sigma}_2\cdot\hat{\mathbf{q}}+F\boldsymbol{\sigma}_1\cdot\hat{\mathbf{Q}}\boldsymbol{\sigma}_2\cdot\hat{\mathbf{Q}}\ , \end{aligned} \tag{4.30}$$

where the coefficients A,B,C,E, and F are complex functions of the energy $E_{\rm CM}$, the scattering angle θ, and the two-body isospin; e.g., $A=A_0+A_1\boldsymbol{\tau}_1\cdot\boldsymbol{\tau}_2$. The subscripts 1 and 2 refer to the coordinates of the two interacting nucleons. The unit vectors $[\hat{\mathbf{Q}},\hat{\mathbf{n}},\hat{\mathbf{q}}]$ form a right-handed coordinate system with $\mathbf{Q}=\mathbf{k}+\mathbf{k}'$, $\mathbf{q}=\mathbf{k}-\mathbf{k}'$, and $\hat{\mathbf{n}}=\hat{\mathbf{q}}\times\hat{\mathbf{Q}}$. The vectors $\hat{\mathbf{q}}$ and $\hat{\mathbf{Q}}$ define the scattering plane while the vector $\hat{\mathbf{n}}$ is directed perpendicular to the scattering plane.

The operator M induces either spin-independent or spin-dependent excitations in the target. The spin-independent excitations are governed by the amplitudes A and C, while the spin excitations are governed by the amplitudes B, C, E, and F. Three different types of spin excitations are possible, namely, a longitudinal one with the spin transfer along the momentum-transfer direction $\hat{\mathbf{q}}$ (term E), and two transverse ones with the spin transfer occurring either in the scattering plane (term F) or perpendicular to the scattering plane (terms B and C). The individual spin components can be measured by performing appropriate spin-flip transfer measurements. For example, a projectile that has its spin polarized perpendicular to the scattering plane, as was assumed in Eq. (4.8), is sensitive only to spin excitations within the scattering plane, i.e., to the coefficients E and F. This is so because only these terms can flip the spin about the $\hat{\mathbf{n}}$ axis. Similarly, the spin of a particle polarized along the $\hat{\mathbf{q}}$ ($\hat{\mathbf{Q}}$) axis flipped by the spin operators with amplitudes B, C, and F (B, C, and E).

The scattering amplitude M can also be written in a longitudinal transverse representation which facilitates

the comparison of the nucleon coupling with that of the other spin probes (Love *et al.*, 1984). Using the relation

$$\begin{aligned}\boldsymbol{\sigma}_1\cdot\boldsymbol{\sigma}_2&=\boldsymbol{\sigma}_1\cdot\hat{\mathbf{q}}\boldsymbol{\sigma}_2\cdot\hat{\mathbf{q}}+\boldsymbol{\sigma}_1\cdot\hat{\mathbf{Q}}\boldsymbol{\sigma}_2\cdot\hat{\mathbf{Q}}+\boldsymbol{\sigma}_1\cdot\hat{\mathbf{n}}\boldsymbol{\sigma}_2\cdot\hat{\mathbf{n}}\\&=\boldsymbol{\sigma}_1\cdot\hat{\mathbf{q}}\boldsymbol{\sigma}_2\cdot\hat{\mathbf{q}}+(\boldsymbol{\sigma}_1\times\hat{\mathbf{q}})\cdot(\boldsymbol{\sigma}_2\times\hat{\mathbf{q}})\ ,\end{aligned}\tag{4.31}$$

one can rewrite Eq. (4.30) in the form (Love *et al.*, 1984)

$$\begin{aligned}M(E_{\rm CM},\theta)=&A+C(\boldsymbol{\sigma}_1+\boldsymbol{\sigma}_2)\cdot\hat{\mathbf{n}}\\&+E\mathcal{O}_l+\frac{B+F}{2}\mathcal{O}_t+\frac{B-F}{2}\mathcal{O}_u\end{aligned}\tag{4.32}$$

with one longitudinal ($\mathcal{O}_l$) and two transverse operators ($\mathcal{O}_t,\mathcal{O}_u$),

$$\mathcal{O}_l=\boldsymbol{\sigma}_1\cdot\hat{\mathbf{q}}\boldsymbol{\sigma}_2\cdot\hat{\mathbf{q}}\tag{4.33}$$

$$\mathcal{O}_t=(\boldsymbol{\sigma}_1\times\hat{\mathbf{q}})\cdot(\boldsymbol{\sigma}_2\times\hat{\mathbf{q}})\tag{4.34}$$

$$\mathcal{O}_u=\boldsymbol{\sigma}_1\cdot\hat{\mathbf{n}}\boldsymbol{\sigma}_2\cdot\hat{\mathbf{n}}-\boldsymbol{\sigma}_1\cdot\hat{\mathbf{Q}}\boldsymbol{\sigma}_2\cdot\hat{\mathbf{Q}}\ .\tag{4.35}$$

For spin excitations the C term is similar to the pion-nucleon coupling (Petrovich *et al.*, 1986), while the $\mathcal{O}_t$ term is similar to the transverse electromagnetic coupling. The latter term can arise from the ρ-meson exchange with the magnetic type of coupling, $(\boldsymbol{\sigma}_1\times\hat{\mathbf{q}})\cdot(\boldsymbol{\sigma}_2\times\hat{\mathbf{q}})$. The longitudinal coupling operator $\mathcal{O}_l$ is unique for hadronic probes and is mainly due to π exchange. The last term $\mathcal{O}_u$ can arise only from nonlocal interactions and from exchange terms.

2. The construction of a local effective interaction in r space

The coefficients A, B, etc., in Eq. (4.30) are defined for free NN kinematics and for antisymmetrized two-nucleon wave functions. In the case of the nucleon-nucleus scattering both the kinematics and the antisymmetrization properties are different. One of the nucleons involved in the scattering process is bound in the target. Therefore the scattering process in general requires a knowledge of the t matrix at momenta that are not available from the free NN kinematics. Moreover, the antisymmetrization has to be performed with bound nuclear wave functions. A partial solution to this problem is to construct a coordinate representation of the t matrix which reproduces the scattering matrix in the physically accessible region and also provides a way to extrapolate to off-shell momenta. This procedure has been carried out by Love and Franey (1981) and Franey and Love (1985). For that purpose they first rewrite Eq. (4.30) into the form

$$\begin{aligned}M(E_{\rm CM},\theta)=&A'\Lambda_S+B'\Lambda_T+C(\boldsymbol{\sigma}_1+\boldsymbol{\sigma}_2)\cdot\hat{\mathbf{n}}\\&+E'S_{12}(\hat{\mathbf{q}})+F'S_{12}(\hat{\mathbf{Q}})\ ,\end{aligned}\tag{4.36}$$

where $S_{12}(\hat{\mathbf{u}})=3\boldsymbol{\sigma}_1\cdot\hat{\mathbf{u}}\boldsymbol{\sigma}_2\cdot\hat{\mathbf{u}}-\boldsymbol{\sigma}_1\cdot\boldsymbol{\sigma}_2$ is the usual tensor operator, and $\Lambda_S=(1-\boldsymbol{\sigma}_1\cdot\boldsymbol{\sigma}_2)/4$ and $\Lambda_T=(3+\boldsymbol{\sigma}_1\cdot\boldsymbol{\sigma}_2)/4$ are the singlet and triplet spin-projection operators, respectively. Here use has been made of the identity $\boldsymbol{\sigma}_1\cdot\hat{\mathbf{u}}\,\boldsymbol{\sigma}_2\cdot\hat{\mathbf{u}}=\frac{1}{3}[S_{12}(\hat{\mathbf{u}})+\boldsymbol{\sigma}_1\cdot\boldsymbol{\sigma}_2]$ and of the completeness of $[\hat{\mathbf{Q}},\hat{\mathbf{n}},\hat{\mathbf{q}}]$. The primed coefficients are just linear combinations of the old coefficients: $A'=A-B-E-F$, $B'=A+(B+E+F)/3$, $E'=(E-B)/3$, and $F'=(F-B)/3$. The amplitudes A' and B' represent the central parts of M, and the terms E' and F' represent tensor interactions.

A practical form of the t_F-matrix interaction is now obtained by assuming a local functional form $V_{12}(\mathbf{r})$ in $\mathbf{r}$ space and by adjusting its parameters until the antisymmetrized NN matrix element in momentum space

$$t_F(\mathbf{q},E_{\rm CM})=\int d\mathbf{r}\exp[-i\mathbf{k}'\cdot\mathbf{r}]V_{12}(\mathbf{r})(1-\mathcal{P}_{12})\exp[i\mathbf{k}\cdot\mathbf{r}]\tag{4.37}$$

reproduces the free t_F matrix in each spin and isospin channel at a given energy $E_{\rm CM}$. In Eq. (4.37) the operator $\mathcal{P}_{12}$ is the exchange operator which generates antisymmetrization.

The tensorial structure of Eq. (4.36) suggests writing the effective interaction as a sum of central (C), spin-orbit (LS), and tensor (T) terms with the following spin-isospin decomposition:

$$\begin{aligned}V_{12}(\mathbf{r})=&V_0^C(r)+V_\sigma^C(r)\boldsymbol{\sigma}_1\cdot\boldsymbol{\sigma}_2+V_\tau^C(r)\boldsymbol{\tau}_1\cdot\boldsymbol{\tau}_2\\&+V_{\sigma\tau}^C(r)\boldsymbol{\sigma}_1\cdot\boldsymbol{\sigma}_2\boldsymbol{\tau}_1\cdot\boldsymbol{\tau}_2\\&+[V^{LS}(r)+V_\tau^{LS}(r)\boldsymbol{\tau}_1\cdot\boldsymbol{\tau}_2)]\mathbf{L}_{12}\cdot\mathbf{S}\\&+[V^T(r)+V_\tau^T(r)\boldsymbol{\tau}_1\cdot\boldsymbol{\tau}_2]S_{12}(\hat{\mathbf{r}})\ ,\end{aligned}\tag{4.38}$$

where $\mathbf{L}_{12}\equiv(\mathbf{r}_1-\mathbf{r}_2)\times(\mathbf{k}_1-\mathbf{k}_2)/2$ is the relative angular momentum operator between nucleons 1 and 2, and $\mathbf{S}=\mathbf{s}_1+\mathbf{s}_2$ is the total two-nucleon spin. The coefficients $V_{\sigma\tau}^C$, etc., depend on the relative coordinate $\mathbf{r}=\mathbf{r}_1-\mathbf{r}_2$ of the two interacting nucleons. Love and Franey (1981) represent these interaction coefficients by a sum of Yukawa functions,

$$V_{12}(r)=\sum_{i=1}^{N}V_i\frac{\exp[-r/R_i]}{r/R_i}\ .\tag{4.39}$$

This functional form is very convenient for numerical calculations, since the Yukawa form has an analytic multipole decomposition in terms of modified Bessel functions, which simplifies the calculation of the two-body matrix elements considerably. The force ranges R_i are free parameters, as well as the force strengths V_i, which, in general, are complex. Both the R_i and the V_i are determined from a best fit to the t_F matrix of Eq. (4.38) and, in general, depend on the incident energy $E_{\rm CM}$.

The representation of the effective interaction in Eq. (4.38) is particularly useful for the description of inelastic-scattering processes because it makes the spin-isospin dependence of the effective interaction explicit. In the single scattering approximation the operator of Eq. (4.38) acts on the projectile as well as on the target system as a one-body operator. All terms that involve the spin operators $\boldsymbol{\sigma}_1\cdot\boldsymbol{\sigma}_2$, $\mathbf{S}$, or S_{12} produce spin-flip

($S=1$) transitions in the projectile and in the target, and all terms that involve the isospin operator $\tau_1 \cdot \tau_2$ induce isospin ($T=1$) transitions. The isospin excitation of the target can occur either through inelastic scattering induced by the isospin operator τ_3, or through charge-exchange reactions mediated by the operators $\tau_\pm$.

3. Properties of the free t_F-matrix interaction

The various force components in Eq. (4.38) are functions of the incident energy E_p and the momentum transfer q. Each of the force components has its own characteristic E_p and q dependence. The energy depen-

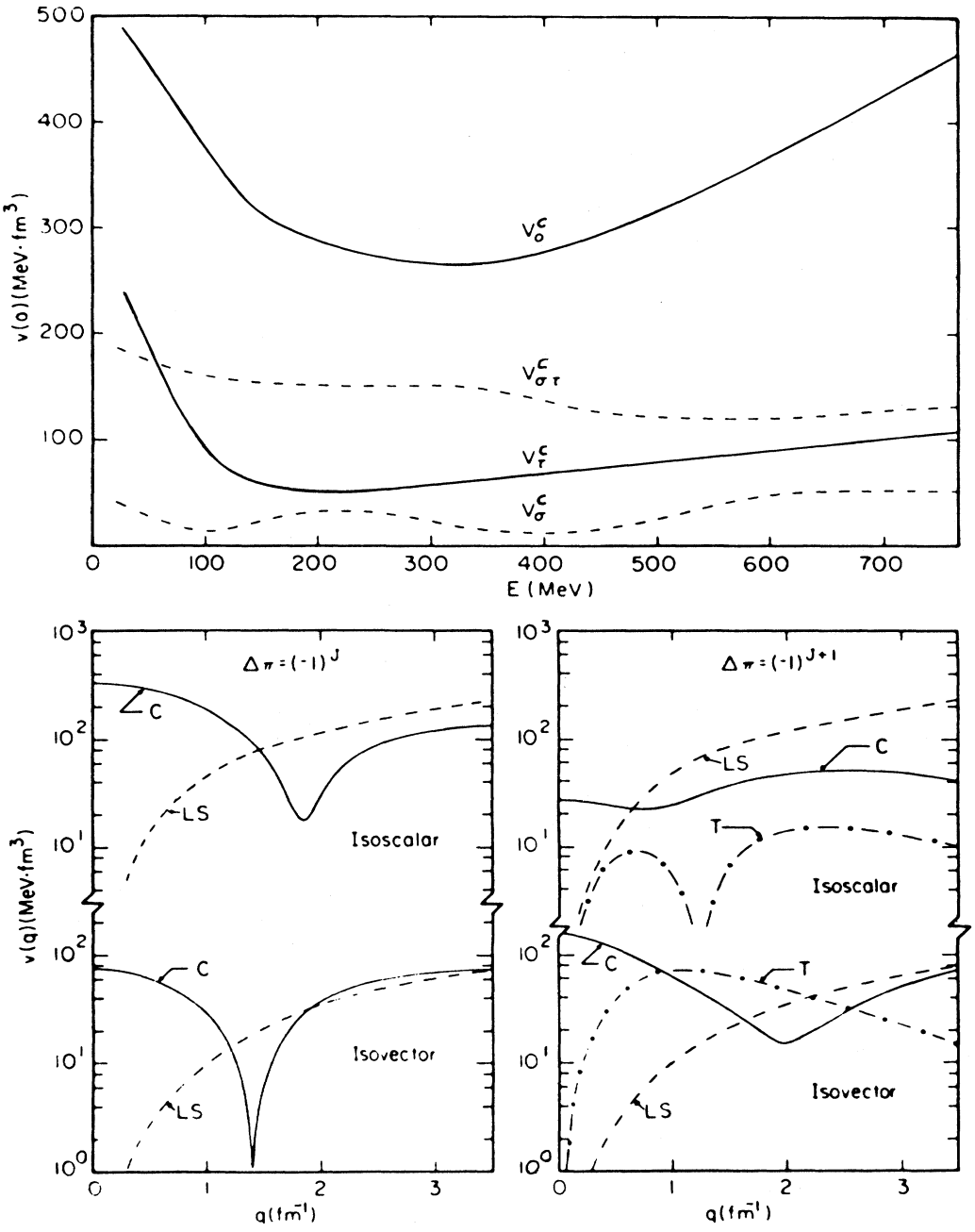

FIG. 15. Energy and momentum dependence of the free nucleon-nucleon t_F matrix. The upper part of the figure shows the energy dependence of the central components of the effective t_F matrix at zero-momentum transfer (including direct and exchange terms). The G-matrix interaction of Bertsch *et al.* (1977) was used below 100 MeV and joined smoothly to the t_F matrix above 100 MeV. The lower figures show the momentum dependence of the 135-MeV t_F matrix for natural-(left figure) and unnatural-(right figure) parity transitions. Isoscalar and isovector central (C), spin-orbit (LS), and tensor (T) components are shown. From Petrovich and Love (1981).

dence of the central parts of the effective interaction at zero-momentum transfer ($q=0$) (Love and Franey, 1981) is shown in the upper part of Fig. 15 for the energy range $10 \leq E_p \leq 750$ MeV. For energies below 100 MeV the values are based on the G-matrix interaction of Bertsch *et al.* (1977), while for energies from 100 to 750 MeV the values are derived from the free t_F-matrix interaction of Love and Franey (1981). The latter interaction was deduced from the Arndt phase shifts (Arndt *et al.*, 1983) supplemented with phase shifts from one-pion exchange in the higher partial waves. The most prominent feature of the curves in the top part of Fig. 15 is that the central scalar-isoscalar interaction V_0^C is dominating the other central spin-, isospin-, and spin-isospin-dependent interaction terms at all energies considered. In the energy region 150 MeV $\leq E_p \leq$ 500 MeV, V_0^C becomes relatively weak and gives rise to the so-called energy window for nuclear structure studies. The origin of this energy window goes back to properties of the $^1S_0$ and $^3S_1$ NN phase shifts, which are strongly attractive at low energies, but vanish at around $E_{\rm lab}=300$ MeV and become repulsive at higher energies (see, for instance, Bohr and Mottelson, 1969). This behavior of the S-wave phase shifts is due to the strong short-range repulsion in the NN potential, which is ineffective at lower, but dominant at higher incident energies.

The incident-energy region around 200–500 MeV is especially well suited for nuclear structure studies for the following reasons. First, the distortion effects on the projectile wave functions are relatively small in this energy region, since they are related to the strength of the scalar-isoscalar interaction V_0^C, which is weak here. Secondly, a weak V_0^C implies a suppression of multistep processes in the nuclear reaction mechanism (Chiang and Hüfner, 1980). Therefore the inelastic nuclear excitation spectrum at moderate excitation energies ($E_x \leq 50$ MeV) is mainly the result of one-step processes and can be calculated within microscopic nuclear structure models (Bertsch and Scholten, 1982; Osterfeld, 1982, 1984; Scholten *et al.*, 1983; Osterfeld *et al.*, 1985). This will be demonstrated in detail in Sec. VI.

From Fig. 15 one can further recognize that the force component $V_{\sigma\tau}^C$ which excites spin-isospin-flip transitions is especially large in the energy window, while the isovector spin-independent component V_τ^C is strongly reduced. This can be better seen from Fig. 16, where the ratio of the volume integrals $|J_{\sigma\tau}/J_\tau|^2 \equiv |V_{\sigma\tau}^C(q=0)/V_\tau^C(q=0)|^2$ is plotted versus E_p at zero-momentum transfer. The ratio is found to be larger than 10 at 200 MeV $\leq E_p \leq$ 500 MeV. It is this dominance of $V_{\sigma\tau}^C$ over V_τ^C which is why nucleon-induced reactions at intermediate energies are an invaluable probe of isovector spin modes in nuclei. This behavior has been known since the work of Kerman, McManus, and Thaler (1959), but was brought into focus with the work of Love and Franey (1981), who calculated the isovector force strength ratio (full curve in Fig. 16) using the NN phase shifts of Arndt *et al.*, (1983) as input to their calculations. The experimental points were later measured at various accelerator laboratories (see Taddeucci, 1983; Alford *et al.*, 1986; King *et al.*, 1986).

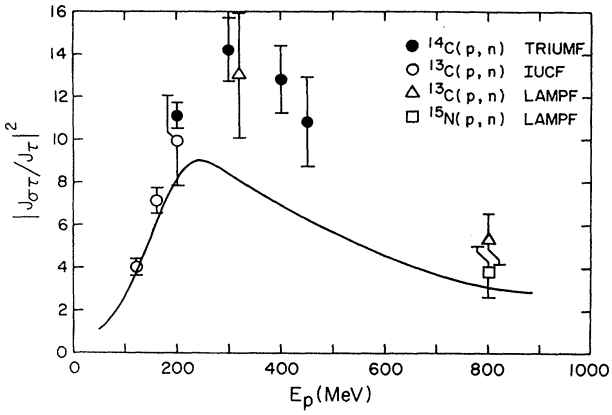

FIG. 16. Energy dependence of the ratio $|J_{\sigma\tau}^C/J_\tau^C|^2$ at zero momentum transfer. The experimental points are measurements of IUCF (○) (Taddeucci, 1983), LAMPF (△ and □) (King *et al.*, 1986), and TRIUMF (●) (Alford *et al.*, 1986). The solid line is the impluse approximation predication of Franey and Love (1985) based on the nucleon-nucleon phase shifts of Arndt *et al.* (1983).

The isoscalar spin-dependent interaction term V_σ^C is rather small at all incident energies, suggesting that the central part of the effective interaction is rather ineffective for exciting isoscalar spin modes. This is indeed the case, as has been observed in the inelastic excitation of the 1^+, $T=0$, $E_x=12.5$ MeV state in ^{12}C by inelastic proton scattering (Comfort *et al.*, 1980, Comfort and Love, 1980; Moss *et al.*, 1980). In this reaction the tensor exchange process is the dominant reaction mechanism, while the direct process governed by V_σ^C is suppressed.

The lower half of Fig. 15 shows the q dependence of the complete t_F-matrix interaction of Love and Franey at $E_p=135$ MeV for natural parity [$\Delta\pi=(-1)^J$] and unnatural parity [$\Delta\pi=(-1)^{J+1}$] transitions. More sophisticated interactions (Nakayama and Love, 1988) behave similarly. One noteworthy feature of the t_F-matrix interaction is the increased importance of the spin-orbit (LS) force at large q transfers relative to the central (C) interaction. The large q transfer behavior can be best studied through the examination of high-spin states ($J^\pi \geq 3^-$), which involve transition densities with large angular momentum ($L \geq 3$) transfer. These transition densities have the property that they peak around momentum transfers of $q \sim 1-2$ fm^{-1}.

The energy and momentum dependence of the isovector parts of the t-matrix interaction displayed in Fig. 15 can be qualitatively understood in the meson-exchange picture of nuclear forces. The simplest interpretation is obtained for the spin-isospin-dependent central and tensor terms, which are mainly mediated by π- and ρ-meson

exchange, modified at short distances by correlations due to ω-meson exchange (Brown *et al.*, 1981). In momentum space the π- and ρ-exchange potentials are given by

$$V_\pi(\omega,\mathbf{q})=J_\pi(\omega,q)\frac{\sigma_1\cdot\mathbf{q}\sigma_2\cdot\mathbf{q}}{\omega^2-q^2-m_\pi^2}\tau_1\cdot\tau_2 \tag{4.40}$$

$$V_\rho(\omega,\mathbf{q})=J_\rho(\omega,q)\frac{(\sigma_1\times\mathbf{q})\cdot(\sigma_2\times\mathbf{q})}{\omega^2-q^2-m_\rho^2}\tau_1\cdot\tau_2\ , \tag{4.41}$$

where $(\omega,\mathbf{q})$ is the four-momentum transfer carried by the exchanged mesons, and where $m_\pi=0.699$ fm^{-1} and $m_\rho=3.9$ fm^{-1} are the corresponding meson masses. The force strength parameters J_π and J_ρ are defined by

$$J_\pi(\omega,q)=4\pi\frac{f_{\pi NN}^2}{m_\pi^2}\left[\frac{\Lambda_\pi^2-m_\pi^2}{\Lambda_\pi^2-\omega^2+q^2}\right]^2 \tag{4.42}$$

$$J_\rho(\omega,q)=4\pi\frac{f_{\rho NN}^2}{m_\rho^2}\left[\frac{\Lambda_\rho^2-m_\rho^2}{\Lambda_\rho^2-\omega^2+q^2}\right]^2 . \tag{4.43}$$

Here $f_{\pi NN}^2=0.08$ and $f_{\rho NN}^2=4.86$ are the πNN and ρNN coupling constants, respectively. The quantities in round brackets are the form factors which describe the finite size of the meson-nucleon vertices. The cut off masses $\Lambda_\pi=6$ fm^{-1} and $\Lambda_\rho=10$ fm^{-1} are determined from appropriate experiments like $p(n,p)n$ charge-exchange scattering (Dominguez and Verwest, 1980) or pion photoproduction (Dominguez and Clark, 1980) and also enter the bare NN potentials as parameters. In the static limit, i.e., for zero energy transfer, we have $\omega\equiv 0$. This limit corresponds to elastic nucleon-nucleon scattering. It is also a good approximation for inelastic nucleon-nucleus scattering as long as the excitation energy E_x is small compared with the pion mass, $m_\pi\equiv 139$ MeV. Therefore, in the following discussion, we shall put $\omega=0$. In Sec. VII, where we shall discuss the physics of the quasifree peak region ($E_x\sim 100$ MeV) and of the Δ-resonance region ($E_x\sim 300$ MeV), the ω dependence of the meson-exchange potentials in Eqs. (4.40) and (4.41) becomes important.

From Eqs. (4.40) and (4.41) it is obvious that both the π- and ρ-exchange potentials vanish for forward scattering ($q=0$), contrary to $V_{\sigma\tau}^C$ in Fig. 15. This is due to the fact that both potentials represent only the first-order Born approximation to the full t_F matrix. The higher-order terms include the short-range correlations which modify $V_{\sigma\tau}^C$ at small q. To understand this effect in a simple manner we first decompose the interactions V_π and V_ρ into irreducible tensors (note that $\omega=0$!),

$$V_\pi(\mathbf{q})=-\tfrac{1}{3}J_\pi(0,q)\left[\frac{3\sigma_1\cdot\mathbf{q}\sigma_2\cdot\mathbf{q}-\sigma_1\cdot\sigma_2 q^2}{q^2+m_\pi^2}-\frac{m_\pi^2}{q^2+m_\pi^2}\sigma_1\cdot\sigma_2+\sigma_1\cdot\sigma_2\right]\tau_1\cdot\tau_2 \tag{4.44}$$

$$V_\rho(\mathbf{q})=-\tfrac{1}{3}J_\rho(0,q)\left[-\frac{3\sigma_1\cdot\mathbf{q}\sigma_2\cdot\mathbf{q}-\sigma_1\cdot\sigma_2 q^2}{q^2+m_\rho^2}-\frac{2m_\rho^2}{q^2+m_\rho^2}\sigma_1\cdot\sigma_2+2\sigma_1\cdot\sigma_2\right]\tau_1\cdot\tau_2\ , \tag{4.45}$$

where we have made use of the operator identity of Eq. (4.31). The first term in the large parentheses is a tensor interaction, the second term is a central interaction of Yukawa type, and the third term is a contact interaction, which in coordinate space leads to a δ-function-like force. Now the short-range correlations keep the nucleons apart so that they never come to the same place. Therefore the δ-function piece will become inoperative and should be removed from the interaction (Ericson and Ericson, 1966; Brown and Weise, 1975). When one considers this effect for the π-exchange potential, one obtains a force strength of 133 MeV fm^3 at $q=0$, which is in good agreement with the experimental $V_{\sigma\tau}^C$ values of Fig. 15, which range from 160 MeV fm^3 near $E_p=100$ MeV to 125 MeV fm^3 near $E_p=750$ MeV.

This simple prescription of dropping the δ-function piece is not accurate enough for the determination of the short-range correlations connected with the ρ-meson exchange. The ρ meson has a larger mass than the pion and consequently a shorter range. Therefore one has to make a better model for the short-range correlations. In principle, this requires a full t-matrix calculation. However, one can simulate the effects of a t-matrix calculation by introducing a two-body correlation function $g(r)$ that multiplies the $\pi+\rho$ potential in coordinate space, that is, $\hat{V}_i(\mathbf{r})\equiv g(r)V_i(\mathbf{r})$ $(i=\pi,\rho)$. In momentum space this gives for the ρ potential

$$\hat{V}_\rho(\mathbf{q})=\int\frac{d^3\mathbf{k}}{(2\pi)^3}V_\rho(\mathbf{k})g(\mathbf{q}-\mathbf{k})\ , \tag{4.46}$$

with $g(\mathbf{q})$ being the Fourier transform of $g(r)$:

$$g(\mathbf{q})=\int d^3\mathbf{r}\,e^{i\mathbf{q}\cdot\mathbf{r}}g(\mathbf{r})\ . \tag{4.47}$$

Now we assume that $g(r)$ arises mainly from the repulsion due to ω-meson exchange in the nucleon-nucleon interaction. Thus the range of $g(r)$ is expected to be comparable to the Compton wavelength of the ω meson. A parametrized form that has been adjusted to reproduce the dominant components of a realistic two-body correlation function calculated with the Reid soft-core potential is (Brown *et al.*, 1977; Anastasio and Brown, 1977)

$$g(r)=1-j_0(q_c r)\ , \tag{4.48}$$

with $q_c=3.93$ fm$^{-1}\simeq m_\omega$ and $j_0(z)$ the spherical Bessel function of order $l=0$. The Fourier transform is

$$g(\mathbf{q})=(2\pi)^3\delta(\mathbf{q})-2\pi^2\frac{1}{q_c^2}\delta(|\mathbf{q}|-q_c)\ ,$$

$$q_c=3.93\ \text{fm}^{-1}\ , \quad (4.49)$$

which, when inserted into Eq. (4.46), results in

$$\hat{\mathbf{V}}_\rho(\mathbf{q})=V_\rho(\mathbf{q})-V_\rho(q_c^2)\ . \quad (4.50)$$

This is the regularized form of the ρ-meson exchange potential.

The short-range correlations strongly affect the central force but affect only slightly the tensor force. This is due to the fact that the latter acts only in a relative D state, where the centrifugal barrier keeps the two nucleons apart. Thus the correlation function can be omitted in this case. The central interaction, on the other hand, is roughly shifted by a constant in momentum space, since the short-range correlations effectively correspond to a short-range interaction. Including the effect of the correlation function we can, to a good approximation, write for the central part of the $V^C_{\sigma\tau}$ interaction

$$V^C_{\sigma\tau}(q)\approx-\int\frac{d^3k}{(2\pi)^3}g(\mathbf{k}-\mathbf{q})\times\left[J_\pi(0,q)\frac{m_\pi^2}{q^2+m_\pi^2}+2J_\rho(0,q)\frac{m_\rho^2}{q^2+m_\rho^2}\right]\boldsymbol{\sigma}_1\cdot\boldsymbol{\sigma}_2\boldsymbol{\tau}_1\cdot\boldsymbol{\tau}_2 \quad (4.51)$$

and for the tensor part

$$V^T_\tau(\mathbf{q})\approx-\tfrac{1}{3}\left[J_\pi(0,q)\frac{q^2}{q^2+m_\pi^2}-J_\rho(0,q)\frac{q^2}{q^2+m_\rho^2}\right]S_{12}(\hat{\mathbf{q}})\boldsymbol{\tau}_1\cdot\boldsymbol{\tau}_2\ . \quad (4.52)$$

It is important to notice that the tensor force contributions of the π- and ρ-meson exchange in Eq. (4.52) have opposite signs. The pionic tensor force is attractive, while that of the ρ meson is repulsive. Both force components tend to cancel each other at large-momentum transfers. This is interesting, since in this way the ρ-meson exchange provides a natural regularization of the otherwise pathologically strong, attractive tensor force of the one-pion exchange at small distances.

A comparison between the results of the correlated $\pi+\rho$ model and the free $t^C_{\sigma\tau}$ interaction at $E_p=140$ MeV has been performed by Petrovich *et al.* (1983). These authors find good agreement between both interactions if the $\pi+\rho$ interaction is supplemented by a contact term of strength 120 MeV fm^3. Petrovich *et al.* also performed the spin-longitudinal/spin-transverse decomposition of the interaction using the interaction representation of Eq. (4.31) as a basis.

The isovector interaction V^C_τ in Fig. 15 shows a strong energy dependence. The force is large and repulsive at small energies ($E_p\leq 50$ MeV) and drops rapidly with increasing E_p. This behavior has been qualitatively explained by Brown *et al.* (1981). These authors argue that since there is no meson that couples directly to the isovector degrees of freedom, the V^C_τ interaction has to come from higher-order meson-exchange processes. Brown *et al.* consider the π- and ρ-meson exchange in second-order perturbation theory, showing that the second-order terms already give the experimentally observed energy dependence of the V^C_τ interaction.

D. The isovector spin-flip and non-spin-flip excitations

With the form of the effective interaction as given in Eq. (4.38) we can now construct the transition potentials for isovector spin-flip ($S=1$, $T=1$) and non-spin-flip ($S=0$, $T=1$) transitions. We again assume that the knockout exchange terms can be incorporated into the formulation via a short-range approximation (Petrovich *et al.*, 1969). Then the effective projectile-target nucleon interaction is local, and only direct matrix elements have to be considered. We also neglect the isovector $\mathbf{L}\cdot\mathbf{S}$ force, which is relatively weak in comparison to the isovector central (C) and tensor (T) forces. With these simplifying assumptions we now extend the formulation of Sec. IV.B to include the nuclear-isospin and spin-isospin degrees of freedom. To start with, we expand the isovector part of V_{pj} in terms of its Fourier components,

$$V^{(\tau)}_{pj}(\mathbf{r}_p-\mathbf{r}_j)=\frac{1}{(2\pi)^3}\int d\mathbf{q}\exp[-i\mathbf{q}\cdot\mathbf{r}_p]\times[V^C_\tau(q)+V^C_{\sigma\tau}(q)\boldsymbol{\sigma}_p\cdot\boldsymbol{\sigma}_j-V^T_\tau(q)S_{pj}(\hat{\mathbf{q}})]\times\exp[i\mathbf{q}\cdot\mathbf{r}_j]\boldsymbol{\tau}_1\cdot\boldsymbol{\tau}_j\ , \quad (4.53)$$

where the tensor operator S_{pj} is defined by

$$S_{pj}=\boldsymbol{\sigma}_p\cdot[3\hat{\mathbf{q}}\hat{\mathbf{q}}-I]\cdot\boldsymbol{\sigma}_j\ ,\quad \hat{\mathbf{q}}=\frac{\mathbf{q}}{q} \quad (4.54)$$

with the unit tensor I. The interaction in Eq. (4.53) is written as a product of two one-body operators, one of which acts in the space of the projectile while the other acts in the space of the target. To the three force components there correspond three different target transition potentials. They can be expressed in terms of the isospin (τ) and spin-isospin ($\sigma\tau$) transition densities (Love *et al.*, 1987),

$$\rho^{(\tau)}_{I_fI_i}(\mathbf{q})=\langle I_fM_f|\sum_{j=1}^{A}\exp[i\mathbf{q}\cdot\mathbf{r}_j]\boldsymbol{\tau}_j|I_iM_i\rangle\ , \quad (4.55)$$

$$\rho^{(\sigma\tau)}_{I_fI_i}(\mathbf{q})=\langle I_fM_f|\sum_{j=1}^{A}\exp[i\mathbf{q}\cdot\mathbf{r}_j]\boldsymbol{\sigma}_j\boldsymbol{\tau}_j|I_iM_i\rangle\ , \quad (4.56)$$

as

$$U^{(\tau)}_{I_fI_i}(\mathbf{q})=V^C_\tau(q)\rho^{(\tau)}_{I_fI_i}(q)\ ,\quad S=0\ , \tag{4.57}$$

$$U^{(\sigma\tau)}_{I_fI_i}(\mathbf{q})=V^C_{\sigma\tau}(q)\rho^{(\sigma\tau)}_{I_fI_i}(\mathbf{q})\ ,\quad S=1\ , \tag{4.58}$$

$$U^{(T)}_{I_fI_i}(\mathbf{q})=V^T_{\sigma\tau}(\mathbf{q})\rho^{(\sigma\tau)}_{I_fI_i}(\mathbf{r})\ ,\quad S=1\ , \tag{4.59}$$

where $V^T_{\sigma\tau}(\mathbf{q})=V^T_\tau(q)(3\hat{\mathbf{q}}\hat{\mathbf{q}}-I)$. It is understood that in Eqs. (4.55) and (4.56) the isospin matrix elements are carried out. This is not indicated explicitly in order to keep the notation simple. Equations (4.55), (4.56), (4.57), and (4.58) represent the extensions of Eqs. (4.14) and (4.16) to include the isospin and spin-isospin degrees of freedom. As in the nuclear structure part, we also have to modify the nuclear reaction part, where we have now to consider the matrix elements of the isospin (τ_p) and spin-isospin ($\sigma_p\tau_p$) operators in the projectile distortion function of Eq. (4.15).

For the consideration of spin observables it is convenient to write the spin-dependent interaction terms of Eq. (4.53) in the longitudinal transverse representation. Using Eqs. (4.32) and (4.54) one easily derives (Love *et al.*, 1987)

$$V^{(\tau)}_{pj}(\mathbf{q})=[V^C_\tau(q)+V^l_\tau(q)\boldsymbol{\sigma}_p\cdot\hat{\mathbf{q}}\boldsymbol{\sigma}_j\cdot\hat{\mathbf{q}} + V^t_\tau(q)(\boldsymbol{\sigma}_p\times\hat{\mathbf{q}})\cdot(\boldsymbol{\sigma}_j\times\hat{\mathbf{q}})]\boldsymbol{\tau}_p\cdot\boldsymbol{\tau}_j\ , \tag{4.60}$$

where V^l_τ and V^t_τ are the spin-longitudinal (l) and spin-transverse (t) isovector components of the interaction:

$$\begin{aligned} V^l_\tau(q)&=V^C_{\sigma\tau}(q)-2V^T_\tau(q)\ ,\\ V^t_\tau(q)&=V^C_{\sigma\tau}(q)+V^T_\tau(q)\ . \end{aligned} \tag{4.61}$$

The corresponding longitudinal and transverse isovector-spin transition densities are defined by

$$\rho^{(l)}_{fi,\tau}(\mathbf{q})=\langle I_fM_f|\sum_{j=1}^{A}\exp[i\mathbf{q}\cdot\mathbf{r}_j]\boldsymbol{\sigma}_j\cdot\hat{\mathbf{q}}\boldsymbol{\tau}_j|I_iM_i\rangle\ , \tag{4.62}$$

$$\rho^{(t)}_{fi,\tau}(\mathbf{q})=\frac{1}{\sqrt{2}}\langle I_fM_f|\sum_{j=1}^{A}\exp[i\mathbf{q}\cdot\mathbf{r}_j]\boldsymbol{\sigma}_j\times\hat{\mathbf{q}}\boldsymbol{\tau}_j|I_iM_i\rangle\ . \tag{4.63}$$

The factor $1/\sqrt{2}$ in Eq. (4.63) has been included for convenience and accounts for the fact that there are two transverse directions, $\hat{\mathbf{n}}$ and $\hat{\mathbf{Q}}$, and only one longitudinal direction, $\hat{\mathbf{q}}$, as can be seen from Eq. (4.32). The longitudinal interaction V^l_τ induces pionlike excitations, while the transverse interaction V^t_τ arises from ρ-meson exchange in lowest-order meson theory.

From Eqs. (4.57)–(4.59) it is obvious that the momentum profiles of the different parts of the effective interaction determine which states are preferentially excited at a given momentum transfer q. At small-momentum transfers ($0\le q\le 0.5$ fm^{-1}) the force components $V^C_\tau(q)$ and $V^C_{\sigma\tau}(q)$ are large and excite the $S=0$ and $S=1$ isovector transitions, respectively. This can be seen from the momentum dependence of the interactions shown in the lower part of Fig. 15. At large-momentum transfers ($q\ge 1$ fm^{-1}) the tensor force dominates and excites only $S=1$ states.

A more detailed specification of the states that are excited at a given momentum transfer requires a multipole expansion of the effective interaction of Eq. (4.53). For that purpose we first expand the plane waves in Eq. (4.53) into partial waves and couple the orbital (L) and spin (S) angular momenta to a total angular momentum J. This leads to an expansion of V_{pj} in terms of the tensor operators

$$M_{LSJM,\mu}(q\mathbf{r},O_S)=j_L(qr)[i^LY_L(\hat{\mathbf{r}})\otimes O_S]^J_M\tau_\mu\ , \tag{4.64}$$

where $O_0=1$ and $O_1=\boldsymbol{\sigma}$. The expansion of the central part of the effective interaction is given by

$$V^C_{pj}=\frac{2}{\pi}\int_0^\infty q^2dq\sum_{LSJ}(-)^{J+S}[V^C_\tau(q)\delta_{S,0}+V^C_{\sigma\tau}(q)\delta_{S,1}] \times M_{LSJ}(p)\cdot M_{LSJ}(j)\ , \tag{4.65}$$

and that of the tensor part takes the form

$$V^T_{pj}=\frac{2}{\pi}\int_0^\infty q^2dq\sum_{LL'J}V^T_\tau(q)i^{L+L'+2} \times Z(L',L,J)M_{L'1J}(p)\cdot M_{L1J}(j)\ . \tag{4.66}$$

Here the $Z(L',L,J)$ are geometrical recoupling coefficients, which can be expressed (Love and Parish, 1970) in terms of the total angular momentum transfer J. For natural parity excitations, i.e., $\Delta\pi=(-)^J$, the only allowed value of L and L' is $L=L'=J$ with $Z(J,J,J)=1$. For unnatural parity transitions, i.e., $\Delta\pi=(-)^{J+1}$, the values of L and L' are restricted to $J\pm1$ and the corresponding coefficients assume the values $Z(J-1,J-1,J)=(J-1)/(2J+1)$, $Z(J+1,J+1,J)=(J+2)/(2J+1)$, and $Z(J-1,J+1,J)=Z(J+1,J-1,J)=3\sqrt{J(J+1)}/(2J+1)$.

From Eqs. (4.65) and (4.66) one recognizes that the nucleon-nucleus scattering induces isovector excitations in the target through the tensors of Eq. (4.64). For small-momentum transfer, that is for $qr_j<1$, we can expand the Bessel function $j_L(qr_j)$ in a Taylor series. We find that for $0^+\to J^\pi$ transitions the hadronic transition operator acting on the target is related to the usual isovector multipole operators, the lowest multipolarities of which are given by (Auerbach and Klein, 1983)

$$\sum_j M_{0000,\mu}(q\mathbf{r}_j)\to\frac{1}{\sqrt{4\pi}}\sum_j\left[1-\frac{(qr_j)^2}{6}\right]\tau_\mu(j)\ , \tag{4.67}$$

$$\sum_j M_{011M,\mu}(q\mathbf{r}_j,\boldsymbol{\sigma}_j) \to\frac{1}{\sqrt{4\pi}}\sum_j\left[1-\frac{(qr_j)^2}{6}\right]\sigma_M(j)\tau_\mu(j)\ , \tag{4.68}$$

$$\sum_j M_{101M,\mu}(q\mathbf{r}_j)\to\sum_j\frac{i}{3}(qr_j)Y_{1M}(\hat{\mathbf{r}}_j)\tau_\mu(j)\ , \tag{4.69}$$

$$\sum_j M_{11JM,\mu}(q\mathbf{r}_j,\boldsymbol{\sigma}_j)\rightarrow\sum_j\frac{i}{3}(qr_j)[Y_1(\hat{\mathbf{r}}_j)\otimes\boldsymbol{\sigma}_j]^J_M\tau_\mu(j)\ , \tag{4.70}$$

$$\sum_j M_{202M,\mu}(q\mathbf{r}_j)\rightarrow\sum_j\frac{(qr_j)^2}{15}Y_{2M}(\hat{\mathbf{r}}_j)\tau_\mu(j)\ , \tag{4.71}$$

$$\sum_j M_{21JM,\mu}(q\mathbf{r}_j,\boldsymbol{\sigma}_j)\rightarrow\sum_j\frac{(qr_j)^2}{15}[Y_2(\hat{\mathbf{r}}_j)\otimes\boldsymbol{\sigma}_j]^J_M\tau_\mu(j)\ . \tag{4.72}$$

The operator on the right-hand side of Eq. (4.67) consists of two parts: the first is proportional to the Fermi operator and the second can be recognized to be proportional to the isovector monopole transition operator. The former excites the isobaric analog state, while the latter excites the isovector monopole resonance. The operator of Eq. (4.68) has a similar structure to that in Eq. (4.67), apart from the fact that now the spin operator $\boldsymbol{\sigma}$ is involved. The first term on the right-hand side of Eq. (4.68) may be recognized as the GT operator, and the second corresponds to the spin-isovector monopole transition operator. The operators in Eqs. (4.69) and (4.70) are associated with isovector dipole transitions which involve either no spin flip (4.69) or spin flip (4.70). The spin-flip dipole transitions can have spin-parity $J^\pi=0^-$, 1^-, or 2^-, and hence, involve three collective modes. A similar spin dependence is found for the isovector quadrupole transitions listed in Eqs. (4.71) and (4.72). The spin-parities for quadrupole spin-flip modes are $J^\pi=1^+$, 2^+, and 3^+.

E. Spectroscopic applications of the (p,n) reaction at small-momentum transfers

The (p,n) reaction is a powerful spectroscopic tool for measuring the Fermi and GT strength functions of nuclei. The experimental situation of these transitions has been reviewed in Sec. III. In this subsection we show how the Fermi and GT transition matrix elements are extracted from the measured forward-angle (p,n) data.

First we notice that at high incident energies and at forward angles the nuclear states are probed at small-momentum transfers ($q\leq 0.2$ fm^{-1}). Therefore, from Fig. 15, it is obvious that only the central parts of the isovector effective interaction contribute to the cross section and that the noncentral parts can be neglected. Furthermore, because of the small q transfer, the multipole expansions of Eqs. (4.67) and (4.68) are applicable, and one may expect a simple relation between the measured 0° (p,n) cross sections and the corresponding allowed β-decay transition rates. There is only one major problem that has to be considered in the derivation of this relation, and that is the projectile distortion effect. The distortions of the projectile wave function have the effect that a range of momentum components of the nuclear transition potential, $U^{(\alpha)}_{fi}(\mathbf{q})=V^C_\alpha(\mathbf{q})\rho^{(\alpha)}_{I_fI_i}(\mathbf{q})$ $(\alpha=\tau,\sigma\tau)$, can contribute to the 0° (p,n) cross section. Therefore the factorization of the nuclear transition amplitude into a nuclear reaction part and a nuclear structure part, which is exact in the plane-wave approximation [see Eq. (4.17)], can only be fulfilled on average for the distorted-wave case. Since, however, the distortion function $D(\mathbf{k},\mathbf{k}',\mathbf{q})$ of Eq. (4.15) peaks at $q=0$ for Fermi and Gamow-Teller ($L=0$) transitions, one might expect that the distorted-wave Born-approximation (DWBA) transition amplitude of Eq. (4.13) would still approximately factorize in this case. Empirically this is indeed the case, and the 0° (p,n) cross section for Fermi and GT transitions can be approximately written as (Goodman, 1980; Goodman *et al.*, 1980; Petrovich, 1980)

$$\begin{aligned}\frac{d\sigma}{d\Omega_{\rm F}}(q\approx 0)&=\left[\frac{\mu}{\pi\hbar^2}\right]^2\frac{k_f}{k_i}N_\tau|J^{NN}_\tau|^2B(\mathrm{F},i\rightarrow f)\ ,\\ \frac{d\sigma}{d\Omega_{\rm GT}}(q\approx 0)&=\left[\frac{\mu}{\pi\hbar^2}\right]^2\frac{k_f}{k_i}N_{\sigma\tau}|J^{NN}_{\sigma\tau}|^2B(\mathrm{GT},i\rightarrow f)\ ,\end{aligned} \tag{4.73}$$

where

$$\begin{aligned}B(\mathrm{F},i\rightarrow f)&=|\langle f|T_-|i\rangle|^2\ ,\\ B(\mathrm{GT},i\rightarrow f)&=\sum_\mu|\langle f|\beta_-(\mu)|i\rangle|^2\ ,\end{aligned} \tag{4.74}$$

are the squares of the Fermi and GT transition matrix elements. In Eq. (4.73), $J^{NN}_\alpha\equiv V^C_\alpha(q=0)$ $(\alpha=\tau,\sigma\tau)$ is the volume integral of the central part of the effective interaction. N_α is the distortion factor, which summarizes the distortion effects in a single constant. In practical calculations N_α is conveniently determined by forming the cross-section ratios

$$N_\alpha=\frac{\sigma^{\rm DW}_\alpha(\theta=0°,Q_{\rm val})}{\sigma^{\rm PW}_\alpha(\theta=0°,Q_{\rm val}=0)}\ , \tag{4.75}$$

where $\sigma^{\rm DW}_\alpha$ ($\sigma^{\rm PW}_\alpha$) is the distorted-wave (plane-wave) cross section at 0° and $Q_{\rm val}$ is the Q value of the reaction. The distortion factors are usually calculated with the complete t_F matrix interaction and with inclusion of the knockout exchange amplitudes in the scattering matrix.

By selecting now F and GT transitions with B values known from β decay, one can extract the force strength ratio $|J_{\sigma\tau}/J_\tau|^2$ from a measurement of the corresponding zero-degree (p,n) cross sections. The ratio $|J_{\sigma\tau}/J_\tau|^2$ determines, to a large extent, which type of mode ($S=0$ or $S=1$) should dominate the spectrum at a given incident energy. In addition, this ratio can be directly compared with the corresponding quantity of the free t_F matrix. This is done in Fig. 16, where the energy dependence of the ratio $|J_{\sigma\tau}/J_\tau|^2$ at zero-momentum transfer is plotted. The experimental points are measurements of IUCF (○) and LAMPF (Δ and □) and TRIUMF (●). A strong energy dependence of the ratio is observed. The ratio peaks at an energy of about 300 MeV, making this a good energy for studying isovector spin excitations in nuclei. Once $|J_{\sigma\tau}/J_\tau|^2$ is known, one can use the (p,n) re-

action to determine the GT matrix elements of states that cannot be populated by β decay. In particular, it is possible to map out the whole GT response function in the 0° spectrum. There are, however, other states with multipolarities $L>0$ which also contribute to the 0° (p,n) cross section. In general, these states reach their maximum cross sections at larger scattering angles, but their angle distributions extend forward to 0°. In order also to guarantee a force-independent analysis of these states, one has to calibrate the momentum dependence of the effective projectile-target nucleon interaction. This can be done as follows: First one selects a GT transition with known B(GT) value and uses Eq. (4.73) to obtain the normalization of the effective projectile-target nucleon interaction at $q=0$. The momentum-transfer dependence of the interaction for $q>0$ is then checked by analyzing angle distributions of inelastic or charge-exchange reactions to high spin states with known nuclear structure. This calibration procedure was carried out, for instance, by Osterfeld *et al.* (1982) for the $\sigma\tau$ central and tensor components of the Love-Franey interaction. The result was that the q dependence of the interaction was found to be essentially in agreement with experiment (see also Rapaport *et al.*, 1981).

The calibration procedure has to be slightly modified if the wave functions of the nuclear states contain Δ-h components explicitly (Osterfeld *et al.*, 1985). In this case one has to fix two independent quantitites, namely, $J_{\sigma\tau}^{NN}$ and $J_{\sigma\tau}^{N\Delta}$, the latter of which is the volume integral of the effective $V_{\sigma\tau}^{N\Delta}$ interaction. But, on the other hand, one also has two known quantities, the measured B(GT) value and the measured 0° (p,n) cross section. Numerically one finds that both the B(GT) value and the 0° (p,n) cross section can be simultaneously reproduced only if the relation

$$\left|\frac{J_{\sigma\tau}^{N\Delta}}{J_{\sigma\tau}^{NN}}\right|=\frac{g_A^*}{g_A} \tag{4.76}$$

holds, where g_A^* is the axial-vector coupling constant of the Δ-isobar sector. In the quark model we have $g_A^*/g_A=\sqrt{72/25}$ (Kokkedee, 1969), while in the Chew-Low theory (Chew and Low, 1956) we have $g_A^*/g_A=2$. Equation (4.76) is an important result, since it shows that the (p,n) probe at high incident energies sees Δ's in nuclei in the same way as the weak interaction in β decay.

With the effective interaction thus calibrated, one can now start to analyze (p,n) spectra. The calibration procedure is usually carried out for the discrete transition $^{42}\mathrm{Ca}(0^+)\rightarrow{}^{42}\mathrm{Sc}(1^+,E_x=0.61\ \mathrm{MeV})$, which possesses a large B(GT) value of 2.57 and a large 0° (p,n) cross section. The same transition is also used in experiments to normalize measured zero-degree (p,n) data to β decay. The only uncertainty in going from ^{42}Ca to another target nucleus is the distortion factor, $N_{\sigma\tau}$, which changes with target. This change can be taken care of by an appropriate choice of the optical potentials. The uncertainties introduced by the choice of the optical potentials are found to be of the order of 10% (Osterfeld *et al.*, 1985).

V. NUCLEAR STRUCTURE

In this section we review the basic microscopic nuclear structure theories suitable for the description of spin and isospin excitations in nuclei. Almost all of these theories have the independent-particle model as a starting point. Here the problem of many interacting nucleons is replaced by that of noninteracting nucleons in a mean field. In this approximation the ground state of the nucleus is described by a single Slater determinant of single-particle orbitals where the energetically lowest single-particle states are occupied. Treating the single-particle potential as a dynamical quantity, one can calculate the vibrations of the nucleus around the ground-state configuration. This is the time-dependent mean-field theory or, equivalently, the random-phase approximation (RPA) theory of vibrations.

The properties of the nuclear vibrations can be most conveniently discussed in terms of the strength function. For an arbitrary one-body operator O the strength function is defined by

$$S(\omega)=\sum_f|\langle\Psi_f|O|\Psi_0\rangle|^2\delta(E_f-E_0-\omega)\ , \tag{5.1}$$

where $|\Psi_0\rangle$ and $|\Psi_f\rangle$ denote the ground (0) and final (f) nucleus eigenstates of energies E_0 and E_f. The major peaks in $S(\omega)$ are identified with the collective states. If the peaks appear in the continuum region of the spectrum they are termed giant resonances. The RPA can describe the excitation energies of the collective states as well as their transition strength, but it cannot reproduce their widths when these states appear in a region of high level density. The reason is that RPA states are only of one-particle/one-hole (1p-1h) character; the coupling to 2p-2h states, which will give rise to the spreading width, is neglected.

The mean-field approach works well for doubly-closed-shell nuclei. For its application to open-shell nuclei, one has to improve the theory by including the pairing correlations between nucleons. This is achieved in the Hartree-Fock-Bogoliubov (HFB) theory. The HFB theory treats simultaneously the long-range, field-producing forces and the short-range pairing forces in the determination of the nuclear ground-state wave function. The latter is also of determinantal structure and is the *vacuum* of the so-called Bogoliubov *quasiparticles.* The Bogoliubov quasiparticles are generalized fermions, which are represented by a linear combination of particle and hole states. They can be used to construct the quasiparticle RPA. The quasiparticle RPA provides a very useful method for the study of collective states in open-shell nuclei.

The description of the width of giant resonances requires a theory which goes beyond the 1p-1h RPA and involves higher-order configurations such as 2p-2h, 3p-3h, etc. One approach, of course, is to try to calculate the complete excitation spectrum using the shell model as a basis. This is, however, impossible in most cases, apart

from light nuclei ($A \leq 40$). Another approach is to compute the mixing of the 1p-1h states with the more complicated nearby configurations. This mixing is calculated approximately within the so-called second RPA. The second RPA considers the coupling of the 1p-1h states with the 2p-2h states, which represent the next level of complexity of nuclear states.

A. The independent-particle model

In the independent-particle model, the nucleons are assumed to move independently of one another in the mean field produced by all the particles. This motion exhibits a shell structure with the major shells spaced at energy intervals of order $\hbar\omega \approx 41\,A^{-1/3}$ MeV. The ground state of the nucleus is described by a single Slater determinant in which the energetically lowest single-particle states are occupied. The single-particle states ϕ_j are eigenfunctions of a single-particle Hamiltonian with eigenvalues ϵ_j. This Hamiltonian is written as the sum of a charge-independent and a charge-dependent term and has a discrete and continuous spectrum. The charge-independent part takes the form

$$H_{sp} = T + U(r) + V_{ls}(r)\boldsymbol{l}\cdot\mathbf{s} \ , \tag{5.2}$$

where T is the kinetic-energy operator, $U(r)$ is a local potential, and $V_{ls}(r)$ is the spin-orbit potential. The charge-dependent part of the Hamiltonian consists of the Coulomb potential $V_C(r)$ and the symmetry potential. The latter favors a nuclear configuration with an equal number of protons and neutrons and is present only for nuclei with neutron excess.

Empirically the single-particle potential $U(r)$ can be well described by a potential of Woods-Saxon form, while the spin-orbit potential V_{ls} is usually taken to be proportional to the derivative of a Woods-Saxon form. The potential parameters are determined from the requirement that the experimentally observed single-particle energies and the mean charge radius of the nucleus be reproduced. This requirement constrains the potentials quite strongly. The potential depths are usually found to depend on the single-particle energies. This reflects the fact that the self-consistently calculated mean field is nonlocal. This nonlocality can be approximately represented by using an energy-dependent effective mass instead of the free-nucleon mass in the kinetic-energy operator T. The effective mass varies from 1.0 (in units of the free-nucleon mass) for single-particle states near the Fermi surface to 0.7 for deep hole states and high-lying particle states (for a recent review of the nuclear shell model, see Mahaux *et al.*, 1985).

Starting from a microscopic many-body theory, the single-particle potential is provided by the Hartree-Fock (HF) self-consistent-field method. Using a variational principle that minimizes the ground-state energy, one extracts from the effective two-nucleon interaction v_{ij} the mean field that each of the nucleons feels due to its interaction with all the others. In configuration-space representation the HF single-particle Hamiltonian is given by

$$\begin{aligned} H_{\rm HF} &= \sum_{k,k'} \left[t_{kk'} + \sum_{j=1}^{A} \bar{v}_{kjk'j} \right] a_k^+ a_{k'} \\ &= \sum_k \epsilon_k a_k^+ a_k \ , \end{aligned} \tag{5.3}$$

where the $t_{kk'}$ denote the matrix element of the kinetic-energy operator T and $\sum_{j=1}^{A} \bar{v}_{kjk'j}$ is the self-consistent HF field. The two-body matrix elements $\bar{v}_{kjk'j} \equiv \langle kj|v|k'j-jk'\rangle$ are antisymmetrized, making the HF potential nonlocal. Moreover, the HF potential is density dependent, as can be immediately recognized from the sum over occupied single-particle orbitals j in the interaction term. This sum performs an average over all two-body interactions.

An essential ingredient in the HF theory is the effective two-nucleon interaction. In principle, this interaction should be calculated from the bare nucleon-nucleon force. The proper framework for such a calculation is the Brueckner theory, which we described in Sec. IV.C. In this theory the effective interaction appears as an infinite sum of scattering processes of two nucleons in the nuclear medium. Since the Brueckner calculations are rather involved, one usually parametrizes the effective interaction by phenomenological forces. Widely used effective interactions are the density-dependent Skyrme forces (Skyrme, 1956, 1959) and the Gogny interaction (Gogny, 1975). These interactions are very successful in reproducing the ground-state properties of many nuclei throughout the periodic table (Vautherin and Brink, 1972; Beiner *et al.*, 1975).

On the right-hand side of Eq. (5.3), the HF Hamiltonian is written in its diagonal form defining the HF single-particle energies ϵ_k and the corresponding single-particle wave functions ϕ_k. The set of ϕ_k is complete and forms the HF basis. The HF ground state of the nucleus is obtained by occupying the lowest single-particle levels up to the Fermi energy ϵ_F. The HF ground state is then used as a vacuum to set up a complete basis of many-particle wave functions. For example, one constructs one-particle/one-hole (1p-1h) excited states by promoting a particle from a state ϕ_j below the Fermi surface ($\epsilon_j \leq \epsilon_F$) to a state ϕ_m above ($\epsilon_m > \epsilon_F$). Correspondingly, one can construct 2p-2h states, 3p-3h states, etc. The set of all multiparticle-multihole states forms a complete orthogonal basis in the many-body Hilbert space. This basis is then used for further investigation of the many-body Hamiltonian, in particular for the diagonalization of the so-called residual interaction

$$V_R = \tfrac{1}{4} \sum_{kk',ll'} \bar{v}_{kk'll'} a_k^\dagger a_{k'}^\dagger a_{l'} a_l \ . \tag{5.4}$$

The residual interaction is that part of the two-body interaction not included in the HF potential.

In the independent-particle model one assumes that

the residual interaction is negligibly small. Under these circumstances the strength function of an arbitrary one-body operator O is given by

$$S(\omega)=\sum_{m,j} n_j(1-n_m)|\langle\phi_m|0|\phi_j\rangle|^2\delta(\omega+\epsilon_j-\epsilon_m)\ , \quad (5.5)$$

where $n_j=0$ or 1 is the occupancy of a given single-particle orbit j.

The strength function takes a very simple form for the Fermi and GT operators. To show this, let us consider the closed-shell nucleus ^{90}Zr. It has all shells filled up to the g orbit. Within the g orbit, only the $g_{9/2}$ neutron orbit is occupied. In this case the strength function of the Fermi operator T_- has a single peak at the excitation energy of $\omega=g^p_{9/2}-g^n_{9/2}$. The corresponding Fermi transition is schematically illustrated in Fig. 3(a). The GT operator $\beta_-(\mu)$ produces two peaks at excitation energies of $\omega_1=\epsilon^p_{9/2}-\epsilon^n_{9/2}$ and $\omega_2=\epsilon^p_{7/2}-\epsilon^n_{9/2}$, respectively [see Fig. 3(b)]. The two GT transitions differ in excitation energy by the spin-orbit splitting $\Delta\epsilon_{ls}=\epsilon^p_{7/2}-\epsilon^p_{9/2}$, the magnitude of which is determined by the spin-orbit potential V_{ls} of Eq. (5.2). In ^{90}Zr this splitting amounts to roughly 5–6 MeV for the g orbits.

If O is one of the more general multipole operators of Eqs. (4.67)–(4.72) with a spatial dependence of, say, $O(\mathbf{r})\sim r^L Y_{LM}(\hat{\mathbf{r}})$, then the single-particle response is characterized by transitions across the major shells with excitation energies of $1\hbar\omega$, $2\hbar\omega$, etc. depending on the value of L. The response for the dipole field ($L=1$), for example, concentrates almost all of its transition strength in a region around the excitation energy of $1\hbar\omega$. The quadrupole field ($L=2$) produces two groups of excitations, one at $0\hbar\omega$ associated with transitions between orbits in the open shells and the other group at $2\hbar\omega$ excitation energy, which exhausts the main part of the total transition strength. The $L=3$ and $L=4$ response functions show some concentration of strength around $1\hbar\omega$ and $3\hbar\omega$ in the former, and around $0\hbar\omega$, $2\hbar\omega$, and $4\hbar\omega$ in the latter case. For these higher multipoles, however, one observes a considerable degree of "smearing out" of the response function.

The energy integral of the strength function gives the total transition strength, which can often be expressed in terms of a sum rule. For the Fermi and GT operator these sum rules are given in Eqs. (2.20) and (2.31), respectively.

So far our discussion has been concerned with 1p-1h transitions. The collective excitations are constructed by a coherent superposition of them. For the description of these states we have to include the residual interaction. This can be done in different ways.

B. The random-phase approximation

If the target ground state can be reasonable well approximated by a single Slater determinant of single-particle orbitals, as is the case, for example, for doubly-closed-shell nuclei, then the random-phase approximation (RPA) gives a good description of the nuclear excitation spectrum. In the RPA the residual interaction of Eq. (5.4) is diagonalized within the model space of 1p-1h excitations. To derive the RPA equations we use the equation-of-motion technique (Rowe, 1968, 1970). Although this derivation has been given many times before, we collect some basic formulas here since we need them below for the discussion of the second RPA.

The equation-of-motion method starts with the observation that an excited state of the A-particle system can be formally represented by a creation operator $Q^\dagger_f$ as

$$|f\rangle=Q^\dagger_f|0\rangle\ , \quad (5.6)$$

where $Q^\dagger_f$ acts on the exact target ground state $|0\rangle$ defined by

$$Q_f|0\rangle=0 \quad \text{for all } f\ . \quad (5.7)$$

The index f labels the eigenstates of the system. From the stationary Schrödinger equation

$$H_A|f\rangle=E_f|f\rangle \quad (5.8)$$

we derive the equation of motion for $Q^\dagger_f$ in the form

$$[H_A,Q^\dagger_j]|0\rangle=(E_f-E_0)Q^\dagger_f|0\rangle=\omega_{f0}Q^\dagger_f|0\rangle\ . \quad (5.9)$$

Here $\omega_{f0}=(E_f-E_0)$ is the excitation energy of state $|f\rangle$ relative to $|0\rangle$. Multiplying Eq. (5.9) from the left with an arbitrary variation $\langle 0|\delta Q$ performed on the wave function $\langle f|$ we get

$$\langle 0|[\delta Q,[H_A,Q^\dagger_f]]|0\rangle=\omega_{f0}\langle 0|[\delta Q,Q^\dagger_f]|0\rangle\ . \quad (5.10)$$

The solution of this equation is completely equivalent to the solution of the Schrödinger equation. In general, the operator $Q^\dagger_f$ will span the complete Hilbert space of np-nh excitations. In the RPA, $Q^\dagger_f$ is truncated at the 1p-1h level

$$Q^\dagger_f=\sum_{m,i}(X^f_{mi}a^\dagger_m a_i-Y^f_{mi}a^\dagger_i a_m) \quad (5.11)$$

and the equations of motion are linearized by imposing Bose commutation relations

$$[Q_f,Q^\dagger_{f'}]=\delta_{f,f'}\ . \quad (5.12)$$

In Eq. (5.11), $a^\dagger_m$ and a_i are single-particle creation and annihilation operators, respectively, which create a particle in orbital ϕ_m above the Fermi surface and annihilate one in orbital ϕ_i below the Fermi surface. The RPA ground state is defined by $Q_f|0\rangle=0$ for all f. Now we specify the nuclear Hamiltonian H_A. We assume it to be the sum of the HF single-particle Hamiltonian of Eq. (5.3) and of the residual interaction of Eq. (5.4):

$$H_A=\sum_k \epsilon_k a^\dagger_k a_k+\tfrac{1}{4}\sum_{kk',ll'}\bar{v}_{kk'll'}a^\dagger_k a^\dagger_{k'}a_{l'}a_l\ , \quad (5.13)$$

Substituting this Hamiltonian and the RPA operator of Eq. (5.11) into Eq. (5.10), we obtain, after linearization of

the commutator [which corresponds to neglecting ground-state correlations in the evaluation of the expectation values of Eq. (5.10)], the well-known RPA equations (Brown, 1971a; Rowe, 1970; Ring and Schuck, 1980)

$$\begin{bmatrix} A_{minj} & B_{minj} \\ B^*_{minj} & A^*_{minj} \end{bmatrix} \begin{bmatrix} X^f_{nj} \\ Y^f_{nj} \end{bmatrix} = \omega_{f0} \begin{bmatrix} X^f_{mi} \\ -Y^f_{mi} \end{bmatrix} . \tag{5.14}$$

Here the matrix elements are defined by

$$A_{minj} = (\epsilon_m - \epsilon_i)\delta_{mn}\delta_{ij} + \bar{v}_{mjin} ,$$
$$B_{minj} = \bar{v}_{mnij} , \tag{5.15}$$

and the eigenvectors are normalized according to

$$\sum_{mi} |X^f_{mi}|^2 - \sum_{mi} |Y^f_{mi}|^2 = 1 . \tag{5.16}$$

The coefficients X^f_{mi} and Y^f_{mi} are the forward and backward-going p-h amplitudes. The matrix A in Eq. (5.14) is Hermitian, and the matrix B is symmetric. Since the interaction matrix elements $\bar{v}_{mjin}$ involve p-h indices only, we call this set of matrix elements the particle-hole residual interaction, $F^{\text{p-h}}$.

The p-h amplitudes X^f_{mi} and Y^f_{mi} have a direct physical meaning: Their absolute squares give the probability of finding the states $a^\dagger_m a_i|0\rangle$ and $a^\dagger_i a_m|0\rangle$ in the excited state $|f\rangle$, that is,

$$X^f_{mi} = \langle f|a^\dagger_m a_i|0\rangle ,$$
$$Y^f_{mi} = \langle f|a^\dagger_i a_m|0\rangle . \tag{5.17}$$

When we use these amplitudes the transition density of Eq. (4.11) takes the explicit form

$$\rho_{fi}(\mathbf{r}) = \sum_{mi} [X^f_{mi}\Phi^*_m(\mathbf{r})\Phi_i(\mathbf{r}) + Y^f_{mi}\Phi^*_i(\mathbf{r})\Phi_m(\mathbf{r})] . \tag{5.18}$$

The transition matrix elements of a one-body operator O acting on the target ground state are then calculated as

$$\langle f|O|0\rangle = \sum_{mi} [X^f_{mi}\langle m|O|i\rangle + Y^f_{mi}\langle i|O|m\rangle] . \tag{5.19}$$

In terms of these matrix elements the strength function of the operator O is given by

$$S(\omega) = \sum_f |\langle f|O|0\rangle|^2 \delta(\omega_{f0} - \omega) . \tag{5.20}$$

One of the important features of the RPA is that it provides a good description of the collective states. The collectivity is created by $F^{\text{p-h}}$, which causes the unperturbed p-h states, $a^\dagger_m a_i|0\rangle$ and $a^\dagger_i a_m|0\rangle$, to mix in such a way that one of the RPA solutions becomes a constructive superposition of many p-h basis states. This collective state is pushed up or down in excitation energy relative to the unperturbed p-h states depending on whether $F^{\text{p-h}}$ is repulsive or attractive (Brown and Bolsterli, 1959).

The transition probability to the collective state is, in general, large since most of the terms in the sum of Eq. (5.19) add up constructively in this case. This means that many nucleons contribute in a constructive manner to the excitation and set up a collective motion in the nucleus. A measure for the collectivity is the amount of the total sum-rule strength exhausted by a state. If this fraction is large, that is, of the order of 50% or so, then the state is termed collective. There are many other noncollective RPA solutions that are the remnants of the original p-h excitations. These states are shifted little in energy and carry much less transition strength. Some of them are of pure p-h nature.

The RPA provides a good description of the nuclear excited states as long as the backward-going amplitudes Y^f_{mi} are not too large compared with the forward-going amplitudes X^f_{mi}. The former are a measure of the ground-state correlations in $|0\rangle$, that is, in how far the true ground state deviates from a single Slater determinant due to the admixtures of 2p-2h and higher-order excitations that are produced by the residual interaction. If the Y^f_{mi} become large, then the ground-state correlations are also large and the RPA becomes questionable. If the ground-state correlations are neglected, the RPA reduces to the Tamm-Dancoff approximation.

C. The RPA with explicit Δ-isobar degrees of freedom

For applications at low energies, the RPA can be easily extended to include Δ-isobar degrees of freedom. In these calculations the Δ_{33} resonance is treated as a stable particle with spin $s=\frac{3}{2}$, isospin $t=\frac{3}{2}$, and mass $m_\Delta = 1232$ MeV. The fermion operators of the nucleonic sector $a^\dagger_N$ are supplemented by corresponding fermion operators $a^\dagger_\Delta$ in the isobaric sector. The fermion anticommutators are generalized to $\{a_N, a^\dagger_\Delta\} = 0$; i.e., if the operators refer to different intrinsic states of the nucleon, they commute. The Hamiltonian describing a nucleus composed of nucleons and Δ's formally resembles the purely nucleonic Hamiltonian of Eq. (5.13). The matrix elements have to be reinterpreted, however. In particular, one has to consider the Δ-nucleon mass difference in the kinetic-energy operator and one has to replace the matrix elements of the residual interaction by the corresponding NΔ and ΔΔ transition potentials, respectively.

The RPA equations (5.14) are now diagonalized in an extended model space including p-h and Δ-h configurations. The generalized RPA wave functions are given by

$$|f\rangle = \sum_{mi} [X^f_{N,mi} a^\dagger_{N,m} a_{N,i} - Y^f_{N,mi} a^\dagger_{N,i} a_{N,m}]|0\rangle + \sum_{mi} [X^f_{\Delta,mi} a^\dagger_{\Delta,m} a_{N,i} - Y^f_{\Delta,mi} a^\dagger_{N,i} a_{\Delta,m}]|0\rangle . \tag{5.21}$$

The amount of Δ-h admixtures in the wave function depends sensitively on the coupling strength of the residual interaction between Δ-h states and p-h states. The properties of this interaction will be discussed in Sec. V.F.4. The effect of the generalized RPA wave functions produced in the analysis of (p,n) data will be shown in Sec. VI.

D. The quasiparticle random-phase approximation

For nuclei away from closed shells the pairing correlations become so important that they have to be explicitly included in the evaluation of the nuclear properties. In order to include pairing one has first to improve the ground-state wave function. This is done in the BCS theory (Bardeen, Cooper, Schrieffer, 1957), which was first applied to nuclei by Bohr, Mottelson, and Pines (1958) and Belyaev (1959). The self-consistent version of the BCS theory is the Hartree-Fock-Bogoliubov (HFB) theory (Bogoliubov, 1959a, 1959b). In the HFB theory one determines the most general wave function of independently moving quasiparticles by minimizing the ground-state energy simultaneously with respect to the long-ranged Hartree-Fock field and the short-ranged, attractive pairing field.

In order to determine the BCS ground state it is convenient to introduce the so-called Bogoliubov quasiparticles (Bogoliubov, 1958; Valatin, 1961). They can be represented by a set of quasiparticle creation and annihilation operators which are linear combinations of the particle and hole operators of Sec. V.A.:

$$\begin{aligned} &\alpha_k^\dagger = v_k a_k^\dagger - v_k a_{\bar{k}} \ , \quad \alpha_k = u_k a_k - v_k a_{\bar{k}}^\dagger \\ &\alpha_{\bar{k}}^\dagger = u_k a_{\bar{k}}^\dagger + v_k a_k \ , \quad \alpha_{\bar{k}} = u_k c_{\bar{k}} + v_k a_{\bar{k}}^\dagger \ . \end{aligned} \tag{5.22}$$

Here $|\bar{k}\rangle$ is the time-reversed state of $|k\rangle$, and v_k^2 and u_k^2 represent the probability that a certain pair state $(k,\bar{k})$ is or is not occupied. These probabilities are determined from the condition that the ground-state energy be minimized. The BCS ground state is defined by

$$\alpha_k|0\rangle = 0 \quad \text{for all } k \ . \tag{5.23}$$

For even-even nuclei the ground-state wave function has the explicit form

$$|0\rangle = \prod_{k>0} (u_k + v_k \alpha_k^\dagger a_{\bar{k}}^\dagger)|\rangle \ , \tag{5.24}$$

where $|\rangle$ is the bare vacuum. It is obvious that this wave function has no definite particle number. The norm of the ground state requires $v_k^2 + u_k^2 = 1$. The parameters u_k and v_k are determined by variation of the energy. This variation is restricted to the subsidiary condition that the expectation value of the particle number operator $\hat{N}$ have on average the value $A = 2\sum_{k>0} v_k^2$. This is achieved by adding the term $-\lambda\hat{N}$ to the Hamiltonian, where λ is a Lagrange multiplier that is adjusted to fulfill the desired condition.

The minimization of $\langle 0|H - \lambda\hat{N}|0\rangle$ leads then to the BCS equations, which can be summarized by the following set of equations (see Ring and Schuck, 1980):

$$E_k = [(\epsilon_k - \lambda)^2 + \Delta_k^2]^{1/2} \ , \tag{5.25}$$

$$\Delta_k = -\sum_{k'>0} \bar{v}_{k\bar{k}k'\bar{k}'} u_{k'} v_{k'} \ , \tag{5.26}$$

$$\begin{aligned} v_k^2 &= \frac{1}{2}\left[1 - \frac{(\epsilon_k - \lambda)}{\sqrt{(\epsilon_k - \lambda)^2 + \Delta_k^2}}\right] , \\ u_k^2 &= \frac{1}{2}\left[1 + \frac{(\epsilon_k - \lambda)}{\sqrt{(\epsilon_k - \lambda)^2 + \Delta_k^2}}\right] , \end{aligned} \tag{5.27}$$

$$u_k^2 + v_k^2 = 1 \ . \tag{5.28}$$

Here E_k is the quasiparticle energy of state k and Δ_k is the gap parameter, which is a measure for the pairing strength between the nucleons. Insertion of the u_k's and v_k's of Eq. (5.27) into Eq. (5.26) results in the gap equation, which is a nonlinear equation in Δ_k. It has only a nonvanishing solution if the pairing force is larger than a certain critical value.

The HFB quasiparticles can now be used to generate the quasiparticle RPA. For that purpose we define in analogy to Eq. (5.11) the excitation operator

$$Q_f^\dagger = \sum_{k>k'} (X_{kk'}^f \alpha_k^\dagger \alpha_{k'}^\dagger - Y_{k'k}^f \alpha_{k'} \alpha_k) \tag{5.29}$$

with

$$Q_f|0\rangle = 0 \quad \text{for all } f \ . \tag{5.30}$$

By inserting $Q_f^\dagger$ into Eq. (5.10) we find—in analogy to the derivation of the RPA equations in Sec. V.B—the quasiparticle RPA equations (Baranger, 1960; Belyaev, 1965), whose matrix form is similar to that of Eq. (5.14). The main difference is that in the quasiparticle RPA there appear also particle-particle (p-p) matrix elements besides the usual p-h matrix elements of the RPA. The appearance of p-p matrix elements can be immediately understood from the structure of the quasiparticle operators of Eq. (5.22) and the excitation operators of Eq. (5.29). Thus one needs two sets of residual interactions for a description of the excitation spectrum of superfluid nuclei: a p-h interaction and a p-p interaction. In Sec. V.I we shall discuss the application of the quasiparticle RPA to the charge-changing reactions.

E. Beyond the RPA

While the RPA gives a good description of the excitation energies, and the transition strengths of the major peaks of the response function, it fails to reproduce the details of the response function, such as the widths and the fine structure of the giant resonances. The RPA energies are discrete as long as only bound or quasibound single-particle states are considered. In the so-called continuum RPA (Krewald *et al.*, 1974; Bertsch and Tsai, 1975) the widths of the single-particle states in the con-

tinuum are included. In this case the RPA equations go over into a set of coupled integral equations (Bertsch and Tsai, 1975). This formulation considers the escape width $\Gamma^{\uparrow}$ of the excited states, i.e., the possibility that one particle can escape from the excited nucleus into the continuum. However, the escape width is, in general, only a small fraction of the total width of a giant resonance state. In order to explain the full width and the fine structure of giant resonances one has to include spreading effects which are due to the mixing of the 1p-1h RPA states with more complicated nuclear configurations. Since the nuclear Hamiltonian contains only one-body and two-body operators, an initially excited 1p-1h state can mix directly only with 2p-2h states. Therefore, for a description of the spreading width it is sufficient to evaluate the mixing of the 1p-1h states with the 2p-2h states. The 2p-2h states mix with still more complicated configurations.

A problem in the calculation of the spreading width is the appropriate choice of the 2p-2h states: i.e., whether they are chosen to be two-phonon states, which include collective effects (Soloviev *et al.*, 1977, 1980; Soloviev, 1987), or whether they can be assumed to be uncorrelated 2p-2h excitations. Which of the two possibilities is the better choice depends mainly on the excitation energy of the mode considered. At low excitation energies the important degrees of freedom are the surface vibrations, and the collective modes will decay by exciting them (Bertsch *et al.*, 1983). Then the two-phonon model (Soloviev *et al.*, 1977, 1980) is appropriate for the description of the damping. At higher excitation energies, however, the level density of the 2p-2h states is very large and all 2p-2h states will contribute to the damping. Therefore all 2p-2h states have to be considered in the calculations. This is possible in the so-called second RPA formulation (Sawicki, 1962; Yannouleas *et al.*, 1983; Drożdż *et al.*, 1986a, 1986b; Yannouleas and Jang, 1986; Wambach, 1988; Drożdż *et al.*, 1990).

In the second RPA the excitation operator of Eq. (5.11) is extended to include 2p-2h excitations, such that

$$Q_f^{\dagger}=\sum_{p,h}(X_{ph}^f a_p^{\dagger}a_h - Y_{ph}^f a_h^{\dagger}a_p) + \sum_{\substack{p_1<p_2\\ h_1<h_2}}(X_{p_1p_2h_1h_2}^f a_{p_1}^{\dagger}a_{p_2}^{\dagger}a_{h_2}a_{h_1} - Y_{p_1p_2h_1h_2}^f a_{h_1}^{\dagger}a_{h_2}^{\dagger}a_{p_2}a_{p_1}) . \tag{5.31}$$

This sum of operators represents the only possible combination of two- and four-fermion operators which creates an excited state orthogonal to the ground state. Inserting $Q_f^{\dagger}$ into the equation of motion (5.10), and performing the variation with respect to the individual expansion coefficients, one obtains the second RPA equations, which formally resemble the usual RPA equations of Eq. (5.14). In the second RPA, however, the matrices A and B of Eq. (5.14) become supermatrices which involve, besides the 1p-1h matrix elements $A_{php'h'}$ and $B_{php'h'}$, the matrix elements $A_{p_1p_2h_1h_2p'h'}$ and $A_{p_1p_2h_1h_2p'_1p'_2h'_1h'_2}$, which describe the coupling of 1p-1h to 2p-2h states and the mixing between 2p-2h states, respectively. It can be shown that as a consequence of the Bose commutation relations (5.12) we have $B_{p_1p_2h_1h_2p'h'}=B_{p_1p_2h_1h_2p'_1p'_2h'_1h'_2}=0$.

Because of the large number of 2p-2h states needed to correctly describe the damping in heavy nuclei, the second RPA equations have a very large dimension. Therefore these matrices cannot be diagonalized as they stand. Since the external field, however, excites only the 1p-1h components of the wave function, only the projected solution of the second RPA equation onto the 1p-1h subspace is needed. The projected solutions obey the RPA equation (5.14), but with a matrix $\tilde{A}(\omega)$ which is now complex and energy (ω) dependent. The matrix $\tilde{A}(\omega)$ has the explicit form (Drożdż *et al.*, 1986a, 1986b)

$$\tilde{A}_{php'h'}(\omega)=A_{php'h'}+\sum_{\substack{p_1<p_2,h_1<h_2\\ p'_1<p'_2,h'_1<h'_2}} A_{php_1p_2h_1h_2}(\omega+i\eta-A_{p_1p_2h_1h_2p'_1p'_2h'_1h'_2})^{-1}A_{p'_1p'_2h'_1h'_2p'h'} , \tag{5.32}$$

where $\eta\to 0$ is an infinitesimal quantity. The imaginary part of $\tilde{A}(\omega)$ gives the spreading width as

$$\Gamma^{\downarrow}_{php'h'}(\omega)=-2\,\mathrm{Im}\,\tilde{A}_{php'h'}(\omega) , \tag{5.33}$$

which is a matrix in the p-h indices. Transforming to a basis in which the interaction in the 2p-2h subspace becomes diagonal with eigenenergies ω_2, the width of a state $|f\rangle$ can be expressed as

$$\Gamma^{\downarrow}_f(\omega_{f0})=2\pi\sum_2 |A_{f2}|^2\delta(\omega_{f0}-\omega_2) \tag{5.34}$$

where

$$A_{f2}=\sum_{ph}(X_{ph}^f+Y_{ph}^f)A_{ph,2} . \tag{5.35}$$

The spreading width of Eq. (5.34) has exactly the form expected from Fermi's golden rule.

The diagrams corresponding to the various decay modes of the state $|f\rangle$ are given in Fig. 17 (From Drożdż *et al.*, 1990). It is instructive to consider these diagrams to lowest order in the residual interaction v as shown in the lower part of Fig. 17. Diagrams of type (a) and (c) involve self-energy insertions on the particle and hole lines, which are closely related to the imaginary part of the optical potential. The last two diagrams, (e) and (f), correspond to medium polarization graphs where a particle and a hole interact via the polarization of the medium. This gives a screening correction to the interaction in the p-h channel, similar to the screening of the Coulomb in-

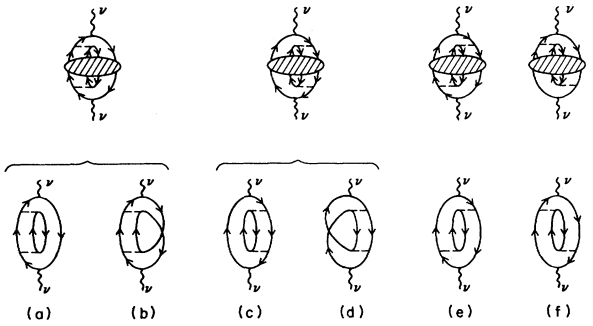

FIG. 17. RPA self-energy in lowest-order approximation. Diagrams (a) and (c) are self-energy insertions on the particle and hole line; diagrams (b) and (d) are particle-particle (p-p) and hole-hole (h-h) interactions; diagrams (e) and (f) correspond to polarization graphs in the crossed channel. From Drożdż *et al.* (1990).

teraction in an electron gas. There also appear p-p and h-h linked diagrams [ladder diagrams (b) and (d)], which renormalize the residual interaction in the p-p channel. In the evaluation of the width, all these decay amplitudes are added coherently and are then squared. Depending on the quantum numbers of the decaying state, important interference effects can occur between the various decay components, leading especially to a narrowing of the width in the case of the scalar-isoscalar ($S=0$, $T=0$) modes. In this case the diagrams (a) and (c) are largely canceled by (e) and (f) (Bertsch *et al.*, 1983; Wambach, 1988). For all other spin and isospin modes, the interference shows fewer coherence effects, making the width of these states large.

F. The residual p-h interaction

The various RPA calculations differ in the choice of the single-particle Hamiltonian and in the choice of $F^{\text{p-h}}$. In the so-called shell-model RPA one starts from the independent-particle model Hamiltonian of Eq. (5.2) and parametrizes $F^{\text{p-h}}$ in a phenomenological way. The most often used phenomenological interactions are the separable multipole-multipole force of Bohr and Mottelson (1975) and the density-dependent Landau-Migdal interaction (Migdal, 1967). In the following we shall discuss the Landau-Migdal interaction in some detail, especially because it has been extended by Migdal (1972) to include one-pion exchange and by Baym and Brown (1975) to include one-rho exchange. These extensions introduce a strong momentum dependence in the $\sigma\tau$ channel. Detailed studies of the magnetic properties of light and heavy nuclei with this generalized interaction support this strong momentum dependence (Speth *et al.*, 1980).

1. The Landau-Migdal interaction

Because of the symmetry properties of nuclear forces, $F^{\text{p-h}}$ can be written in the general form

$$\begin{aligned} F^{\text{p-h}}(\mathbf{r}_1,\mathbf{r}_2)=[\,&V_0^{\text{p-h}}(\mathbf{r}_1,\mathbf{r}_2)+V_\tau^{\text{p-h}}(\mathbf{r}_1,\mathbf{r}_2)\boldsymbol{\tau}_1\cdot\boldsymbol{\tau}_2 \\ &+V_\sigma^{\text{p-h}}(\mathbf{r}_1,\mathbf{r}_2)\boldsymbol{\sigma}_1\cdot\boldsymbol{\sigma}_2 \\ &+V_{\sigma\tau}^{\text{p-h}}(\mathbf{r}_1,\mathbf{r}_2)\boldsymbol{\sigma}_1\cdot\boldsymbol{\sigma}_2\boldsymbol{\tau}_1\cdot\boldsymbol{\tau}_2 \\ &+\text{tensor terms}+\cdots\,], \end{aligned} \tag{5.36}$$

where the dependence of the interaction on spin and isospin has been made explicit. Since the microscopic calculation of $F^{\text{p-h}}$ is very involved, one usually introduces phenomenological interactions. In the following we discuss the Landau-Migdal interaction. This interaction was originally developed by Landau (1956, 1957, 1959) in the context of Fermi-liquid theory and later applied to finite nuclei by Migdal (1967). In the Landau-Migdal theory the nucleons on the Fermi surface are considered as weakly interacting quasiparticles. A quasiparticle can be thought of as a nucleon (or nucleon hole) which has surrounded itself with a polarization cloud of nucleon particle-nucleon hole excitations. This so-called "dressed" nucleon behaves like a particle with an effective mass m^*. Starting from the ground state of an even-even nucleus, the quasiparticles are defined as the low-lying single-particle or single-hole excitations in the neighboring odd-mass nuclei. The excited states in the even-even system are then constructed from a superposition of quasiparticle-quasihole states.

Landau originally defined the quasiparticle interaction for an infinite medium like symmetric nulcear matter. In this case the quasiparticle states are represented by plane waves $|\mathbf{k}\rangle$. Landau showed that for small excitations close to the Fermi surface the excitation energy of the interacting system can be expressed as a functional of the quasiparticle occupation numbers $n(\mathbf{k})$:

$$\begin{aligned} \delta E=&\sum_k \epsilon^0(\mathbf{k})\delta n(\mathbf{k}) \\ &+\tfrac{1}{2}\sum_{\mathbf{k}_1\mathbf{k}_2} F^{\text{p-h}}(\mathbf{k}_1,\mathbf{k}_2)\delta n(\mathbf{k}_1)\delta n(\mathbf{k}_2)\,. \end{aligned} \tag{5.37}$$

Here $\epsilon^0(\mathbf{k})$ is the quasiparticle energy, and $F^{\text{p-h}}(\mathbf{k}_1,\mathbf{k}_2)$ is the interaction between a quasiparticle and a quasihole. The variation $\delta n(\mathbf{k})$ represents the deviation of the occupation numbers of the interacting system from the sharp Fermi distribution function of the noninteracting system.

According to Eq. (5.37), the p-h interacting has to be identified with the second derivative of the energy functional with respect to the occupation numbers:

$$F^{\text{p-h}}(\mathbf{k}_1,\mathbf{k}_2)=\frac{\delta^2 E}{\delta n(\mathbf{k}_1)\delta n(\mathbf{k}_2)}\,. \tag{5.38}$$

For isospin-symmetric nuclear matter, $F^{\text{p-h}}$ has the explicit form

$$\begin{aligned} F^{\text{p-h}}(\mathbf{k}_1,\mathbf{k}_2)=&F(\mathbf{k}_1,\mathbf{k}_2)+F'(\mathbf{k}_1,\mathbf{k}_2)\boldsymbol{\tau}_1\cdot\boldsymbol{\tau}_2 \\ &+G(\mathbf{k}_1,\mathbf{k}_2)\boldsymbol{\sigma}_1\cdot\boldsymbol{\sigma}_2 \\ &+G'(\mathbf{k}_1,\mathbf{k}_2)\boldsymbol{\sigma}_1\cdot\boldsymbol{\sigma}_2\boldsymbol{\tau}_1\cdot\boldsymbol{\tau}_2\,. \end{aligned} \tag{5.39}$$

For small excitations near the Fermi surface, $F^{\text{p-h}}$ describes the forward scattering of a particle and a hole in the limit of vanishing energy and momentum transfer ($\omega \to 0$, $q \to 0$). This is the so-called Landau limit. In this limit the quasiparticle momenta $\mathbf{k}_1$ and $\mathbf{k}_2$ are close to the Fermi momentum, so that $|\mathbf{k}_1| \simeq \mathbf{k}_F$ and $|\mathbf{k}_2| \simeq k_F$. Hence the interaction depends only on the so-called Landau angle θ_L between $\mathbf{k}_1$ and $\mathbf{k}_2$. Expanding in terms of Legendre polynomials we obtain for the first interaction component of Eq. (5.39)

$$F(\mathbf{k}_1,\mathbf{k}_2)=\sum_l F_l P_l(\cos\theta_L) \ . \tag{5.40}$$

The expansion coefficients F_l are called Landau parameters. It is customary to introduce dimensionless quantities

$$f_l = C_0^{-1} F_l \ , \tag{5.41}$$

where

$$C_0^{-1} = \frac{dN}{d\epsilon_F} = \frac{g}{2\pi^2}\frac{m^* k_F}{\hbar^2} \tag{5.42}$$

is the density of states at the Fermi surface per unit energy and unit volume, and m^* is the effective mass of the quasiparticle. The factor g in Eq. (5.42) denotes the spin-isospin degeneracy of states, which amounts to 4 for symmetric nuclear matter. Using $k_F = 1.36\ \text{fm}^{-1}$ and the bare nucleon mass, we obtain $C_0 = 151\ \text{MeV fm}^3$. In the literature there exist other choices for the normalization constant C_0. The Jülich group, for instance, uses the spin-degeneracy factor $g=2$, which leads to $C_0 = 302$ MeV fm^3. Sometimes also slightly different values of m^* are used. Another unit is the so-called pionic unit, which expresses the force strength in units of $J_\pi = 4\pi f_{\pi NN}^2 / m_\pi^2 = 392$ MeV fm^3.

For a short-range interaction only the first few terms in the Legendre expansion of Eq. (5.40) will be significant. For a zero-range interaction only the $l=0$ term is important. In this limit we obtain

$$\begin{aligned} F^{\text{p-h}}(\mathbf{k}_1,\mathbf{k}_2) = C_0 (f_0 + f_0' \boldsymbol{\tau}_1\cdot\boldsymbol{\tau}_2 + g_0 \boldsymbol{\sigma}_1\cdot\boldsymbol{\sigma}_2 \\ + g_0' \boldsymbol{\sigma}_1\cdot\boldsymbol{\sigma}_2 \boldsymbol{\tau}_1\cdot\boldsymbol{\tau}_2) \ , \end{aligned} \tag{5.43}$$

where f_0, f_0', g_0 and g_0' are the four zero-order Landau parameters. In Midgal's (1967) extension of this interaction to finite nuclei, the Landau parameters become density dependent. Only the non-spin-flip terms f_0 and f_0' are found to show a strong density dependence (Ring and Speth, 1974; Speth *et al.*, 1977).

According to Landau's ansatz, the p-h interaction of Eq. (5.43) is an effective force, which acts only between p-h states and which does not have to be antisymmetrized. The influence of the more complicated nuclear configurations as well as the exchange contributions to the matrix elements are assumed to be incorporated into the Landau-Migdal parameters. The parameters are adjusted to experimental data, such as the excitation energies and transition strengths of the collective states and the electromagnetic moments and transition probabilities of odd-A nuclei. This adjustment is a sensible procedure, since the various types of collective states are selectively sensitive to specific interaction terms. For example, the excitation energies of the electric isoscalar modes associated with nuclear shape vibrations depend strongly on the attractive interaction term f_0, while those of the electric isovector modes associated with neutron-proton polarization oscillations are related to the repulsive interaction term f_0'. Similarly, the spin excitations are governed by the spin-dependent interaction parameters g_0 and g_0'.

2. The $\pi+\rho+g_0'$ model

Despite its simple structure, the Landau interaction performs very well in correlating the properties of collective nuclear excitations both in light and in heavy nuclei. Its success is due to the fact that most collective states are sensitive only to the small-momentum-transfer behavior of the interaction. In particular, many natural parity non-spin-flip states as, for example, the electric giant resonances, can be well described by the Landau-Migdal interaction (For reviews see Speth and van der Woude, 1981; Goeke and Speth, 1982). For magnetic or spin-flip transitions, however, a zero-range interaction is too simple, since the pion and the ρ meson play a significant role there. Because of its small mass the pion introduces a strong momentum dependence into the p-h interaction. Moreover, it provides a tensor interaction which turns out to be very attractive at large-momentum transfers, $q \sim 2\ \text{fm}^{-1}$. This fact was first recognized by Migdal (1972, 1978, 1979) in his discussion of pion condensates. The attraction of the tensor force of the pion is partly balanced by the tensor force of the ρ meson, which is repulsive (Baym and Brown, 1975). A sensible $F^{\text{p-h}}$ in the $\sigma\tau$ channel should therefore include the π- and ρ-meson exchange potentials. These potentials alone, however, cannot describe the short-range behavior of the p-h interaction, since they vanish for small-momentum transfers. The short-range behavior is characterized by the Landau-Migdal parameter g_0', which has to be extracted from experiment. A semimicroscopic method of introducing short-range terms into the p-h interactions is to fold the π and ρ exchange potentials into the correlation function $g(r)$ of Eq. (4.48). One finds that this correlation function accounts for a large fraction (72%) of the empirical g_0' value. But still a phenomenological correction term has to be added to the correlated π and ρ exchange potentials in order to reproduce the experimental data. This correction term is usually assumed to be of zero-range form, involving a parameter $\delta g_0'$. Thus most models for the residual p-h interaction in the $\sigma\tau$ channel have the form

$$\begin{aligned} F^{\text{p-h}}(\mathbf{r}_1,\mathbf{r}_2) = \hat{V}_\pi(\mathbf{r}_1,\mathbf{r}_2) + \hat{V}_\rho(\mathbf{r}_1,\mathbf{r}_2) \\ + \delta g_0' C_0 \boldsymbol{\sigma}_1\cdot\boldsymbol{\sigma}_2 \boldsymbol{\tau}_1\cdot\boldsymbol{\tau}_2 \ . \end{aligned} \tag{5.44}$$

As previously mentioned, for the zero-range term only direct matrix elements are calculated, while for the finite-range part of the force both direct and exchange matrix elements have to be considered. Several p-h interactions with π- and ρ-meson exchange have been constructed, for example, by the Jülich-Stony Brook group (Speth *et al.*, 1980; Nakayama *et al.*, 1984; Krewald *et al.*, 1988). There are other residual interactions which consider either only the π exchange plus a short-range Landau-Migdal term (Meyer-ter-Vehn, 1981) or the full one-boson exchange potential including π, ρ, σ, and ω exchange (Towner and Khanna, 1983; see also Arima *et al.*, 1983; Towner, 1987). In all cases a Landau-Migdal parameter has to be added to the finite-range interaction in order to reproduce the empirical spin-isospin properties of nuclei. Complete Brueckner G-matrix calculations show a very similar behavior in the $\sigma\tau$ channel to that of the phenomenological interactions (Dickhoff *et al.*, 1983; Nakayama *et al.*, 1984).

The $\sigma\tau$ interaction is strongly repulsive at small-momentum transfers. With increasing momentum transfer q, however, the interaction decreases rapidly and vanishes around $q=2.5$ fm^{-1}. The small-momentum transfer behavior of the interaction is well tested by the energetics of the GT resonance, which is pushed up in excitation energy. The energy shift is very sensitive to the repulsion of $F^{\text{p-h}}$ at small q. In order to test the high-momentum transfer behavior of $F^{\text{p-h}}$, one has to consider magnetic excitations of high multipolarities ($J^{\pi}\geq 2^{-}$). These states have transition densities peaking at large-momentum transfers ($q\sim 1$–2 fm^{-1}). Although these states are not very collective, one may deduce from their energetics that the residual p-h interaction is weak in this momentum-transfer region. For a more detailed discussion of this point, see Krewald and Speth (1980), Speth *et al.* (1984), and Krewald *et al.*, 1988.

3. The effective G-matrix interaction and the medium polarization

There have been various attempts to calculate the Landau parameters microscopically starting from the Brueckner G matrix. Pioneering work in this field was performed by Brown (1971b), who pointed out the connections between Landau-Migdal theory on the one hand and the Brueckner-Bethe theory on the other hand (see also: Bäckmann *et al.*, 1985). In Fig. 18 we show the lowest-order contributions to the p-h interaction within the Bethe-Brueckner approach. The antisymmetrized G is evaluated by solving the Bethe-Goldstone equation (4.28) for the scattering of two particles in nuclear matter with the particle momenta $|\mathbf{k}_1|$ and $|\mathbf{k}_2|$ restricted to k_F. The Landau parameters are then functions of the momentum transfer $\mathbf{q}$ and of the Fermi momentum k_F (density).

Calculations of this form have been carried out by the Tübingen group (Dickhoff *et al.*, 1981, 1983; Dickhoff, 1983), the Jülich group (Nakayama *et al.*, 1984, 1986; see also Krewald *et al.*, 1988), and the Brooklyn group (Celenza *et al.*, 1982; Anastasio *et al.*, 1983). In Table I, set (I), we compare the theoretical Landau parameters calculated within the G-matrix approach with the empirical values. The theoretical values correspond to the Landau limit $|\mathbf{q}|\to 0$. Especially for the f_0 parameter of the scalar-isoscalar channel there is a large discrepancy between the empirical and the theoretical value. The latter is too attractive and even violates the stability condition of nuclear matter, which requires $f_0>-1$ (Sjöberg, 1973). This means that in the G-matrix approximation nuclear matter at normal density is unstable against small density fluctuations. The important physics missing in the G-matrix approach is the medium polarization effect.

It has been shown by Sjöberg (1973) and Babu and Brown (1973) that, in particular, the screening effect in the so-called crossed channel reduces strongly the attraction of the G matrix. The lowest-order diagram associat-

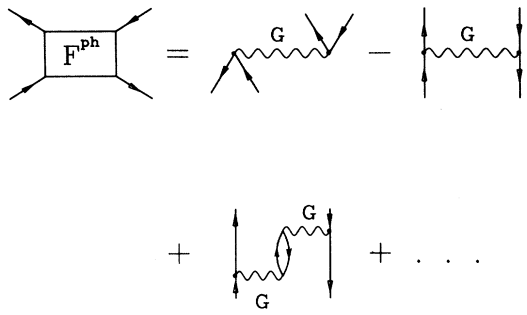

FIG. 18. Lowest-order contributions to the effective particle-hole interaction in the Bethe-Brueckner approach.

TABLE I. Landau parameters at normal densities ($k_f=1.4$ fm^{-1}) in pionic units ($C_0=392$ MeV fm^3). The G-matrix calculations of the Tübingen group (Dickhoff *et al.*, 1983), the Jülich group (Nakayama *et al.*, 1984), and the Brooklyn group (Celenza *et al.*, 1982) are compared to the empirical Landau parameters. The various calculations labeled by roman numerals were performed with different input and different approximations. Set I: Bare (nonrelativistic) G matrix derived from the Bonn potential (Holinde *et al.*, 1972). Set II: Bare G matrix plus induced interaction. Set III: Bare G matrix plus induced interaction plus relativistic corrections. Set IV: Bare G matrix plus relativistic corrections. From Towner (1987).

		f_0	f_0'	g_0	g_0'
Tübingen	I	−0.78	0.17	0.16	0.44
	II	−0.38	0.16	0.13	0.49
Jülich	I	−0.90	0.25	0.15	0.49
	II	−0.22	0.05	−0.05	0.58
	III	0.18	0.12	−0.12	0.56
Brooklyn	I	−0.76	0.19	0.13	0.44
	IV	−0.23	0.23	0.14	0.38
Empirical		0±0.1	∼0.6	∼0.15	∼0.7

ed with the medium polarization is shown in the lower part of Fig. 18. Schematically, the equation to be solved is

$$F^{\text{p-h}} = G^{\text{p-h}} \pm F_{\text{induced}}(F^{\text{p-h}}) , \tag{5.45}$$

where the induced interaction sums all p-h bubbles in the crossed channel. This equation has to be solved self-consistently. The major effect of the induced interaction is on the parameter f_0, reducing the strong attraction. This is shown in Table I, set (II). There is a mild repulsive effect on the g'_0 parameter but essentially no effect on the other Landau parameters.

A further improvement in the theoretical description of the Landau parameters is achieved if relativistic effects are considered in the G-matrix calculations. The first calculation of this type was perfomed by the Brooklyn group (Table I, set IV). It can be seen that the relativistic G matrix stabilizes the Landau parameter f_0. A further improvement is obtained if, in addition, the induced interaction is considered, as was done by the Jülich group (set III).

4. The Δ-hole residual interaction

The interaction between p-h and Δ-h states is obtained from Eq. (5.44) by replacing the operators σ and τ by the corresponding spin and isospin transition operators **S** and **T**, respectively, which convert a nucleon into a Δ isobar (Brown and Weise, 1975). For the nucleon-isobar coupling constant the Chew-Low (Chew and Low, 1956) value $f_{\pi N\Delta} = 2f_{\pi NN}$ is assumed and correspondingly $f_{\rho N\Delta} = 2f_{\rho NN}$. A problem is the contact interaction term of Eq. (5.44). In analogy to the purely nucleonic case, one would expect that in the case of the p-h→Δ-h transition potential a contact interaction of the form $\delta g'_{N\Delta}(f_{\pi N\Delta}/f_{\pi NN})C_0\sigma_1\cdot\mathbf{S}_2\tau_1\cdot\mathbf{T}_2$ would have to be added to the correlated π and ρ exchange in order to obtain the complete $F^{\Delta\text{-h}}$ interaction. The question arises whether there exists a relation between the Landau parameters g'_0 of the nucleonic sector and the corresponding parameter $g'_{N\Delta}$ appearing in the coupling of the nucleonic and the Δ sector. Using chiral-symmetry arguments, Oset and Rho (1979) have advocated that $g'_{N\Delta} \equiv g'_0$ (see also Bohr and Mottelson, 1981; Brown and Rho, 1981). This so-called "universality" assumption leads to a large quenching of GT strength due to Δ isobars. However, one-boson exchange models for the $F^{\Delta\text{-h}}$ interaction (Arima *et al.*, 1983; Towner, 1987), as well as complete microscopic G-matrix calculations (Dickoff *et al.*, 1981; Dickhoff, 1983; Nakayama *et al.*, 1984), do not support this assumption. They give $g'_{N\Delta}$ values that are 30 to 40% smaller than g'_0. The results of these calculations are listed in Table II. The reason for the small value of $g'_{N\Delta}$ is rather simple: In the microscopic calculation of g'_0 and $g'_{N\Delta}$, direct and exchange interaction terms appear which, in general, interfere destructively. The exchange terms reduce the direct terms, but for the p-h→Δ-h transition matrix elements this reduction is much stronger than for purely nucleonic p-h matrix elements. This different interference pattern is due to a simple property of the spin-isospin exchange operator $\mathcal{P}_{\sigma\tau}$, which is four times larger for p-h→Δ-h transitions than for p-h→p-h transitions.

TABLE II: Calculated Landau parameters g'_0 and $g'_{N\Delta}$. The value of g'_0 is measured in units of $C_0 = 392$ MeV fm^3, while $g'_{N\Delta}$ is measured in units of $2\times C_0 = 784$ MeV fm^3. Listed are results of G-matrix calculations performed by the Jülich group (Nakayama *et al.*, 1984) and by the Tokyo group (Cheon *et al.*, 1983). The various calculations were performed with different input and different approximations. Set I: Bare nonrelativistic G matrix based on the Bonn potential (Holinde *et al.*, 1972). Set II: Bare G matrix plus induced interaction. Set III: Bare G matrix plus induced interaction plus relativistic corrections. From Towner, 1987.

		g'_0	$g'_{N\Delta}$
Jülich	I	0.49	0.35
	II	0.58	0.56
	III	0.56	0.68
Tokyo	I	0.52	0.35
	II	0.61	0.45

Cheon *et al.* (1984) find, in addition, that the magnitude of the $g'_{N\Delta}$ value depends quite sensitively on the nuclear density. Its magnitude decreases with decreasing density, thus favoring a small value of $g'_{N\Delta}$ near the nuclear surface. Some enhancement of the G-matrix value of $g'_{N\Delta}$ can be obtained if the induced interaction of Eq. (5.45) is considered. Only a mild enhancement of $g'_{N\Delta}$ over the G-matrix value is found (set II in Table II) (Cheon *et al.*, 1984; Nakayama *et al.*, 1984). The Jülich group also studied relativistic corrections and obtained a further slight enhancement of the $g'_{N\Delta}$ value (set III in Table II). In summary, all microscopic models for the evaluation of the $g'_{N\Delta}$ parameter given much smaller values than the "universality" relation of Oset and Rho (1979) assumes *ad hoc*. This indicates that the Δ-h quenching mechanism may be much less important than originally thought.

G. Applications to spin-isospin modes

1. Excitation energy of the Gamow-Teller resonance

In order to calculate the excitation energy of the GT resonance we have to solve the RPA equations of Eq. (5.14) with an appropriate residual interaction. In principle we should start from the finite-range interaction of Eq. (5.44), calculate direct and exchange matrix elements, and diagonalize the residual interaction in a given model space of p-h configurations. This procedure has been car-

ried out by many groups by now. For a first understanding, however, it is sufficient to consider simplified residual interactions such as the Landau-Migdal force or a separable interaction of the multipole-multipole form. For a description of the isobaric analog and GT states a separable interaction is very appropriate, since both types of excitation involve no change of the orbital motion of the nucleons. With a radially independent separable interaction we obtain for the GT matrix elements

$$v_{mjin}=\kappa_{\sigma\tau}\langle mi^{-1}|\sigma(1)\tau_-(1)|0\rangle \times\langle nj^{-1}|\sigma(2)\tau_-(2)|0\rangle\ , \tag{5.46}$$

and similarly for the isobaric analog matrix elements

$$v_{mjin}=\kappa_{\tau}\langle mi^{-1}|\tau_-(1)|0\rangle\langle nj^{-1}|\tau_-(2)|0\rangle\ . \tag{5.47}$$

This amounts to the field approximation of Bohr and Mottelson (1975), where the coherent states are generated by oscillating average fields which, in the present case, are proportional to the operators τ and $\sigma\tau$. By inserting the matrix elements of Eq. (5.46) into the RPA equations (5.14) we can eliminate the amplitudes X^f_{mi} and Y^f_{mi} because of the separability of the interaction and obtain the following dispersion relation for the excitation energy ω_{f0} of the collective GT state (e.g., for the 1^+ state with spin projection $M=0$):

$$\sum_{pn}\frac{|\langle(pn^{-1})J^\pi=1^+,M=0|\sigma_0\tau_{-1}|0\rangle|^2}{(\epsilon_p-\epsilon_n)-\omega_{f0}} +\sum_{pn}\frac{|\langle(np^{-1})J^\pi=1^+,M=0|\sigma_0\tau_{+1}|0\rangle|^2}{(\epsilon_n-\epsilon_p)+\omega_{f0}}=\frac{1}{\kappa_{\sigma\tau}}\ . \tag{5.48}$$

Here ϵ_p and ϵ_n are the proton and neutron single-particle energies. For nuclei with a large neutron excess the second sum in Eq. (5.48) will be approximately zero, since all relevant β_+ transitions are Pauli blocked. This means that the effect of ground-state correlations on the GT resonance is small. Gaarde *et al.* (1981) have solved Eq. (5.48) for various nuclei. They used experimental single-particle and single-hole energies and adjusted $\kappa_{\sigma\tau}$ in such a way that the experimentally observed GT energy is reproduced. They found the value $\kappa_{\sigma\tau}=23/A$ MeV. From the isobaric analog state they determined the coupling constant $\kappa_\tau=28/A$. This value is slightly larger than that of $\kappa_{\sigma\tau}$.

An even simpler and more instructive method for determining the GT energy systematics is the sum-rule method (Bertsch, 1981, 1983; Suzuki, 1982, 1984; Bertsch and Esbensen, 1987). Since the ground-state correlations are small for the isobaric analog state and the GT state, the Tamm-Dancoff approximation is sufficient for the evaluation of their excitation energies. The Tamm-Dancoff theory respects the sum rules of Eqs. (2.20) and (2.31). For charge-exchange modes with a narrow width, it is convenient to identify the peak energy of the resonance with the average excitation energy of the strength function. The latter is defined by the linearly energy-weighted sum over the non-energy-weighted sum of the excitation strengths. In the Tamm-Dancoff theory the average excitation energy is given by the commutation expression

$$\langle E\rangle=\int_0^\infty dE\,ES_{\rm TDA}(E)=\frac{\langle 0|O^\dagger[H,O]|0\rangle}{\langle 0|O^\dagger O|0\rangle}\ , \tag{5.49}$$

where the expectation value is taken with respect to the independent-particle-model ground-state wave function of the parent nucleus. The operator in Eq. (5.49) is calculated by explicitly summing over intermediate p-h states which are calculated within the Tamm-Dancoff approximation.

Let us first show that we can evaluate the excitation energy of the isobaric analog state in this way. For that purpose we divide the total Hamiltonian into the single-particle Hamiltonian of Eq. (5.2), the spin- and/or isospin-dependent two-body interactions, and the Coulomb interaction:

$$H=H_{sp}+\sum_{i<j}\left[\kappa_\tau\boldsymbol{\tau}_i\cdot\boldsymbol{\tau}_j+\kappa_\sigma\boldsymbol{\sigma}_i\cdot\boldsymbol{\sigma}_j+\kappa_{\sigma\tau}\boldsymbol{\tau}_i\cdot\boldsymbol{\tau}_j\boldsymbol{\sigma}_i\cdot\boldsymbol{\sigma}_j +\frac{e^2(1-\tau_{i3})(1-\tau_{j3})}{4|\mathbf{r}_i-\mathbf{r}_j|}\right]. \tag{5.50}$$

According to Eq. (5.50), we can make the corresponding separation of the mean excitation energy as

$$\langle E\rangle=\Delta E_{\rm orbit}+\Delta E_{ls}+\Delta E_\tau +\Delta E_\sigma+\Delta E_{\sigma\tau}+\Delta E_C\ , \tag{5.51}$$

where we have split the single-particle energy into an orbital *(orbit)* and a spin-orbit (*ls*) part. Of the various interaction terms of Eq. (5.50), only the Coulomb force does not commute with the Fermi operator T_-. Therefore, from Eq. (5.49), the mean excitation energy of the isobaric analog state is given by

$$\langle E_{\rm IAS}\rangle=\frac{1}{N-Z}\langle 0|T_+[V_C,T_-]|0\rangle\ . \tag{5.52}$$

Here the commutator

$$[V_C,T_-]=\tfrac{1}{4}\sum_{i<j}\frac{e^2}{|\mathbf{r}_i-\mathbf{r}_j|} \times[(1-\tau_{i3})\tau_{j-}+(1-\tau_{j3})\tau_{i-}] \tag{5.53}$$

represents a two-body force, which changes a neutron-proton pair into a proton-proton pair. The use of (5.53) in (5.52) yields

$$\langle E_{\rm IAS}\rangle=\Delta E_C =e^2\int d^3\mathbf{r}\int d^3\mathbf{r}'\frac{\rho_p(\mathbf{r})[\rho_n(\mathbf{r}')-\rho_p(\mathbf{r}')]}{(N-Z)|\mathbf{r}-\mathbf{r}'|}\ , \tag{5.54}$$

where we have kept only the direct Coulomb matrix element, since the exchange matrix element is comparatively small because of the long range of the Coulomb in-

teraction. We remark that the κ_τ interaction of Eq. (5.50) contributes to $\Delta E_{\rm orbit}$ via the symmetry potential and to ΔE_τ via the residual p-h interaction. Both contributions to $\langle E_{\rm IAS}\rangle$ necessarily cancel, so that Eq. (5.54) is fulfilled.

Let us next calculate the mean excitation energy of the GT resonance. It is defined by

$$\langle E_{\rm GTS}\rangle = \frac{\langle 0|\beta_+(0)[H,\beta_-(0)]|0\rangle}{\langle 0|\beta_+(0)\beta_-(0)|0\rangle} \tag{5.55}$$

where, for convenience, we have considered only the $\mu=0$ component of the GT operator. In the following we shall apply Eq. (5.55) to nuclei with a large neutron excess, like ^{48}Ca, ^{90}Zr, or ^{208}Pb, in which all the spin-orbit partners of the proton states are occupied by neutrons. When we insert the Hamiltonian of Eq. (5.50) into the commutator of Eq. (5.55) we find that only the orbital part of the Hamiltonian commutes with $\beta_-(0)$.

As the first of the noncommuting terms we evaluate the expectation value of the spin-isospin-dependent two-body interaction.

$$\Delta E_{\sigma\tau} = \frac{\langle 0|\beta_+(0)\sum_{i>j}\kappa_{\sigma\tau}\tau_i\cdot\tau_j\sigma_i\cdot\sigma_j\beta_-(0)|0\rangle}{\langle 0|\beta_+(0)\beta_-(0)|0\rangle} . \tag{5.56}$$

In order to make a nonvanishing expectation value in Eq. (5.56), the operators $\beta_+(0)$ and $\beta_-(0)$ must act on particles i and j, respectively. Decomposing the isospin operator according to $\tau_i\cdot\tau_j=\frac{1}{2}(\tau_{i+}\tau_{j-}+\tau_{i-}\tau_{j+})+\tau_{i3}\tau_{j3}$ and inserting the explicit form of the GT operator from Eq. (2.29), we find that the numerator of Eq. (5.56) is equal to $2(N-Z)^2\kappa_{\sigma\tau}$. The denominator has the value $\langle 0|\beta_+(0)\beta_-(0)|0\rangle=(N-Z)$, so that

$$\Delta E_{\sigma\tau}=2(N-Z)\kappa_{\sigma\tau}=4\kappa_{\sigma\tau}T_0 , \tag{5.57}$$

where $T_0=(N-Z)/2$ is the isospin of the parent nucleus.

Next we consider the Coulomb energy ΔE_C and the isovector single-particle energies that contribute the same amount to the GT energy as to the isobaric analog state. From Eq. (5.54) we know that $\Delta E_C=\langle E_{\rm IAS}\rangle$. However, the isobaric analog state has an additional energy contribution from the residual κ_τ interaction, which we have to subtract. We can calculate this contribution by noticing first that $\sum_{i<j}\tau_i\cdot\tau_j=2\mathbf{T}^2-3A/2$ and then using the fact that the isobaric analog state and the GT resonance have isospin quantum numbers T_0 and (T_0-1), respectively. This gives the energy difference

$$\begin{aligned}&\langle T_0T_0|\kappa_\tau\sum_{i<j}\tau_i\cdot\tau_j|T_0T_0\rangle\\ &-\langle T_0-1T_0-1|\kappa_\tau\sum_{i<j}\tau_i\cdot\tau_j|T_0-1T_0-1\rangle\\ &=4\kappa_\tau T_0 .\end{aligned} \tag{5.58}$$

Subtraction of this energy difference from $\langle E_{\rm IAS}\rangle$ gives the desired result.

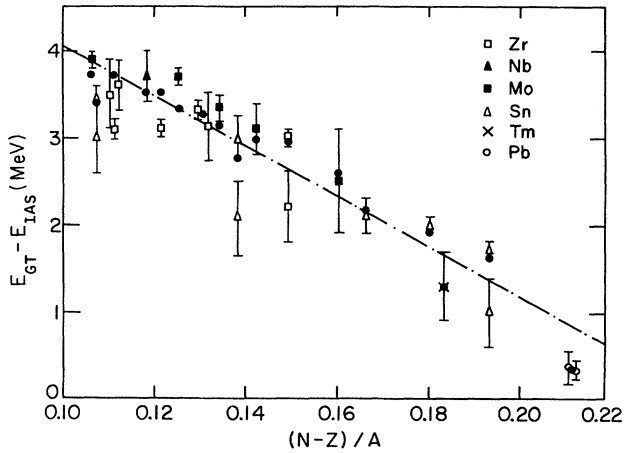

FIG. 19. Energy difference of the Gamow-Teller and the isobaric analog state for different nuclei as a function of the relative neutron excess. From Nakayama *et al.* (1982).

The remaining term of Eq. (5.51) is the spin-orbit potential. For nuclei like ^{48}Ca or ^{90}Zr only the $j_>$ neutron shell is filled, while the daughter nucleus has both $j_>$ and $j_<$ proton shells empty. Since the GT operator has roughly equal strength for spin-flip and non-spin-flip transitions, the expectation value of the spin-orbit value is given by

$$\Delta E_{ls}=\tfrac{1}{2}(\epsilon_{j_>}-\epsilon_{j_<}) . \tag{5.59}$$

Now, putting all the pieces together, we obtain the following mass formula for the mean excitation energy of the GT resonance relative to that of the isobaric analog state

$$\begin{aligned}\langle E_{\rm GTS}\rangle-\langle E_{\rm IAS}\rangle&=\Delta E_{ls}+4(\kappa_{\sigma\tau}-\kappa_\tau)T_0\\ &=\Delta E_{ls}+\frac{\tilde\kappa_{\sigma\tau}-\tilde\kappa_\tau}{A}2(N-Z) .\end{aligned} \tag{5.60}$$

In the last step we have made the A dependence of the coupling constants κ_τ and $\kappa_{\sigma\tau}$ explicit by defining $\kappa_\tau\equiv\tilde\kappa_\tau/A$ and $\kappa_{\sigma\tau}\equiv\tilde\kappa_{\sigma\tau}/A$, respectively.

Figure 19 shows the data on the position of the GT resonance compared with the functional form of Eq. (5.60) (from Nakayama *et al.*, 1982). For nuclei with small neutron excess the spin-orbit energy ΔE_{ls} dominates and the GT state lies above the isobaric analog state. For heavy nuclei such as ^{208}Pb, the second term balances the first and the GT state appears at the same position as the isobaric analog state. The slope of the straight line requires that $\tilde\kappa_\tau$ be larger than $\tilde\kappa_{\sigma\tau}$. Their values are found to be $\tilde\kappa_\tau=28$ and $\tilde\kappa_{\sigma\tau}=23$, respectively, as was noted at the beginning of this section.

2. The fragmentation and the width of the Gamow-Teller states

While the excitation energy of the GT resonance can be estimated from the sum rule, a more detailed descrip-

tion of the GT strength function needs a full RPA calculation. The random-phase approximation can accurately describe the excitation energies of the low-lying weak GT states as well as the fragmentation of the strength between these states and the high-lying GT resonance. The width of the GT states can only be described if one goes to the second RPA. In the following we shall apply both the RPA and the second RPA to the evaluation of the GT strength function.

In Fig. 20 we show theoretical GT response functions for the nuclei ^{48}Ca, ^{90}Zr, and ^{208}Pb. The response functions were either calculated in RPA (dashed curve) or in the second RPA (solid curve) (from Drożdż *et al.*, 1986b). As expected, in case of ^{48}Ca and ^{90}Zr the RPA strength functions show two major peaks. In ^{48}Ca the two peaks correspond to the mixing between the $f^n_{7/2}\rightarrow f^p_{7/2}$ and the $f^n_{7/2}\rightarrow f^p_{5/2}$ transitions, while in the case of ^{90}Zr the mixing occurs between the $g^n_{9/2}\rightarrow g^p_{9/2}$ and $g^n_{9/2}\rightarrow g^p_{7/2}$ transitions. In both cases most of the strength is concentrated in the high-lying GT resonance. This is the result of the repulsive residual p-h interaction, which couples, for example in ^{90}Zr, the two p-h transitions $g^n_{9/2}\rightarrow g^p_{9/2}$ and $g^n_{9/2}\rightarrow g^p_{7/2}$ to form two new 1^+ states. Only some strength remains in the state at the lower excitation energy. This renormalization of the low-lying transition strength of the independent-particle model was, in fact, the main empirical evidence available when Ikeda *et al.* (1963) first proposed that the GT strength might be concentrated in a state at high excitation energies.

Because of the large neutron excess more p-h transitions can couple in ^{208}Pb, and the situation is therefore somewhat different. Already on the RPA level, 27% of the total GT strength is located above 20 MeV excitation energy. This strength originates mostly from the coupling of the GT resonance to $2\hbar\omega$ 1^+ excitations. Otherwise a large fraction of the strength resides in the collective GT state (see also Sagawa and Van Giai, 1982). Note that except for ^{208}Pb the calculated energy position of the GT resonance is in good agreement with the experimental centroid energies, which are indicated by the arrows.

The full curves on the right panel of Fig. 20 represent the GT response functions of second RPA calculations including 2p-2h correlations. The second RPA predicts a width of about 4 MeV at half maximum for the GT resonance in ^{48}Ca and ^{90}Zr—in good agreement with experiment. The most important result of Fig. 20 is, however, that the damping widths of the GT states predicted by the second RPA are strongly asymmetric, with a very long high-energy tail. By contrast, in the experimental analysis of the data one usually fits the strength distribution of states to a Gaussian function, which cuts off the

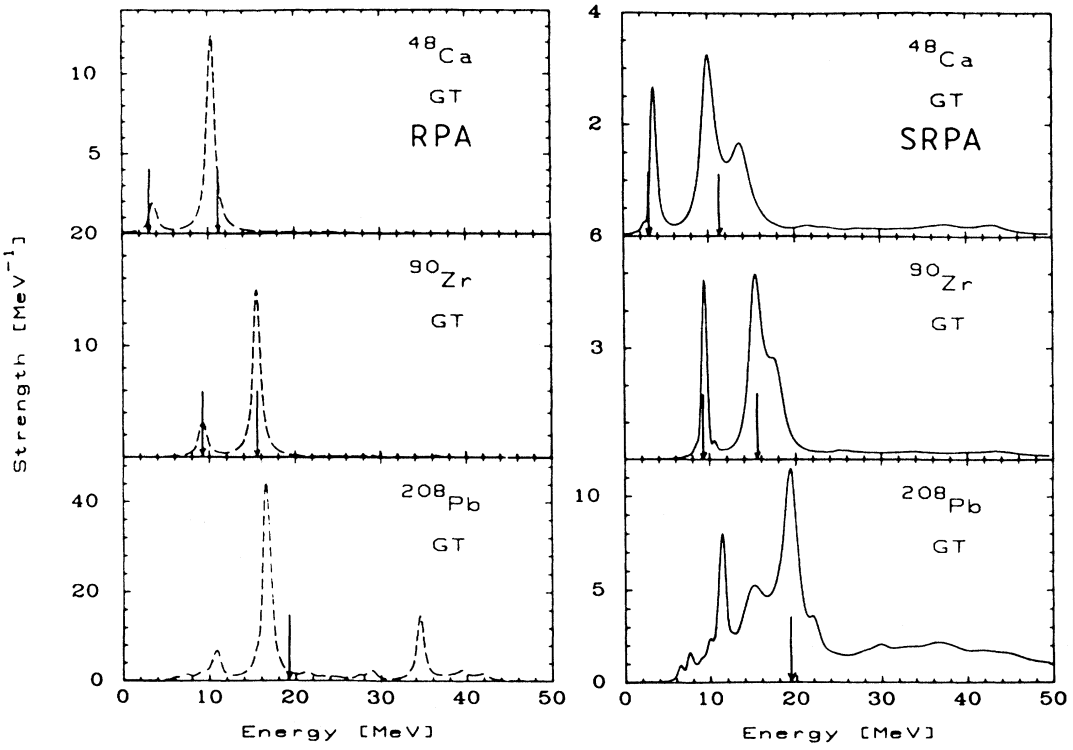

FIG. 20. Gamow-Teller distributions in various closed-shell nuclei. The left panel displays the RPA results, while the right panel shows the effect of 2p-2h admixtures on the Gamow-Teller strength distribution functions. The arrows indicate the centroid energies of the experimental resonances. The RPA results were folded into a width of 1 MeV. From Drożdż *et al.* (1986b).

strength in the wings of the strength function. This leads to an underestimate of the total transition strength of the peak. From the outset there is no theoretical justification for this special choice of a Gaussian form for the width of a peak. Rather, one expects that in the giant-resonance region the spreading width $\Gamma^{\downarrow}$ increases with excitation energy due to the increasing number of 2p-2h states. This is, indeed, observed for the GT strength functions in Fig. 20. Roughly 29% of the minimal sum-rule bound $S_{\beta^-}^{\min}(\mathrm{GT})=3(N-Z)$ is found beyond $E_x=20$ MeV in the nuclei ^{48}Ca and ^{90}Zr. In ^{208}Pb this amounts even to 40%. Most of this high-energy strength originates from central spin-isospin interactions and from tensor interactions. The relative contribution of both depends on the strength of the tensor force. Note that the second RPA calculations reproduce the position of the GT states rather well in all three nuclei. It should be stressed that theoretically the high-energy tails necessarily accompany the local broadening of resonance. They are a direct consequence of the strong increase in level density of 2p-2h states as the excitation energy increases.

H. Higher spin-isospin modes

In Fig. 21 the calculated strength distribution functions for the 0^-, 1^-, and 2^- components of the giant spin-flip dipole ($L=1$, $S=1$) resonance are shown. Again the dashed curves denote the RPA results and the full curves denote the second RPA results. While in the case of the 1p-1h RPA the 0^- and 1^- strength is essentially concentrated in a single collective state, in the second RPA the strength is spread out over a large energy interval. The widths of the states become larger than 10 MeV, with an appreciable fraction of strength being shifted into the high excitation energy region. For the 0^- and 1^- states approximately 35% of the strength is

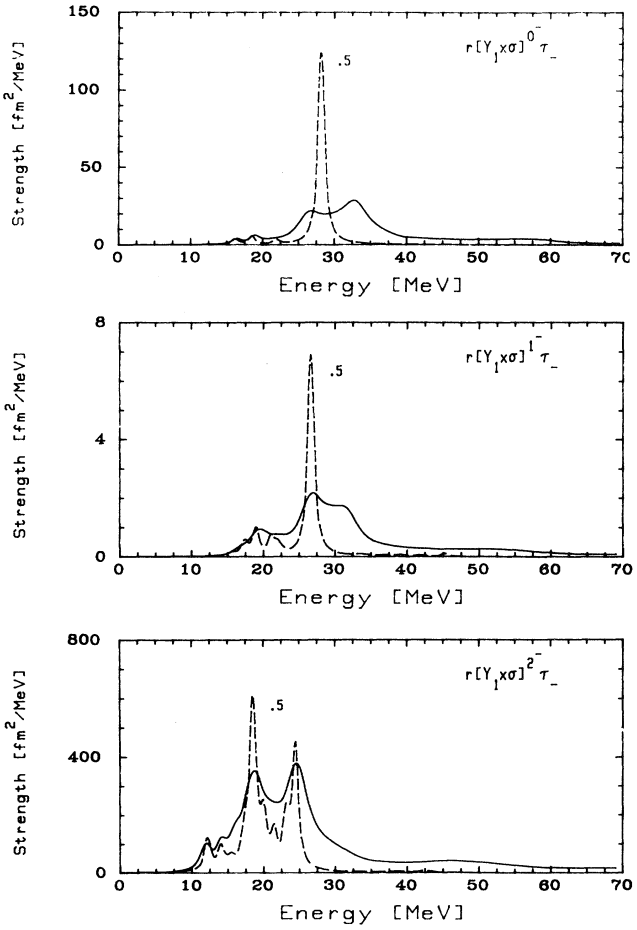

FIG. 21. Strength distribution functions for the $L=1$, $J^\pi=0^-$, 1^-, and 2^- resonances in ^{90}Zr. The dashed curve is the RPA result, while the solid curve represents the full second RPA calculation. The RPA strength is multiplied by a factor 0.5. From Drożdż *et al.* (1987).

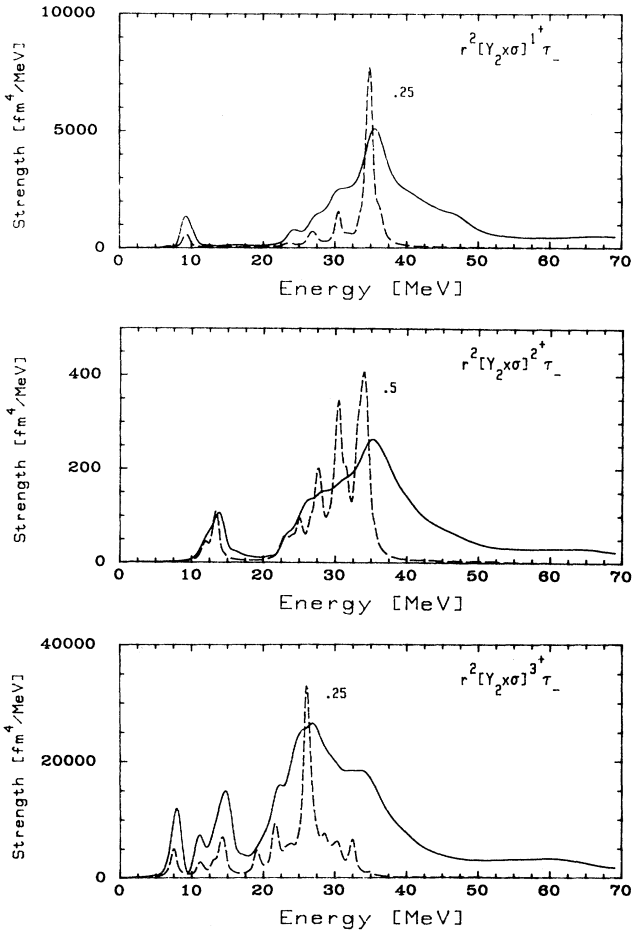

FIG. 22. Same as in Fig. 21 but now for the $L=2$, $J^\pi=1^+$, 2^+, and 3^+ strength distribution functions in ^{90}Zr. Note that the RPA strengths for the 1^+ and 3^+ states shown in the upper and lower parts of the figure, respectively, have been multiplied by a factor 0.25, while the RPA strength of the 2^+ states in the middle part of the figure has been multiplied by a factor 0.5. From Drożdż *et al.* (1987).

located beyond $E_x = 35$ MeV (Drożdż *et al.*, 1987).

The 2^- strength distribution in the lower part of Fig. 21 differs from the 0^- and 1^- distributions in that it already shows a strong fragmentation on the 1p-1h RPA level. The principal effect of the second RPA is then to reduce the 2^- strength in the lower excitation energy region ($E_x < 30$ MeV) and move it into the high excitation energy region at $E_x \geq 30$ MeV. A similar effect can also be observed for the $2\hbar\omega$, $J^\pi = 1^+$, 2^+, and 3^+ quadrupole modes, the strength distributions of which are shown in Fig. 22. Again the second RPA predicts a strong, asymmetric spreading of the strength. The calculated widths of the individual resonances are now larger than 15 MeV. The second RPA moves at least 50 percent of the strength out of that energy region where the 1p-1h RPA would predict it to be. This strength is moved into the high excitation energy tail, $E_x \geq 40$ MeV. Comparing the results of Figs. 20, 21, and 22, one observes that the spreading of the multipole strength is larger the higher the excitation energy and the higher the spin of the mode. Note that the spreading width $\Gamma^\downarrow$ calculated in the second RPA provides a lower limit to the total width of a state because the escape width $\Gamma^\uparrow$ is not included yet. The sum of escape width $\Gamma^\uparrow$ and spreading width $\Gamma^\downarrow$ gives the total width $\Gamma = \Gamma^\uparrow + \Gamma^\downarrow$.

The second RPA mainly includes 2p-2h mixing in the excited state, while the 2p-2h mixing in the ground state is only treated on the RPA level. Several authors (Desplanques and Noguera, 1986; MacFarlane, 1986; Hirsch *et al.*, 1988; Nishizaki *et al.*, 1988; Takayanagi *et al.*, 1988a, 1988b; see also Drożdż *et al.*, 1990; Mariano *et al.*, 1990) have improved on this by including 2p-2h mixing in the ground state via perturbation theory. This inclusion of ground-state correlations beyond the random-phase approximation effectively renormalizes the one-body transition operators (Speth *et al.*, 1977; Towner, 1987). In the case of the GT operators the total sum-rule strength S_{β^-}(GT) is enhanced (Towner and Khanna, 1979; Bertsch and Hamamoto, 1982; see also, Towner, 1984 and 1987), but accurate calculations (Nishizaki *et al.*, 1988; Takayanagi *et al.*, 1988a, 1988b), which treat all second-order 2p-2h diagrams in a consistent manner, show that this enhancement is only of the order of 10% or less. The resulting strength distribution is therefore quite similar to the one in the usual second RPA.

I. The quasiparticle RPA and the β_+ strength function

While the β_- strength function is well described by the RPA theory, the β_+ strength function is much less well understood. In nuclei with a sizable neutron excess the $\sigma\tau_+$ transitions are suppressed due to Pauli blocking of the accessible neutron orbitals. In general, many fewer p-h configurations are available for $\sigma\tau_+$ transitions than for $\sigma\tau_-$, while the ground-state correlations become much more important for the $\sigma\tau_+$ transitions than they are for the $\sigma\tau_-$ transitions. There are two major reasons for the latter effect: The first is that the ground-state correlations associated with β_+ transitions are due to the strong GT resonance, which is only reached by the $\sigma\tau_-$ operator. The second is that β_+ transitions mostly take place in open-shell nuclei which have additional ground-state correlations. Therefore β_+ transitions in these nuclei are severely suppressed with respect to the single-particle values from the independent-particle model.

The appropriate nuclear structure theory for the description of the β_+ transitions is either the shell model or the quasiparticle RPA. The shell-model calculations can be performed only in light nuclei. The quasiparticle RPA, which was originally introduced by Halbleib and Sorensen (1967) to the calculation of Gamow-Teller β decay, therefore provides a valuable method for studying these transitions in heavy-mass nuclei. Cha (1983) was the first to apply the quasiparticle RPA to β_+ decay in the $A = 100-150$ region. He found that the RPA correlations suppress the low β_+ transitions by a factor of 3 to 10 with respect to the independent quasiparticle model. However, the observed experimental transition strength is even more suppressed—typically by an additional factor of 4.

Recently, Vogel and Zirnbauer (1986) have shown that additional suppression can be obtained in the quasiparticle RPA if the *pp* residual interaction is adjusted in an appropriate way. Cha (1983) had adjusted this interaction by fitting to energies of low-lying states which are not very sensitive to the *pp* interaction. Vogel and Zirnbauer, on the other hand, used strongly suppressed β_+ transitions in semimagic neutron-deficient nuclei like ^{148}Dy, ^{150}Er, or ^{152}Yb to fix the *pp* coupling strength. These nuclei with the magic neutron number $N = 82$ (and others like ^{94}Ru and ^{96}Pd with $N = 50$) are expected to undergo very fast positron decay. In the extreme single-particle model, their decay rates are determined by the $h^p_{11/2} \rightarrow h^n_{9/2}$ transition in the case of $N = 82$, and by the $g^p_{9/2} \rightarrow g^n_{7/2}$ transition in the case of $N = 50$. The single-particle B(GT) value for these even-mass systems is simply given by $B(\mathrm{GT})_{\mathrm{s.p.}} = N_p 4l/(2l+1)$, where l is the orbital angular momentum of the corresponding subshell and N_p is the number of protons in the partially filled $j = l + \frac{1}{2}$ shell. For these nuclei the measured B(GT) values are ~ 7 times smaller than the single-particle values (Nolte *et al.*, 1982, 1983; Kleinheinz *et al.*, 1985). Therefore the total β_+ strength in these nuclei is strongly quenched. Engel *et al.* (1988) have shown that pairing and particle-hole interactions together reduce the strength by approximately a factor of 2 with respect to the single-particle value in the above semimagic nuclei. After taking into account these effects and other possible effects from Δ-hole quenching, their calculated β_+ strengths are still a factor of 2 to 3 larger than the experimental value. If, however, the *pp* interaction is additionally included with an adjusted strength of $V_{pp} = -400$

MeV fm^3, then Engel *et al.* (1988) can explain the data.

These findings have an enormous influence on the interpretation and calculation of double β-decay matrix elements. In double β-decay the GT transitions appear as intermediate virtual transitions. Recently several groups (Civitarese *et al.*, 1987; Tomoda and Faessler, 1987; Muto and Klapdor, 1988; Muto *et al.*, 1989a, 1989b; Hirsch and Krmpotić, 1990a, 1990b; Hirsch *et al.*, 1990) have performed calculations for the double β-decay transitions. All groups find a strong reduction of the double β-decay matrix elements if the *pp* interaction is included. Therefore the extremely small decay rates for both 2ν and 0ν double β decay can be explained as a nuclear structure effect. In case of 2ν decay this suppression is observed experimentally in several nuclei. The substantial suppression of 0ν double β decay means that limits on the neutrino mass deduced from limits on the half-lives obtained in experimental searches for 0ν double β decay are less stringent than commonly thought. (For recent reviews on double β decay, see Haxton and Stephenson, 1984; Doi *et al.*, 1985; Grotz and Klapdor, 1990; Tomoda, 1991).

The quasiparticle RPA calculations for the β_+ strength function have been tested against shell-model calculations (Lauritzen, 1988). The quasiparticle RPA predicts a β_+ decay rate larger by a factor of about 2 than the full shell-model calculations and than experiment. The β_+ transitions are weaker in the shell model, probably due to the correlations not included in the quasiparticle RPA.

J. Shell-model calculations

If the target ground state is strongly mixed among various A-particle Slater determinants, as is the case, for example, for nuclei in between closed shells, then a large shell-model calculation is needed to obtain a reliable description of the nuclear excitation spectrum. The shell-model approach starts with the definition of a model space of single-particle orbitals and a corresponding effective many-body Hamiltonian consisting of the single-particle potential and of the effective two-body interaction. The Hamiltonian is diagonalized in the multinucleon configuration space to obtain eigenvalues and eigenfunction[5] of the excited states as well as transition densities between the states. The shell-model calculations have the advantage that they allow for a direct comparison with many experimental data. Unfortunately, the number of A-nucleon configurations to be treated increases dramatically with the number of single-particle states defining the model space. This limits the shell-model calculations to light nuclei or nuclei near shell closures. The most extensive and successive shell-model calculations have been performed for p-shell nuclei ($5 < A < 14$) (Cohen and Kurath, 1965, 1967), for *sd*-shell nuclei ($17 \leq A \leq 39$) (Wildenthal, 1984; Brown and Wildenthal, 1988), and for *pf*-shell nuclei (McGrory and Wildenthal, 1981; Muto, 1986). For the former two mass regions the active model space includes all configurations within the major shell, while for the *pf*-shell nuclei the model space becomes so large that it has to be restricted in real calculations and becomes incomplete.

To demonstrate the strength of the shell-model calculations, let us consider the reaction ^{26}Mg$(p,n)^{26}$Al, which has a complex spectroscopy. This can be seen from Fig. 23, where the experimental (Madey *et al.*, 1987a, 1987b) GT strength distribution of ^{26}Mg is compared with a shell-model calculation of Brown and Wildenthal (1988). Both the theoretical and the experimental results have been Gaussian averaged over 2 MeV in order to emphasize the gross structure of the strength function. The calculated GT strength function is larger than experiment at all excitation energies considered. However, the shape is in quantitative agreement with experiment. This shows that the shell-model calculation can describe the energetics and the fine structure of the strength distribution much better than any other method. In Fig. 23 theory and experiment can be brought into agreement when the theoretical results are multiplied by $(0.77)^2 = 0.6$. This quenching factor is consistent with the GT strength extraction of Fig. 6. Similar quenching factors are found for all other *sd*-shell nuclei (Brown and Wildenthal, 1988). In Fig. 24 a comparison of the measured and the calculated GT matrix elements of various *sd*-shell nuclei is made. For perfect agreement the points should lie on the diagonal line. However, they cluster about a line with a slope of 0.77, showing the overall quenching of the experimental GT matrix elements. Part of this quenching is due to the configurations excluded from the model space, such as the $2\hbar\omega$ and higher $\hbar\omega$ excitations.

Careful studies of the quenching effect were carried out by Arima *et al.* (1983) and by Towner and Khanna

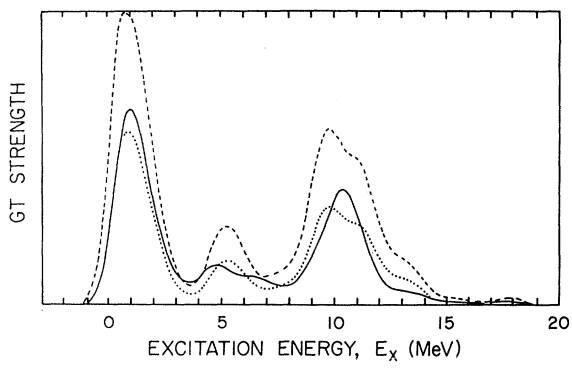

FIG. 23. Excitation energy spectrum of the GT operator in ^{26}Mg. The solid curve is the experimental GT strength distribution as extracted from the forward-angle (p,n) reaction at $E_p = 135$ MeV (Madey *et al.*, 1987a, 1987b). The dashed curve is the theoretical prediction of a multiconfiguration shell-model calculation of Brown and Wildenthal (1988). Both theoretical and experimental spectra were averaged with a width of 2 MeV to simplify the comparison. The dotted curve is the theoretical spectrum renormalized by a factor of 0.6.

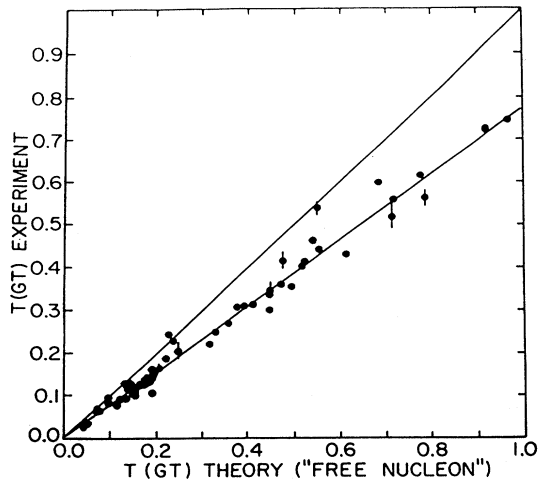

FIG. 24. Theoretical vs experimental GT matrix elements for *sd*-shell nuclei (Brown and Wildenthal, 1988). The matrix elements should lie on the diagonal for perfect agreement between theory and experiment; however, they cluster at a line with slope 0.77, showing the overall quenching of the GT strength.

(1983) for the magnetic moments and the β-decay matrix elements of nuclei with a valence nucleon or hole outside an *LS* doubly closed shell. They found that approximately $\frac{2}{3}$ of the quenching comes from higher-order configuration mixing and $\frac{1}{3}$ from Δh admixtures to the wave functions. (For recent reviews see Towner, 1984, 1987; Arima *et al.*, 1987).

As was pointed out in Sec. III.G, the experimental transition strength to high-spin stretched states is also strongly quenched. The measured strength is typically a small fraction of that expected for pure p-h excitations—generally less than $\frac{1}{3}$ for isoscalar excitations and less than $\frac{1}{2}$ for isovector excitations. This depletion of strength cannot be due to the Δ-isobar effect, since the Δ cannot couple to the isoscalar states. Furthermore, the Δ coupling to the isovector stretched states is weak because of the high angular momentum transfer. Therefore the observed quenching must be due to the nuclear configuration mixing effect. That this supposition is correct was first proven for the high-spin 12^- and 14^- states in ^{208}Pb by Krewald and Speth (1980). These authors showed that the fragmentation of the $1j_{15/2}$ and $1i_{13/2}$ single-particle strength due to phonon coupling (Hamamoto, 1974) is the main reason for the reduction of the cross section to the high-spin states. In this approach the p-h strength, missing in the low-lying states, is fragmented into many states at higher excitation energies (see also, Suzuki and Hyuga, 1983; Pandharipande *et al.*, 1984). This strength escapes experimental detection.

Krewald and Speth (1980) used the Jülich-Stony Brook potential of Eq. (5.44) for the residual p-h interaction. They found that the strong momentum dependence of this interaction is important to reproduce the experimental excitation energies of the magnetic high-spin states. Therefore these states provide a sensitive test of the high-momentum components of the p-h interaction in the $\sigma\tau$ channel.

Recently large-basis shell-model calculations have been performed for the stretched 6^- states in ^{28}Si and ^{32}S (Amusa and Lawson, 1983; Carr *et al.*, 1989; Clausen *et al.*, 1990; see also the rotational model with Coriolis mixing by Zamick, 1984, and Liu and Zamick, 1985). These calculations give an excellent description of the experimental data and can explain the experimentally observed fragmentation of the strength as well as the quenching.

VI. MICROSCOPIC ANALYSES OF INELASTIC SCATTERING AND CHARGE-EXCHANGE SPECTRA

With the reaction theory of Sec. IV and the nuclear structure information of Sec. V at hand, we can now proceed to discuss the analyses of the experimental data. The basic model assumption in these analyses is that for inelastic scattering and charge-exchange reactions at intermediate bombarding energies ($E_p \geq 100$ MeV/nucleon) the cross section at forward angles is dominated by direct one-step processes in which the scattered projectile excites the 1p-1h response function of the target. The (p,n), (n,p), and $(^3\text{He},t)$ spectra as shown, for example, in Figs. 12, 13, and 14, are therefore believed to be a superposition of cross sections of 1p-1h excitations, which are calculable within microscopic nuclear structure and reaction models. The contributions of multistep processes to the cross section are assumed to be suppressed. This assumption is corroborate by various two-step reaction calculations (Chiang and Hüfner, 1981; Esbensen and Bertsch, 1985; Smith and Wambach, 1988), which show that at high bombarding energies the two-step cross section is relatively small (of the order of 10% or so) compared with the one-step cross section. This is especially true for moderate excitation energies ($E_x \leq 50$ MeV) and for forward-angle scattering. The two-step background cross section starts to be become significant only at relatively high excitation energies and large scattering angles.

In the (p,n) reaction at intermediate energies the cross section is dominated by $\sigma\tau$ excitations because the scattering matrix elements of these transitions are larger by at least an order of magnitude than those of the τ excitations. This is due to the dominance of the $V^C_{\sigma\tau}$ component of the effective projectile-target nucleon interaction over the V^C_τ component, as was discussed in Sec. IV.C.3. Hence the (p,n) reaction at intermediate energies is a unique example of a hadron-induced reaction that excites states very selectively in only one channel. Since the impulse approximation is found to be rather accurate at intermediate energies, one can calculate the cross sections within the DWIA and focus attention on the nuclear structure aspects being probed.

A. Gamow-Teller strength from (p,n) data

In course of time the determination of the total GT strength from the measured (p,n) data has involved several methods and prescriptions. Here we give a short historical overview of the various ways in which GT strength was extracted from the data. Initially Gaarde *et al.*, (1981) compared the measured GT cross section with an absolute DWIA calculation based on the Love and Franey (1981) t_F matrix. They found that only 30% of the expected total GT strength lay in the peaks of the forward-angle spectrum. Of course, a DWIA calculation is not reliable enough for the determination of the absolute magnitude of a cross section because of the uncertainties involved in the effective projectile-target nucleon interaction. Therefore Goodman and Bloom (1984) calibrated the interaction to β-decay using the prescription of Sec. IV.E. They concluded that 50–60% of the total sum-rule strength was present in nuclei ranging from $A=13$ to $A=90$.

In heavier nuclei, the GT resonance is located on top of a broad continuum whose shape and magnitude is not known. Therefore a smooth background beneath the GT resonance (see the dashed line in Fig. 25) was subtracted from the spectrum to extract the GT cross section (see Gaarde *et al.*, 1981). Osterfeld (1982, 1984), however, showed that this procedure is not correct. He calculated the forward-angle (p,n) cross section in the DWIA, including many multipolarities of transitions in the independent-particle model. The result of his calculation, obtained for the ^{48}Ca$(p,n)^{48}$Sc reaction at $E_p=160$ MeV, is shown in Fig. 25. The calculation predicts that

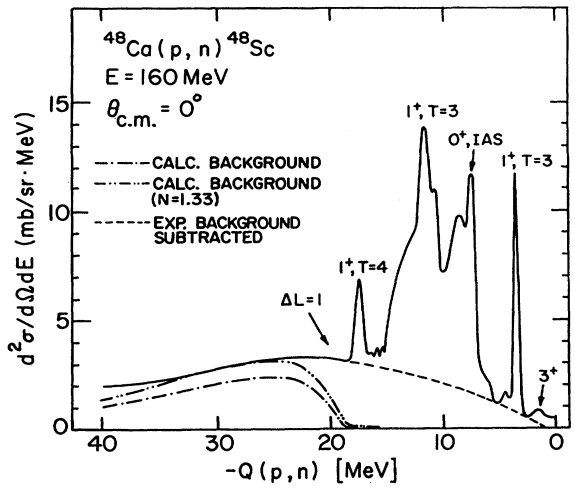

FIG. 25. Zero-degree spectrum for the reaction ^{48}Ca$(p,n)^{48}$Sc at $E_p=160$ MeV. The solid curve represents the experimental data (Anderson *et al.*, 1985a). The dashed curve indicates the experimental background subtraction. The dash-dotted curve denotes the calculated background which, when multiplied by a factor of 1.33 (dashed-double dotted curve), reproduces the experimental cross section at high excitation energies. From Osterfeld (1982).

there is essentially no background just below the GT resonance. On the other hand, the calculation reproduces the continuous spectrum at higher excitation energies rather well. This result indicated that most of the background subtracted in the experimental analysis of the GT resonance was actually GT strength (see also Osterfeld and Schulte, 1984). It was then soon verified from an experimental multipole decomposition of the cross section (Anderson *et al.*, 1985a, 1985b; Moinester, 1987) that, indeed, all the cross section below the GT peak was GT strength. This increased the total GT strength to 50–60% of the total sum-rule value (see the shaded area in Fig. 6).

The next question to ask is how much GT strength might be located beyond the main peak in the high-energy tail of the nuclear excitation spectrum? This question was first discussed by Bertsch and Hamamoto (1982), who performed a perturbative calculation for the mixing of Gamow-Teller strength with 2p-2h configurations at high excitation energies. They found that roughly 50% of the total GT strength could be shifted into the region of 10–45 MeV excitation energy for the nucleus ^{90}Zr. This amount of strength would make a significant contribution to the 0° (p,n) cross section beyond the GT resonance. Therefore, several experimental and theoretical attempts have been made to localize this GT strength.

Experimentally it is not easy to check this conjecture because the cross section in the high excitation energy region is structureless. Furthermore, as one goes up in excitation energy, the GT cross section decreases rapidly per unit GT strength because of the momentum-transfer dependence of both the projectile-target nucleon interaction $V^C_{\sigma\tau}(q)$ and the GT transition density $\rho^{(\sigma\tau)}_{1^+}(q)$. Both fall off rapidly with increasing momentum transfer, thus making it easy to hide GT strength in (p,n) reactions, as the strength is pushed up in excitation energy.

One experimental method of looking for GT strength in the continuum is to compare 0° (p,n) spectra of neighboring nuclei which differ only in neutron excess. This procedure was applied by Goodman and Bloom (1984) to the targets ^{40}Ca and ^{42}Ca. The nucleus ^{42}Ca has a strong low-lying GT state at $E_x=0.61$ MeV and several other weak GT states at higher excitation energies, summing to a total B(GT) value $\sum B(\mathrm{GT})=3.2\pm0.2$. This value is far less than the required minimum value of 6 for two excess neutrons. Since ^{40}Ca has essentially zero GT strength, one can use its 0° (p,n) spectrum as a reference point for the background level in ^{42}Ca(p,n). Hence Goodman and Bloom (1984) subtracted the 0° ^{40}Ca from the 0° ^{42}Ca spectrum to see the effect of the neutron excess in the continuum. Although these authors concluded that only 50% of the sum rule is present in the ^{42}Ca spectrum, their plot of the difference spectrum shows a consistent excess cross section up to 30 MeV excitation energy. If this excess cross section were all $L=0$ GT strength, over 80% of the sum-rule limit would be present.

Various theoretical attempts (Izumoto, 1983; Bang

et al., 1985; Klein *et al.*, 1985; Osterfeld *et al.*, 1985; Cha and Osterfeld, 1989) have been made to calculate the complete forward-angle (p,n) spectra using RPA wave functions for the description of the nuclear excitation spectrum. The use of the RPA method is of particular importance in this connection since it describes the energetics of the collective modes properly. Furthermore, it allows for the use of large model spaces, including many $\hbar\omega$ excitations. Such large model spaces are needed to exhaust the total transition strength of the relevant multipole operators.

Izumoto (1983) was the first to calculate the continuum cross section for the ^{90}Zr(p,n) reaction at $E_p=200$ MeV using large basis continuum RPA wave functions for the nuclear structure. The RPA response was calculated in two ways: once with and once without the inclusion of Δ-isobar degrees of freedom. The single-particle wave functions used in the RPA were generated from a Woods-Saxon potential. The residual p-h interaction was assumed to consist of one-pion exchange plus a repulsive zero-range Landau-Migdal term with a force strength of $g_0'=0.7$ in pionic units. The coupling between p-h and Δ-h states was obtained by following the prescription of Sec. V.F.4 using a short-range repulsion between p-h and Δ-h states modeled according to the "universality" argument of Oset and Rho (1979), with $g'_{N\Delta}=g'_0$. A quenching of 30% of the total GT strength was found due to the coupling of p-h with Δ-h states. From the RPA wave functions Izumoto calculated the inclusive ^{90}Zr(p,n) cross section using a simplified effective projectile-target

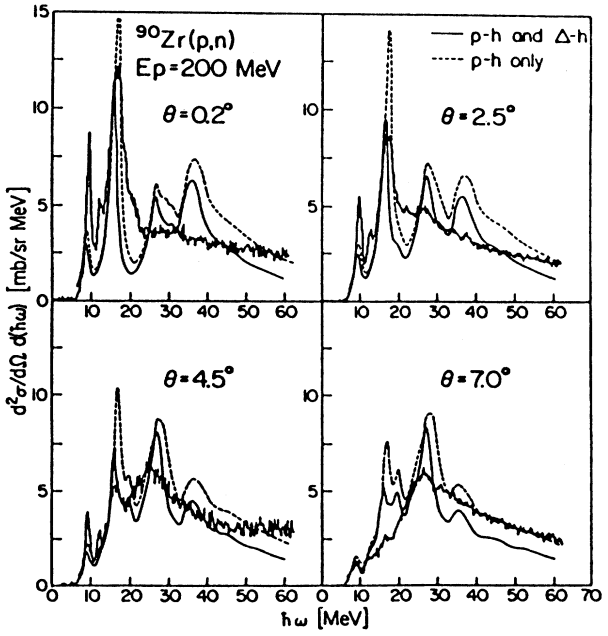

FIG. 26. Neutron spectra for the reaction ^{90}Zr$(p,n)^{90}$Nb at angles of 0° and 4.5°. The data are from Gaarde *et al.* (1981). The theoretical spectra (Izumotu, 1983) were calculated either with the usual RPA wave functions (heavy solid) or with generalized RPA+Δ wave functions (dashed line). From Izumotu (1983).

nucleon interaction normalized to the t_F-matrix interaction of Love and Franey. The results of his calculations are compared to the 200-MeV ^{90}Zr$(p,n)^{90}$Nb data of Gaarde *et al.* (1981) in Fig. 26. The solid and dashed line represent the theoretical spectra calculated either with (full curve) or without (dashed curve) Δ-isobar degrees of freedom. The magnitude of the calculated cross section is seen to be in fair agreement with the data, although the theoretical spectra show too much structure. This is due to the fact that the continuum RPA only includes the escape width ($\Gamma^{\uparrow}$), but not the spreading width ($\Gamma^{\downarrow}$) of the nuclear states. In Izumoto's calculations a constant spreading width of $\Gamma=2$ MeV was assumed for all final nucleus states.

Similar calculations to those of Izumoto were also carried out by Osterfeld *et al.* (1985) with the major difference that Osterfeld *et al.* treated both the nuclear structure and the nuclear reaction calculations on a more quantitative level. In their calculations the nuclear structure wave functions were generated from a large basis RPA calculation using a discretized continuum and the Jülich-Stony Brook residual interaction of Secs. V.F.2 and V.F.4. The finite-range part of $F^{\text{p-h}}$ was properly antisymmetrized. The reaction calculations were performed with exact inclusion of knockout exchange amplitudes for both the nucleonic and the Δ-isobar sector. The Love-Franey t_F matrix was employed for the effective projectile-target nucleon interaction and was calibrated to β decay as described in Sec. IV.E. The continuous theoretical spectra were then generated by folding the cross sections to the discrete RPA final states into an asymmetric Breit-Wigner weight function with widths either taken from experiment or adjusted phenomenologically. Strongly asymmetric spreading widths with large high-energy tails were needed to describe the data. This folding procedure effectively simulates the damping of the 1p-1h RPA doorway states due to their coupling to 2p-2h states and more complicated configurations. The results of Osterfeld *et al.* (1985) are shown in Fig. 27. The theoretical spectra describe the experimental data rather well in the Q value range $0\geq Q\geq -40$ MeV. Apparently there is not much need for quenching of GT strength to bring theory and experiment into agreement. Actually the calculations with explicit Δ-isobar degrees of freedom underestimate the data quite appreciably. It is important to notice that the projectile-target nucleon coupling was calibrated to β decay. Hence there is no freedom to readjust the magnitude of the cross section. Part of the cross section is simply lost from the low-lying spectrum due to the Δ-isobar mechanism. Within the framework of the RPA theory there is obviously no need for a large Δ-isobar quenching mechanism.

Similar calculations for the ^{90}Zr(p,n) spectrum were also carried out by Bang *et al.* (1985) and by Klein *et al.* (1985), arriving at conclusions similar to those of Osterfeld *et al.* (1985). Bang *et al.* used a local Woods-Saxon potential to generate the single-particle wave functions and a Landau-Migdal-type residual interaction supple-

mented by a renormalized π exchange potential. Klein *et al.* performed a continuum RPA calculation using the Skyrme III force to generate the Hartree-Fock potential and the single-particle wave functions. The residual p-h interaction was chosen self-consistently, i.e., to be of Skyrme type. The continuum RPA calculations were solved in a large 1p-1h configuration space truncated at 200 MeV. The calculated strength function was smoothed with a Lorentzian function whose full width at half maximum was taken to be 2 MeV. All multipoles with $J^{\pi} \leq 5^{+}$ were included. The (p,n) spectrum was calculated with the Love-Franey (1981) t_F-matrix interaction. The results of Klein *et al.* (1985) are shown in Fig. 28. The shape of the calculated spectra is very similar to that of Izumoto in Fig. 26. While the experimental cross section at forward angles and low excitation energies is overestimated by the theoretical spectra, it is underestimated at high excitation energies. The energy-integrated theoretical and experimental cross sections, however, agree well for the angular range $0 \leq \theta \leq 10°$. Moreover, there is a good agreement between the calculated energy-integrated cross sections of Klein *et al.* (1985) and Osterfeld *et al.* (1985). Hence the picture that is emerging from these various independent analyses of the (p,n) data is that at least part of the GT strength which is missing from the low-energy portion of the experimental spectrum is present at excitation energies well beyond the values predicted by the 1p-1h RPA.

This picture is supported by calculations for other target nuclei. Bang *et al.* (1985) and Cha and Osterfeld (1989), for instance, have also calculated energy spectra for the reaction ^{208}Pb(p,n) at 200 MeV incident energy. The nucleus ^{208}Pb is especially interesting because the RPA works best in this case and describes excitation energies, $B(E\lambda)$ values, and transition densities of many low- and high-lying states in a quantitative way. In Fig. 29 the calculated spectra of Cha and Osterfeld (1989) are compared to the data. One sees that the experimental data at all scattering angles are described rather well by the microscopic cross-section calculations. In general the theoretical cross sections tend to overestimate the data at lower excitation energies ($0 \leq E_x \leq 40$ MeV) and underestimate them at higher excitation energies. In the high excitation energy region, two-step processes will certainly contribute to the cross section (Bertsch and Scholten, 1982; Scholten *et al.*, 1983; Smith and Wambach, 1988). In Fig. 29 the background cross section with respect to the GT resonance is also shown. One sees

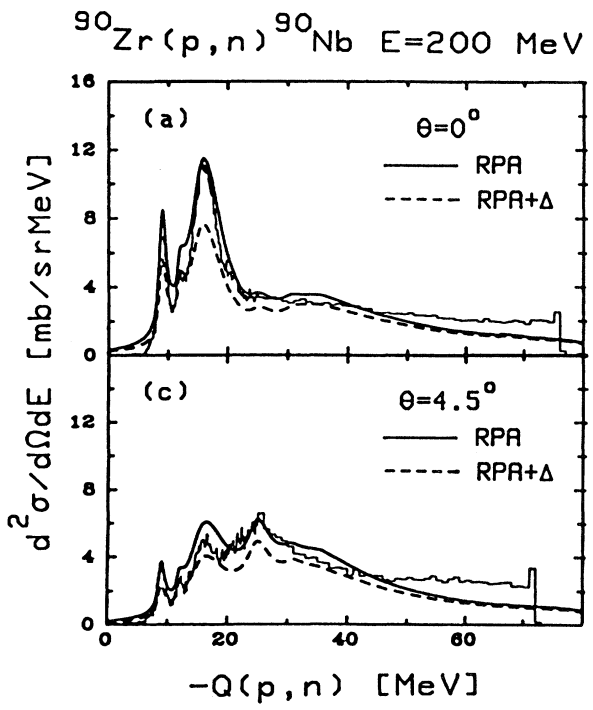

FIG. 27. Continuum cross sections of the reaction ^{90}Zr$(p,n)^{90}$Nb for $E_p = 200$ MeV at various scattering angles. The solid and dashed lines are theoretical predictions (Osterfeld *et al.*, 1985) calculated with and without inclusion of Δ-isobar hole states, respectively. The data are from Gaarde *et al.* (1981).

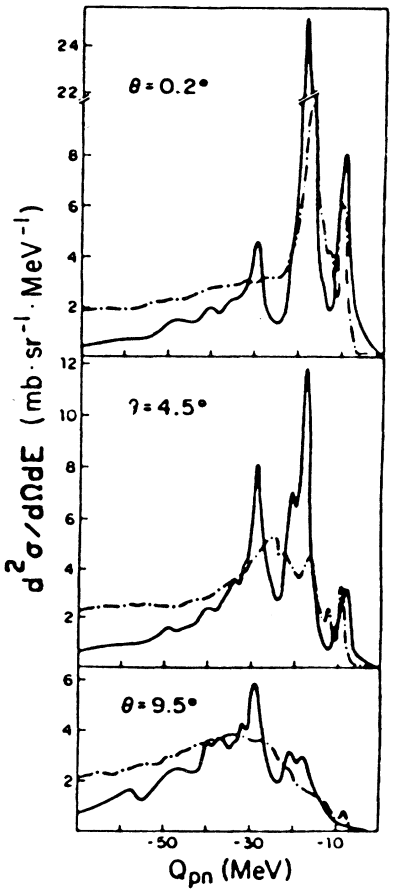

FIG. 28. Spectra for the reaction ^{90}Zr$(p,n)^{90}$Nb at $E_p = 200$ MeV. The continuous lines represent the calculated cross sections (Klein *et al.*, 1985), and the dot-dashed lines represent the data (Gaarde *et al.*, 1981). From Klein *et al.* (1985).

that the GT strength is spread out up to $E_x = 40$ MeV. An analysis of the data suggests that the quenching of GT strength due to Δ isobars can only be of the order of 10–20% in order not to destroy the good description of the data. The energy-integrated experimental and theoretical cross sections agree at all scattering angles within 10%. This is a further strong indication that quenching due to Δ's is not large.

B. Spin observables in the charge-exchange continuum

The measurement of polarization transfer observables in the (**p**,**n**) reaction can help to identify the spin and parity decomposition of the continuum. In particular, the measurement, of the transverse polarization transfer coefficient D_{nn} makes it possible to separate the spin-flip from the non-spin-flip cross section. In these experiments the incoming proton is polarized transversely to the beam direction with its spin pointing perpendicular to the scattering plane (parallel to $\hat{\mathbf{n}}$). The polarization of the outgoing particle is then measured for orientations parallel and antiparallel to the $\hat{\mathbf{n}}$ direction. Moss (1984) has shown that, within the limits of the plane-wave impulse approximation, the spin-observable D_{nn} is sensitive to the total (J), orbital (L), and spin (S) angular momentum transfers associated with a nuclear transition. This implies that D_{nn} can serve as a J^π meter and can help to determine the strength distribution functions of states with different J^π. Of particular interest is the GT strength function and the issue of the "missing" GT strength in the continuum.

To study the various properties of D_{nn}, we first note that $D_{nn} = D_{yy}$, as defined in Eq. (4.8). From Eq. (4.30) we notice that only the spin operators $\sigma_p \cdot \hat{\mathbf{q}}$ and $\sigma_p \cdot \hat{\mathbf{Q}}$ can flip the projectile spin around the $\hat{\mathbf{n}}$ axis, while all

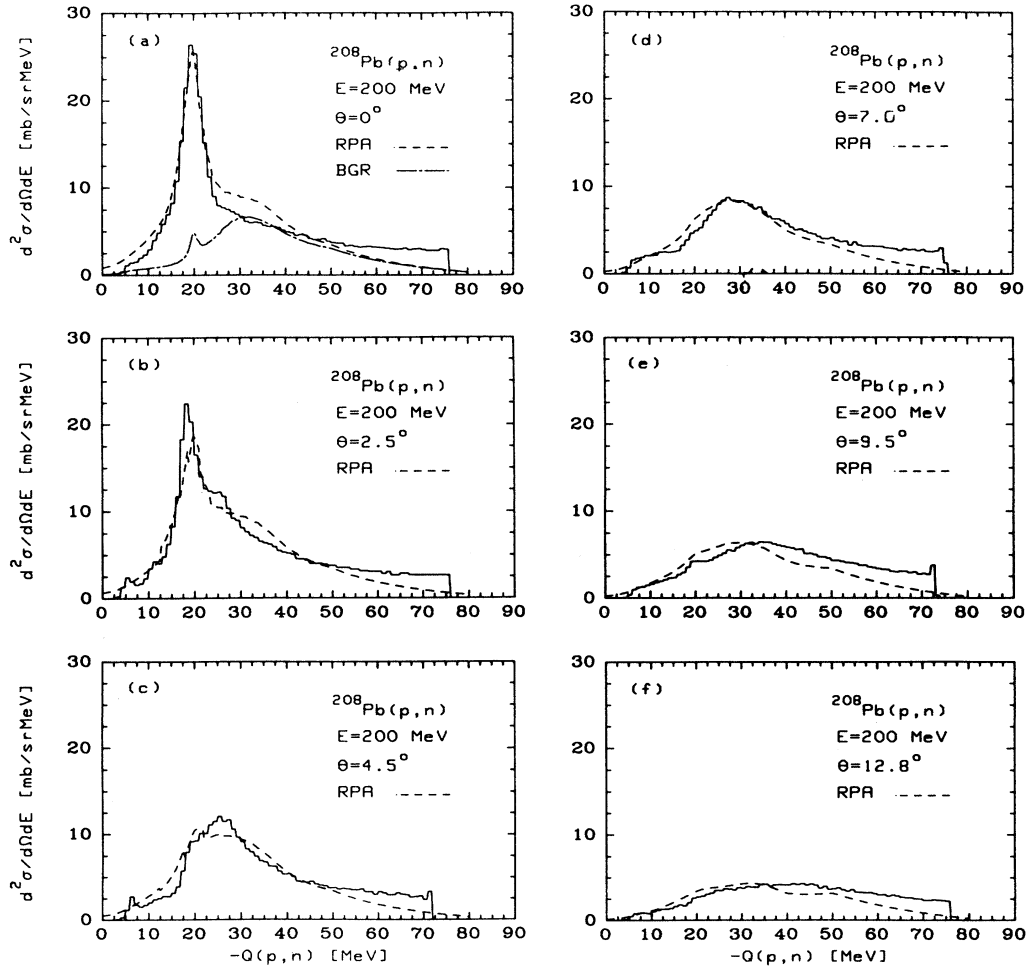

FIG. 29. Neutron spectra for the reaction ^{208}Pb$(p,n)^{208}$Bi. The data (solid curve) were taken from Gaarde *et al.* (1981). The complete theoretical spectra (Cha and Osterfeld, 1988) were calculated with RPA wave functions (dashed curve). The long-short dashed curve in (a) shows the background with respect to the GT resonance. From Cha and Osterfeld (1988).

other terms—including the spin operator $\sigma_p \cdot \hat{\mathbf{n}}$—leave the spin untouched. Using Eq. (4.60) together with Eq. (4.33) we can specify the various spin-flip and non-spin-flip contributions to the charge-exchange cross section within the plane-wave-impulse approximation. For natural-parity transitions we obtain (Love *et al.*, 1987)

$$D_{nn}=\frac{\sigma^0+\sigma^t(\hat{\mathbf{n}})-\sigma^t(\hat{\mathbf{Q}})}{\sigma^0+\sigma^t(\hat{\mathbf{n}})+\sigma^t(\hat{\mathbf{Q}})}$$
$$=\frac{1}{1+2\sigma^t/\sigma^0}\ , \quad \Delta\pi=(-)^J \tag{6.1}$$

and for unnatural-parity transitions we have (Love *et al.*, 1987)

$$D_{nn}=\frac{\sigma^t(\hat{\mathbf{n}})-\sigma^t(\hat{\mathbf{Q}})-\sigma^l(\hat{\mathbf{q}})}{\sigma^t(\hat{\mathbf{n}})+\sigma^t(\hat{\mathbf{Q}})+\sigma^l(\hat{\mathbf{q}})}$$
$$=\frac{-1}{1+2\sigma^t/\sigma^l}\ , \quad \Delta\pi=(-)^{J+1}\ . \tag{6.2}$$

Here σ_0 is the non-spin-flip cross section produced by the isovector transition potential $V_\tau^C(q)\rho_{I_f I_i}^{(\tau)}(\mathbf{q})$ of Eq. (4.57), and σ^t and σ^l are the transverse (t) and longitudinal (l) spin-flip cross sections produced by the transition potentials $V_\tau^t(q)\rho_{fi,\tau}^{(t)}(\mathbf{q})$ and $V_\tau^l(q)\rho_{fi,\tau}^{(l)}(\mathbf{q})$, respectively. The longitudinal cross section σ^l is nonvanishing only for unnatural-parity ("pionlike") states, hence its appearance in Eq. (6.2) but not in Eq. (6.1). Observing that $\sigma^t(\hat{\mathbf{n}})=\sigma^t(\hat{\mathbf{Q}})=\sigma^t$, one easily verifies the second equality in Eqs. (6.1) and (6.2).

An immediate result of Eq. (6.1) is that for natural-parity $S=0$ transitions $D_{nn}=1$, since $\sigma^t\equiv 0$ in this case. On the other hand, for natural-parity $S=1$ transitions $D_{nn}\approx 0$, because now $\sigma^0\equiv 0$. For unnatural-parity transitions D_{nn} is always negative, as follows from Eq. (6.2). In this case D_{nn} depends on the ratio

$$\frac{\sigma^t}{\sigma^l}=\left|\frac{\rho_{fi,\tau}^{(t)}(\mathbf{q})}{\rho_{fi,\tau}^{(l)}(\mathbf{q})}\frac{V_\tau^t(q)}{V_\tau^l(q)}\right|^2\ , \tag{6.3}$$

where the nuclear structure and reaction aspects of the problem enter through the ratios $\rho_{fi,\tau}^{(t)}(\mathbf{q})/\rho_{fi,\tau}^{(l)}(\mathbf{q})$ and $V_\tau^t(q)/V_\tau^l(q)$, respectively. Both the transition-density ratio and the force strength ratio depend on the momentum transfer q. The q dependence of the interaction terms V_τ, V_τ^t, and V_τ^l is shown in Fig. 30 for the 210-MeV t_F-matrix interaction parametrized by Franey and Love (1981). One observes that V_τ^t and V_τ^l dominate V_τ^C for $q\leq 2$ fm^{-1}. This makes spin excitations the dominant states at this bombarding energy and in this momentum-transfer range. Furthermore, the linear momentum profiles of V_τ^l and V_τ^t are such that for $0\leq q\leq 1$ fm^{-1} the longitudinal interaction V_τ^l varies strongly with q, while the transverse interaction V_τ^t changes only slowly with q. This different behavior of the spin-dependent interaction terms is qualitatively understood from the underlying meson-exchange picture. The longitudinal interaction V_τ^l obtains a large contribution from the one-pion exchange interaction, which causes a strong q dependence because

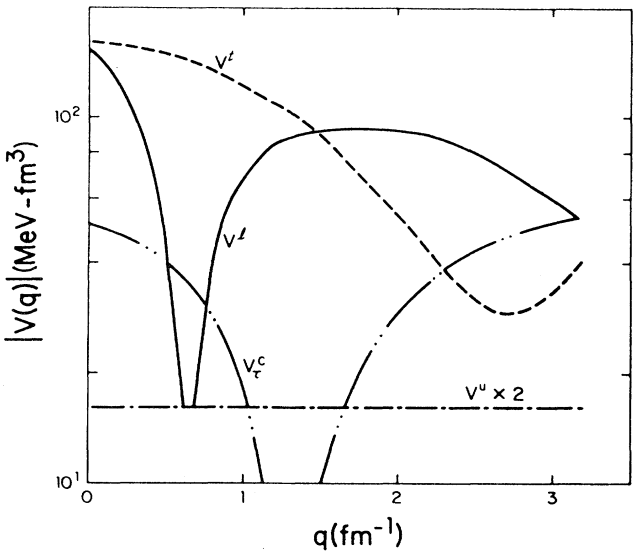

FIG. 30. The isovector spin-independent (V_τ^C), spin-longitudinal (V^l), spin-transverse (V^t), and exchange spin-transverse (V^u), parts of the free t_F-matrix interaction vs q at $E_p=210$ MeV. From Love *et al.* (1987).

of the light pion mass. On the other hand, V_τ^t is driven by one-ρ meson exchange, which varies slowly with q because of the large ρ-meson mass.

From Fig. 30 it is clear that the relative magnitude of $V_\tau^t(q)$ and $V_\tau^l(q)$ will mainly determine which value is taken on by D_{nn} for unnatural-parity transitions at a given momentum transfer q. For small q values ($q\leq 0.2$ fm^{-1}) one expects $D_{nn}\approx -\frac{1}{3}$ for states that have longitudinal and transverse transition densities of comparable magnitude. For larger q values, however, D_{nn} will tend to zero because of the weak V_τ^l. This result suggests that the sensitivity of D_{nn} to natural versus unnatural-parity transitions is most pronounced at small-momentum transfers ($q\leq 0.5$ fm^{-1}). From a nuclear structure point of view, the value of D_{nn} becomes more negative the more a nuclear transition is of longitudinal character. A purely longitudinal excitation like a 0^- transition has $D_{nn}=-1$. Summarizing, we can say that a positive value of D_{nn} is a signature of $S=0$ strength, while a vanishing or negative value is a signature of $S=1$ strength. The more negative D_{nn} becomes, the more important is the contribution of the spin-longitudinal response to the cross section. It can be shown that distortion effects do not alter these results as long as there are no strong spin-orbit terms in the optical potentials.

Transverse polarization transfer measurements of (**p**,**n**) reactions to the continuum have recently been performed at IUCF with beam energies up to 200 MeV (Taddeucci *et al.*, 1986). Figure 31(b) shows 0° spectra for the ^{90}Zr(**p**,**n**)^{90}Nb reaction at $E_p=160$ MeV. In the top and in the middle part of the figure, the differential spin-flip

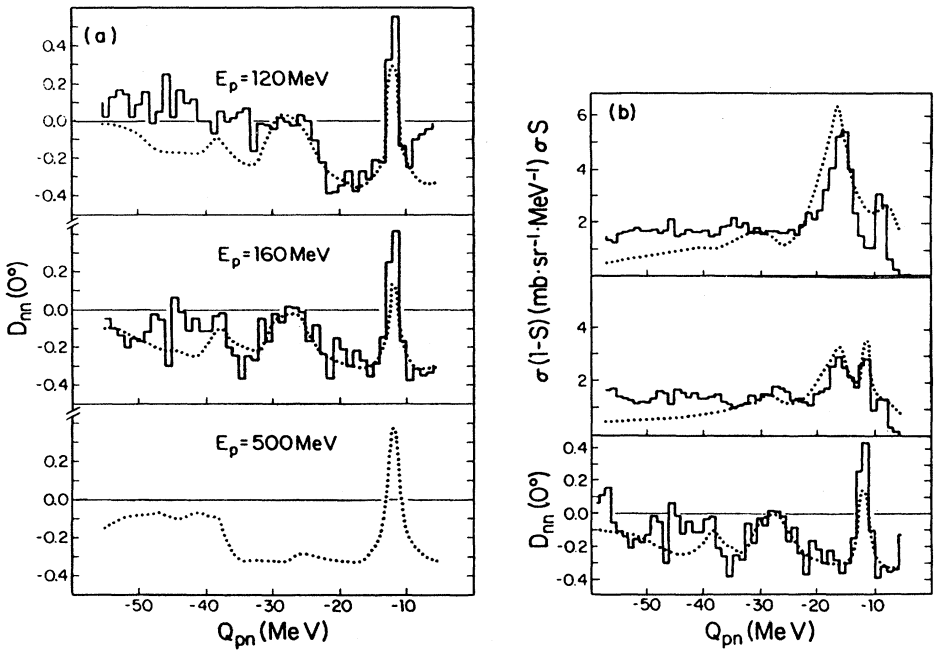

FIG. 31. (a) Spectra of $D_{nn}(0°)$ for the ^{90}Zr$(p,n)^{90}$Nb reaction at different incident energies. The continuous lines represent the data (Taddeucci, 1987). The dotted lines represent the polarization transfer coefficients calculated using the DWIA. (b) The 0° spectra for the spin-flip cross section σS_{nn} and the non-spin-flip cross section $\sigma(1-S_{nn})$, for the ^{90}Zr$(p,n)^{90}$Nb reaction at $E_p=160$ MeV. The $D_{nn}(0°)$ values are also shown. The continuous lines represent the data; the dotted lines denote the theoretical results. From Love *et al.* (1987).

and non-spin-flip cross sections are shown as a function of the Q_{pn} value of the reaction. Both cross sections are expressed in terms of the spin-flip probability S_{nn}, which is defined by $S_{nn}:=(1-D_{nn})/2$. The value of S_{nn} is zero for $S=0$ transitions and lies between zero and one for $S=1$ transitions. Some interesting features emerge from Fig. 31(b). The giant GT resonance stands out in both the spin-flip (σS_{nn}) and the non-spin-flip [$\sigma(1-S_{nn})$] spectrum. On the other hand, the isobaric analog state transition, for which $D_{nn}=1$, stands out only in the non-spin-flip spectrum, as expected. The GT resonance and the low-lying GT states have a negative value of $D_{nn}=-\frac{1}{3}$, as expected for pure GT transitions. This can be seen from the lower part of Fig. 31(b), where the D_{nn} spectrum is shown. The $D_{nn}=-\frac{1}{3}$ value extends over the range -22 MeV $\leq Q_{pn} \leq -15$ MeV. This result is consistent with the theoretical prediction (Bang *et al.*, 1985; Klein *et al.*, 1985; Osterfeld *et al.*, 1985) that most of the strength in this energy region should be due to GT excitations. The data, however, cannot exclude the possibility of other unnatural-parity excitations.

Another noteworthy feature of the data in Figs. 31(a) and 31(b) is that $D_{nn} \approx 0$ near $Q_{pn}=-27$ MeV. This is the excitation energy about which the giant spin-flip dipole resonance is centered. The data indicate that a large fraction of the strength observed in this energy region at 0° has natural parity, i.e., $J^\pi=1^-$. Around $Q_{pn} \approx -35$ MeV there seems to be again a concentration of unnatural-parity strength.

The dotted curves in Figs. 31(a) and 31(b) are the calculations of Klein and Love (1986), which are in remarkable agreement with the measured cross sections and with the measured D_{nn} values in the Q_{pn} range of $-32 \leq Q_{pn} \leq -15$ MeV. The calculations were performed in the same way as described in Sec. VI.A, apart from the fact that now the continuum RPA cross sections are smoothed (Klein *et al.*, 1985; Klein and Love, 1986) using a Lorentzian function with a full width at half maximum of 6 MeV. Especially interesting is the prediction for D_{nn} at $E_p=500$ MeV, since the signature for the $J^\pi=1^-$ strength at $Q_{pn}=-27$ MeV disappears. The D_{nn} values up to $Q_{pn}=-35$ MeV are now dominated by the $J^\pi=1^+$ excitations (GT and spin-isovector monopole), which produce $D_{nn} \approx -\frac{1}{3}$. The $J^\pi=1^-$ excitation is suppressed at forward angles ($\theta=0°$) and high incident energies ($E_p=500$ MeV) because it involves an $L=1$ angular distribution that yields a very small cross section near $q \approx 0$. Simultaneously there is practically no cross-section loss for the redistributed GT strength because of the small change in momentum transfer for increasing Q values. The 200-MeV $(\mathbf{p},\mathbf{n})$ data of Taddeucci *et al.* (1986) already show a tendency towards this behavior. Spin-flip transfer experiments were also performed by Watson *et al.* (1986) for the ^{48}Ca$(\mathbf{p},\mathbf{n})^{48}$Sc reaction at $E_p=135$ MeV with very similar results. In these experiments 75% of the GT strength could be identified.

C. The (p, p') spin-flip transfer reaction

Recently, cross sections, analyzing powers, and spin-flip probabilities have been measured at small angles in the polarized proton inelastic scattering from targets in the mass range from ^{12}C to ^{90}Zr (Nanda *et al.*, 1983, 1984; Glashausser *et al.*, 1987; Häusser *et al.*, 1988). These measurements reveal a large cross section for spin excitations distributed roughly uniformly over the excitation energy region from 8 to 40 MeV. This is a very interesting result, particularly in connection with the identification of the $M1$ and $M2$ strength in the inelastic channel.

In ^{90}Zr the spin-flip measurements can clearly identify the $M1$ resonance (Nanda *et al.*, 1983, 1984), but a large amount of spin-flip strength is also observed in the continuum region above the giant $M1$ resonance. It is important to understand this spin-flip strength in order to draw firm conclusions concerning the quenching mechanism of the magnetic strength.

In ^{40}Ca first evidence has been reported for the spin-flip dipole and spin-flip quadrupole resonances (Glashausser *et al.*, 1987). The strength distributions of the individual modes were obtained by performing a multipole decomposition of the spin-flip cross section at various scattering angles. This multipole decomposition was based on the assumption that the measured cross section is background free; that is, that it receives little contributions from two-step processes. This assumption is supported by microscopic cross-section calculations, as we shall now show.

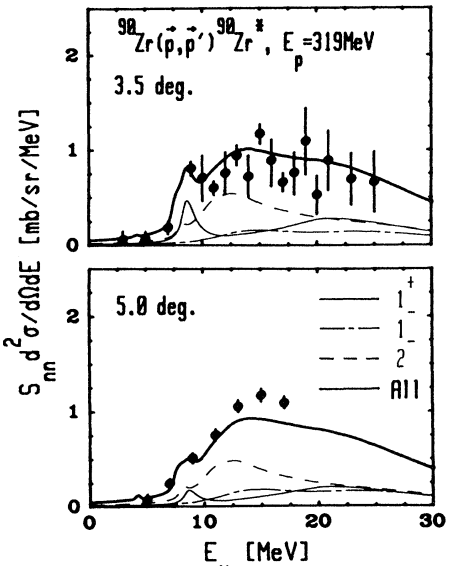

FIG. 32. Spin-flip spectra for the ^{90}Zr(p,p') reaction at scattering angles of 3.5° and 5°, respectively. The solid circles are the experimental data (from Nanda *et al.*, 1983). The heavy-solid curve shows a DWIA calculation, including many multipoles of transitions (Yabe *et al.*, 1986). For comparison, the cross-section contributions of 1^+, 1^-, and 2^- states are also given. From Yabe *et al.* (1986).

As an example of a multipole decomposition of an inelastic spin-flip spectrum we choose the ^{90}Zr(p,p') reaction at $E_p = 319$ MeV. In Fig. 32 the spin-flip spectra calculated by Yabe *et al.* (1986) are compared to the data of Nanda *et al.*, (1983, 1984) at scattering angles of 3.5° and 5°, respectively. The theoretical spectra (Yabe *et al.*, 1986) were calculated within the DWIA using RPA wave functions for the nuclear structure description. The cross sections to the discrete RPA states were folded into an energy-dependent phenomenological width Γ. From Fig. 32 it can be seen that the theoretical spectra reproduce the experimental data rather well. The theoretical spectra are the incoherent sum of cross sections with multipolarities $L=0$ through $L=3$ ($J^\pi = 0^-, 1^+, 1^-, 2^+, 2^-, 3^+$). The largest contribution to the total spin-flip cross section comes from the 2^- states, which generate roughly 40% of the theoretical spin-flip cross section. The 2^- strength distribution shown in Fig. 32 is rather similar to that of elaborate 2p-2h calculations performed by Drożdż *et al.* (1987). The energy-integrated ^{90}Zr(p,p') spin-flip cross section is in good agreement with the transition strength predictions obtained from the RPA. A similar result was obtained by Esbensen and Bertsch (1984) using a semi-infinite nuclear slab model for the nuclear structure description.

D. Some results from the (^{3}He,t) reaction

The decomposition of the spectra into the various multipoles described in the previous paragraphs is, of course, model dependent. To reduce the model dependence it is helpful to have data from other probes which show a different selectivity for the excitation of the various spin-flip modes. Such data are provided by the (^{3}He,t) reaction at intermediate energies ($E=200$–400 MeV/nucleon). Here an interesting observation is made in that the high excitation energy cross section of the 0°(^{3}He,t) spectrum appears to be much larger than that of the corresponding cross section in the (p,n) spectrum. From the analyses of the (p,n) data in Sec. VI.A one would expect that this enhancement is due to a stronger excitation of the $1\hbar\omega$ and $2\hbar\omega$ modes in (^{3}He,t) than in (p,n). An analysis of the (^{3}He,t) data shows that this expectation is, indeed, correct. The enhancement factor is about 10 and is a result of the strong surface character of the (^{3}He,t) reaction. The (^{3}He,t) data thus provide different nuclear structure information from that of the (p,n) data.

In Fig. 33 spectra are shown for the ^{90}Zr(^{3}He,t) reaction at $E=600$ MeV incident energy and at scattering angles of 0°, 2.5°, and 4.3°. The solid lines represent the experimental data (Ellegaard *et al.*, 1983) and the dashed curves are the calculated spectra (Udagawa *et al.*, 1987). The calculations were performed in a similar manner to that for the ^{90}Zr(p,n) reaction described in Sec. VI.A. In the case of the (^{3}He,t) reaction the finite size of the projectile has to be considered. This was done (Udagawa *et al.*, 1987) by folding the effective projectile nucleon-target nucleon interaction into the magnetic projectile

density distribution of ^{3}He, which was taken from experiment (McCarthy *et al.*, 1977). Similarly, the optical potentials in the incident and exit channels were generated from the 200-MeV proton optical potentials of Nadasen *et al.* (1981) by following the single folding procedure.

The low-energy part of the 0° spectrum in Fig. 33 is clearly dominated by the GT transitions and is described well by the calculations. The high-energy part of the spectrum, i.e, the energy region 15 MeV $\leq E_x \leq$ 40 MeV, is underestimated by the calculations. This part of the spectrum is dominated by the $2\hbar\omega$, $L=0$, $J^\pi=1^+$, and $2\hbar\omega$, $L=2$, $J^\pi=1^+$, 2^+, and 3^+ transitions. In the (p,n) reaction at $E=200$ MeV the contributions of the $2\hbar\omega$ modes to the 0° spectrum are small. The enhancement of the $2\hbar\omega$ modes in the (^{3}He,t) spectrum can be explained by the surface character of the (^{3}He,t) reaction (see Udagawa *et al.*, 1987).

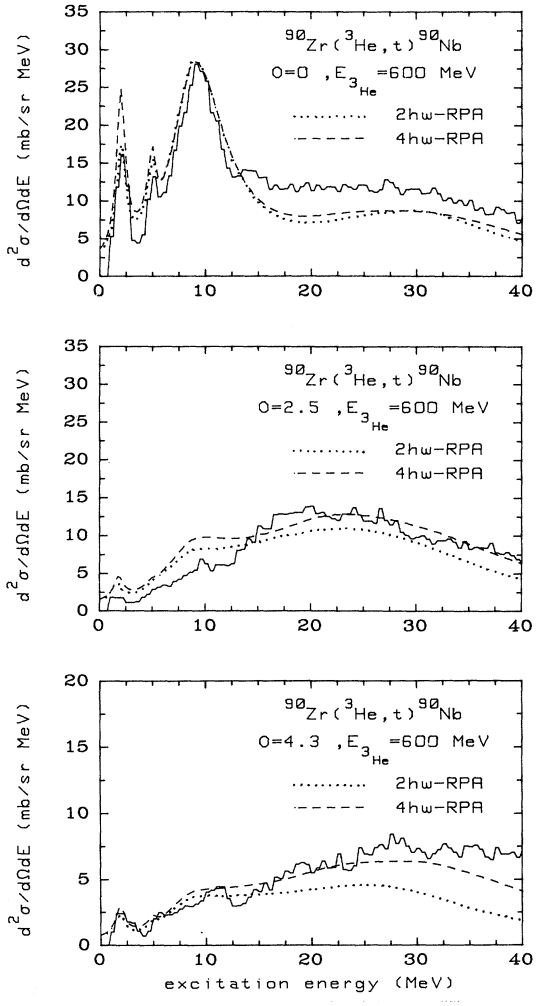

FIG. 33. Spectra of the reaction ^{90}Zr(^{3}He,t)^{90}Nb at 600 MeV bombarding energy for scattering angles of $\theta=0°$, 2.5°, and 4.3°. The data (solid line) are taken from Ellegaard *et al.* (1985). The dotted curves are the calculations performed in a $2\hbar\omega$ RPA model space, while the dashed curves are the results obtained in a $4\hbar\omega$ RPA model space. From Udagawa *et al.* (1987).

VII. SPIN-ISOSPIN RESPONSE IN THE QUASIFREE AND Δ-RESONANCE REGIONS

A. The quasifree region

In this section we discuss the continuum spectra obtained with high-energy beams. The quasifree region represents a broad bump in the nuclear continuum which, to a first approximation, can be interpreted as due to the incident particles, being directly scattered by the individual nucleons in the target, the nucleons being knocked out of the nucleus. This process becomes visible at momentum transfers above about 1 fm^{-1}, where the recoil nucleon gets free of Pauli blocking. The peak of the bump is expected near the excitation energy of $\omega=q^2/2m$, with m the nucleon mass and q the three-momentum transfer. The large width of the bump is a result of the Fermi motion of the nucleons in the nucleus.

One of the major aims of the experiments performed in the quasifree region ($\omega \leq 150$ MeV, $q \approx 1.0-2.5$ fm^{-1}) is to separate the spin-longitudinal ($\sigma\cdot\mathbf{q}$) from the spin-transverse ($\sigma\times\mathbf{q}$) nuclear response. The corresponding response functions are connected with the transition densities of Eqs. (4.62) and (4.63) by $R^{(l)}(\omega,q)=|\rho_\tau^{(l)}(\omega,\mathbf{q})|^2$ and $R^{(t)}(\omega,q)=|\rho_\tau^{(t)}(\omega,\mathbf{q})|^2$. Here an interesting question is whether the virtual pion field inside the nucleus is strong enough to cause a collective enhancement of $R^{(l)}(\omega,q)$ over $R^{(t)}(\omega,q)$; that is, whether or not $R^{(l)}(\omega,q)>1$. The existence of such a phenomenon would be very significant because of its direct relation to Migdal's original suggestion of the existence of a pion condensate at sufficiently high nuclear densities (Migdal, 1972, 1973, 1978). So far, all searches for so-called precritical phenomena of pion condensation have produced negative results.

In 1982 Alberico *et al.* (1982) proposed that the appropriate place to look for pionic effects in the nucleus would be the quasifree region. These authors argued that, in spite of the repulsive short-range correlations at small-momentum transfers, the p-h interaction in the $\sigma\tau$ channel might still become sufficiently attractive in the high (ω,q)-transfer region to induce an enhancement and shift of the spin-longitudinal response towards lower excitation energies relative to the free-Fermi-gas response. The transverse response $R^t(\omega,q)$ should instead be quenched and shifted upwards in excitation energy because of the repulsiveness of the p-h interaction in this channel. The arguments of Alberico *et al.* (1982) are easily understood from the $(\pi+\rho+g'_0)$ model for the residual p-h interaction. In this model the spin-longitudinal (l) and spin-transverse (t) particle-hole interactions are given by

$$V^{(l)}_{\text{p-h}}(\omega,q)=J_\pi(\omega,q)\left[g'_0+\frac{q^2}{\omega^2-q^2-m_\pi^2}\right]\sigma_1\cdot\hat{\mathbf{q}}\sigma_2\cdot\hat{\mathbf{q}}\tau_1\cdot\tau_2 \tag{7.1}$$

$$V^{(t)}_{\text{p-h}}(\omega,q)=J_\pi(\omega,q)\left[g'_0+\frac{J_\rho(\omega,q)}{J_\pi(\omega,q)}\frac{q^2}{\omega^2-q^2-m_\rho^2}\right](\sigma_1\times\hat{\mathbf{q}})\cdot(\sigma_2\times\hat{\mathbf{q}})\tau_1\cdot\tau_2\ , \tag{7.2}$$

where the force strength parametes $J_\pi(\omega,q)$ and $J_\rho(\omega,q)$ are defined in Eqs. (4.42) and (4.43). Note that the Landau-Migdal parameter g'_0 in Eqs. (7.1) and (7.2) is measured in pionic units here. The q dependence of $V^{(l)}_{\text{p-h}}(\omega,q)$ and $V^{(t)}_{\text{p-h}}(\omega,q)$ resembles the graphs shown in Fig. 30: In the high-q-transfer region [$q\sim(1-2)$ fm^{-1}] $V^{(l)}_{\text{p-h}}$ is attractive, while $V^{(t)}_{\text{p-h}}$ is repulsive there.

It is well established from inealstic electron scattering to the nuclear continuum that there are no large collective effects in the transverse spin-isospin response (Meziani *et al.*, 1985). There might be a slight reduction of the cross section in this channel, but even this small effect is not well established (O'Connell *et al.*, 1984, 1987; Meziani *et al.*, 1985). The first measurements of the spin-longitudinal response were carried out at LAMPF by Carey *et al.* (1984) and Rees *et al.* (1987). These experimentors performed a complete $(\mathbf{p},\mathbf{p}')$ spin-flip transfer experiment using longitudinal (L), sideways (S), and normal (N) polarized beams to measure the tarnsverse polarization transfer coefficients D_{qq}, D_{QQ}, and D_{nn}. They performed the experiments at $E_p=500$ MeV and at a fixed momentum transfer of $q=1.75$ fm^{-1}, where the precritical effects of pion condensation are expected to be largest. From the measurement of the coefficients D_{qq}, D_{QQ}, and D_{nn} one can extract the transverse and longitudinal spin-flip cross sections $\sigma^l(\omega,q)$ and $\sigma^t(\omega,q)$, by using for D_{qq} and D_{QQ} similar expressions to those derived for $D_{nn}=D_{yy}$ in Eq. (4.8) (for details see Carey *et al.*, 1984; Moss, 1984; Rees *et al.*, 1987). Assuming that the cross sections can be factorized into a product of nucleon-nucleon cross section (σ_{NN}) times the response function $R^{(r)}(\omega,q)$ $(r=l,t)$ times an effective number of nucleons participating in the reaction, N_{eff}, the cross section can be written as

$$\sigma^r(\omega,q)=N_{\text{eff}}\sigma_{NN}R^{(r)}(\omega,q)\quad(r=l,t)\ . \tag{7.3}$$

The response function ratio $R^{(l)}(\omega,q)/R^{(t)}(\omega,q)$ is then

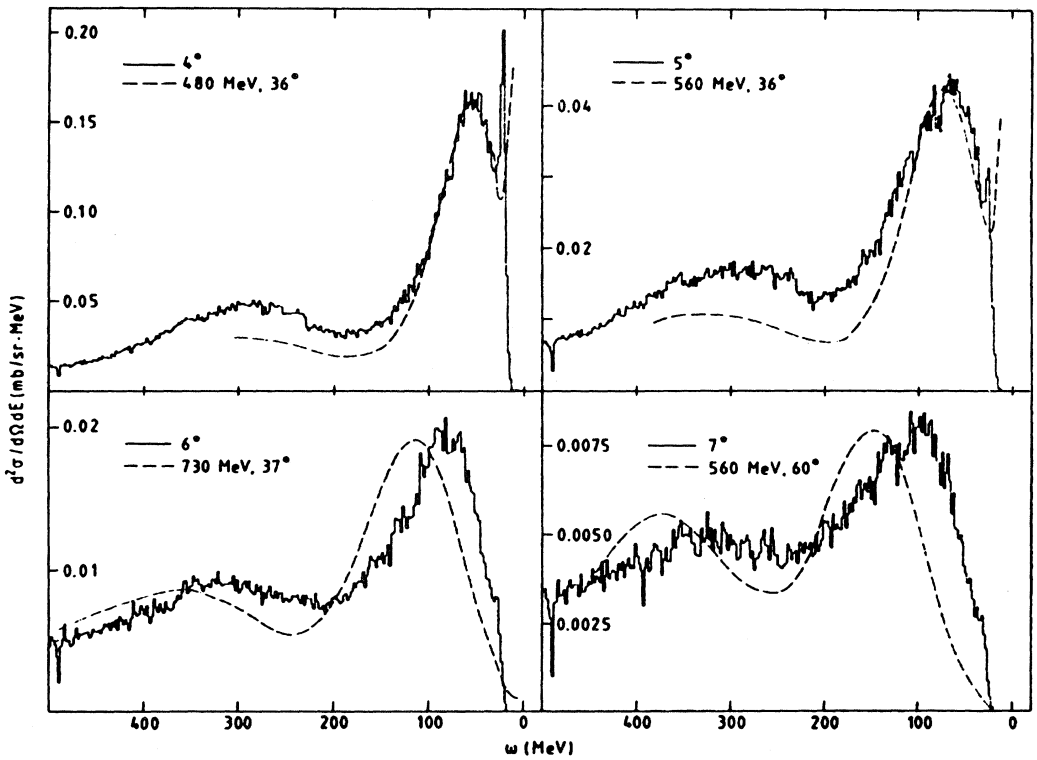

FIG. 34. Comparison between spectra from ^{12}C(^{3}He,t) (Bergqvist *et al.*, 1987) and ^{12}C(e,e') (Bareau *et al.*, 1983, O'Connell *et al.*, 1984, 1987). The solid curves denote the (^{3}He,t) data, while the dashed curves denote the (e,e') data. The (^{3}He,t) and (e,e') spectra have been chosen to have the same transferred momentum q near the quasifree peak. From Bergqvist *et al.* (1987).

easily determined. This ratio should deviate appreciably from unity if a collective enhancement in the spin-longitudinal channel is present. However, a ratio of $R^{(l)}(\omega,q)/R^{(t)}(\omega,q)\leq 1$ was found, which completely contradicts the prediction.

Inelastic proton scattering has the disadvantage that it is a mixed isoscalar-isovector ($T=0$ and $T=1$) probe and that it thus does not provide the single spin-isospin response that a charge-exchange ($T=1$) reaction can provide. Therefore a ^{12}C(^{3}He,t) charge-exchange experiment (Bergqvist *et al.*, 1987) was performed at Saturne at $E=2$ GeV incident energy. In this experiment for the first time a shift of the quasielastic peak position relative to that of the ^{12}C(e,e') experiments (O'Connell *et al.*, 1984, 1987; Meziani *et al.*, 1985) was observed. This is shown in Fig. 34, where the ^{12}C(^{3}He,t) and ^{12}C(e,e') spectra are compared at four different momentum transfers ($\omega,\mathbf{q}$). It can be seen that the (^{3}He,t) spectrum at 4° ($q=1.4$ fm^{-1}) is quite similar to the (e,e') spectrum at 480 MeV and 36°, and gives the same centroid energy and width of the peak. However, with increasing momentum transfer a relative shift takes place between the (^{3}He,t) and (e,e') bumps, amounting to about 25 MeV at $q=2.1$ fm^{-1} and to about 45 MeV at $q=2.5$ fm^{-1}.

It is also interesting to compare these results with those using other probes. This is done in Fig. 35, where the quasifree peak positions measured in the reactions (e,e') (O'Connell *et al.*, 1984, 1987), (p,p') (Moss, 1984; Rees *et al.*, 1987), (^{3}He,t) (Bergqvist *et al.*, 1987), (p,n) (Taddeuci, 1988), and (n,p) (Taddeucci, 1988) are plotted in the (ω,q) plane. One of the eminent features seen in Fig. 35 is the gradual softening of the (^{3}He,t) peak with respect to the (e,e') peak as the momentum transfer q increases. The experimental results are compared with the theoretical prediction $\omega=q^2/2m$ of a relativistic (solid line) or nonrelativistic (dashed line) Fermi gas.

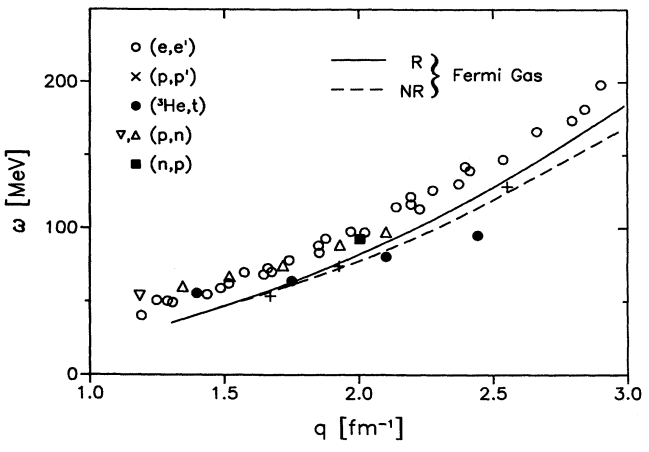

FIG. 35. Peak position of the quasifree bump in the reactions ^{12}C(e,e'), ^{12}C(p,p'), ^{12}C(p,n), ^{12}C(^{3}He,t), and ^{6}Li(n,p). The excitation energy ω of the quasifree peak is plotted vs the three-momentum transfer q. The solid and dashed lines represent the peak position of the nonrelativistic and relativistic Fermi-gas responses, respectively. From Rapaport (1989).

Several causes have been suggested to explain this relative shift of the quasifree peak positions between the (^{3}He,t) and (e,e') experiments. The most interesting one is related to the softening (hardening) of the longitudinal (transverse) spin response of the nucleus in the high-q-transfer region (Chanfray and Ericson, 1984; Ericson, 1984). Recent RPA calculations by Alberico *et al.* (1988); by De Pace and Viviani (1990, 1991), and by Ichimura *et al.* (1989) do, indeed, support such a possibility. These calculations, however, cannot simultaneously reproduce the ($\mathbf{p},\mathbf{p}'$) and the (^{3}He,t) data. Ichimura *et al.* (1989) performed a full DWIA calculation and found that projectile distortions can also produce a shift (see also Okuhara *et al.*, 1987 and Shigehara *et al.*, 1988).

The fact that recent (p,n) and (n,p) results from LAMPF (Taddeucci, 1988) seem not to show agreement with the shifts observed in the (^{3}He,t) experiments throws doubts on the interpretation of the (^{3}He,t) data. The interpretation can only be kept if one can show that there is an essential difference between the (^{3}He,t) and (p,n) reactions in exciting the spin-longitudinal and spin-transverse nuclear responses. Such a difference could be due to the (^{3}He,t) form factor, which might favor one excitation over the other, but this has yet to be proven.

The ($d,2p$) reaction has also been used to study the quasifree peak region (Ellegaard *et al.*, 1987; Gaarde, 1988). The quasifree peak position is observed to fall on the same line as the (^{3}He,t) results in Fig. 35.

B. The Δ-resonance region

The charge-exchange reactions at intermediate energies have been successfully used to measure the isovector spin response of nuclei in the Δ-resonance region. Figure 36 displays zero-degree triton spectra of the (^{3}He,t) reaction at 2 GeV bombarding energy on various targets (Contardo *et al.*, 1986). A considerable energy shift of ~70 MeV is observed between the elementary Δ excitation in the proton and the Δ excitation in a nucleus. The spectra are plotted versus the kinetic energy T of the outgoing triton. For our discussions it is more convenient to express everything in terms of excitation energy, which we define as $\omega\equiv E_{^3\mathrm{He}}-T$. For the proton target the Δ peak occurs then at $\omega\approx 325$ MeV, while for nuclear targets with mass number $A\geq 12$ it appears at $\omega\approx 255$ MeV. This phenomenon is also found to persist, although to a variable extent, at higher bombarding energies (Ableev *et al.*, 1984). A similar situation prevails for the (p,n) reaction at $E_p=800$ MeV. Here the Δ peak appears at $\omega\approx 365$ MeV in the $p(p,n)\Delta^{++}$ reaction (Glass *et al.*, 1977) and at $\omega\approx 295$ MeV for targets with $A\geq 12$ (Cassapakis *et al.*, 1976; Bonner *et al.*, 1978; Lind, 1987). Again the shift of the Δ peak position amounts to ~70 MeV. In contrast to this, in the case of γ absorption (Ziegler, 1979; Mecking, 1979; Ahrends, 1980; Arends *et al.*, 1981) and inelastic electron-scattering experiments (Barreau *et al.*, 1983, Meziani *et al.*, 1985; Sealock *et al.*,

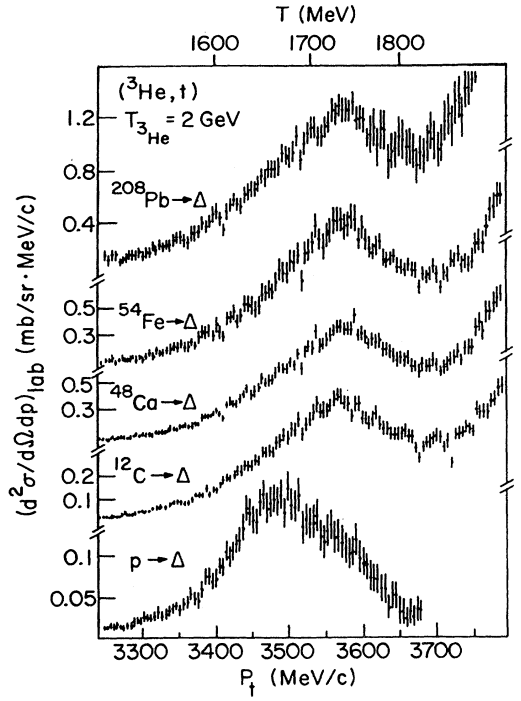

FIG. 36. Triton spectra observed in (^{3}He,t) reactions at 2 GeV incident energy for a number of targets. The important feature of the spectra is the relative shift of the Δ peak position between the proton target and the nuclear targets. From Contardo *et al.* (1986).

1989), the Δ peak does not show such a pronounced displacement.

The energy shift of the Δ peak as observed by the charge-exchange reactions has two different origins. The first is due to the Fermi motion of the nucleons in the nucleus. This effect accounts for roughly 40 MeV of the observed energy shift, leaving 30 MeV unexplained (Esbensen and Lee, 1985). This latter part of the shift is the interesting one. The question is whether it is due to a nuclear medium effect or whether it is a trivial consequence of the reaction mechanism and of the reaction kinematics.

Before we try to answer this question, let us first note that the apparent shift of ~40 MeV between the (p,n) and ^{3}(He,t) spectra is a trivial effect of the finite projectile size. The probability that the triton can survive the (^{3}He,t) scattering process is rapidly decreasing with increasing momentum transfer, so that the cross section is heavily weighted towards low excitation energy. This weighting factor is evident from the (ω,q) dependence of the ^{3}He-t form factor (Ellegaard *et al.*, 1985).

Soon after the first (^{3}He,t) experiment (Ellegaard *et al.*, 1983), Chanfray and Ericson (1984) speculated that the nontrivial part of the shift might be related to a nuclear medium effect in the isovector spin-longitudinal channel. That is, if the Δ-isobar nucleon hole (Δ-h) residual interaction becomes strongly attractive at large-momentum transfers $|\mathbf{q}|\approx 1-2$ fm^{-1}, then this attraction might lead to a lowering of the Δ mass produced in the target. Along this line of reasoning, no shift of the Δ peak position is to be observed with the electromagnetic probes, since they excite the Δ transversely, i.e., by the transition operator $\mathbf{S}\times\mathbf{q}\mathbf{T}$. Here $\mathbf{S}$ and $\mathbf{T}$ are the spin and isospin transition operators, respectively.

Several model calculations were performed to explain the shift of the Δ bump in nuclei. All of these calculations are based on the isobar-hole model, which has been successfully used in the description of pion-nucleus scattering (Hirata *et al.*, 1977, 1979; see also the reviews of Oset, Toki, and Weise, 1982; Ericson and Weise, 1988) and γ absorption (Koch *et al.*, 1984, Ericson and Weise, 1988).

In the isobar-hole model the elementary excitations of the nucleus are the Δ-h states. The Δ is assumed to move in a complex one-body potential, the imaginary part of which describes the increase of the Δ width in nuclei due to decay channels other than $\Delta\rightarrow\pi+N$, such as $\Delta N\rightarrow NN$. The real part of the Δ nucleus potential incorporates a variety of effects, like (i) the average single-particle potential experienced by the Δ, (ii) Pauli blocking effects, etc. (see Ericson and Weise, 1988).

The correlations between the Δ-h states are introduced by solving RPA-like equations with a residual interaction of the form

$$V_{\Delta\text{-h}}(\omega,q)=[V^{(l)}_{\Delta\text{-h}}(\omega,q)\mathbf{S}_1\cdot\hat{\mathbf{q}}\mathbf{S}_2^{\dagger}\cdot\hat{\mathbf{q}} + V^{(t)}_{\Delta\text{-h}}(\omega,q)(\mathbf{S}_1\times\hat{\mathbf{q}})\cdot(\mathbf{S}_2^{\dagger}\times\hat{\mathbf{q}})]\mathbf{T}_1\cdot\mathbf{T}_2^{\dagger} \quad (7.4)$$

where

$$V^{(l)}_{\Delta\text{-h}}(\omega,q)=J_{\pi}(\omega,q)\left[\frac{f_{\pi N\Delta}}{f_{\pi NN}}\right]^2 \times\left[g'_{\Delta\Delta}+\frac{q^2}{\omega^2-q^2-m_{\pi}^2+i\epsilon}\right] \quad (7.5)$$

and

$$V^{(t)}_{\Delta\text{-h}}(\omega,q)=J_{\pi}(\omega,q)\left[\frac{f_{\pi N\Delta}}{f_{\pi NN}}\right]^2 \left[g'_{\Delta\Delta}+\frac{J_{\rho}(\omega,q)}{J_{\pi}(\omega,q)}\frac{q^2}{\omega^2-q^2-m_{\rho}^2+i\epsilon}\right]. \quad (7.6)$$

Here $g'_{\Delta\Delta}$ is the Landau-Migdal parameter, which describes the short-range correlations for Δ-h→Δ-h transitions. Note that $V^{l}_{\Delta\text{-h}}(\omega,q)$ has a singularity at $q=q_{\text{pole}}=\sqrt{\omega^2-m_{\pi}^2}$ when the excitation energy ω is larger than m_{π}. This singularity appears for the Δ excitations because the excitation energy is larger than the pion mass. The interaction $V^{l}_{\Delta\text{-h}}$ is repulsive for $q<q_{\text{pole}}$, but attractive for $q>q_{\text{pole}}$.

Chanfray and Ericson (1984) and Dmitriev and Suzuki (1985) calculated the longitudinal and transverse spin-response of the Δ resonance in nuclear matter. They obtained a large energy shift of ~200 MeV for the Δ peak position in the longitudinal channel. Such nuclear

matter calculations are, of course, unrealistic because the finite size effects of the nucleus are important. Esbensen and Lee (1985) applied the surface response model of Esbensen and Bertsch (1984) to the problem. They found only a small shift of 5 MeV from RPA correlations. They could, however, reproduce the Δ peak position by introducing an effective mass of the Δ in the medium. This effective mass was introduced *ad hoc* and was found to be ~ 30 MeV smaller than the free-Δ mass. Esbensen and Lee, however, could not give the mechanism that produces such an effective mass.

Recent RPA calculations performed by Delorme and Guichon (1989, 1991) and by Udagawa *et al.* (1990) for finite nuclei consistently find a downward energy shift of ~ 30 MeV for the Δ peak position in nuclei. The energy shift is due to the energy (ω)-dependent π-exchange interaction of Eq. (7.5). The calculations of Udagawa *et al.* (1990) especially show in a very transparent way how the energy shift comes about. These authors calculate the Δ-h transition densities explicitly in momentum space for all relevant multipolarities J^π and find that these transition densities have their peak positions in the attractive region of $V^{(l)}_{\Delta\text{-h}}(\omega,q)$. This is illustrated in Fig. 37, where the real part of the spin-longitudinal residual interaction is plotted along with the real part of a $J^\pi=1^+$, $L=0$ transition density (dashed curve) versus momentum transfer. As can be seen, the peak appears in the attractive region. This reflects the fact that the squared four-momentum transfer $t\equiv(\omega^2-q^2)$ is negative in the reaction. By folding the transition densities into $V^{(l)}_{\Delta\text{-h}}(\omega,q)$ Udagawa *et al.* obtain a net attractive energy shift. This is shown in Fig. 38, where cross sections calculated either with or without residual interaction are compared to the ^{12}C(p,n) data of Lind *et al.*, (1987). One can see a strong energy shift in the Δ peak position between the correlated and uncorrelated calculations. This energy shift amounts to ~ 30 MeV. The strong energy shift occurs in

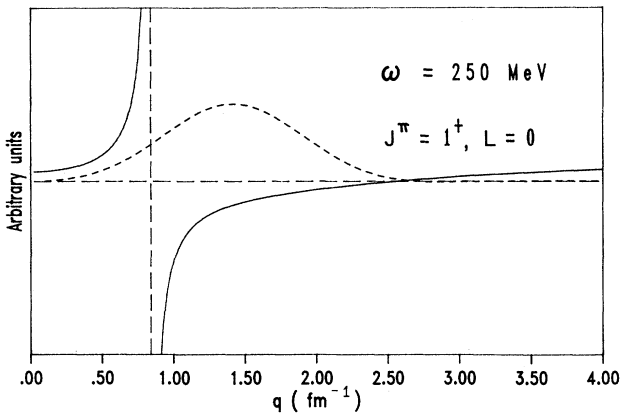

FIG. 37. The Δ-h residual interaction in the spin-longitudinal channel (solid curves) and the longitudinal transition density for the $J^\pi=1^+$, $L=0$ state (dashed curve) as function of momentum transfer q. From Udagawa *et al.* (1990).

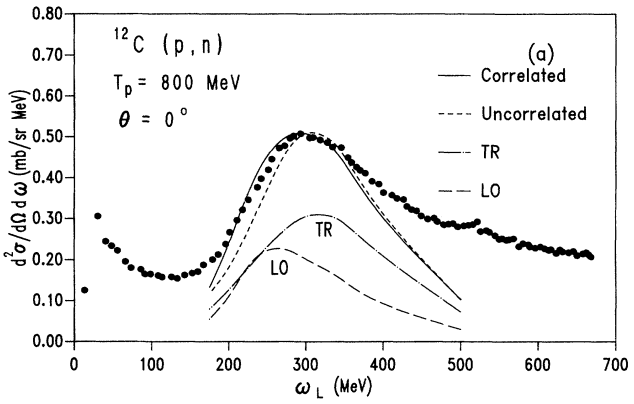

FIG. 38. Zero-degree neutron spectra for the reaction ^{12}C(p,n) at 800 MeV incident energy. The data are from Lind *et al.* (1987). The theoretical cross sections are calculated with (solid curve) or without (dashed curve) Δ-h correlations. The longitudinal and transverse cross sections are shown separately for the case in which correlations are included. The theoretical cross sections were multiplied by a normalization factor of $N=1.5$. From Udagawa *et al.* (1990).

the spin-longitudinal channel. The spin-transverse interaction $V^{(t)}_{\Delta\text{-h}}(\omega,q)$, on the other hand, is weakly repulsive in the important momentum-transfer range; therefore no shift occurs in the spin-transverse channel. This is in agreement with what is observed in the electroexcitation of the Δ. Udagawa *et al.* had to use a small $g'_{\Delta\Delta}$ parameter of about $\frac{1}{3}$ (in units of $J_{\pi\Delta\Delta}=4\pi\hbar c f_{\pi N\Delta}f_{\pi N\Delta}/m_\pi^2\approx 1600$ MeV fm^3) in order to reproduce the Δ peak position. This value corresponds to minimal short-range correlations. Apparently $g'_{\Delta\Delta}$ is much smaller than g'_0. One may view the shift of the Δ bump as a tool for determining experimentally the Landau-Migdal parameter $g'_{\Delta\Delta}$. Of course, further studies are needed to confirm this result. In particular, the (ω,q) dependence of the $t_{N\Delta}$ transition potential in the Δ excitation process has to be understood better in order to draw firm conclusions on the Δ-h correlations in nuclei. This is particular true for the longitudinal and transverse components of the $t_{N\Delta}$ operator. Studies of the $p(\mathbf{d},2p)\Delta^0$ reaction (Ellegaard *et al.*, 1989) indicate that there is a strong transverse component in $t_{N\Delta}$. However, this conclusion depends on assumptions about the deuteron form factor. Therefore other reactions should also be used to determine the longitudinal and transverse spin character of the $t_{N\Delta}$ interaction (see also the review paper by Gaarde, 1991).

VIII. CONCLUSIONS AND OUTLOOK

Over the last decade great progress has been made in our understanding of collective spin-isospin excitations in nuclei. Today, the main properties of the collective spin-isospin modes, like, for example, the excitation energies and the damping widths of the giant Gamow-Teller resonances and other isovector magnetic resonances, are

known. The progress was initiated by investigations into the (p,n) charge-exchange reaction at intermediate energies, which triggered various other investigations with the (p,p'),(e,e'), (γ,γ'), and (n,p) reactions as well as with other probes. The combined effort of all these studies made it possible for us now to have a working knowledge of the nuclear spin-isospin response function over a wide range of excitation energies and momentum transfers.

The collective spin-isospin modes give information on the spin-isospin-dependent interaction in the nucleus. In particular, the short-range spin-isospin correlations between nucleons in the medium, as well as the role played by pions in the nucleus, can be determined.

From a theoretical point of view the question of the so-called "missing" Gamow-Teller strength seems essentially to be solved. All microscopic nuclear structure calculations, as well as the extensive analyses of the experimental spectra, indicate that most of the "missing" strength is located in the continuum region of the nuclear excitation spectrum just beyond the collective mode. The configuration mixing of the 1p-1h modes with the 2p-2h states and more complicated nuclear configurations leads to a strong fragmentation of the GT strength, shifting a large amount of GT strength (20%–30%) up to excitation energies from 30 to 70 MeV. In this way a strongly asymmetric damping width of the collective spin-isospin modes is produced. The asymmetry is a consequence of the increasing level density of 2p-2h states with increasing excitation energy. Furthermore, it is found that the higher the excitation energy of a mode, the larger is its spreading width.

The admixture of Δ-h configurations to the low-lying GT modes seems now to be much less important than early work suggested. It probably pushes 5% to—at most—20% of the nucleonic GT strength up to the Δ region. A decisive experimental test of this conjecture, however, is still lacking.

The question of the "missing" GT strength has led the experimentalists to measure the isovector spin response of nuclei in the Δ resonance region. The result was unexpected and surprising. A strong energy shift of the Δ peak position towards lower excitation energies was observed in nuclear targets as compared with the proton target. The origin of this shift is not yet completely clear, but there are strong indications that the Δ-hole correlations mediated by the energy-dependent, attractive, π-exchange interaction in the spin-longitudinal channel shifts the Δ peak position downwards in energy by 30 MeV. No significant shift is observed in the electroexcitation of the Δ that probes the spin-transverse channel. The shift observed in the charge-exchange reactions provides strong support for the assumption that baryon resonances can feel strong nuclear medium effects. This history of spin and isospin excitations in nuclei over the last decade indicates that still more unexpected phenomena await discovery and that nuclear physics will continue to be challenging and exciting.

ACKNOWLEDGMENTS

The author thanks D. Cha, S. Drożdż, C. Gaarde, S. Krewald, V. A. Madsen, K. Nakayama, J. Speth, T. Udagawa, and J. Wambach for many stimulating discussions and helpful exchanges. He thanks G. F. Bertsch for his continuous support and helpful advice in the preparation of this article. Special thanks go to J. Durso and J. Speth for a careful reading of the whole manuscript and for many helpful comments. Finally the author is grateful to S. M. Austin and G. F. Bertsch for the warm hospitality extended to him during two visits, in 1990 and 1991, to the Michigan State University, where part of this article was written.

REFERENCES

Ableev, V. G., G. G. Vorob'ev, S. M. Eliseev, S. A. Zaporozhets, V. I. Inozemtsev, A. P. Kobushkin, A. B. Kurepin, D. K. Nikitin, A. A. Nomofilov, N. M. Piskunov, I. M. Sitnik, E. A. Strokovskiĭ, L. N. Strunov, and V. I. Sharov, 1984, JETP Lett. **40**, 763.

Adams, G. S., A. D. Bacher, G. T. Emery, W. P. Jones, R. T. Kouzes, D. W. Miller, A. Picklesimer, and G. E. Walker, 1977, Phys. Rev. Lett. **38**, 1387.

Adler, S. L., 1965, Phys. Rev. B **140**, 736.

Adler, S. L., and R. F. Dashen, 1968, Current Algebras (Benjamin, New York).

Ahrens, J., 1980, Nucl. Phys. A **335**, 67.

Alberico, W. M., M. Ericson, and A. Molinari, 1982, Nucl. Phys. A **379**, 429.

Alberico, W. M., A. De Pace, M. Ericson, M. B. Johnson, and A. Molinari, 1988, Phys. Rev. C **38**, 109.

Alford, W. P., R. L. Helmer, R. Abegg, A. Celler, O. Häusser, K. Hicks, K. P. Jackson, C. A. Miller, S. Yen, R. E. Azuma, D. Frekers, R. S. Henderson, H. Baer, and C. D. Zafiratos, 1986, Phys. Lett. B **179**, 20.

Amusa, A., and R. D. Lawson, 1983, Phys. Rev. Lett. **51**, 103.

Anantaraman, N., B. A. Brown, G. M. Crawley, A. Galonsky, C. Djalali, N. Marty, M. Morlet, A. Willis, J. C. Jourdain, and B. H. Wildenthal, 1984, Phys. Rev. Lett. **52**, 1409.

Anantaraman, N., G. M. Crawley, A. Galonsky, C. Djalali, N. Marty, M. Morlet, A. Willis, and J. C. Jourdain, 1981, Phys. Rev. Lett. **46**, 1318.

Anastasio, M. R., and G. E. Brown, 1977, Nucl. Phys. A **285**, 516.

Anastasio, M. R., L. S. Celenza, W. S. Pong, and C. M. Shakin, 1983, Phys. Rep. **100**, 327.

Anderson, B. D., T. Chittrakarn, A. R. Baldwin, C. Lebo, R. Madey, R. J. McCarthy, J. W. Watson, B. A. Brown, and C. C. Foster, 1985a, Phys. Rev. C **31**, 1147.

Anderson, B. D., T. Chittrakarn, A. R. Baldwin, C. Lebo, R. Madey, P. C. Tandy, J. W. Watson, B. A. Brown, and C. C. Foster, 1985b, Phys. Rev. C **31**, 1161.

Anderson, B. D., J. N. Knudson, P. C. Tandy, J. W. Watson, R. Madey, and C. C. Foster, 1980, Phys. Rev. Lett. **45**, 699.

Anderson, J. D., and C. Wong, 1961, Phys. Rev. Lett. **7**, 250.

Arends, J., J. Eyink, A. Hegerath, K. G. Hilger, B. Mecking, G. Nöldeke, and H. Rost, 1981, Phys. Lett. B **98**, 423.

Arima, A., T. Cheon, K. Shimizu, H. Hyuga, and T. Suzuki,

1983, Phys. Lett. B **122**, 126.
Arima, A., and H. Horie, 1954a, Prog. Theor. Phys. **11**, 509.
Arima, A., and H. Horie, 1954b, Prog. Theor. Phys. **12**, 623.
Arima, A., K. Shimizu, W. Bentz, and H. Hyuga, 1987 in *Advances in Nuclear Physics,* Vol. 18, edited by J. W. Negele and E. Vogt (Plenum, New York), p. 1.
Arndt, R. A., L. D. Roper, R. A. Bryan, R. B. Clark, B. J. VerWest, and P. Signell, 1983, Phys. Rev. D **28**, 97.
Auerbach, N., 1971, Phys. Lett. B **36**, 293.
Auerbach, N., 1974, Nucl. Phys. A **182**, 247.
Auerbach, N., and A. Klein, 1983, Nucl. Phys. A **395**, 77.
Auerbach, N., F. Osterfeld, and T. Udagawa, 1989, Phys. Lett. B **219**, 184.
Babu, S., and G. E. Brown, 1973, Ann. Phys. (NY) **78**, 1.
Bacher, A. D., G. T. Emery, W. P. Jones, D. W. Miller, G. S. Adams, F. Petrovich, and W. G. Love, 1980, Phys. Lett. B **97**, 58.
Bäckmann, S.-O., G. E. Brown, and J. A. Niskanen, 1985, Phys. Rep. **124**, 1.
Bainum, D. E., J. Rapaport, C. D. Goodman, D. J. Horen, C. C. Foster, M. B. Greenfield, and C. A. Goulding, 1980, Phys. Rev. Lett. **44**, 1751.
Baker, F. T., L. Bimbot, R. W. Fergerson, C. Glashausser, K. Jones, A. Green, K. Nakayama, and S. Nanda, 1988, Phys. Rev. C **37**, 1350.
Baker F. T., L. Bimbot, R. W. Fergerson, C. Glashausser, A. Green, K. Jones, W. G. Love, and S. Nanda, 1989, Phys. Rev. C **40**, 1877.
Baldwin, G. C., and G. S. Klaiber, 1947, Phys. Rev. **71**, 3.
Baldwin, G. C., and G. S. Klaiber, 1948, Phys. Rev. **73**, 1156.
Bang, J., S. A. Fayans, F. A. Gareev, S. N. Ershov, and N. I. Pyatov, 1985, Nucl. Phys. A **440**, 445.
Baranger, M., 1960, Phys. Rev. **120**, 957.
Bardeen, J., L. N. Cooper, and J. R. Schrieffer, 1957, Phys. Rev. **108**, 1175.
Barreau, P., M. Bernheim, J. Duclos, J. M. Finn, Z. Meziani, J. Morgenstern, J. Mougey, D. Royer, B. Saghai, D. Tarnowski, S. Turck-Chieze, M. Brussel, G. P. Capitani, E. DeSanctis, S. Frullani, F. Garibaldi, D. B. Isabelle, E. Jans, I. Sick, and P. D. Zimmerman, 1983, Nucl. Phys. A **402**, 515.
Barschall, H. H., and W. Haeberli, 1970, Eds., *Polarization Phenomena in Nuclear Reactions: Proceedings of the 3rd International Symposium* (University of Wisconsin, Madison).
Baym, G., and G. E. Brown, 1975, Nucl. Phys. A **247**, 395.
Beiner, M., H. Flocard, Nguyen Van Giai, and P. Quentin, 1975, Nucl. Phys. A **238**, 29.
Belyaev, S. T., 1959, K. Dan. Vidensk. Selsk. Mat. Fys. Medd. **31**, 11.
Belyaev, S. T. , 1965, Nucl. Phys. **64**, 17.
Berg, G. P. A., W. Hürlimann, I. Katayama, S. A. Martin, J. Meissburger, J. Roemer, B. Styczen, F. Osterfeld, G. Gaul, R. Santo, and G. Sondermann, 1982, Phys. Rev. C **25**, 2100.
Bergqvist, I., A. Brockstedt, L. Carlén, L. P. Ekström, B. Jakobsson, C. Ellegaard, C. Gaarde, J. S. Larsen, C. Goodman, M. Bedjidian, D. Contardo, J. Y. Grossiord, A. Guichard, R. Haroutunian, J. R. Pizzi, D. Bachelier, J. L. Boyard, T. Hennino, J. C. Jourdain, M. Roy-Stephan, M. Boivin, and P. Radvanyi, 1987, Nucl. Phys. A **469**, 648.
Berman, B. L., and S. C. Fultz, 1975, Rev. Mod. Phys. **47**, 713.
Bernstein, A., 1970, in *Advances in Nuclear Physics,* Vol. 3, edited by M. Baranger, E. Vogt, and A. M. Bernstein (Plenum, New York), p. 325.
Bertrand, F. E., E. E. Gross, D. J. Horen, J. R. Wu, J. Tinsley, D. K. McDaniels, L. W. Swenson, and R. Liljestrand, 1981, Phys. Lett. B **103**, 326.
Bertsch, G. F., 1981, Nucl. Phys. A **354**, 157c.
Bertsch, G. F., 1983, Prog. Theor. Phys. Suppl. **74&75**, 115.
Bertsch, G. F., P. F. Bortignon, and R. A. Broglia, 1983, Rev. Mod. Phys. **55**, 287.
Bertsch, G. F., J. Borysowicz, H. McManus, and W. G. Love, 1977, Nucl. Phys. A **284**, 399.
Bertsch, G. F., and H. Esbensen, 1987, Rep. Prog. Phys. **50**, 607.
Bertsch, G. F., and I. Hamamoto, 1982, Phys. Rev. C **26**, 1323.
Bertsch, G. F., and O. Scholten, 1982, Phys. Rev. C **25**, 804.
Bertsch, G. F., and S. F. Tsai, 1975, Phys. Rep. C **18**, 125.
Bethe, H. A., 1971, Annu. Rev. Nucl. Sci. **21**, 93.
Bethe, H. A., and J. Goldstone, 1957, Proc. R. Soc. London, Ser. A **238**, 551.
Blair, J. S., 1959, Phys. Rev. **115**, 928.
Blin-Stoyle, R. J. 1953, Proc. Phys. Soc. London, Ser. A **66**, 1158.
Bloom, S. D., and G. M. Fuller, 1985, Nucl. Phys. A **440**, 511.
Bogoliubov, N. N., 1958, Sov. Phys. JETP **7**, 41.
Bogoliubov, N. N., 1959a, Sov. Phys. Usp. **2**, 236.
Bogoliubov, N. N., 1959b, Usp. Fiz. Nauk. **67**, 549.
Bohle, D., Th. Guhr, U. Hartmann, K. D. Hummel, G. Kilgus, U. Milkau, and A. Richter, 1986, in *Proceedings of the International Symposium on Weak and Electromagnetic Interactions,* edited by H. V. Klapdor (Springer, Berlin), p. 311.
Bohr, A., and B. Mottelson, 1969, *Nuclear Structure Vol. I* (Benjamin, New York).
Bohr, A., and B. Mottelson, 1975, *Nuclear Structure Vol. II* (Benjamin, New York).
Bohr, A., and B. Mottelson, 1981, Phys. Lett. B **100**, 10.
Bohr, A., B. Mottelson, and D. Pines, 1958, Phys. Rev. **110**, 936.
Bonner, B. E., J. E. Simmons, C. R. Newsom, P. J. Riley, G. Glass, J. C. Hiebert, Mahavir Jain, and L. C. Northcliffe, 1978, Phys. Rev. C **18**, 1418.
Bowman, J. D., H. W. Baer, R. Bolton, M. D. Cooper, F. H. Cverna, N. S. P. King, M. Leitch, H. S. Matis, A. Erell, J. Alster, A. Doron, M. A. Moinester, E. Blackmore, and E. R. Siciliano, 1983, Phys. Rev. Lett. **50**, 1195.
Bardy, F.P., C. M. Castaneda, G. A. Needman, J. L. Ullmann, J. L. Romero, T. D. Ford, M. L. Johnson, N. S. King, C. M. Morris, F. Petrovich, and R. H. Howell, 1982, Phys. Rev. Lett. **48**, 860.
Brady, F., G. A. Needman, J. L. Romero, C. M. Castaneda, T. D. Ford, J. L. Ullmann, and M. L. Webb, 1983, Phys. Rev. Lett. **51**, 1320.
Brieva, F. A., and J. R. Rook, 1977a, Nucl. Phys. A **291**, 299.
Brieva, F. A., and J. R. Rook, 1977b, Nucl. Phys. A **291**, 317.
Brieva, F. A., and J. R. Rook, 1978, Nucl. Phys. A **307**, 493.
Brieva, F. A., H. V. von Geramb, and J. R. Rook, 1978, Phys. Lett. B **79**, 177.
Brown, B. A., and B. H. Wildenthal, 1983, Phys. Rev. C **28**, 2397.
Brown, B. A., and B. H. Wildenthal 1987, Nucl. Phys. A **474**, 290.
Brown, B. A., and B. H. Wildenthal, 1988, Annu. Rev. Nucl. Sci. **38**, 29.
Brown, G. E. 1971a, *Unified Theory of Nuclear Models and Forces* (North-Holland, New York).
Brown, G. E., 1971b, Rev. Mod. Phys. **43**, 1.
Brown, G. E., S.-O. Bäckman, E. Oset, and W. Weise, 1977, Nucl. Phys. A **286**, 191.
Brown, G. E., and M. Bolsterli, 1959, Phys. Rev. Lett. **3**, 472.

Brown, G. E., and S. Raman, 1980, Comments Nucl. Part. Phys. **9**, 79.
Brown, G. E., and M. Rho, 1981, Nucl. Phys. A **72**, 397.
Brown, G. E., J. Speth, and J. Wambach, 1981, Phys. Rev. Lett. **46**, 1057.
Brown, G. E., and W. Weise, 1975, Phys. Rep. C **22**, 279.
Brueckner, K. A., 1954, Phys. Rev. **96**, 508.
Brueckner, K. A., and C. A. Levinson, 1955, Phys. Rev. **97**, 1344.
Buenerd, M., C. Bonhomme, D. Lebrun, P. Martin, J. Chauvin, G. Duhamel, G. Perrin, and P. de Saintignon, 1979, Phys. Lett. B **84**, 305.
Carey, T. A., K. W. Jones, J. B. McClelland, J. M. Moss, L. B. Rees, N. Tanaka, and A. D. Bacher, 1984, Phys. Rev. Lett. **53**, 144.
Carr, J. A., S. D. Bloom, F. Petrovich, and R. J. Philpott, 1989, Phys. Rev. Lett. **62**, 2249.
Cassapakis, C. G., H. C. Bryant, B. D. Dieterle, C. P. Leavitt, D. M. Wolfe, B. E. Bonner, J. E. Simmons, C. W. Bjork, P. J. Riley, M. L. Evans, G. Glass, J. C. Hiebert, M. Jain, R. A. Kenefick, L. C. Northcliffe, and D. W. Werren, 1976, Phys. Lett. B **63**, 35.
Cecil, F. E., G. T. Garvey, and W. J. Braithwaite, 1974, Nucl. Phys. A **232**, 22.
Celenza, L. S., W. S. Pong, and C. M. Shakin, 1982, Phys. Rev. C **25**, 3115.
Cha, D., 1983, Phys. Rev. C **27**, 2269.
Cha, D., and F. Osterfeld, 1989, Phys. Rev. C **39**, 694.
Cha, D., B. Schwesinger, J. Wambach, and J. Speth, 1984, Nucl. Phys. A **430**, 321.
Chanfray, G., and M. Ericson, 1984, Phys. Lett. B **141**, 163.
Cheng, T. P., and L. F. Li, 1984, *Gauge Theory of Elementary Particles* (Clarendon, Oxford).
Cheon, T., K. Shimizu, and A. Arima, 1984, Phys. Lett. B **138**, 345.
Chew, G. F., and F. E. Low, 1956, Phys. Rev. **101**, 1570.
Chiang, H. C., and J. Hüfner, 1980, Nucl. Phys. A **349**, 466.
Civitarese, O., A. Faessler, and T. Tomoda, 1987, Phys. Lett. B **194**, 11.
Clausen, B. L., R. A. Lindgren, M. Farkhondeh, L. W. Fagg, D. I. Sober, C. W. de Jager, H. de Vries, N. Kalantar-Nayestanaki, B. L. Berman, K. S. Dhuga, J. A. Carr, F. Petrovich, and P. E. Burt, 1990, Phys. Rev. Lett. **65**, 547.
Cohen, S., and D. Kurath, 1965, Nucl. Phys. A **73**, 1.
Cohen, S., and D. Kurath, 1967, Nucl. Phys. A **101**, 1.
Comfort, J. R., Sam M. Austin, P. T. Debevec, G. L. Moake, R. W. Finlay, and W. G. Love, 1980, Phys. Rev. C **21**, 2147.
Comfort, J. R., and W. G. Love, 1980, Phys. Rev. Lett. **44**, 1656.
Contardo, D., M. Bedjidian, J. Y. Grossiord, A. Guichard, R. Haroutunian, J. R. Pizzi, C. Ellegaard, C. Gaarde, J. S. Larsen, C. Goodman, I. Bergqvist, A. Brockstedt, L. Carlén, P. Ekström, D. Bachelier, J. L. Boyard, T. Hennino, J. C. Jourdain, M. Roy-Stephan, M. Boivin, and P. Radvanyi, 1986, Phys. Lett. B **168**, 331.
Cornelius, W. D., J. M. Moss, and T. Yamaya, 1981, Phys. Rev. C **23**, 1364.
Crawley, G. M., N. Anantaraman, A. Galonsky, C. Djalali, N. Marty, M. Morlet, A. Willis, and J. C. Jourdain, 1983, Phys. Lett. B **127**, 322.
Crawley, G. M., C. Djalali, N. Marty, M. Morlet, A. Willis, N. Anantaraman, B. A. Brown, and A. Galonsky, 1989, Phys. Rev. C **39**, 311.
Czerski, P., W. H. Dickhoff, A. Faessler, and H. Müther, 1984, Nucl. Phys. A **427**, 224.
Day, B. D., 1967, Rev. Mod. Phys. **39**, 719.
Day, B. D., 1981, Phys. Rev. C **24**, 1203.
de Alfaro, V., S. Fubini, G. Furlan, and C. Rossetti, 1973, *Currents in Hadron Physics* (North-Holland, Amsterdam).
De Pace, A., and M. Viviani, 1990, Phys. Lett. B **236**, 397.
De Pace, A., and M. Viviani, 1991, Phys. Lett. B **254**, 20.
Delorme, J., M. Ericson, A. Figureau, and C. Thevenet, 1976, Ann. Phys. (Paris) **102**, 273.
Delorme, J., M. Ericson, and P. Guichon, 1982, Phys. Lett. B **115**, 86.
Delorme, J., and P. A. M. Guichon, 1989, in *Proceedings 10e Biennale de Physique Nucléaire (Aussois),* IPN Lycen Report No. LYCEN 8906, p. C4-1.
Delorme, J., and P. A. M. Guichon, 1991, Phys. Lett. B **263**, 157.
Desplanques, B., and S. Noguera, 1986, Phys. Lett. B **174**, 361.
Dickhoff, W. H., 1983, Nucl. Phys. A **399**, 287.
Dickhoff, W. H., A. Faessler, J. Meyer-ter-Vehn, and H. Müther, 1981, Phys. Rev. C **23**, 1154.
Dickhoff, W. H., A. Faessler, H. Müther, and S. S. Wu, 1983, Nucl. Phys. A **405**, 534.
Dmitriev, V. F., and T. Suzuki, 1985, Nucl. Phys. A **438**, 697.
Djalali, C., 1984, J. Phys. (Paris) C **4**, 375.
Doering, R. R., A. Galonsky, D. M. Patterson, and G. F. Bertsch, 1975, Phys. Rev. Lett. **35**, 1691.
Doi, M., T. Kotani, and E. Takasugi, 1985, Prog. Theor. Phys. Suppl. **83**, 1.
Dominguez, C. A. and R. B. Clark, 1980, Phys. Rev. C **21**, 1944.
Dominguez, C. A. and B. J. VerWest, 1980, Phys. Lett. B **89**, 333.
Donnelly, T. W., J. D. Walecka, I. Sick, and E. B. Hughes, 1968, Phys. Rev. Lett. **21**, 1196.
Drożdż, S., V. Klemt, J. Speth, and J. Wambach, 1986a, Nucl. Phys. A **451**, 11.
Drożdż, S., V. Klemt, J. Speth, and J. Wambach, 1986b, Phys. Lett. B **166**, 18.
Drożdż, S., S. Nishizaki, J. Speth, and J. Wambach, 1990, Phys. Rep. **197**, 1.
Drożdż, S., F. Osterfeld, J. Speth, and J. Wambach, 1987, Phys. Lett. B **189**, 271.
Eisenberg, J. M., and D. S. Koltun, 1980, *Theory of Meson Interactions with Nuclei* (Wiley, New York).
Ellegaard, C., 1987, Can. J. Phys. **65**, 600.
Ellegaard, C., C. Gaarde, J. S. Larsen, C. Goodman, I. Bergqvist, L. Carlén, P. Ekström, B. Jakobsson, J. Lyttkens, M. Bedjidian, M. Chamcham, J. Y. Grossiord, A. Guichard, M. Gusakow, R. Haroutunian, J. R. Pizzi, D. Bachelier, J. L. Boyard, T. Hennino, J. C. Jourdain, M. Roy-Stephen, M. Boivin, and P. Radvanyi, 1983, Phys. Rev. Lett. **50**, 1745.
Ellegaard, C., C. Gaarde, J. S. Larsen, V. Dmitriev, O. Sushkov, C. Goodman, I. Bergqvist, A. Brockstedt, L. Carlén, P. Ekström, M. Bedjidian, D. Contardo, J. Y. Grossiord, A. Guichard, R. Haroutunian, J. R. Pizzi, D. Bachelier, J. L. Boyard, T. Hennino, M. Roy-Stephan, M. Boivin, and P. Radvanyi, 1985, Phys. Lett. B **154**, 110.
Ellegaard, C., C. Gaarde, T. S. Jørgensen, J. S. Larsen, C. Goodman, I. Bergqvist, A. Brockstedt, P. Ekström, M. Bedjidian, D. Contardo, J. Y. Grossiord, A. Guichard, D. Bachelier, J. L. Boyard, T. Hennino, J. C. Jourdain, M. Roy-Stephen, P. Radvanyi, and J. Tinsley, 1987, Phys. Rev. Lett. **59**, 974.
Ellegaard, C., C. Gaarde, T. S. Jørgensen, J. S. Larsen, B. Million, C. Goodman, A. Brockstedt, P. Ekström, M. Österlund,

M. Bedjidian, D. Contardo, D. Bachelier, J. L. Boyard, T. Hennino, J. C. Jourdain, M. Roy-Stephen, P. Radvanyi, and P. Zupranski, 1989, Phys. Lett. B **231**, 365.
Engel, J., P. Vogel, and M. R. Zirnbauer, 1988, Phys. Rev. C **37**, 731.
Erell, A., J. Alster, J. Lichtenstadt, M. A. Moinester, J. D. Bowman, M. D. Cooper, F. Irom, H. S. Matis, E. Piasetzky, and U. Sennhauser, 1986, Phys. Rev. C **34**, 1822.
Ericson, M., 1971, Ann. Phys. (N.Y.) **63**, 562.
Ericson, M., 1984, in *Proceedings of the International Conference on Spin Excitations in Nuclei,* edited by F. Petrovich, G. E. Brown, G. T. Garvey C. D. Goodman, R. A. Lindgren, and W. G. Love (Plenum, New York), p. 27.
Ericson, M., and T. E. O. Ericson, 1966, Ann. Phys. (N.Y.) **36**, 323.
Ericson, M., A. Figureau, and C. Thevenet, 1973, Phys. Lett. B **45**, 19.
Ericson, T. E. O., and W. Weise, 1988, *Pions and Nuclei* (Oxford University, New York/London).
Erkelenz, K., 1974, Phys. Rep. **13**, 191.
Esbensen, H., and G. F. Bertsch, 1984, Ann. Phys. (N.Y.) **157**, 255.
Esbensen, H., and G. F. Bertsch, 1985, Phys. Rev. C **32**, 553.
Esbensen, H., and T.-S. H. Lee, 1985, Phys. Rev. C **32**, 1966.
Fagg, L. W., 1975, Rev. Mod. Phys. **47**, 683.
Fermi, E., 1934a, Nuovo Cimento **11**, 1.
Fermi, E., 1934b, Z. Phys. **88**, 161.
Fetter, A. L., and J. D. Walecka, 1971, *Quantum Theory of Many Particle Systems* (McGraw-Hill, New York).
Feynman, R. P., and M. Gell-Mann, 1958, Phys. Rev. **109**, 193.
Franey, M. A., and W. G. Love, 1985, Phys. Rev. C **31**, 488.
Fubini, S., and G. Furlan, 1965, Physics, **1**, 229.
Fujita, Y., M. Fujiwara, S. Morinobu, T. Yamazaki, T. Itahashi, S. Imanishi, H. Ikegami, and S. I. Hayakawa, 1982, Phys. Rev. C **25**, 678.
Gaarde, C., 1985, in *Proceedings of the Niels Bohr Centennial Conference on Nuclear Structure,* Copenhagen (North-Holland, Amsterdam), p. 449c.
Gaarde, C., 1988, Nucl. Phys. A **478**, 475c.
Gaarde,C., 1991, Annu. Rev. Nucl. Sci. **41**, 187.
Gaarde, C., J. S. Larsen, M. N. Harakeh, S. V. Van der Werf, M. Igarashi, and A. Müller-Arnke, 1980, Nucl. Phys. A **334**, 248.
Gaarde, C., J. Rapaport, T. N. Taddeucci, C. D. Goodman, C. C. Foster, D. E. Bainum, C. A. Goulding, M. B. Greenfield, D. J. Horen, and E. Sugarbaker, 1981, Nucl. Phys. A **369**, 258.
Galonsky, A., J. P. Didelez, A. Djaloeis, and W. Oelert, 1978, Phys. Lett. B **74**, 176.
Gell-Mann, M., 1962, Phys. Rev. **125**, 1067.
Gell-Mann, M., 1964, Phys. Lett. **8**, 214.
Gell-Mann, M., and M. Levy, 1960, Nuovo Cimento **16**, 705.
Gershtein, S. S., and Ia. B. Zeldovich, 1956, Sov. Phys. JETP **2**, 576 [Zh. Eksp. Teor. Fiz. **29**, 698 (1956)].
Glashausser, C., K. Jones, F. T. Baker, L. Bimbot, H. Esbensen, R. W. Fergerson, A. Green, S. Nanda, and R. D. Smith, 1987, Phys. Rev. Lett. **58**, 2404.
Glass, G., Mahavir Jain, M. L. Evans, J. C. Hiebert, L. C. Northcliffe, B. E. Bonner, J. E. Simmons, C. Bjork, P. Riley, and C. Cassapakis, 1977, Phys. Rev. D **15**, 36.
Goeke, K., and J. Speth, 1982, Annu. Rev. Nucl. Part. Sci. **32**, 65.
Gogny, D., 1975, Nucl. Phys. A **237**, 399.
Goldhaber, M., and E. Teller, 1948, Phys. Rev. **74**, 1046.
Goodman, C. D., 1980, in *The (p,n) Reaction and the Nucleon-Nucleon Force,* edited by C. D. Goodman, Sam M. Austin, S. D. Bloom, J. Rapaport, and G. R. Satchler (Plenum, New York), p. 149.
Goodman, C. D., and S. D. Bloom, 1984, in *Proceedings of the International Conference on Spin Excitations in Nuclei,* edited by F. Petrovich, G. E. Brown, G. T. Garvey, C. D. Goodman, R. A. Lindgren, and W. G. Love (Plenum, New York), p. 143.
Goodman, C. D., C. A. Goulding, M. B. Greenfield, J. Rapaport, D. E. Bainum, C. C. Foster, W. G. Love, and F. Petrovich, 1980, Phys. Rev. Lett. **44**, 1755.
Grotz, K., and H. V. Klapdor, 1990, *The Weak Interaction in Nuclear, Particle and Astrophysics* (Hilger, Bristol/ N.Y.).
Härting, A., W. Weise, H. Toki, and A. Richter, 1981, Phys. Lett. B **104**, 261.
Häusser, O., R. Abegg, R. G. Jeppesen, R. Sawafta, A. Celler, A. Green, R. L. Helmer, R. Henderson, K. Hicks, K. P. Jackson, J. Mildenberger, C. A. Miller, M. C. Vetterli, S. Yen, M. J. Iqbal, and R. D. Smith, 1988, Phys. Rev. Lett. **61**, 822.
Halbleib, J. A., and R. A. Sorensen, 1967, Nucl. Phys. A **98**, 542.
Hamamoto, I., 1974, Phys. Rep. **10**, 63.
Hanna, S. S., 1974, Nukleonika **19**, 655.
Hanna, S. S., 1977, in *Photonuclear Reactions,* Lecture Notes in Physics No. 67, edited by S. Costa and C. Schaerf (Springer, Berlin), p. 275.
Hanna, S. S., 1980, in *Proceedings of the Giant Multipole Resonance Topical Conference,* Oak Ridge, edited by F. E. Bertrand (Harwood Academic, New York), p. 1.
Harakeh, M. N., K. van der Borg, T. Ishimatsu, H. P. Morsch, A. van der Woude, and F. E. Bertrand, 1977, Phys. Rev. Lett. **38**, 676.
Harakeh, M. N., B. van Heyst, K. van der Borg, and A. van der Woude, 1979, Nucl. Phys. A **327**, 373.
Hartmann, U., D. Bohle, Th. Guhr, K. D. Hummel, G. Kilgus, U. Milkau, and A. Richter, 1987, Nucl. Phys. A **465**, 25.
Haxton, W. C., and G. J. Stephenson, Jr., 1984, Prog. Part. Nucl. Phys. **12**, 409.
Hayakawa, S. I., M. Fujiwara, S. Imanishi, Y. Fujita, I. Katayama, S. Morinobu, T. Yamazaki, T. Itahashi, and H. Ikegami, 1982, Phys. Rev. Lett. **49**, 1624.
Helmer, R., 1987, Can. J. Phys. **65**, 588.
Hirata, M., J. H. Koch, F. Lenz, and E. J. Moniz, 1977, Phys. Lett. B **70**, 281.
Hirata, M., J. H. Koch, F. Lenz, and E. J. Moniz, 1979, Ann. Phys. (N.Y.) **120**, 205.
Hirsch, J., and F. Krmpotić, 1990a Phys. Lett. B **264**, 6.
Hirsch, J., and F. Krmpotić, 1990b, Phys. Rev. C **41**, 792.
Hirsch, J., E. Bauer, and F. Krmpotić, 1990, Nucl. Phys. A **516**, 304.
Hirsch, J., A. Mariano, M. Faig, and F. Krmpotić, 1988, Phys. Lett. B **210**, 55.
Holinde, K., 1981, Phys. Rep. **68**, 121.
Holinde, K., K. Erkelenz, and R. Alzetta, 1972, Nucl. Phys. A **194**, 161.
Holinde, K., and R. Machleidt, 1977, Nucl. Phys. A **280**, 429.
Horen, D. J., C. D. Goodman, C. C. Foster, C. A. Goulding, M. G. Greenfield, J. Rapaport, D. E. Bainum, E. Sugarbaker, T. G. Masterson, F. Petrovich, and W. G. Love, 1980, Phys. Lett. B **95**, 27.
Horen, D. J., C. D. Goodman, D. E. Bainum, C. C. Foster, C. Gaarde, C. A. Goulding, M. B. Greenfield, J. Rapaport, T. N. Taddeucci, E. Sugarbaker, T. Masterson, S. M. Austin, A. Galonsky, and W. Sterrenburg, 1981, Phys. Lett. B **99**, 383.
Ichimura, M., K. Kawahigashi, T. S. Jørgensen, and C. Gaarde,

1989, Phys. Rev. C **39**, 1446.
Ikeda, K. S. Fujii, and J. I. Fujita, 1963, Phys. Lett. **3**, 271.
Izumoto, T., 1983, Nucl. Phys. A **395**, 189.
Jeukenne, J. P., A. Lejeune, and C. Mahaux, 1976, Phys. Rep. **25**, 83.
Kerman, A. K., H. McManus, and R. M. Thaler, 1959, Ann. Phys. (N.Y.) **8**, 551.
Kim, C. W., and H. Primakoff, 1965, Phys. Rev. **139**, B1447.
King, N. S. P., P. W. Lisowski, G. L. Morgan, P. N. Craig, R. G. Jeppesen, D. A. Lind, J. R. Shepard, J. L. Ullmann, C. D. Zafiratos, C. D. Goodman, and C. A. Goulding, 1986, Phys. Lett. B **175**, 279.
Klein, A., and W. G. Love, 1986, Phys. Rev. C **33**, 1920.
Klein, A., W. G. Love, and N. Auerbach, 1985, Phys. Rev. C **31**, 710.
Kleinheinz, P., K. Zuber, C. Conci, C. Protop, J. Zuber, C. F. Liang, P. Paris, and J. Blomqvist, 1985, Phys. Rev. Lett. **55**, 2664.
Klemt, E., P. Bopp, L. Hornig, J. Last, S. J. Freedman, D. Dubbers, and O. Schärpf, 1988, Z. Phys. C **37**, 179.
Knüpfer, W., M. Dillig, and A. Richter, 1980, Phys. Lett. B **95**, 349.
Knüpfer, W., R. Frey, A. Friebel, W. Mettner, D. Meuer, A. Richter, E. Spamer, and O. Titze, 1978, Phys. Lett. B **77**, 367.
Koch, J. H., E. J. Moniz, and N. Ohtsuka, 1984, Ann. Phys. (N.Y.) **154**, 99.
Kokkedee, J. J. J., 1969, *The Quark Model* (Benjamin, New York).
Krewald, S., J. Birkholz, A. Faessler, and J. Speth, 1974, Phys. Rev. Lett. **33**, 1386.
Krewald, S., K. Nakayama, and J. Speth, 1988, Phys. Rep. **161**, 103.
Krewald, S., F. Osterfeld, J. Speth, and G. E. Brown, 1981, Phys. Rev. Lett. **46**, 103.
Krewald, S., and J. Speth, 1980, Phys. Rev. Lett. **45**, 417.
Krmpotić, F., 1981a Phys. Rev. Lett. **46**, 1261.
Krmpotić, F., 1981b, Nucl. Phys. A **351**, 365.
Krmpotić, F., and F. Osterfeld, 1980, Phys. Lett. B **93**, 218.
Krmpotić, F., K. Ebert, and W. Wild, 1980, Nucl. Phys. A **342**, 497.
Krmpotić, F., K. Nakayama, and A. P. Galeaõ, 1983, Nucl. Phys. A **399**, 478.
Lacombe, M., B. Loiseau, J. M. Richard, R. Vinh Mau, J. Côté, P. Pirès, and R. de Tourreil, 1980, Phys. Rev. C **21**, 861.
Landau, L. D., 1956, Sov. Phys. JETP **3**, 920.
Landau, L. D., 1957, Sov. Phys. JETP **5**, 101.
Landau, L. D., 1959, Sov. Phys. JETP **8**, 70.
Laszewski, R. M., R. Alarcon, and S. D. Hoblit, 1987, Phys. Rev. Lett. **59**, 431.
Laszewski, R. M., R. Alarcon, D. S. Dale, and S. D. Hoblit, 1988, Phys. Rev. Lett. **61**, 1710.
Laszewski, R. M., P. Rullhusen, S. D. Hoblit, and S. F. LeBrun, 1985, Phys. Rev. Lett. **54**, 530.
Laszewski, R. M., P. Rullhusen, S. D. Hoblit, and S. F. LeBrun, 1986, Phys. Rev. C **34**, 2013.
Laszewski, R. M., and J. Wambach, 1985, Comments Nucl. Part. Phys. **14**, 321.
Lauritzen, B., 1988, Nucl. Phys. A **489**, 237.
Lebrun, D., M. Buenerd, P. Martin, P. de Saintignon, and G. Perrin, 1980, Phys. Lett. B **97**, 358.
Lewis, M. B., and F. E. Bertrand, 1972, Nucl. Phys. A **196**, 337.
Lichtenstadt, J., J. Heisenberg, C. N. Papanicolas, C. P. Sargent, A. N. Courtemanche, and J. S. McCarthy, 1979, Phys. Rev. C **20**, 497.
Lind, D. A., 1987, Can. J. Phys. **65**, 637.
Lindgren, R. A., W. J. Gerace, A. D. Bacher, W. G. Love, and F. Petrovich, 1979, Phys. Rev. Lett. **42**, 1524.
Lindgren, R. A., M. Leuschner, B. L. Clausen, R. J. Peterson, M. A. Plum, and F. Petrovich, 1987, Can. J. Phys. **65**, 666.
Lindgren, R. A., and F. Petrovich, 1984, in *Proceedings of the International Conference on Spin Excitations in Nuclei,* edited by F. Petrovich, G. E. Brown, G. T. Garvey, C. D. Goodman, R. A. Lindgren, and W. G. Love. (Plenum, New York), p. 323.
Liu, H., and L. Zamick, 1985, Phys. Rev. C **32**, 1754.
Love, W. G., 1978, Nucl. Phys. A **312**, 160.
Love, W. G., 1980, in *The (p,n) Reaction and the Nucleon-Nucleon Force,* edited by C. D. Goodman, Sam M. Austin, S. D. Bloom, J. Rapaport, and G. R. Satchler (Plenum, New York), p. 23.
Love, W. G., and M. A. Franey, 1981, Phys. Rev. C **24**, 1073.
Love, W. G., M. A. Franey, and F. Petrovich, 1984, in *Proceedings of the International Conference on Spin Excitations in Nuclei,* edited by F. Petrovich, G. E. Brown, G. T. Garvey, C. D. Goodman, R. A. Lindgren, and W. G. Love (Plenum, New York), p. 205.
Love, W. G., A. Klein, M. A. Franey, and K. Nakayama, 1987, Can. J. Phys. **65**, 536.
Love, W. G., and L. J. Parish, 1970, Nucl. Phys. A **157**, 625.
MacFarlane, M. H., 1986, Phys. Lett. B **182**, 265.
MacGregor, M. H., M. J. Moravcsik, and H. P. Stapp, 1960, Annu. Rev. Nucl. Sci. **10**, 291.
Machleidt, R., K. Holinde, and Ch. Elster, 1987, Phys. Rep. **149**, 1.
Madey, R., B. S. Flanders, B. D. Anderson, A. R. Baldwin, C. Lebo, J. W. Watson, Sam M. Austin, A. Galonsky, B. H. Wildenthal, and C. C. Foster, 1987a, Phys. Rev. C **35**, 2011.
Madey, R., B. S. Flanders, B. D. Anderson, A. R. Baldwin, C. Lebo, J. W. Watson, Sam M. Austin, A. Galonsky, B. H. Wildenthal, and C. C. Foster, 1987b, Phys. Rev. C **36**, 1647.
Mahaux, C., 1983, Nucl. Phys. A **396**, 9c.
Mahaux, C., P. F. Bortignon, R. A. Broglia, and C. H. Dasso, 1985, Phys. Rep. **120**, 1.
Mariano, A., J. Hirsch, and F. Krmpotić, 1990, Nucl. Phys. A **518**, 523.
Marty, N., M. Morlet, A. Willis, V. Comparat, and R. Frascaria, 1975, in *Proceedings of the International Conference on Highly Excited States in Nuclei,* Vol. I, edited by A. Faessler, C. Mayer-Böricke, and P. Turek (KFA Jülich), p. 17.
McCarthy, J. S. S., I. Sick, and R. R. Whitney, 1977, Phys. Rev. C **15**, 1396.
McClelland, J. B., J. M. Moss, B. Aas, A. Azizi, E. Bleszynski, M. Bleszynski, J. Geaga, G. Igo, A. Rahbar, J. B. Wagner, G. S. Weston, C. Whitten Jr., K. Jones, S. Nanda, M. Gazzaly, and N. Hintz, 1984, Phys. Rev. Lett. **52**, 98.
McGrory, J. B., and B. H. Wildenthal, 1981, Phys. Lett. B **103**, 173.
Mecking, B., 1979, in *Proceedings of the International Conference on Nuclear Physics with Electromagnetic Interactions,* Lecture Notes in Physics No. 108, edited by H. Arenhövel and D. Drechsel (Springer, Berlin), p. 382.
Meuer, D., R. Frey, D. H. H. Hoffmann, A. Richter, E. Spamer, O. Titze, and W. Knüpfer, 1980, Nucl. Phys. A **349**, 309.
Meyer-ter-Vehn, J., 1981, Phys. Rep. **74**, 323.
Meziani, Z. E., P. Barreau, M. Bernheim, J. Morgenstern, S. Turck-Chieze, R. Altemus, J. McCarthy, L. J. Orphanos, R. R. Whitney, G. P. Capitani, E. DeSanctis, S. Frullani, and F. Garibaldi, 1985, Phys. Rev. Lett. **54**, 1233.
Migdal, A. B., 1967, *Theory of Finite Fermi Systems and Appli-*

cations to Atomic Nuclei (Wiley, New York).
Migdal, A. B., 1972, Sov. Phys. JETP **34**, 1184.
Migdal, A. B., 1978, Rev. Mod. Phys. **50**, 107.
Migdal, A. B., 1979, in *Meson in Nuclei,* Vol. III, edited by M. Rho and D. Wilkinson (North-Holland, New York), p. 941.
Moake, G. L., L. J. Gutay, R. P. Scharenberg, P. T. Debevec, and P. W. Quin, 1979, Phys. Rev. Lett. **43**, 910.
Moffa, P. J., and G. E. Walker, 1974, Nucl. Phys. A **222**, 140.
Moinester, M. A., 1987, Can. J. Phys. **65**, 660.
Morpurgo, G., 1958, Phys. Rev. **110**, 721.
Morpurgo, G., 1959, Phys. Rev. **114**, 1075.
Moss, J. M., 1984, in *Proceedings of the International Conference on Spin Excitations in Nuclei,* edited by F. Petrovich, G. E. Brown, G. T. Garvey, C. D. Goodman, R. A. Lindgren, and W. G. Love (Plenum, New York), p. 355.
Moss, J. M., C. Glashausser, F. T. Baker, R. Boudrie, W. D. Cornelius, N. Hintz, G. Hoffmann, G. Kyle, W. G. Love, A. Scott, and H. A. Thiessen, 1980, Phys. Rev. Lett. **44**, 1189.
Müller, S., A. Richter, E. Spamer, W. Knüpfer, and B. C. Metsch, 1983, Phys. Lett. B **120**, 305.
Muto, K., 1986, Nucl. Phys. A **451**, 481.
Muto, K., E. Bender, and H. V. Klapdor, 1989a, Z. Phys. A **334**, 177.
Muto, K., E. Bender, and H. V. Klapdor, 1989b, Z. Phys. A **334**, 187.
Muto, K., and H. V. Klapdor, 1988, Phys. Lett. B **201**, 420.
Nadasen, A., P. Schwandt, P. P. Singh, W. W. Jacobs, A. D. Bacher, P. T. Debevec, M. D. Kaitchuck, and J. T. Meek, 1981, Phys. Rev. C **23**, 1023.
Nagels, M. M., T. A. Rijken, and J. D. de Swart, 1979a, Phys. Rev. D **17**, 768.
Nagels, M. M., T. A. Rijken, and J. D. de Swart, 1979b, Phys. Rev. D **20**, 1633.
Nakayama, K., A. Pio Galeão, and F. Krmpotić, 1982, Phys. Lett. B **114**, 217.
Nakayama, K., S. Krewald, J. Speth, and W. G. Love, 1984, Nucl. Phys. A **431**, 419.
Nakayama, K., S. Krewald, and J. Speth, 1986, Nucl. Phys. A **451**, 243.
Nakayama, K., and W. G. Love, 1988, Phys. Rev. C **38**, 57.
Nanda, S. K., C. Glashausser, K. W. Jones, J. A. McGill, T. A. Carey, J. B. McClelland, J. M. Moss, S. J. Seestrom-Morris, H. Ohnuma, M. Franey, M. Gazzaly, and N. Hintz, 1983, Phys. Rev. Lett. **51**, 1526.
Nanda, S. K., C. Glashuasser, K. W. Jones, J. A. McGill, T. A. Carey, J. B. McClelland, J. M. Moss, S. J. Seestrom-Morris, H. Ohnuma, M. Franey, M. Gazzaly, and N. Hintz, 1986, Phys. Rev. C **34**, 2013.
Negele, J. W., 1970, Phys. Rev. C **1**, 1260.
Nishizaki, S., S. Drożdż, J. Wambach, and J. Speth, 1988, Phys. Lett. B **215**, 231.
Nolte, E., S. Z. Gui, G. Colombo, G. Korschinek, and K. Eskola, 1982, Z. Phys. A **306**, 223.
Nolte, E., G. Korschinek, and C. Setzensack, 1983, Z. Phys. A **309**, 33.
O'Connell, J. S., W. R. Dodge, J. W. Lightbody, Jr., X. K. Maruyama, J.-O. Adler, K. Hansen, B. Schröder, A. M. Bernstein, K. I. Blomqvist, B. H. Cottman, J. J. Comuzzi, R. A. Miskimen, and B. P. Quinn, 1984, Phys. Rev. Lett. **53**, 1627.
O'Connell, J. S., W. R. Dodge, J. W. Lightbody, Jr., X. K. Maruyama, J.-O. Adler, K. Hansen, B. Schröder, A. M. Bernstein, K. I. Blomqvist, B. H. Cottman, J. J. Comuzzi, R. A. Miskimen, B. P. Quinn, J. H. Koch, and N. Ohtsuka, 1987, Phys. Rev. C **35**, 1063.
Ohlsen, G. G., 1972, Rep. Prog. Phys. **35**, 717.
Ohta, K., and M. Wakamatsu, 1974, Nucl. Phys. A **234**, 445.
Okuhara, Y., B. Castel, I. P. Johnstone, and H. Toki, 1987, Phys. Lett. B **186**, 113.
Olmer, C., B. Zeidman, D. F. Geesaman, T.-S. H. Lee, R. E. Segel, L. W. Swenson, R. L. Boudrie, G. S. Blanpied, H. A. Thiessen, C. L. Morris, and R. E. Anderson, 1979, Phys. Rev. Lett. **43**, 612.
Oset, E., and M. Rho, 1979, Phys. Rev. Lett. **42**, 47.
Oset, E., H. Toki, and W. Weise, 1982, Phys. Rep. **83**, 283.
Osterfeld, F., 1982, Phys. Rev. C **26**, 762.
Osterfeld, F., 1984, in *Proceedings of the International Conference on Spin Excitations in Nuclei,* edited by F. Petrovich, G. E. Brown, G. T. Garvey, C. D. Goodman, R. A. Lindgren, and W. G. Love (Plenum, New York), p. 403.
Osterfeld, F., D. Cha, and J. Speth, 1985, Phys. Rev. C **31**, 372.
Osterfeld, F., S. Krewald, H. Dermawan, and J. Speth, 1981, Phys. Lett. B **105**, 257,
Osterfeld, F., S. Krewald, J. Speth, and T. Suzuki, 1982, Phys. Rev. Lett. **49**, 11.
Osterfeld, F., and A. Schulte, 1984, Phys. Lett. B **138**, 23.
Osterfeld, F., J. Wambach, H. Lenske, and J. Speth, 1979, Nucl. Phys. A **318**, 45.
Ovazza, D., A. Willis, M. Morlet, N. Marty, P. Martin, P. de Saintignon, and M. Buenerd, 1978, Phys. Rev. C **18**, 2438.
Pandharipande, V. R., C. N. Papanicolas, and J. Wambach, 1984, Phys. Rev. Lett. **53**, 1133.
Petrovich, F., 1980, in *The (p,n) Reaction and the Nucleon-Nucleon Force,* edited by C. D. Goodman, Sam M. Austin, S. D. Loom, J. Rapaport, and G. R. Satchler (Plenum, New York), p. 115.
Petrovich, F., J. A. Carr, R. J. Philpott, and H. McManus, 1983, in *Electromagnetic Properties of Atomic Nuclei,* edited by H. Horie and H. Ohnuma (Tokyo Institute of Technology, Meguro, Tokyo), p. 312.
Petrovich, F., J. A. Carr, and H. McManus, 1986, Annu. Rev. Nucl. Part. Sci. **36**, 29.
Petrovich, F., and W. G. Love, 1981, Nucl. Phys. A **354**, 499c.
Petrovich, F., W. G. Love, A. Picklesimer, G. E. Walker, and E. R. Siciliano, 1980, Phys. Lett. B **95**, 166.
Petrovich, F., H. McManus, V. A. Madsen, and J. Atkinson, 1969, Phys. Rev. Lett. **22**, 895.
Petrovich, F., R. J. Philpott, A. W. Carpenter, and J. A. Carr, 1984, Nucl. Phys. A **425**, 609.
Pitthan, R., and Th. Walcher, 1971, Phys. Lett. B **36**, 563.
Raman, S., 1979, in *Neutron Capture Gamma-Ray Spectroscopy,* edited by R. E. Chrien and W. R. Kane (Plenum, New York), p. 193.
Raman, S., L. W. Fagg, and R. S. Higgs, 1991, in *Electric and Magnetic Giant Resonances in Nuclei,* edited by J. Speth (World Scientific, Singapore), p. 355.
Rapaport, J., 1983, in *The Interaction Between Medium Energy Nucleons in Nuclei,* AIP Conference Proceedings No. 97, edited by H. O. Meyer (AIP, New York), p. 365.
Rapaport, J., 1989, in *Workshop on Fundamental Symmetries and Nuclear Structure,* Santa Fe, New Mexico, edited by J. N. Ginocchio and S. P. Rosen (World Scientific, Singapore), p. 186.
Rapaport, J., T. Taddeucci, C. Gaarde, C. D. Goodman, C. C. Foster, C. A. Goulding, D. J. Horen, E. Sugarbaker, T. G. Masterson, and D. Lind, 1981, Phys. Rev. C **24**, 335.
Rapaport, J., T. Taddeucci, T. P. Welch, C. Gaarde, J. Larsen, D. J. Horen, E. Sugarbaker, P. Koncz, C. C. Foster, C. D. Goodman, C. A. Goulding, and T. Mastesron, 1983, Nucl.

Phys. A **410**, 371.
Rees, L. B., J. M. Moss, T. A. Carey, K. W. Jones, J. B. McClelland, N. Tanaka, A. D. Bacher, and H. Esbensen, 1987, Phys. Rev. C **34**, 627.
Rehm, K. E., P. Kienle, D. W. Miller, R. E. Segel, and J. J. Comfort, 1982, Phys. Lett. B **114**, 15.
Rho, M., 1974, Nucl. Phys. A **231**, 493.
Richter, A., 1979, in *Nuclear Physics with Electromagnetic Interactions,* Lecture Notes in Physics No. 108, edited by H. Arenhoevel and D. Drechsel (Springer, Berlin), p. 19.
Richter, A., 1982, Nucl. Phys. A **374**, 177c.
Rikus L., and H. V. von Geramb, 1984, Nucl. Phys. A **426**, 496.
Rikus, L., K. Nakano, and H. V. von Geramb, 1984, Nucl. Phys. A **414**, 413.
Ring, P., and P. Schuck, 1980, *The Nuclear Many-Body Problem* (Springer, New York).
Ring, P., and J. Speth, 1974, Nucl. Phys. A **235**, 315.
Rosza, C. M., D. H. Youngblood, J. D. Bronson, Y.-W. Lui, and U. Garg, 1980, Phys. Rev. C **21**, 1252.
Rowe, D. J., 1968, Rev. Mod. Phys. **40**, 153.
Rowe, D. J., 1970, *Nuclear Collective Motion* (Methuen, London).
Sagawa, H., and N. Van Giai, 1982, Phys. Lett. B **113**, 119.
Satchler, G. R., 1983, *Direct Nuclear Reactions* (Oxford University Press, New York).
Sawicki, J., 1962, Phys. Rev. **126**, 2231.
Sawyer, R. F., 1972, Phys. Rev. Lett. **29**, 382.
Sawyer, R. F., 1979, in *Mesons in Nuclei,* Vol. III, edited bv M. Rho and D. Wilkinson (North-Holland, New York), p. 992.
Scalapino, D. J. 1972, Phys. Rev. Lett. **29**, 386.
Scholten, O., G. F. Bertsch, and H. Toki, 1983, Phys. Rev. C **27**, 2975.
Schulte, A., T. Udagawa, F. Osterfeld, and D. Cha, 1987, Phys. Lett. B **183**, 243.
Sealock, R. M., K. L. Giovanetti, S. T. Thornton, Z. E. Meziani, O. A. Rondon-Aramayo, S. Auffret, J.-P. Chen, D. G. Christian, D. B. Day, J. S. McCarthy, R. C. Minehart, L. C. Dennis, K. W. Kemper, B. A. Mecking, and J. Morgenstern, 1989, Phys. Rev. Lett. **62**, 1350.
Seestrom-Morris, S. J., D. Dehnhard, M. A. Franey, G. S. Kyle, C. L. Morris, R. L. Boudrie, J. Piffaretti, and H. A. Thiessen, 1982, Phys. Rev. C **26**, 594.
Shigehara, T., K. Shimizu, and A. Arima, 1988, Nucl. Phys. A **477**, 583.
Shimizu, K., M. Ichimura, and A. Arima, 1974, Nucl. Phys. A **226**, 282.
Sick, I., E. B. Hughes, T. W. Donnelly, J. D. Walecka, and G. E. Walker, 1969, Phys. Rev. Lett. **23**, 1117.
Siemens, P. J., 1970, Nucl. Phys. A **141**, 225.
Sjöberg, O., 1973, Ann. Phys. (N.Y.) **78**, 39.
Skyrme, T. H. R., 1956, Philos. Mag. **1**, 1043.
Skyrme, T. H. R., 1959, Nucl. Phys. **9**, 615.
Smith, D. M., and J. Wambach, 1988, Phys. Rev. C **38**, 100.
Soloviev, V. G., 1987, Prog. Part. Nucl. Phys. **19**, 107.
Soloviev, V. G., Ch. Stoyanov, and A. I. Vdovin, 1977, Nucl. Phys. A **288**, 376.
Soloviev, V. G., Ch. Stoyanov, and A. I. Vdovin, 1980, Nucl. Phys. A **342**, 261.
Speth, J., V. Klemt, J. Wambach, and G. E. Brown, 1980, Nucl. Phys. A **343**, 382.
Speth, J., S. Krewald, F. Osterfeld, and T. Suzuki, 1984, in *Proceedings of the International Conference on Spin-Excitations in Nuclei,* edited by F. Petrovich, G. E. Brown, G. T. Garvey, C. D. Goodman, R. A. Lindgren, and W. G. Love (Plenum, New York), p. 445.
Speth, J., E. Werner, and W. Wild, 1977, Phys. Rep. **33**, 127.
Speth, J., and A. van der Woude, 1981, Rep. Prog. Phys. **44**, 719.
Sterrenburg, W. A., S. M. Austin, R. P. DeVito, and A. Galonsky, 1980, Phys. Rev. Lett. **45**, 1839.
Steffen, W., H. D. Gräf, W. Gross, D. Meuer, A. Richter, E. Spamer, O. Titze, and W. Knüpfer, 1980, Phys. Lett. B **95**, 23.
Steinwedel, H., and J. H. D. Jensen, 1950, Z. Naturforsch. **5a**, 413.
Suzuki, T., 1982, Nucl. Phys. A **379**, 110.
Suzuki, T., 1984, Ann. Phys. (Paris) **9**, 535.
Suzuki, T., and H. Hyuga, 1983, Nucl. Phys. A **402**, 491.
Suzuki, T., S. Krewald, and J. Speth, 1981, Phys. Lett. B **107**, 9.
Taddeucci, T. N., 1983, in *The Interaction Between Medium Energy Nucleons in Nuclei,* AIP Conference Proceedings No. 97, edited by H. O. Meyer (AIP, New York), p. 228.
Taddeucci, T. N., 1987, Can. J. Phys. **65**, 557.
Taddeucci, T. N., 1988, Bull. Am. Phys. Soc. **33**, 1597.
Taddeucci, T. N., T. A. Carey, C. Gaarde, J. Larsen C. D. Goodman, D. J. Horen, T. Masterson, J. Rapaport, T. P. Welch, and E. Sugarbaker, 1984, Phys. Rev. Lett. **52**, 1960.
Taddeucci, T. N., C. D. Goodman, R. C. Byrd, I. J. van Heerden, T. A. Carey, D. J. Horen, J. S. Larsen, C. Gaarde, J. Rapaport, T. P. Welch, and E. Sugarbaker, 1986, Phys. Rev. C **33**, 746.
Takayanagi, K., K. Shimizu, and A. Arima, 1988a, Nucl. Phys. A **477**, 205.
Takayanagi, K., K. Shimizu, and A. Arima, 1988b, Nucl. Phys. A **481**, 321.
Toki, H., and W. Weise, 1980, Phys. Lett. B **97**, 12.
Tomoda, T., 1991, Rep. Prog. Phys. **54**, 53.
Tomoda, T., and A. Faessler, 1987, Phys. Lett. B **199**, 45.
Towner, I. S., 1984, Prog. Part. Nucl. Phys. **11**, 91.
Towner, I. S., 1987, Phys. Rep. **155**, 263.
Towner, I. S., and F. C. Khanna, 1979, Phys. Rev. Lett. **42**, 51.
Towner, I. S., and F. C. Khanna, 1983, Nucl. Phys. A **399**, 334.
Udagawa, T., S. W. Hong, and F. Osterfeld, 1990, Phys. Lett. B **245**, 1.
Udagawa, T., A. Schulte, and F. Osterfeld, 1987, Nucl. Phys. A **474**, 131.
Valatin, J. G., 1961, Phys. Rev. **122**, 1012.
Vautherin, D., and D. M. Brink, 1972, Phys. Rev. C **5**, 626.
Vetterli, M. C., O. Häusser, R. Abegg, W. P. Alford, A. Celler, D. Frekers, R. Helmer, R. Henderson, K. H. Hicks, K. P. Jackson, R. G. Jeppesen, C. A. Miller, K. Raywood, and S. Yen, 1989, Phys. Rev. C **40**, 559.
Vetterli, M. C., O. Häusser, W. P. Alford, D. Frekers, R. Helmer, R. Henderson, K. Hicks, K. P. Jackson, R. G. Jeppesen, C. A. Miller, M. A. Moinester, K. Raywood, and S. Yen, 1987, Phys. Rev. Lett. **59**, 439.
Vogel, P., and M. R. Zirnbauer, 1986, Phys. Rev. Lett. **57**, 3148.
Wambach, J., 1988, Rep. Prog. Phys. **51**, 989.
Watson, J. W., P. J. Pella, B. D. Anderson, A. R. Baldwin, T. Chittrakarn, B. S. Flanders, R. Madey, C. C. Foster, and I. J. van Heerden, 1986, Phys. Lett. B **181**, 47.
Watson, J. W., B. D. Anderson, and R. Madey, 1987, Can. J. Phys. **65**, 566.
Weisberger, W. I., 1966, Phys. Rev. **143**, 1302.
Wienhard, K., K. Ackermann, K. Bangert, U. E. P. Berg, C. Bläsing, W. Naatz, A. Ruckelshausen, D. Rück, R. K. M. Schneider, and R. Stock, 1982, Phys. Rev. Lett. **49**, 18.
Wildenthal, B. H., 1984, Prog. Part. Nucl. Phys. **11**, 5.
Wilkinson, D. H., 1973a, Phys. Rev. C **7**, 930.

Wilkinson, D. H., 1973b, Nucl. Phys. A **209**, 470.
Wilkinson, D. H., 1974, Nucl. Phys. A **225**, 365.
Wilkinson, D. H., 1977, Phys. Lett. B **66**, 105.
Wolfenstein, L, and J. Ashkin, 1952, Phys. Rev. **85**, 947.
Yabe, M., F. Osterfeld, and D. Cha, 1986, Phys. Lett. B **178**, 5.
Yamaguchi, N., S. Nagata, and T. Matsuda, 1983, Prog. Theor. Phys. **70**, 459.
Yannouleas, C., M. Dworzecka, and J. J. Griffin, 1983, Nucl. Phys. A **397**, 239.
Yannouleas, C., and S. Jang, 1986, Nucl. Phys. A **455**, 40.
Yen, S., 1987, Can. J. Phys. **65**, 595.
Yen, S., R. Sobie, H. Zarek, B. O. Pich, T. E. Drake, C. F. Williamson, S. Kowalski, and C. P. Sargent, 1980, Phys. Lett. B **93**, 250.
Youngblood, D. H., P. Bogucki, K. D. Bronson, U. Garg, Y.-W. Lui, and C. M. Rozsa, 1981, Phys. Rev. C **23**, 1997.
Youngblood, D. H., C. M. Rozsa, J. M. Moss, D. R. Brown, and J. D. Bronson, 1977, Phys. Rev. Lett. **39**, 1188.
Zamick, L., 1984, Phys. Rev. C **29**, 667.
Ziegler, B., 1979, in *Proceedings of the International Conference on Nuclear Physics with Electromagnetic Interactions,* Lecture Notes in Physics No. 108, edited by H. Arenhoevel and D. Dreschel (Springer, Berlin), p. 148.
Zweig, G., 1964, CERN Report No. 8182/TH 401.